FLOW INJECTION WITH CHEMILUMINESCENCE DETECTION FOR THE DETERMINATION OF IRON IN SURFACE ATLANTIC WATERS

by

Andrew Ross Bowie

A thesis submitted to the University of Plymouth

in partial fulfilment for the degree of

DOCTOR OF PHILOSOPHY

Department of Environmental Sciences

Faculty of Science

In collaboration with

Centre for Coastal and Marine Sciences – Plymouth Marine Laboratory

October 1999

ABSTRACT

Flow Injection with Chemiluminescence Detection for the Determination of Iron in Surface Atlantic Waters

Andrew R. Bowie

This thesis describes the design, optimisation and shipboard deployment of a flow injection - chemiluminescence (FI-CL) technique for the determination of iron (Fe) in seawater. Chapter One presents an overview of the marine biogeochemistry of Fe, including its speciation, sources and sinks, abundance and limitation for phytoplankton growth in the World's oceans. Current analytical methods for the determination of Fe in natural waters are also reviewed.

Chapter Two reports the instrumental development of the FI-CL method. Each component is described and its suitability to the flow manifold discussed. Different CL detection systems are evaluated and a charge coupled device used to investigate the spectral profile of the Fe-catalysed luminol reaction. Automation of the FI manifold is also detailed along with acquisition of CL signals. Chapter Three details the optimisation of a FI-CL procedure for the determination of Fe in seawater. Reagent clean-up techniques, blank procedures and a standard addition operating routine are detailed. Fe(III) reduction using sulphite is treated theoretically. Matrix effects are investigated and the synthesis of an 8-hydroxyquinoline resin used for in-line matrix elimination and preconcentration is reported. The optimised method is selective to Fe(II+III) in the linear range 0.04-10 nM, with a precision of 3.2% (n=5) for a 1.0 nM standard and a limit of detection (3s) of 40 pM for a load time of 1 min. Chapter Four presents the results of an investigation into the kinetic effect of Fe on luminol CL using the continuous addition of reagent (CAR) technique. Instrumental and chemical parameters are optimised, interferences investigated and the CAR-CL technique compared with alternative flow configurations.

In Chapter Five, the application of the FI-CL method to the shipboard determination of Fe in the surface North and South Atlantic (50°N to 50°S) is presented. Data are reported for samples collected from the upper water column (<200 m) in eight different biogeochemical provinces, which represent coastal, upwelling and oligotrophic regions of the Atlantic Ocean. Total dissolvable iron (unfiltered, TD-Fe) levels range from <0.1 to 6.1 nM and indicate that high and spatially variable TD-Fe (>2 nM) concentrations exist in Equatorial and tropical North Atlantic regions influenced by atmospheric deposition from the West African continent. Away from strong input mechanisms, TD-Fe concentrations in the upper water column average 0.6 nM. Input sources are fingerprinted *via* correlation with other trace metals (Al, Co, Ni), nutrients and hydrography, whilst active biological uptake is shown to be the dominant sink. TD-Fe vertical distributions through the upper mixed layer display strong relationships with chlorophyll *a* concentrations, and measurements in the deep chlorophyll maximum of the South Atlantic oligotrophic gyre show that, despite elevated nitrate at such depths, Fe concentrations are at a minimum (ca. 0.1 nM) and may be low enough to (co-)limit phytoplankton growth.

ACKNOWLEDGEMENTS

I would like to express my sincere thanks to all of my supervisors for their advice throughout my PhD. research and for their critical comments on this manuscript. Firstly to Paul Worsfold, who has been a good friend and very supportive throughout our many projects (how much over budget?); to Eric Achterberg, who has given me intuitive advice and guidance during my studies (but not on the squash court). Many thanks to Fauzi Mantoura, to whom I am indeed very grateful, for his wise comments and for providing me with excellent opportunities and contacts which have inspired me into exploring oceanic trace element biogeochemistry.

I am very grateful to those whom have helped me in a variety of ways during the field studies and oceanographic cruises. I would like to acknowledge the Atlantic Meridional Transect steering group for providing a platform to deploy the iron monitor. Thanks to Ray Barlow for his insights and friendship during AMT-3 and 6. Tony Bale for his support as principle scientist, Jim Aiken, Malcolm Woodward, Emilio Marañón and all other participants of the AMT project who have helped with data and interpretation and who contributed to some wondrous experiences during the voyages. Many thanks also to the crew and officers of the magnificent *R.R.S James Clark Ross*. I would like to acknowledge Tim Fileman for his advice and field support during the Tamar Estuary axial transects and David Whitworth for design and implementation of the tidal cycle survey and for his contribution to the AMT data set. A big thanks to Jeroen de Jong for his analytical advice and for exchange of ideas. Big thanks also to Phil Boyd (well done, you did it!), Cliff Law and the 1999 SOIREE "ring in the ocean" team – an unforgettable and momentous experience.

Thanks also to members of the "106" research group and other companions, past and present, who have provided friendship and support in (and out of) the lab. Cheers to Dazza (good luck with the family), Phil (reliable rugby partner), Vincenzo and Paolo (separated at birth?), Thierry, Ana, Grady, Dan, Simon, Richard, Sandrine, Belen and to all the new boys and girls. You all have good opportunities, so best wishes for all.

A big cheers to David Whitworth for socially great memories and scientific inspiration in the early years. Hope to see you down south. Best wishes to Véro Herzl, thanks for your friendship and for the Barbican year; Lesley Johns (you're next!) and Matt "the phat" Shaw. Big hóla to all my Spanish friends who helped make my time in Córdoba a great cultural experience. Good luck to Angela Hayes, to Raj "Bob" Birring (who will never change), The Chief, Ghost and other dubious characters, and to all the Leeds and Manchester chaps for fantastic memories from the crazy student years. Many thanks to Mum and Dad and my family for your support – it has been unflinching and for this I am very grateful. And most importantly for me, "un gros bisou" to Sophie Mai, who has made the past year and a half very special. I hope our dreams come true.

I will not cease from mental fight,

Nor shall my sword sleep in my hand.

William Blake (1757-1827)

AUTHOR'S DECLARATION

At no time during the registration for the degree of Doctor of Philosophy has the author been registered for any other University award. This study was financed with the aid of a studentship from the University of Plymouth and carried out in collaboration with CCMS – Plymouth Marine Laboratory. The field work performed during the Atlantic Meridional Transect forms part of larger, multi-disciplinary project and the assistance of all those involved is duly and gratefully acknowledged.

A programme of advanced study was undertaken which included guided reading in topics related to environmental analytical chemistry and chemical oceanography, and training in the analysis of trace metals using a variety of ultra-clean analytical techniques. Relevant scientific seminars and conferences were regularly attended at which work was often presented; external institutions were visited for consultation purposes, several papers prepared for publication and data disseminated *via* password-protected sites on the World Wide Web.

All data presented in this thesis (unless otherwise stated in the text and appendices) was prepared by the author, whom the ownership rests with. Before using this data in any presentation or printed publication, please contact the author and include full acknowledgements. All enquiries regarding the sampling, analysis and data preparation can be directed to:

Andrew R. Bowie
Dept. of Environmental Sciences
University of Plymouth
Drake Circus
Plymouth PL4 8AA
United Kingdom
Tel +44 1752 233128
Fax +44 1752 233035
E-mail abowie@plymouth.ac.uk

Signed..... Andrew Bowie.....

Date..... 29th November 1999.....

PUBLICATIONS

Bowie A.R., Fielden P.R., Lowe R.D. and Snook R.D., 1995. Sensitive determination of manganese using flow injection and chemiluminescent detection, *Analyst*, **120**, 2119-2127.

Bowie A.R., Sanders M.G. and Worsfold P.J., 1996. Analytical applications of liquid phase chemiluminescence reactions - a review, *Journal of Bioluminescence and Chemiluminescence*, **11**, 61-90.

Bowie A.R., Achterberg E.P., Mantoura R.F.C. and Worsfold P.J., 1997. Iron distributions along the Atlantic Meridional Transect, 50°N – 50°S. In *"Proceedings of the Marc'h Mor Workshop"*, IUEM, Brest, France, 208-212.

Bowie A.R., Achterberg E.P., Mantoura R.F.C. and Worsfold P.J., 1998. Determination of sub-nanomolar levels of iron in seawater using flow injection with chemiluminescence detection, *Analytica Chimica Acta*, **36**, 189-200.

Bowie A.R., 1999. Sources, Sinks and Distributions of Iron in Seawater. Data contribution, Chapter in: de Baar H.J.W., *"Biogeochemistry of Iron in Seawater"*, Turner D.R. and Hunter K.A. (eds.), IUPAC/SCOR project, in press.

Bowie A.R., Achterberg E.P., Mantoura R.F.C. and Worsfold P.J., 1999. Iron biogeochemistry in the surface waters of the Atlantic Ocean, *Deep Sea Research*, in preparation.

Bowie A.R., Silva M., Perez-Bendito D. and Worsfold P.J., 1999. The kinetic effect of iron species on luminol chemiluminescence under the continuous addition of reagent technique, *Talanta*, in preparation.

Boyd P.W., Watson A.J., Law C.S., Abraham E., Trull T., Murdoch R., Bakker D.C.E., Bowie A.R. and 25 other authors, 1999. Diatoms bloom upon mesoscale iron fertilisation of polar Southern Ocean waters, co-author, *Nature*, in submitted.

Cannizzaro V., Bowie A.R., Achterberg E.P. and Worsfold P.J., 1999. Determination of cobalt and iron in estuarine and coastal waters using flow injection – chemiluminescence, *Analyst*, accepted, in press.

Croot P.L., Bowie A.R., Frew R.D. and Maldonado M.T., 1999. Persistence of dissolved iron and Fe(II) during an iron induced phytoplankton bloom in the Southern Ocean. co-author, in preparation.

Segura-Carretero A., Rodriguez-Fernandez J., Bowie A.R. and Worsfold P.J., 1999. Acquisition of chemiluminescence spectral profiles using a continuous flow manifold with two-dimensional CCD detection, *Analytical Communications*, submitted.

Worsfold P.J., Achterberg, E.P., Bowie, A.R. and Sandford, R.C., 1999. Flow Injection with Chemiluminescence Detection for the Shipboard Monitoring of Trace Metals, Chapter in: *"Chemical Sensors in Oceanography"*, Varney M.S. (ed.), in press.

Worsfold P.J., Achterberg E.P., Bowie A.R. and Cannizzaro V., 1999. Marine Monitoring of Trace Metals using Flow Injection with Chemiluminescence Detection. In: *"Environmental Monitoring and Management, Proceedings of the Winter Conference"*, University of the West Indies, in press.

PRESENTATIONS AND CONFERENCES ATTENDED

Techniques for Water Quality Monitoring, Royal Society of Chemistry, one day meeting, University of Plymouth (UK), June 1996.

Atlantic Meridional Transect Workshop II, Plymouth Marine Laboratory (UK). *'Iron Distributions along AMT cruise 3"*, poster presentation, February 1997.

Progress in Chemical Oceanography II, Southampton Oceanography Centre (UK). *"Oceanic Iron Analyses using Flow Injection – Chemiluminescence"*, poster presentation, September 1997.

MARC'H MOR International Workshop, Brest (France). *"Determination of Iron Species in Marine Waters"*, oral and poster presentations, paper in conference proceedings, November 1997.

Iron in the Marine Environment, Challenger Society Meeting, London (UK). *"Iron Determinations by FI-CL and Distributions during AMT-3 Cruise"*, oral presentation, December 1997.

Young Researchers' Meeting and National Congress, Royal Society of Chemistry, Durham (UK). *"Shipboard Determinations of Iron in Seawater using a Novel FI-CL Manifold"**, oral presentation, April 1998. *Awarded prize for best oral presentation.

Water, Water Everywhere, one day meeting, Zeneca Brixham (UK), April 1998.

Trace Metal Monitoring in Surface Marine Waters and Estuaries, EU MAST progress meeting, Oviedo (Spain). *"Luminescence Methods for the in situ Monitoring of Trace Metals in Marine Systems"*, September 1998.

UK Oceanography, University of Southampton (UK). *"Iron Biogeochemistry along two Atlantic Meridional Transects"*, poster presentation, September 1998.

Biogeochemistry of Iron in Seawater, SCOR Working Group 109, Amsterdam (Netherlands). *"Iron Biogeochemistry in the Surface Atlantic Ocean"**, oral presentation, November 1998. *Invited lecture

Ronald Belcher Memorial Lecturer*, Royal Society of Chemistry, Greenwich, London (UK). *"Investigating Marine Trace Metal Biogeochemistry using Novel Analytical Techniques"*, April 1999, *Prize lectureship for outstanding research during Ph.D. studentship.

LabVIEW programming, National Instruments one day seminar, Cheltenham (UK), July 1999.

Symposium of Analytical Chemistry, Royal Society of Chemistry, Dublin (Ireland). *"Iron Mapping and Speciation through the First Mesoscale Iron Enrichment Experiment in the Southern Ocean"*, July 1999.

3rd European Conference on Environmental Analytical Chemistry, Chalkidiki (Greece). *"Investigating Iron Biogeochemistry During a Mesoscale Enrichment in the Southern Ocean using Flow Injection Chemiluminescence"*, October 1999.

CONTENTS

LIST OF FIGURES

LIST OF TABLES

GLOSSARY OF COMMONLY-USED ABBREVIATIONS

A/D	analogue to digital
AdCSV	adsorptive cathodic stripping voltammetry
AMT	Atalntic Meridional Transect
BFCC	Brazilian and Falkland currents convergence
BSF	brilliant sulfoflavin
CAR	continuous addition of reagent
CASS	coastal surface seawater
CCD	charge coupled device
CL	chemiluminescence
CLE	competitive ligand equilibration
CO_2	carbon dioxide
CRM	certified reference material
CZCS	colour zone coastal scanner
CTD	conductivity, tepmerature, depth
DCM	deep chlorophyll maximum
diss	dissolved
DMS	dimethylsulphide
EDTA	ethylenediaminetetraacetate
EFS	East Falkland shelf
Eq	Equator
FI	flow injection
FRRF	fast repetition rate fluorometry
GFAAS	graphite furnace atomic absorption spectrometry
H_2O_2	hydrogen peroxide
HDPE	high density polyethylene
HNLC	high nutrient, low chlorophyll
HNO_3	nitric acid
8-HQ	8-hydroxyquinoline
IDA	iminodiacetic acid
ID-ICPMS	isotope dilution inductively coupled plasma mass spectrometry
ITCZ	inter-tropical convergence zone
LISW	low iron seawater
LOD	limit of detection
MLW	wind mixed layer
MOW	Mediterranean outflow water
MQ	Milli-Q
Na_2CO_3	sodium carbonate
Na_2SO_3	sodium sulphite
NaOH	sodium hydroxide
NASS	North Atlantic surface seawater
NEAOG	North-east Atalntic oligotrophic gyre
NH_3	ammonia
NH_4OAc	ammonium acetate
NO_2	nitrite
NO_3	nitrate
NWAUp	North-west African upwelling
PAR	photosynthetically available radiation
P-I	photosynthesis-irradiance

PMT	photomultiplier tube
PO_4	phosphate
PTFE	polytetrafluoroethylene (Teflon®)
PVC	polyvinyl chloride
Q-HCl	sub-boiled, quartz distilled hydrochloric acid
RSD	relative standard deviation
SAOG	South Atlantic oligotrophic gyre
SeaWiFS	Sea-viewing wide field-of-view sensor
$Si(OH)_4$	silicate
SOIREE	Southern Ocean iron release experiment
SPM	suspended particulate matter
SST	sea surface temperature
STB	screw terminal board
SUp/NEq	south of upwelling / north of Equator
SW	seawater
SWApp	South-west approaches
TCNQ	tetracyanoquinodimethane
TD	total dissolvable
T-S	temperature – salinity
TTL	transistor-transistor logic
UHP	ultra high purity

FLOW INJECTION WITH CHEMILUMINESCENCE DETECTION FOR THE DETERMINATION OF IRON IN SURFACE ATLANTIC WATERS

by

Andrew Ross Bowie

INTRODUCTION

I.1 CHEMICAL AND PHYSICAL PROPERTIES OF IRON

Originating from the Anglo-Saxon word "*iren*", its chemical symbol taken from the Latin "*ferrum*", the element iron (Fe) has been known to humans since ancient times and no other element has played a more important role in man's material progress. Fe is a vital constituent of plant and animal life. With a relative abundance of 5.6%, it is the fourth most abundant element in the Earth's crust (Taylor, 1964), existing in numerous crystalline forms and is widely distributed in the lithosphere as oxides and carbonates such as haematite (Fe_2O_3), magnetite (Fe_3O_4), limonite ($\sim 2Fe_2O_3.3H_2O$), siderite ($FeCO_3$) and pyrite (FeS_2). Compounds of Fe are present in two oxidation states in natural waters, the Fe(II) or *ferrous* form and the Fe(III) or *ferric* form. Some physico-chemical properties of Fe are given in Table I.1.

Property	*Value*
Atomic number	26
Relative atomic mass	55.847 g mol^{-1}
Electronic configuration	$[Ar]3d^64s^2$
No. of naturally occurring isotopes	5
Melting point at 1 atm (°C)	1535
Boiling point at 1 atm (°C)	2750
Density at 300K (g cm^{-3})	7.874

Table I.1. Physical and chemical properties of Fe

Metallic Fe is a silvery, lustrous material which has important magnetic properties. The pure solid is usually alloyed with carbon or other metals, is very reactive chemically, and rapidly corrodes, especially in moist air or at elevated temperatures. Most Fe produced commercially is used in the steel industry. The ubiquitous usage of Fe as a structural element has severely compromised historical seawater analyses due to many contamination problems originating from the tools used by marine chemists, e.g. water samplers, research vessels, laboratories and many manufactured materials.

I.2 MARINE BIOGEOCHEMISTRY OF IRON

The World's oceans cover about 70% of the surface of the Earth and play an important role in the global climate system, acting as an important buffer for heat and gases (e.g. carbon dioxide, CO_2). Plankton productivity in the ocean exhibits high spatial and temporal variability

and is dependent on several key nutrients, one of which is Fe. However, there remain large gaps in the knowledge of Fe chemistry and its biological importance to marine life (Wells *et al.*, 1995). Its extreme insolubility and biogeochemical reactivity in seawater results in very low ambient dissolved Fe concentrations (<1.0 nM). Only recently has the development of new clean sampling and analytical methodologies enabled the generation of reliable profiles in traditional dissolved (<0.2 μm or <0.45 μm), total dissolvable (unfiltered) and particulate (>0.2 μm or 0.45 μm) operationally defined classes, although the chemical forms within each fraction are largely speculative. Figure I.1 provides a schematic summary of the marine biogeochemical processes of Fe in seawater, which are discussed in detail in the following sections.

I.2.1 Composition of Seawater

The major constituents of seawater that make up >99% by weight of sea-salts are shown in Table I.2. In contrast to many trace elements and classical nutrients whose concentrations are strongly influenced by biogeochemical cycling, these major seawater ions act conservatively. Their abundance results in an almost invisible Fe signal in seawater, hidden behind the high salt matrix.

Ion	*Concentration (g l^{-1})*[a]	*Percent by weight*[b]
Chloride (Cl^-)	19.87	55.07
Sodium (Na^+)	11.05	30.62
Sulphate (SO_4^{2-})	2.712	7.72
Magnesium (Mg^{2+})	1.326	3.68
Calcium (Ca^{2+})	0.422	1.17
Potassium (K^+)	0.416	1.10
Bicarbonate (HCO_3^{2-})	0.142	0.39
Bromide (Br^-)	0.0674	0.19
Strontium (Sr^{2+})	0.0079	0.02
Boron (H_3BO_3)	0.00445	0.01
Fluoride (F^-)	0.00128	<0.01
Ionic strength (M)	0.6-0.7	
Salinity	~35 (range 32-37)	
pH	7.5-8.3	

[a] Ocean water of salinity = 35; data from Riley and Chester, 1971
[b] Data from Gross, 1996
Note: Oceanic mean [dissolved Fe] = 0.04 μg l^{-1}, $1x10^{-7}$ % (Johnson *et al.*, 1997)

Table I.2. Major constituents of seawater

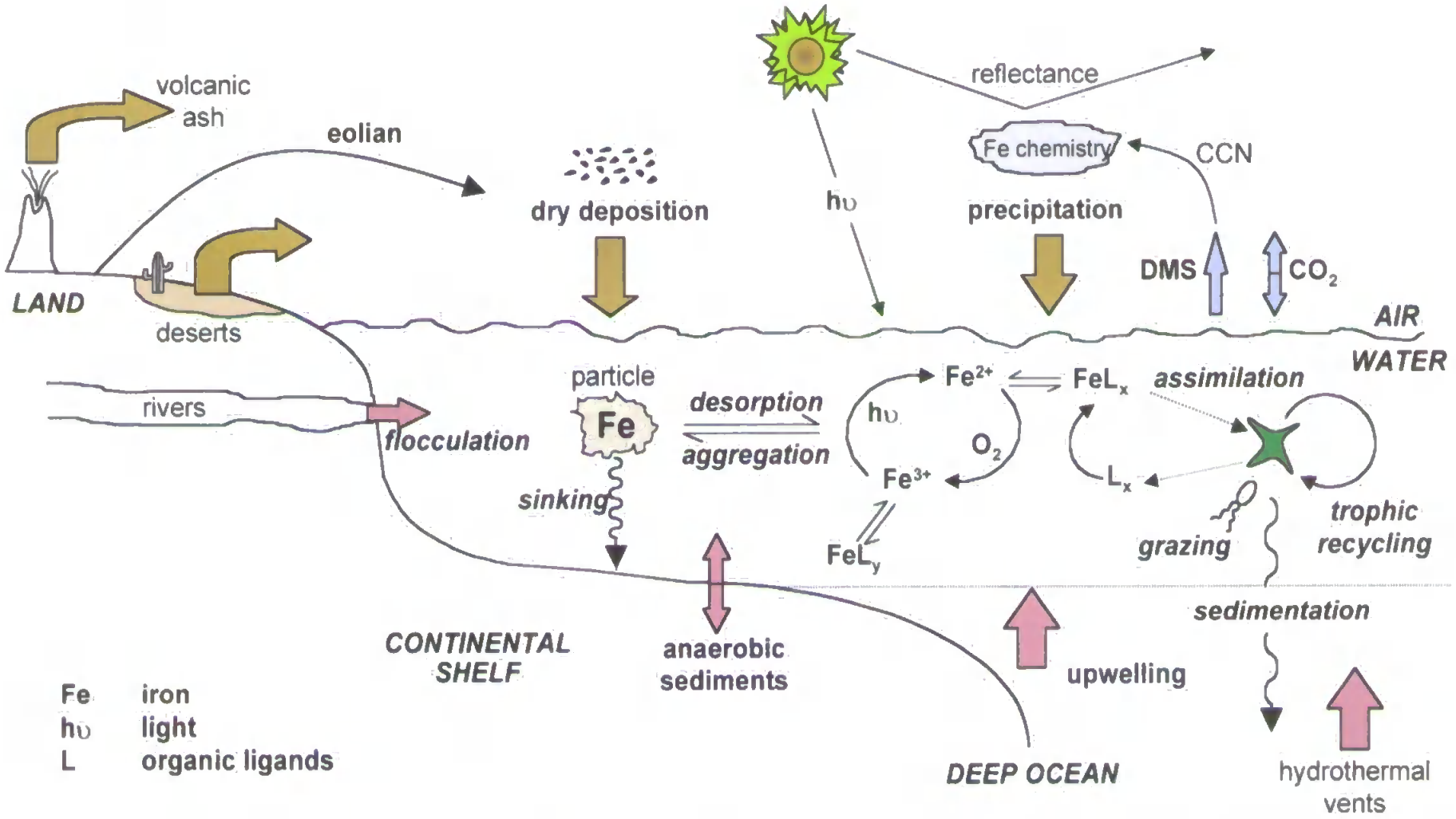

Figure I.1. Biogeochemistry of Fe in coastal and oceanic waters, illustrating sources, transport, cycling and interaction with phytoplankton and biogases

I.2.2 Speciation, Solubility and Bioavailability

The speciation of Fe in natural waters affects its thermodynamic solubility (Byrne and Kester, 1976; Zhu *et al.*, 1992; Millero, 1998), redox transformations (Millero, 1990, Millero *et al.*, 1995a, Zhu *et al.*, 1993) and interaction of Fe with biota (Anderson and Morel, 1982; Sunda *et al.*, 1991; Sunda and Huntsman, 1995a). Figure I.2 schematically illustrates the speciation and cycling of Fe in the marine environment.

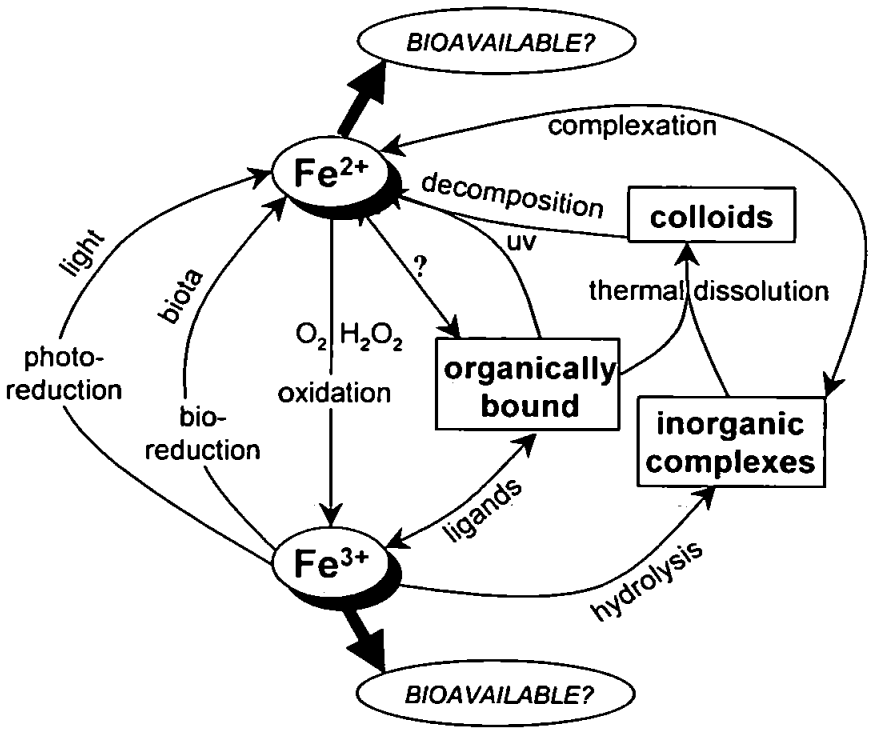

Figure I.2. Speciation and redox cycling of Fe in seawater

I.2.2.1 Inorganic Complexation

From a thermodynamic perspective, Fe(III) at pH 8 in oxygenated seawater rapidly ($k_f > 10^4\ M^{-1}\ s^{-1}$; T=20 °C) hydrolyses with OH^- to yield $Fe(OH)_2^+$, $Fe(OH)_3$, $Fe(OH)_4^-$ and insoluble oxy-hydroxide species (Stumm and Morgan, 1996; Byrne *et al.* 1988; Millero *et al.* 1995a). The solid Fe(III) oxy-hydroxide present in seawater may be more amorphous, more labile and more soluble than well-crystallised forms of FeOOH and Fe_2O_3 because of reversible photoredox cycling in the euphotic zone cycling (Waite and Morel, 1984a; Waite *et al.*, 1995; see Section I.2.2.4). Previous studies (Kuma and Matsunaga, 1995, Kuma *et al.*, 1996) have also shown that Fe(III) hydroxide solubility values are higher in coastal waters than in the open-

ocean, probably due to the increased presence of strong organic ligands (Kuma *et al.*, 1998). The inorganic colloidal fraction may play an important role in the supply of bioavailable Fe to coastal marine phytoplankton (Kuma and Matsunaga, 1995). Multiligand and multimetal equilibrium models exist (e.g. Haltafall, WaterQ, MINEQL+; Westall *et al.*, 1976; Stumm and Morgan 1996) to esti nate trace metal speciation in seawater and in heterogeneous sorption and redox systems. Millero *et al.* (1995a) thoroughly investigated and modelled the inorganic speciation of Fe(II) and Fe(III) in natural waters, and the published diagrams are reproduced in Figure I.3.

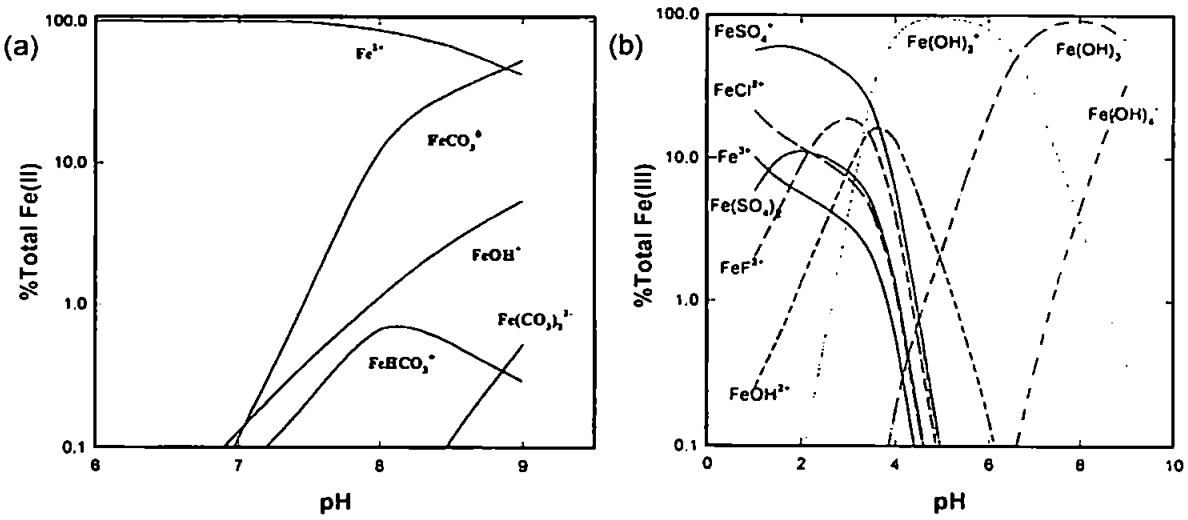

Figure I.3. The inorganic speciation of (a) Fe(II) and (b) Fe(III) in seawater (S=35) as a function of pH (reproduced from Millero *et al.*, 1995a)

I.2.2.2 Organic Complexation

As much as 99.9% of dissolved Fe has been reported to be organically complexed in seawater (Rue and Bruland, 1995; Gledhill and van den Berg, 1994; Kuma *et al.*, 1996). Two classes of Fe(III)-binding ligands are thought to exist, a stronger class (L_1), complexing the majority of total dissolved Fe(III), and a weaker one (L_2). In the equatorial Pacific, [L_1] has been calculated to exist at a mean concentration of 310 pM with a conditional stability constant of $K^{cond}_{FeL_1,Fe(III)'}=4.7\times10^{12}$ M^{-1}, and [L_2] has been reported to be present at a mean concentration of 190 pM with a conditional stability constant of $K^{cond}_{FeL_2,Fe(III)'}=6.5\times10^{11}$ M^{-1} (Rue and Bruland, 1997). Under these conditions, the sum of dissolved inorganic Fe(III) species, or Fe(III)', would therefore exist at an extremely low equilibrium concentration (0.01 pM; Rue and Bruland, 1997). The source of such ligands remains uncertain, although they may originate from phytoplankton

via cell exudation and degradation products or from bacteria as an assemblage of siderophores (Section I.2.2.7). Recent work by Emmenegger *et al.* (1998) showed that Fe(II) oxidation in lake water is consistent with reported redox models based on carbonate speciation (King, 1998) above pH 7.5, but showed elevated oxidation rates at lower pH, which was ascribed to the presence of Fe(II) ligands. Such Fe(II)-organic complexes may in turn oxidise to Fe(III)-organic complexes and become available to algae by cell-surface reduction, ligand-exchange or photochemical processes (Rue and Bruland, 1997). Conversely, oxidation of Fe(II) on oxide surfaces would reduce the bioavailability of Fe. Reliable analytical methods do not presently exist to determine Fe(II) ligand concentrations in seawater.

I.2.2.3 Colloids

Existing as oxyhydroxides in nearshore waters (Wells and Goldberg, 1992) and hydrothermal plumes (Feely *et al.*, 1990), and mainly as organic complexes in surface oceanic waters (Wells and Goldberg, 1994), the marine colloidal phase may serve as a reservoir of Fe in seawater. Results indicate that 20-40% of filterable Fe in surface North Atlantic waters occurs in the organic colloidal phase (Wu and Luther, 1994; Powell *et al.*, 1997). However, a poor understanding of the colloidal abundance, distribution, species, photochemical reactivity and exchange processes with soluble and particulate forms presently exists.

I.2.2.4 Redox Cycling

The redox cycling of Fe in marine (O'Sullivan *et al.*, 1991; King *et al.*, 1995), terrestrial (McKnight *et al.*, 1988) and atmospheric (Zhu *et al.*, 1992, 1993; Zhuang *et al.*, 1992) systems is critically linked to its solubility, bioavailability and oxygen radical chemistry. An appreciable dynamic concentration of Fe(II) is thought to exist *via* a combination of photochemical (O'Sullivan *et al.*, 1991; Johnson *et al.*, 1994), thermal, enzymatic and microbial pathways (Tortell *et al.*, 1999; Maldonado and Price, 1999). Photochemical Fe(II) formation proceeds through the reductive dissolution of Fe(III) (hydr)oxides and the photolysis of dissolved Fe(III)-organic complexes (e.g. fulvic or humic acids; Stumm and Morgan, 1996; Wells and Mayer, 1991a; Waite and Morel, 1984b). The Fe(II) formed is rapidly re-oxidised by O_2, H_2O_2 and other oxidants

(half life of the order of 10 min in coastal seawater, pH 8, T=22 °C; Holland, personal communication). Millero and Sotolongo (1989) and King *et al.* (1995) found similar half lives (several minutes, dependant on factors such as pH, temperature, [Fe], [oxidant]) in seawater based on model calculations and experimental measurements, assuming a pseudo first-order rate constant, and Emmenegger *et al.* (1998) reported a value between 7 and 60 s for surface waters of a eutrophic lake. Oxidation rates are enhanced if ferrous ions are adsorbed onto a mineral or biogenic particle surface, producing $Fe(OH)_3$ as soft colloids or surface-bound molecules that are less polymeric and less crystalline than aged oxyhydroxides, and thus more soluble and in faster equilibrium with monomeric species. Such species may be more available for uptake by phytoplankton (Bruland *et al.*, 1991; Rich and Morel, 1990).

The deposition of photochemically transformed aerosols may be a significant direct source of Fe(II) to surface waters, especially following rain events (Zhu *et al.*, 1993; Zhuang *et al.*, 1995). Fe(III) reduction may also be mediated by membrane-bound redox proteins or by intracellular enzymes secreted as a result of cell damage, and reduction rates have been reported to increase as Fe-limited growth rates decrease, suggesting that the reductant pumping mechanism may be related to Fe-deficiency (Maldonado and Price, 1999). Elevated Fe(II) concentrations have also been observed during spring blooms (Kuma *et al.*, 1992). The acidic, reducing microenvironment contained within the gut of a planktonic grazer may also provide suitable conditions for Fe(III) reduction.

Fe(II) oxidation has been previously studied at micromolar levels (Kuma *et al.*, 1992; O'Sullivan *et al.*, 1997) and more recently at oceanic (i.e. nanomolar) concentrations (Millero *et al.*, 1987; Millero and Sotolongo, 1989; King *et al.*, 1995; Emmenegger *et al.*, 1988). A generally accepted mechanism for the oxidation of Fe(II) by O_2 is the four-step Haber-Weiss mechanism which involves oxidation of Fe(II) by both O_2 and H_2O_2 (eqns. 1 and 3) as rate-limiting reactions and by fast reactions involving radical intermediates, $O_2^{\cdot-}$ and $HO^{\cdot}$ (eqns. 2 and 4) (Haber and Weiss, 1934):

$$Fe(II) + O_2 \xrightarrow{k_1} Fe(III) + O_2^{\cdot-} \qquad (1)$$

$$Fe(II) + O_2^{\cdot-} \xrightarrow{k_2,\ 2H^+} Fe(III) + H_2O_2 \qquad (2)$$

$$Fe(II) + H_2O_2 \xrightarrow{k_3} Fe(III) + HO^{\cdot} + OH^- \qquad (3)$$

$$Fe(II) + HO^{\cdot} \xrightarrow{k_4} Fe(III) + OH^- \qquad (4)$$

The rate expression of Fe(II) oxidation is thus given by :

$$-\frac{d[Fe(II)]}{dt} = 2k_1[O_2][Fe(II)] + 2k_3[H_2O_2][Fe(II)]$$
$$= k'_{O_2}[Fe(II)] + k'_{H_2O_2}[Fe(II)]$$
$$= k_{appl}[Fe(II)] \qquad (5)$$

where k'_{O_2} and $k'_{H_2O_2}$ include, respectively, the O_2 and H_2O_2 concentrations and a stoichiometric factor that accounts for the fast oxidation of a second Fe(II) in reactions 2 and 4. This mechanism has been proven to account for the oxidation of Fe(II) under conditions that maintain the 1:4 O_2 to Fe(II) stoichiometry (Millero *et al.*, 1987; Millero and Sotolongo, 1989). However, the application of the mechanism to natural waters must include a full appreciation of the species composition and further verification is still required at open-ocean seawater concentrations.

In situ determinations of Fe(II) are inherently difficult, due to its rapid oxidation at ambient seawater pH, complex reduction processes and the strong interaction of labile ferrous species with particles and biota. O'Sullivan *et al.* (1991) reported variable Fe(II) concentrations in the range 0.12 to 0.53 nM in the surface waters of the equatorial Pacific, with higher values at the surface and at the depth of the chlorophyll *a* maximum. Gledhill and van den Berg (1995) observed similar concentrations in the North Sea ($[Fe(II)]_{max}$=1.2 nM), with highest levels occurring in the upper 20 m. Measurements of significant concentrations of Fe(II) in seawater imply that the species is more stable than oxidation models predict, possibly due to binding by organic ligands. Such observations will have important ramifications for bioavailability, since the inorganic species Fe(II)' is substantially more soluble and kinetically more labile than Fe(III)'. Johnson *et al.* (1994) studied Fe photochemistry through decktop incubations in the equatorial

Pacific and found clear diurnal patterns, resulting from photoreductive dissolution of colloidal Fe, its subsequent oxidation and biological uptake of dissolved Fe(III). Studies of redox chemistry across the oxic/anoxic boundary of the Pettaquamscutt Estuary (Rhode Island, USA; O'Sullivan *et al.*, 1997) showed that Fe(II) ranged from <4 nM in oxygenated surface water to 8 μM at the dissolved Fe maximum (>95 % of total).

I.2.2.5 Solubility

Studies earlier this century examining Fe seawater chemistry and speciation using hydrolysis constants resulted in the prediction of extreme insolubility and supersaturation of this bio-essential element and its potentially limiting effect on phytoplankton growth (Cooper, 1935, 1937, 1948a,b). However, in a anoxic primordial ocean, prior to the evolution of oxygen-producing photosynthesis about 3 billion years ago, Fe was present at much higher concentrations in the Fe(II) oxidation state (Geider, 1999). This would have been accompanied by an increased solubility of 6-7 orders of magnitude and led to the development of cellular systems requiring large amounts of Fe used in both photosynthetic and respiratory electron-transfer chains (Raven, 1988). There is no present day clear consensus on the thermodynamic solubility of inorganic Fe(III) in oxic seawater, and estimates for Fe(III)' vary between ~10^{-8} M and ~10^{-10} M, depending on the presence of dissolved $Fe(OH)_3$ species (Wells *et al.*, 1995). Recent studies by Kuma *et al.* (1996) and Millero (1998) have examined the earlier work of Byrne and Kester (1976) and addressed the uncertainty concerning the effect of hydroloysis on the solubility of Fe species in coastal and oceanic waters. Organic ligands are now thought to increase the solubility (32-65%) at pH=8.1 through the formation of organic complexes. Kuma *et al.* (1996) reported high and variable Fe solubility values (0.3-0.6 nM) in the surface mixed layer of the eastern Indian Ocean generally corresponding with the chlorophyll *a* concentrations, with solubility minima (0.15-0.2 nM) occurring in the depths below (50-200 m). Model speciation calculations in the pH range 6-8 have yielded ligand concentrations that are in good agreement with those found in ocean waters using voltammetric methods. Millero (1998) estimated the solubility of Fe(III) to be 0.2 nM at pH=8.1 and 0.6 nM at pH=7.65, values also in good agreement with dissolved Fe measurements conducted for open-ocean surface and deep

water samples respectively (Johnson *et al*, 1997). Table I.3 summarises the equilibrium constants for Fe hydrolysis species used in the construction of Figure I.4, which illustrates the Fe species distribution in equilibrium with solid amorphous FeOOH.

Components		FeOOH(s)	H^+	log K
Species	Fe^{3+}	1	3	2.5
	$FeOH^{2+}$	1	2	0.31
	$Fe(OH)_2^+$	1	1	-3.17
	$Fe(OH)_3$	1	0	-12(?)
	$Fe(OH)_4^-$	1	-1	-19.1
	$Fe_2(OH)_2^{4+}$	2	4	2.05
	$Fe_3(OH)_4^{5+}$	3	5	1.2
	H^+	0	1	0
		{FeOOH(s)} = 1	pH given	
$Fe(III)_{total} = [Fe^{3+}] + [FeOH^{2+}] + [Fe(OH)_2^+] + [Fe(OH)_3] + [Fe(OH)_4^-] + 2[Fe_2(OH)_2]^{4+} + 3[Fe_3(OH)_4]^{5+}$				

Table I.3. (Hydr)oxide solubility as influenced by hydrolysis for amorphous FeOOH; data from Baes and Mesmer (1976)

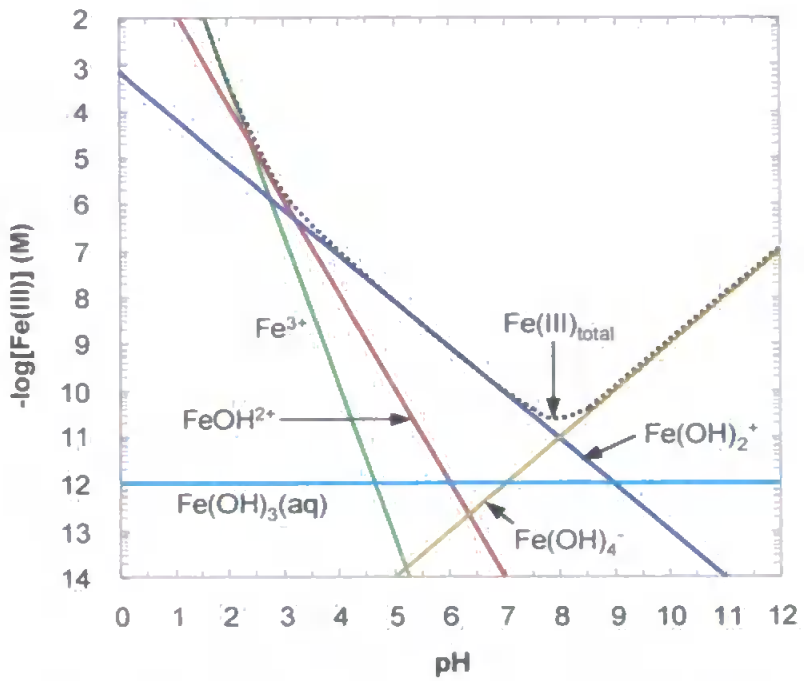

Figure I.4. The effect of hydrolysis on the solubility of Fe (hydr)oxides in equilibrium with FeOOH; multinuclear species are omitted; adapted from Stumm and Morgan (1996)

I.2.2.6 Functions within the Cell

Fe is bio-essential to phytoplankton (Raven 1990), its major physiological role being in electron transfer processes within the algal cell (Geider and La Roche, 1994; Hutchins, 1995; van Leeuwe, 1997). Fe is essential in several steps of the photosynthetic route of CO_2 fixation and for several Fe-containing enzymes involved in the Calvin cycle. It is involved in: (1) the electron transfer protein ferredoxin (LaRoche *et al.*, 1996), (2) the photosynthetic catalyst cytochrome *f*, and (3) Fe-storage complexes (e.g. ferretin), thereby repressing free Fe from producing damaging free radicals. Fe is required for the synthesis of the photon-harvesting molecule chlorophyll *a* and in the enzymes nitrate- and nitrite- reductase necessary for the reduction of nitrate and nitrite to ammonium for the synthesis of amino acids (Rueter and Ades, 1987; Timmermans *et al.*, 1994). Several other cellular and enzymatic functions require Fe (Geider and La Roche, 1994). Because of the multiplicity of functions, Fe limitation is likely to affect many cellular processes simultaneously, and further study is required to identify and quantify the nature and extent of Fe limitation on separate components of the diverse marine planktonic assemblage. Novel non-intrusive approaches have been developed for examining the metabolic status of phytoplankton assemblages. Fast repetition rate fluorometry (FRRF) measures a change in quantum yield of *in vivo* chlorophyll fluorescence resulting from exciting photosystem II (PSII) with a train of subsaturating flashes, and has recently been exploited to show that Fe may limit phytoplankton populations in the Equatorial (Greene *et al.*, 1994) and South Pacific Ocean (Behrenfeld and Kolber, 1999).

I.2.2.7 Bioavailability

Many questions remain unanswered as to which fractions of Fe that coexist in seawater are available to biological organisms. The availability of Fe depends on various environmental parameters: pH, light and mixing conditions, chemical oxidation-reduction, photochemical and microbial reduction, photodissolution of colloidal and particulate phases and (in)organic complexation processes. A reciprocal interaction exists between trace metals and phytoplankton. Trace metals may limit microbial activity and have a major role in determining species composition or taxonomy. Conversely, phytoplankton assist in regulating the

concentrations and speciation of many trace metal nutrients, through the exudation of high-affinity, relatively specific complexing ligands and through cell-surface reactions, in an attempt to facilitate its acquisition or for the storage of excess ambient Fe. This capacity for "luxurious" uptake differs among species and may be an important strategy for organisms which bloom episodically. Algae assimilate macro-nutrients and trace metal in the euphotic zone. Microbial degradation of sinking biogenic particles will release these nutrients into solution deeper in the water column, generating a nutrient-type profile (e.g. see later Figure I.6). This cycling depletes concentrations of nutrients in surface waters (and enriches them in deeper waters) in the atomic ratios in which they occur in phytoplankton, as indicated by the Redfield ratios (Redfield, 1934; Redfield *et al.*, 1963; updated by de Baar and Boyd, 1999):

$$C : N : P : Fe : = 106 : 16 : 1 : 10^{-3.5}$$

Marine algae have the potential for multiple uptake systems which shift in importance in response to changes in species taxonomy and Fe inputs and speciation, and micro-organisms use a variety of strategies for extracting Fe from the surrounding environment (Figure I.5). Dissolved inorganic, labile Fe(III)' and Fe(II)' are known to be bioavailable *via* a transport ligand process involving cell surface complexation and internalisation (Morel *et al.*, 1991). However, strong Fe(III) complexation by organic ligands (Section I.2.2.2) would result in an ambient Fe(III)' concentration <0.1 pM (Rue and Bruland, 1997), which would be far too low for diffusion of inorganic Fe across membranes to support measured growth rates (Sunda and Huntsman, 1995a). Cell-surface mediated reduction of organically-bound Fe (Maldonado and Price, 1996) in combination with dynamic redox cycling (Waite *et al.*, 1995) may buffer or enhance the steady state concentration of both Fe(II)' and Fe(III)' and facilitate uptake *via* membrane-bound, Fe' based transport systems (Sunda, 1989; Morel *et al.*, 1991; Wells and Mayer, 1991a). Cyanobacteria and some algae have also been reported to produce extracellular siderophores in response to Fe deficiency in culture media, which out compete naturally occurring ligands (Trick *et al.*, 1983; Brown and Trick, 1992; Wilhelm and Trick, 1994; Wilhelm *et al.*, 1996). Fe-siderophore chelates are transported into the cell by membrane transport proteins and the Fe released internally for metabolism. However, no soluble siderophore complexes have been observed in naturally occurring seawater samples. Recent radiotracer

studies investigating the uptake of ^{55}Fe bound to various chelates and in inorganic form in both culture media and natural assemblages (Hutchins *et al.*, 1999) suggest that prokaryotes and eukaryotes compete for organically-bound Fe using different uptake strategies. Eukaryotic phytoplankton efficiently assimilate Fe complexed by porphyrin molecules released following mechanical breakdown of cells, whilst prokaryotic picoplankton (cyanobacteria) utilise siderophore-bound Fe. Thus the chemical nature of organically complexed Fe will in turn influence the outcome of competition between picoplanktonic cyanobacteria and large eukaryotic diatom species, and changes in the source of complexed Fe will drive changes in the community cell size structure and consequentially carbon export from the euphotic zone (Boyd and Newton, 1999).

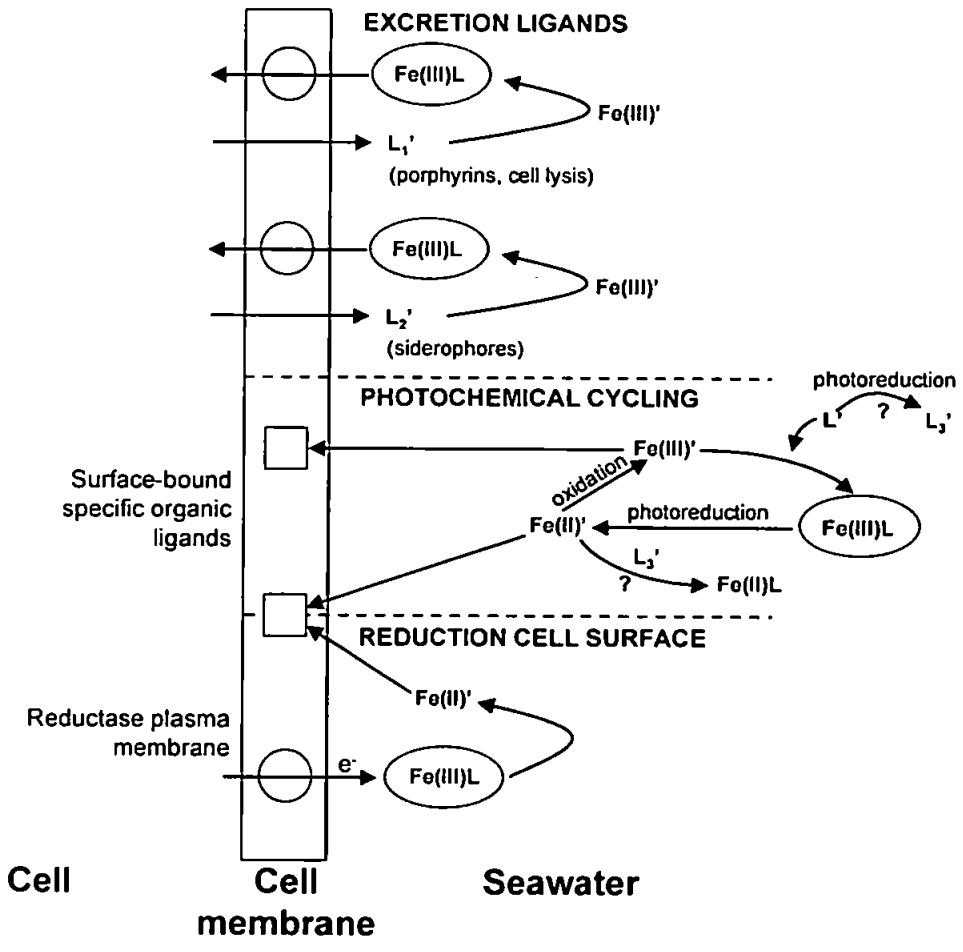

Figure I.5. Schematic diagram showing multiple algal Fe uptake systems

At present, there is no direct evidence that particulate Fe is available to phytoplankton. However, particulate and colloidal species may become accessible *via* dissolution processes, and

the particulate fraction has been reported to contain the majority of easily exchangeable Fe (Wells and Meyer, 1991b). In addition, evidence exists that microbes can help meet their Fe requirements by adsorption and leaching of atmospheric dust particles. For example, the nitrogen-fixing bacteria *Trichodesmium* has been observed to bloom in response to Saharan dust storms in the tropical North Atlantic (Rueter *et al.*, 1990; Rueter and Unsworth, 1991), and aerosols supplied from Asia or Alaska triggered a physiological response in the Northeast Pacific (Boyd *et al.*, 1998, Boyd and Harrison, 1999).

I.2.3 Sources of Iron in Seawater

Elemental distributions are affected by a number of processes. Fe is a recycled trace metal demonstrating a nutrient-type distribution in the ocean. In addition, it exhibits particle-sorption characteristics with residence times in surface waters ranging from weeks to a few years depending on the local oceanography regime. Fe is supplied to the ocean surface from above *via* atmospheric deposition, laterally by rivers, from below by vertical mixing during upwelling events, in shelf regions through reductive re-suspension of sediments, and in deep ocean ridges by hydrothermal venting.

I.2.3.1 Atmospheric Transport

The atmosphere is a major pathway for mineral aerosols containing Fe bound within an aluminosilicate lattice, entering the open-ocean through dry (e.g. dust storms) or wet (e.g. rain) deposition. Much of the particulate discharge from rivers will be trapped and settle in estuarine and coastal zones rather than reaching the open sea. In contrast, wind erosion of arid soils, generating dust and mineral particles capable of long-range transport, is recognised as the major source of atmospheric Fe for the open-ocean. Airborne transport from the continents is estimated to supply approximately three times as much total Fe to the oceans as that delivered by rivers (Duce and Tindale, 1991). However, Fe aerosol solubilities and surface water speciation and bioavailability after deposition events are poorly constrained. Most aeolian Fe will be in the form of crystalline phases, which may undergo several stages of dissolution before deposition. Duce and Tindale (1991) predicted between 10 and 50 % of mineral Fe will be

soluble at seawater pH, although more recent estimates (Jickells and Spokes, 1999) suggest an overall atmospherically transported limit of 0.8 - 2.1 %. Moreover, a dynamic loop between dissolved and particulate phases will exist in surface waters, an accurate knowledge of which is critical for calculating the residence time of Fe in the mixed layer. Importantly, a significant fraction (56±32 %) of dissolved aerosol Fe may enter the ocean as Fe(II) (Zhuang *et al.*, 1990) due to photochemical reduction reactions in an acidic (pH 2.5-5.0) rainwater micro-environment and will therefore be the dominant source of nutrient Fe in the remote euphotic zone. Strong Fe-organic complexes are already known to exist in seawater (Gledhill and van den Berg, 1994; Rue and Brualnd, 1995), and rates of formation of complexes appear to be rapid (Kuma *et al.*, 1996) and ligand concentrations to increase in response to elevated Fe levels (Rue and Bruland, 1997; Croot, unpublished data). Similar organic complexation may also provide a mechanism to maintain Fe in solution in the atmosphere and through the sea-surface micro-layer (Jickells and Spokes, 1999).

Duce and Tindale (1991) estimated that approximately eight times more atmospheric Fe is deposited to the ocean in the northern hemisphere compared with the southern hemisphere, the result of the presence of large mineral aerosol sources (e.g. desert regions). The Saharan dust plume is known to extend across the equatorial Atlantic Ocean reaching the southeastern United States (Prospero *et al.*, 1999), and has been reported to supply as much as 1000 mg m^{-2} yr^{-1} of Fe (dissolved plus particulate) to waters near the west coast of Africa (Duce and Tindale, 1991). However, dust deposition to the oceans is highly pulsed and seasonally dependent. This is as a result of variability in the dust generation processes at source, mixing, photochemical reworking and reprecipitation during transportation and the sporadic nature of dry deposition or washout during rain events. Further study is required to understand how physical characteristics (e.g. stratification) and biological cycling in the water column, coupled with the frequency and the intensity of the atmospheric inputs, regulate the Fe biogeochemical cycle in the ocean. In regions where other nutrients are present in high concentrations, the flux of aerosol Fe may limit primary productivity. Martin (1990) proposed that increased dust fluxes over the Southern Ocean during the last glacial maximum (Kumar *et al.*, 1995) could have resulted in Fe-stimulated

increases in primary productivity. An alternative scenario is that increased dust fluxes at more temperate latitudes (e.g. equatorial Atlantic Ocean) would have elevated deep water dissolved Fe concentrations if there was a concurrent increase in strong organic ligands within the oceanic interior preventing loss to the solid phase (Watson *et al.*, 1999). Such elevated Fe levels could then be translated to other ocean areas through the global deep water circulation pattern (Broecker and Peng, 1982), and raise euphotic zone Fe concentrations in the Southern Ocean *via* upwelling events.

I.2.3.2 Riverine Inputs

The contribution of Fe to the oceans through fluvial input is small. The land – sea margin exhibits large property gradients and acts as a filter of river transported signals. Large amounts of dissolved Fe in rivers are present mainly as colloids which rapidly precipitate, flocculate and settle out as salinity increases, and are therefore trapped in estuaries (Millward, 1995). Furthermore, enhanced productivity in coastal regions results in significant attenuation of enhanced coastal signals through biological uptake and irreversible scavenging, thus preventing riverine inputs from penetrating into the oceanic interior. Such processes were observed in a transect from the mouth of Delaware Bay into the Gulf Stream (Wu and Luther, 1996). Fe levels in these coastal waters were therefore the product of a balance between inputs of high concentrations from rivers and flushing with oceanic waters containing low concentrations. This relationship was considerably modified by interactions with sediments or suspended particles, plankton growth and decay, atmospheric deposition and anthropogenic inputs within the mixing zone.

I.2.3.3 Sedimentary Regeneration

Interstitial waters, the pore spaces between particles in rocks and sediments, are sites of intense chemical, physical and biological reactions, leading to diagenesis, the formation or altering of mineral phases and accompanied changes to the composition of the overlying waters. Consistent horizontal gradients of dissolved and particulate Fe have been reported from open-oceans towards continental margins (Johnson *et al.*, 1997; Blain *et al.*, 1998), suggesting that

reductive mobilisation through diagenetic chemical reactions in marine sediments provides a large source of Fe to the oceanic rim. An inverse exponential relationship has been observed with decreasing Fe concentrations existing versus increasing distance away from the shore, and Johnson *et al.* (1997) reported that dissolved Fe concentrations reflected oceanic values (<0.2 nM) only 50 km from the Gulf of Alaska coastline.

Many of the chemical changes that take place during early diagenesis are redox-mediated, which are in turn dependent on the degree to which organic carbon undergoes decomposition in the sediment complex. A diagenetic sequence of catabolic processes exists in sediments as organic matter is metabolised by a particular oxidising agent, donating electrons to several oxidised components in the interstitial water-sediment complex and fuelling bacterial respiration. When oxygen is present it is the preferred electron acceptor, however the terminal electron accepting species alters during the diagenetic sequence as the oxidants are consumed in order of decreasing thermodynamic advantage (Chester, 1990). Diagenesis proceeds in a general sequence in which the oxidants are utilised for the destruction of organic carbon in the order: oxygen > nitrate ≥ manganese oxides > iron oxides > sulphate (Berner, 1980), setting up a downward vertical gradient, although the oxidants may not always be limiting and processes can occur simultaneously. A reduction and dissolution of solid Fe oxides in hemi-pelagic or anoxic shelf sediments may therefore result in a net diffusion of Fe(II) from porewaters into the overlying nepheloid layer as well as leading to the formation of pyrite (FeS_2). Such processes, when in combination with lateral and vertical mixing induced by strong bottom water currents, will deliver dissolved Fe to oceanic surface waters. This source of Fe has yet to be quantified through field studies, although previous studies have observed the exchange of other trace elements at the sediment-water interface (Peterson *et al.*, 1995) and used concentrations of Ni, Cd, Cu and Mn in bottom waters and hemi-pelagic interstitial waters in the Pacific to set up diagenetic models (Klinkhammer *et al.*, 1982). The greater input of Fe to coastal and shelf regions compared with the open-ocean is accompanied by higher Fe requirements of neritic phytoplankton species (Sunda *et al.*, 1991), and such ecosystems have the potential to be Fe (co-)limited (Hutchins and Bruland, 1998; Hutchins *et al.*, 1998).

I.2.3.4 Hydrothermal Venting

Trace elements may be supplied to deep and intermediate waters above the sea floor from processes that occur in the oceanic crust. Such processes involve low temperature weathering of ocean basement rocks (e.g. basalts) and high temperature water-rock reactions associated with hydrothermal activity at spreading ridge centres. Large amounts of ore-forming minerals, such as Fe, Mn, Zn, Cu and Pb, are leached from the crust during hydrothermal venting (Elderfield, 1976). Although they are mainly precipitated on mixing with seawater, either in the vents or on the sea floor, a fraction of dissolved elements will penetrate into the base of the water column over, for example, the mid Atlantic (Hydes *et al.*, 1986) or Juan de Fuca Ridges (Chin *et al.*, 1994; Massoth *et al.*, 1994). The particulate phases in these plumes (predominantly Fe and Mn oxides and hydroxides) also scavenge P, V, As, Pb, Po and several rare-earth elements from seawater. Thus, on a global scale, hydrothermal plumes are both a source for some elements and a sink for others. Hydrothermal venting is a temporally and spatially variable phenomenon and the extent to which material released through such events is dispersed throughout the ocean interior is poorly constrained.

I.2.3.5 Biogenic Recycling

The single largest reservoir of Fe in the surface waters of remote oceanic basins may well be the biota itself. Evidence exists that the biological pool of Fe may be recycled on the time scale of days (Hutchins *et al.*, 1993; Hutchins and Bruland, 1995; Price *et al.*, 1994), and this regenerated Fe may satisfy the demand by phytoplankton (mainly picoplankton) in high nutrient low chlorophyll regions and oligotrophic gyres. However, the chemical form and organic complexation of recycled Fe and its potential to be directly assimilated is currently poorly understood.

I.2.4 Sinks of Iron from Seawater

The major sink of dissolved Fe is its active uptake by photosynthesising organisms. Biogenic scavenging and the sedimentation of oxidised mineral particulate Fe will also remove the

element from the water column, although the mechanics of such removal processes require investigation.

I.2.4.1 Biological Uptake

The active uptake of micro-nutrients from seawater by plankton species is believed to remove the majority of dissolved Fe from the euphotic zone. Uptake mechanisms may involve the incorporation of Fe within the cell as well as adsorption onto the outside of plankton particles. The fractions of Fe which are available to different biological species has been the topic of much debate.

I.2.4.2 Particle Scavenging

Scavenged-type trace elements (e.g. Al, Mn, Pb) have vertical distribution profiles in the ocean which exhibit surface enrichment and sub-surface depletion. Such elements retain the most identifiable open-ocean surface water fingerprints from atmospheric deposition, which can be used to identify sources of Fe entering surface waters. Sinking biogenic and lithogenic particles can both scavenge dissolved species from seawater, and the large surface area of organic colloidal matter has the potential for sorption and aggregation. Increased production will result in a higher concentration of sinking biogenic particles, and therefore a higher scavenging rate will exist in upwelling systems.

I.2.4.3 Sedimentation

Particulate Fe will tend to aggregate above its solubility threshold, which has been predicted to be 0.2 nM at pH 8.1 and 0.6 nM at pH 7.65 (Millero, 1998). Such coagulated material will tend to sink out of the upper mixed layer into deeper water, where it may undergo bacterial remineralisation before reaching the sedimentary layer. The signal due to high aerosol Fe entering the ocean in areas of strong atmospheric deposition is reflected in a high vertical flux of settling particulate Fe in the water column, as collected in sediment traps in the northeast Atlantic Ocean (Kremling and Streu, 1993; Kuss and Kremling, 1999). Standing stocks of

suspended particulate Fe are also higher in such regions (Helmers, 1996), and by analogy, elevated concentrations of dissolved Fe would be expected.

I.2.5 Abundance and Distribution of Iron in the Oceans

Improvements in sampling and analytical methodologies over recent years have resulted in dramatic decrease in the reported concentration of Fe in seawater (Table I.4), although current literature still presents dissolved Fe values in seawater varying over an order of magnitude. However, coherent trends are beginning to emerge for many oceanic basins. Table I.5 briefly summarises the recently reported concentrations of dissolved Fe in the World's oceans. Very low concentrations (0.05-1.0 nM) exist in surface waters of remote oceans, rising to 0.6-2.0 nM in deeper waters (>500 m) of the ocean interior and resulting in a recycled or nutrient-type vertical profile. In enclosed seas, dissolved Fe levels range between 1-10 nM and coastal regions typically have elevated concentrations (up to 100 nM). In regions which receive high atmospheric loadings, dissolved Fe is likely to show a scavenged-type vertical structure, with a surface enrichment and depletion at depth, similar to elements Al and Pb. There has been relatively few studies on the vertical distribution of Fe in sub- or anoxic waters (e.g. Indian Ocean, Black Sea), where dissolved Fe may be expected to show a concentration maximum at depth through the oxygen minimum zone (similar to Mn), due to a redox shift to the more soluble Fe(II) oxidation state. Saager *et al.* (1989) did however report a mid-depth Fe maximum (surface: ca. 1 nM; intermediate: ca. 3 nM; deep: ca. 1.4 nM) in the northwest Indian Ocean, associated with a broad intermediate oxygen minimum zone. Particulate Fe ranges from sub-nanomolar in the open-ocean to several hundred nanomolar in coastal waters. The natural enrichment of open-ocean surface waters (>1.0 nM) is consistent with atmospheric transport, whilst reductive mobilisation in marine sediments is the major source for higher Fe levels near continental margins. Minima in the fine structure of vertical profiles through the euphotic zone are predominantly due to active uptake by photosynthesising plankton, although passive scavenging onto particles also plays a role.

Year	Concentration (nM)
1924	25,000
1931	500-1400
1935	100-800
1954	60
1989	0.2-2.0
1996	**0.6-0.7** (deep ocean)

Table I.4. Historical data of Fe concentrations in the World's oceans

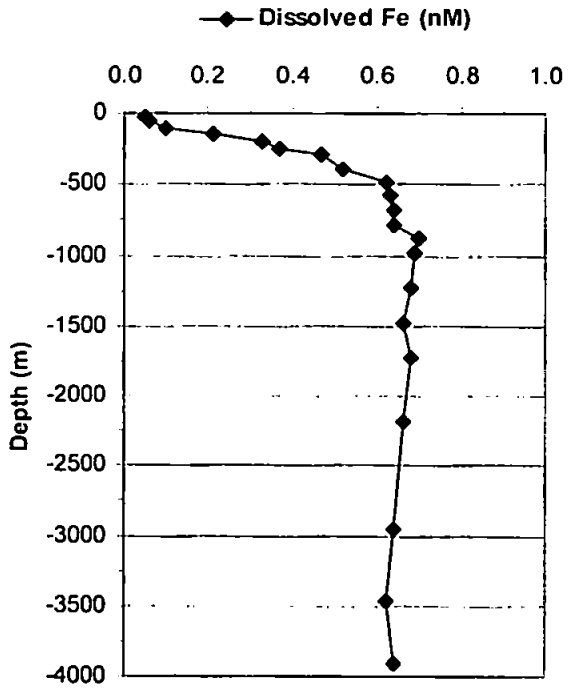

Figure I.6. Nutrient-type distribution of dissolved Fe in the North Pacific (data from Martin *et al.*, 1989[1])

The distributions of dissolved and particulate Fe in World's oceans were recently reviewed and modelled by Johnson *et al.* (1997) and showed a recycled-type vertical structure correlating with classical nutrients, as one might expect for a limiting nutrient (Figure I.6). However, Fe did not appear to show the inter-ocean fractionation seen with nitrate, phosphate and other bioactive trace metals (e.g. Zn and Cd; Bruland and Franks 1983). Martin and Whitfield (1983) predicted an intermediate mean oceanic residence time (MORT) of 1.8×10^3 yr for Fe, indicating an association with reactive biogenic particles and a influence from water mixing processes.

[1] http://color.mlml.calstate.edu/www/data/irondata.htm

Region	Surface [Fe] (nM)	Deep [Fe] (nM)	Reference
ATLANTIC OCEAN			
Northeast Atlantic	0.1-0.5	0.9	Landing *et al.*, 1995
	1.7	0.8	Gledhill and van den Berg, 1994
	0.2	0.6	Martin *et al.*, 1993
	1.0	3.9	Danielsson *et al.*, 1985
Northwest Atlantic	0.4	1.9	Witter and Luther, 1998
	0.6	1.4	Wu and Boyle, 1998
	0.2-0.6	0.7-0.9	Wu and Luther, 1994
Equatorial and South Atlantic	0.5-3.1	1.0-2.6	Landing and Powell, 1998
Atlantic surface water transects	0.5-10*	n.o.	Powell *et al.*, 1995
PACIFIC OCEAN			
North Pacific	0.04-1.0	0.04-0.88	Johnson *et al.*, 1997
	0.2	0.6	Rue and Bruland, 1995
	0.05-0.1	0.1-0.8	Obata *et al.*, 1993
	0.05	0.7	Martin *et al.*, 1989
	0.06	0.8	Martin and Gordon, 1988
	0.1	0.7	Landing and Bruland, 1987
	0.2-0.7	0.6-1.5	Gordon *et al.*, 1982
Equatorial Pacific	0.05	0.4	Gordon *et al.*, 1997
	0.02	n.o.	Rue and Bruland, 1997
	0.4	2.0	Landing and Bruland, 1987
	0.4	1.0	Gordon *et al.*, 1982
South Pacific	0.1	0.7	Landing and Bruland, 1987
SOUTHERN OCEAN			
Atlantic Sector	0.1	0.3	de Jong *et al.*, 1998
	0.3-3.8	0.4-2.8	Löscher *et al.*, 1997[3]
	0.2-1.5	0.6-1.5	Löscher *et al.*, 1997[4]
	0.17-0.50	1.0	de Baar *et al.*, 1995
	1.2	2.0	Westerlund and Öhman, 1991
	0.10-0.16	0.6-0.7	Martin *et al.*, 1990a
Pacific Sector	0.01-0.05	0.3-1.0	Coale *et al.*, 1998
	0.2-0.3	0.7-0.9	Sedwick and DiTullio, 1997
Indian-Australasian Sectors	0.3-12.6	0.3-12.6	Blain *et al.*, 1998
	0.2-0.6*	0.4-1.2*	Sedwick *et al.*, 1997
INDIAN OCEAN			
	0.01	0.1-0.6	Obata *et al.*, 1997
	0.3	n.o.	Takeda *et al.*, 1995
	0.3	1.0	Saager *et al.*, 1989

Notes
1. All values dissolved, except * (unfiltered, TD-Fe)
2. Surface sample collected from <500 m depth; all others considered deep samples
3. Polar Front
4. Southern Antarctic Circumpolar Current (sACC)
5. n.o.: no observations

Table I.5. Summary of the distributions of dissolved Fe in the World's oceans

Such estimates, however, ignore a number of important input (e.g. atmospheric deposition, hydrothermal venting) and output terms. Sarthou *et al.* (1997) estimated the residence time of Fe in the surface layers of the Southern Ocean to be 3.7 yr, whilst Bruland *et al.* (1994) predicted its residence time in the deep sea to be 70-140 yr, typical of 'scavenged' metals (e.g. Mn, Al, Pb, Th). However, unlike these metals, Fe concentrations are constant in deep waters (ca. 0.7 nM; Johnson *et al.*, 1997) and between oceanic provinces. Two mechanisms can retain Fe near its solubility limit of ca. 1 nM (Zhu *et al.* 1992): binding by organic ligands (Gledhill and van den Berg, 1994; Rue and Bruland, 1995; Kuma *et al.* 1995; Witter and Luther, 1998) and reversible exchange with amorphous $Fe(OH)_3$ or surface-binding sites on marine particles (Zhuang *et al.*, 1992). Particulate Fe concentrations (ca. 1 nM) may serve to buffer the sub-nanomolar levels of dissolved Fe. There remains large gaps in knowledge of dissolved Fe distributions in the oceans and few reliable profiles exist in coastal shelf sections, upwelling, polar regimes and waters receiving significant atmospheric inputs.

I.2.6 Iron Limitation

Fe is an essential plant micro-nutrient and its low concentrations limit biological productivity in 40% of the oceans (de Baar and Boyd, 1999). Moreover, it has recently been proven to act as a (co-)limitant in significant regions of the remaining 60% of surface waters, including the oligotrophic gyres (Behrenfeld and Kolber, 1999) and coastal upwelling regimes (Hutchins and Bruland, 1998; Hutchins *et al.*, 1998). Marine ecosystems are now thought to be limited by not one, but several nutrients simultaneously, and photosynthetic efficiency and biomass will in addition be regulated by light deficiency and grazing control. Temporal or spatial variations in Fe supply may alter algal size structure, species composition, trophic dynamics and ultimately export production. This role of Fe in controlling productivity and consequentially CO_2 fixation will intimately be linked to the atmosphere – ocean CO_2 flux (Cooper *et al.*, 1996) and global transitions in climate between glacial and interglacial times (Martin, 1990). Moreover, it has been suggested that oceanic Fe fertilisation aimed at the enhancement of phytoplankton production may turn out to be a feasible method of stimulating active removal of the

greenhouse gas CO_2 from the atmosphere (Martin, 1990; Watson, personal communication, 1999), although such ideas remain contentious.

I.2.6.1 High Nutrient, Low Chlorophyll Regions

Vast areas of remote oceans, such as the polar and sub-polar regions and the equatorial upwelling zones consistently maintain high classical nutrient levels throughout the year, while phytoplankton stocks remain low (Chisholm and Morel, 1991). Such regions are often referred to as High Nutrient, Low Chlorophyll (HNLC; Minas *et al.*, 1996), despite comprising very different oceanic regimes. For such HNLC regions, limitation by Fe has been suggested (Gran, 1931; Hart, 1934, 1942; Martin and Fitzwater, 1988).

I.2.6.2 Iron Enrichment Studies

SHIPBOARD INCUBATIONS

During the latter part of the 1980s, the first uncontaminated, experimental tests of Fe limitation were reported for the sub-arctic Pacific (Martin and Fitzwater, 1988). Since then, many expeditions have further tested the hypothesis through enclosed, bottle experiments in the Southern Ocean (Martin *et al.*, 1990b; de Baar *et al.*, 1990; Coale *et al.*, 1998) and the Equatorial and subarctic Pacific (Martin *et al.*, 1991; Coale, 1991; Johnson *et al.*, 1994; Kolber *et al.*, 1994; Price *et al.*, 1994; Coale *et al.*, 1996a). The extrapolation of *in vitro* shipboard and laboratory incubation results to whole ecosystems has been strongly criticised (Banse, 1990; Dugdale and Wilkerson, 1990; Frost, 1991), since experiments do not represent the *in situ* phytoplankton grazer community, allow for advection or adjust for adsorption and contamination effects from the vessel walls.

IN SITU FERTILISATIONS

In autumn of 1993, the first *in situ* Fe fertilisation experiment was initiated at a site some 500 km south of the Galapagos Islands (IronEx I; Martin *et al.*, 1994). Surface seawater was enriched with a single 4 nM infusion of dissolved Fe and labelled with SF_6 tracer for tracking the dispersing patch. The experiment demonstrated a clear physiological response to the addition of

Fe which resulted in a doubling of plant biomass, a threefold increase in chlorophyll *a* concentrations and a fourfold increase in phytoplankton productivity. Unfortunately, within about four days, the enriched patch was subducted by a cold water mass and the experiment ended prematurely, resulting in a smaller biological and geochemical response than bottle experiments had predicted. Nitrate draw-down during IronEx I was undetectable (<0.2 μM), and CO_2 fugacity was only reduced by 10 μatm, well below the apparent expectation based on Redfield stoichiometry (Watson *et al.*, 1994).

A second *in situ* perturbation experiment, IronEx II, was conducted during May 1995 in the equatorial Pacific, where Fe was added in three sequential infusions over a week in order to mimic a natural continual flux (Coale *et al.*, 1996b). The fertilised patch remained in the surface layers, and a massive phytoplankton bloom resulted over a 17 d period, which was dominated by diatoms and not significantly checked by grazing or secondary nutrient limitation, consistent with the natural ecosystem observations observed in the Antarctic Polar Front (de Baar *et al.*, 1995). The added Fe during IronEx II triggered an immediate biophysical response before any changes in species composition, observed *via* improved performance of photosystem II of the local picoplankton community (Behrenfeld *et al.*, 1996). A decrease in CO_2 fugacity (90 μatm; Cooper *et al.*, 1996) within the patch was observed, together with a strong increase in dimethylsulphide (DMS; Turner *et al.*, 1996), the oxidation of which is involved in the formation of atmospheric sulphate particles which can exert a climate cooling effect, both through scattering and absorption of solar radiation and by altering of cloud albedo (Charlson *et al.*, 1987).

A natural corollary to the Fe hypothesis is the suggestion that biological production in the ocean, stimulated by increased Fe availability during the Last Glacial Maximum, was responsible for the observed low atmospheric levels of CO_2 (Martin, 1990). Support for this theory comes from the observation of increased export of carbon to sub-Antarctic sediments during the Last Glacial Maximum at times of higher Fe flux (Kumar *et al.*, 1995). An unenclosed Fe enrichment experiment in the Southern Ocean, which encompasses the majority of HNLC waters, would

have the greatest significance for palaeoclimatic interpretations. Such an experiment was conducted during February 1999 in the vicinity of 61°S, 140°W, approximately 500 km from the Antarctic ice (Southern Ocean Iron RElease Experiment, SOIREE; Boyd *et al.*, 1999a,b). Four infusions of Fe were conducted over a 13 day period, maintaining the dissolved Fe concentration above 0.3-0.4 nM (Bowie, unpublished results[2]). Despite challenging conditions of high seas and strong winds, a coherent patch was mapped continuously, enabling the observation of significant increases in algal photosynthetic competence and algal biomass after the fifth day. Chlorophyll *a* concentrations increased markedly, and macro-nutrient levels and the partial pressure of CO_2 decreased from the levels observed at the beginning of the experiment. In addition, upper ocean levels of DMS increased. Such preliminary results suggest that in this region of the Southern Ocean, Fe availability plays a fundamental role in controlling photosynthetic competence, algal biomass and ocean-atmosphere CO_2 flux, despite a relatively deep mixed layer, cold temperatures and the presence of grazers.

I.3 Sampling and Analytical Methods for the Determination of Iron in Natural Waters

It is clear, therefore, that the importance of Fe for marine algae requires that Fe measurements are performed routinely and accurately as part of any attempt to understand factors that control phytoplankton growth and biomass in the oceans. A number of sampling and analytical methods have been developed over the past two decades for the quantification and speciation of Fe in natural waters.

I.3.1 Sampling Methods for Iron

A sampling scheme will ideally be frequent enough to avoid bias from dynamic biogeochemical processes occurring on a short (seconds to minutes) time scale. The observed metal concentrations at any one time are the result of input, uptake, scavenging and vertical mixing processes. Investigators use different kinds of sampling equipment and methods that may

[2] http://www.tracer.env.uea.ac.uk/soiree

contaminate their samples to different degrees, leading to elevated and variable metal concentrations. Conversely, samplers may provide sites for adsorption of dissolved or colloidal Fe onto the container's interior surfaces, lowering the amount of Fe in solution. Fe is strongly associated with particulate and colloidal phases, so the size fraction analysed will determine, to some extent, what concentration is measured. Some investigators filter their samples through 0.45 µm filters, others use 0.2 µm filters and others analyse unfiltered samples. At sea, prevention of contamination of the samples is the highest priority, resulting in the use of a clean air van equipped with a laminar flow bench. In addition to discrete sampling devices, a variety of surface pumping systems and configurations are also used to deliver seawater to the shipboard laboratory (e.g. towed torpedo fish). The type and location of the pumping system intake are critical in order to avoid contamination from the ship's hull and any overboard discharges, as are the materials used in the tubing, pump housing and filtration devices. Reliable designs for vertical profiling are currently based on Go-Flo bottles with metal components replaced or modified and suspended on a Nylon® or Teflon® coated rosette frame using Kevlar® hydroline (Hunter *et al.*, 1996). A rubber zodiac operated remotely from the main research vessel has often been employed to sample surface seawater, where contamination from the ship is suspected (Nolting and de Jong, 1994).

I.3.2 Chelation Solvent Extraction – GFAAS Detection

Pre-1980 determinations of nanomolar levels of dissolved Fe in seawater were severely compromised and contaminated. With the advent of ultra-clean sampling and dedicated container labs (Nolting and de Jong, 1994), reliable Fe methodologies have been developed, based on shipboard filtration and acid preservation of ca. 0.5-1.0 l volumes of seawater, followed by shore-based complexation with pyrrolidine dithiocarbamate (PDC) and diethyl-dithiocarbamate (DDC) and extraction into an organic phase, either chloroform or freon. After back extraction into HNO_3, analyses were performed using graphite-furnace atomic absorption spectrometry (GFAAS; Bruland *et al.*, 1979; Danielsson *et al.*, 1982; Gordon *et al.*, 1982; Landing and Bruland, 1987; Johnson *et al.*, 1997; Löscher *et al.*, 1997). Utilising a 300 ml sample, the detection limit of this method was 0.05 nM and the precision was in the range 3-7 % (Landing

and Bruland, 1987). These methods are multi-metal but the many sample handling stages are tedious (e.g. 2-3 d to complete one oceanic profile of 24 samples), thus increasing the risk of contamination. Furthermore, the technique provided no information on the oxidation state of Fe, possessed an inherently poor precision which compromised reliable low level determinations, and was clearly impractical to use at sea.

In contrast, field-based measurements may provide high resolution data with the ability to modify cruise strategy in real time as well as the opportunity to identify and eliminate sampling contamination problems. The lack of rigorous intercomparison exercises and appropriate seawater reference material (dissolved Fe in NASS-4 CRM is 1.88±0.29 nM; BCR CRM 403 is not certified for Fe), has led to reported Fe concentrations in surface seawater varying over several orders of magnitude. This has prevented reliable correlations between data reported by different workers and reduced the ability to distinguish between environmental variability and analytical data quality.

Recently, to elucidate Fe speciation in natural waters, a number of analytical techniques have been reported that are able to distinguish between Fe(II), inorganic Fe(III) and organically chelated Fe. If the method only responds to one oxidation state, treating the samples with an appropriate strong oxidising or reducing agent can facilitate the determination of a total, or at least "chemically reactive" Fe concentration.

I.3.3 Spectrophotometry

Spectrophotometric analytical methods are based on the formation of a specific Fe(II)- or Fe(III)- ligand complex with a characteristic absorption wavelength. Chelating agents utilised for this purpose include 1,10-phenanthroline (Chalk and Tyson, 1994) and ferrozine (King *et al.*, 1991; Blain and Tréguer, 1995). Major interferences include transition metal ions such as Cu(I) and strong oxidising and complexing agents, although liquid-liquid extraction may be used to overcome these. The sensitivity (and selectivity to some extent) of these spectrophotometric techniques may be increased by incorporating an in-line preconcentration step, whereby the

complexing agent (e.g. ferrozine) is adsorbed onto a C_{18} Sep-Pak cartridge, and Fe(II) can then be retained on the column as the sample is passed through it. The Fe(II)-ferrozine complex may be extracted by methanol before its absorption is measured.

A method has been reported which simultaneously measures both oxidation states of Fe, using sorbent extraction preconcentration coupled to FI-AAS. Fe(III) is directly injected into the flame spectrometer, whereas a Fe(II)-ferrozine complex is retained in-line on a C_{18}-modified silica column and subsequently eluted with methanol (Krekler *et al.*, 1994). Chelating agents are available which can form complexes with both the Fe(II) and Fe(III) forms. However, successful application of techniques such as this requires a knowledge of the fundamental thermodynamic properties of the complexes.

A very sensitive (LOD 0.1 nM) spectrophotometric method based on the Fe(III) catalysis of the oxidation of N,N-dimethyl-p-phenylenediamine (DPD) by H_2O_2 has been reported (Measures *et al.*, 1995; Kolotyrkina *et al.*, 1995). However, the technique is non-redox specific and the reaction kinetics are very sensitive to temperature fluctuations which may result in difficulties in applying such a catalytic method in the field. All of the above spectrophotometric techniques suffer from interferences caused by complexation by naturally occurring Fe(III) binding ligands. Only if the stability and dissociation rate constants of the added Fe-chelator complex are reliably known, and the concentration of the added chelator is an order of magnitude greater than those occurring naturally, will measurements be reliable.

I.3.4 Voltammetry

Competitive ligand equilibration adsorptive cathodic stripping voltammetry (CLE/CSV) has proved a useful method for investigating the organic complexation of Fe in seawater (Gledhill and van den Berg, 1994; Rue and Bruland, 1995; Wu and Luther, 1995; Witter and Luther, 1998). The technique relies on the specific adsorption of a complex of the metal ion with an added chelator onto a hanging mercury drop electrode followed by a voltammetric scan to determine the amount of adsorbed metal ions. The complexation by natural ligands is then

determined in competition with the added chelator by titration with added Fe. Gledhill and van den Berg (1995) also reported a catalytic CSV method for measuring the redox speciation of Fe, based on the selective masking of Fe(II) by 2,2-dipyridyl (Dp). The sensitivity of the method was good, with detection limits at the sub-nanomolar level, although sample throughput was slow and voltammetric methods can often only be carried out over a narrow pH range, introducing uncertainties into the speciation of Fe in the sample. One complicating factor in analysing Fe by voltammetry is the presence a variety of Fe(III) (oxy)hydroxides with a range of reduction potentials with respect to Fe(II). Surfactants and interfering chelators in natural samples may also affect the kinetics of the stripping step in anodic stripping voltammetry, and any adsorption of organically bound Fe on the hanging mercury drop electrode would negate complexing capacity measurements. In addition, CSV electrodes can be sensitive to vibration, electrostaticity and power surges common on ships, and are less robust compared to automated wet chemistry manifolds.

I.3.5 Chemiluminescence

Several CL methods have been developed for the determination of Fe in natural waters. Elrod *et al.* (1991) measured dissolved Fe(II) using the CL reagent brilliant sulfoflavin. Total Fe was determined after reduction of Fe(III) with ascorbic acid. The moderate detection limit (0.45 nM) of the method confined it to mapping high Fe levels encountered in hydrothermal plumes and coastal waters. Obata *et al.* (1993, 1997) reported a sensitive CL method for Fe(III) based on a luminol - NH_3 - H_2O_2 reaction, but samples required careful pH adjustment prior to analysis to eliminate interferents. The limit of detection was reported to be 0.05 nM, although the CL emission for this standard was indistinguishable from that of the blank. An unspecified modification of Obata's CL method was used by Coale *et al.* (1996b) to track the dispersion of added Fe during the IronEx II fertilisation experiment, and more recently de Jong and co-workers (1998) have used a variant of this system for dissolved Fe determinations in the Southern Ocean. Powell *et al.* (1995) and O'Sullivan *et al.* (1995) adapted the classical luminol CL reaction for laboratory Fe determinations using FI and stopped-flow manifolds respectively, whilst Bowie *et al.* (1998) developed FI shipboard instrumentation and validated the luminol

assay for Fe(II+III) determinations. King *et al.* (1995) monitored the rates of Fe(II) oxidation in 0.7M NaCl solutions using a luminol FI-CL method, and Emmenegger *et al.* (1988) have investigated Fe(II) oxidation kinetics and photoredox cycling in freshwater systems using the technique. Many of the above techniques incorporated a solid phase cation-exchange column in the FI manifold to separate and preconcentrate the analyte from the sea-salt matrix.

I.3.6 Other Techniques

Recently, Wu and Boyle (1998) developed a method for the determination of Fe in seawater by high-resolution isotope dilution inductively coupled plasma mass spectrometry (ID-ICPMS) after $Mg(OH)_2$ co-precipitation. The sensitivity was good (LOD 0.05 nM) and validated through oceanographically consistent profiles in the eastern North Atlantic, but was clearly impractical for shipboard analyses. In addition, a method based on the formation of a Fe(III) spectrofluorimetric complex has been reported (Yan *et al.*, 1992), where the sensitivity of the reaction was enhanced in a micellar environment. Novel techniques are available based on electrospray mass spectrometry (Kebarle and Tang, 1993), HPLC-ICP-MS (Carey *et al.*, 1994) and ASV-ICP-MS, and have been used for the determination of As(III), Se(IV), Cr(VI), V(V) and Pb (II) species. These methods should provide very powerful tools for studying trace metal speciation in aquatic samples. Not only is it possible to determine the oxidation state of Fe, but also to identify Fe(II) and Fe(III) ligand complexes without interfering with the pre-existing equilibrium in natural waters. Finally, it should be noted that any technique which requires sample acidification may substantially alter the form of Fe in the original sample matrix, particularly the speciation of Fe(III) and/or the oxidation state of the metal. Fe data is operationally defined and all reported profiles should come with a complete characterisation of sample handling, filtration, acidification and storage protocols together with an evaluation of the intrusive nature of the analytical method. The oceanographic community will only be able to differentiate between natural variability and analytical artefacts through shipboard intercomparison exercises or the design of Fe test species, whereby the detectability of methods will be investigated against a suite of model pre-bound Fe complexes (e.g. Fe^{3+}-EDTA, Fe^{3+}-siderophore, Fe^{3+}-NTA, etc.).

I.4 CHEMILUMINESCENCE DETECTION

The desire to map the global oceanic distribution of Fe, to elucidate the effect its limitation may play on biological processes, and to clarify its chemical species has created a demand for analytical methodologies that can provide highly precise, accurate and rapid Fe determinations at sub-nanomolar levels on-board ships. Such techniques must be based on simple and portable yet reliable and sensitive detection systems. For these reasons, considerable recent research has been focussed on the development of chemiluminescence-based analytical monitors.

I.4.1 Theory

Luminescence is a general term applied to the emission of electromagnetic radiation by an atomic or molecular species, originating from the decay of that species from a higher to a lower quantized energy state. Figure I.7 shows a Jablonski diagram, illustrating processes defined as absorption, fluorescence, internal conversion, intersystem crossing, phosphorescence and other (non)radiative transitions that can take place for a photon-absorbing molecule excited between the ground state and electronically excited states. Chemiluminescence (CL) can be defined as the production of electromagnetic radiation (ultraviolet, visible or infrared) by a chemical reaction, the term being first used by Eilhardt Weidemann in 1888. Bioluminescence consists of visible wavelength CL produced by (bio)chemical systems of living organisms. Despite most chemical reaction systems releasing energy as heat, CL reactions can been observed in solid, liquid and gas phases and have been exploited for analytical purposes. CL emissions have been identified as direct or indirect (e.g. sensitised) depending on their origin. In a generic, direct CL reaction between analyte A and reagent B, a primary electronically excited fluorophore (P*) is produced, which can subsequently relax to the ground state with the emission of a photon, hυ:

$$A + B \xrightarrow{k_1} P^* + other\ products \xrightarrow{k_2} P + h\upsilon \qquad (6)$$

where $k_2 >> k_1$ and k_1 is therefore the reaction rate limiting value. A higher emission intensity is achieved through a more efficient production of the excited state:

$$I_{CL} = \Phi_{CL}\frac{dP}{dt} = \Phi_{Ex}\,\Phi_{Em}\frac{dP}{dt} \qquad (7)$$

where:

- I_{CL} is the CL emission intensity (photons emitted per second)
- Φ_{CL} is the CL quantum yield (photons emitted per molecule reacted)
- dP/dt is the rate of chemical reaction (molecules reacting per second)
- Φ_{Ex} is the excitation quantum yield (excited states produced per molecule reacted), and
- Φ_{Em} is the emission quantum yield (photons emitted per excited state molecule produced).

The quantum yield (Φ_{CL}) of a reaction is therefore the product of the efficiencies of the excitation and emission steps and values ranging from 0.001 to 0.8 have been observed (Campbell, 1988), higher Φ_{CL} usually being associated with effective biological systems. CL emissions are characterised by their colour, intensity, and rates of production and decay. Since rate constants are usually not known however, CL procedures require empirical standardisation.

Four conditions must be satisfied for CL emissions to occur:

1. The reaction enthalpy must be suitably exothermic, with typically a free-energy change of between 170-300 kJ mol^{-1}.
2. An energetically favourable reaction pathway must exist for generation of an excited state species.
3. The reaction rate must be high enough for detection ($k_2 >> k_1$).
4. A favourable deactivation pathway must exist to allow CL emission.

However, such guidelines are general and in many cases CL behaviour cannot be predicted. The advantages of CL reactions for analysis include their high sensitivities, wide linear dynamic ranges and speeds of response, all of which can be achieved with relatively simple instrumentation. The absence of an emission source (as in fluorescence spectrophotometry) eliminates noise due to Raman or Rayleigh scattering and detection systems can therefore be operated at extreme photomultiplier voltages for improvement in signal-to-noise ratios. Femtomole detection limits have been attained for the detection of certain enzymes.

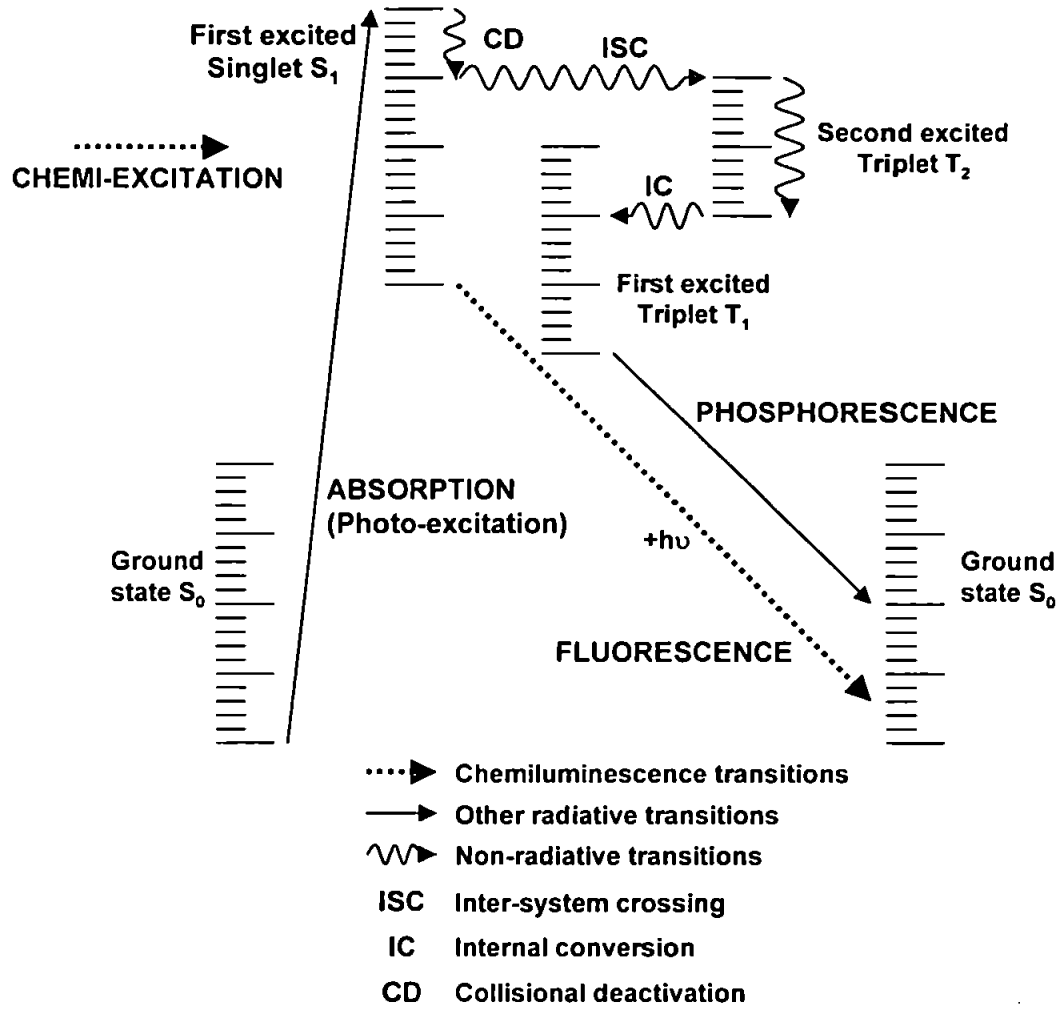

Figure I.7. Jablonski diagram; processes involving absorption or emission of a photon are shown as straight lines and non-radiative processes are shown as wavy lines (modified from Campbell, 1988)

I.4.2 Analytical Applications of Liquid-Phase Chemiluminescence Reactions

The potential of CL-based analytical techniques in environmental, biomedical, toxicological and related areas has been documented in detail in a number of recent reviews, covering various aspects of its application (e.g. Robards and Worsfold, 1992; Lewis *et al.*, 1993; Bowie *et al.*, 1996). In solution-phase, CL has recently found many applications in analytical chemistry for the determination of metal ions, inorganic anions, biomolecules, carcinogens and drugs in a variety of environmental and clinical matrices. Many such systems employ flow injection (Section I.5) as a means of mixing sample and reagent solutions. To illustrate the research interest in FI-CL over the last decade, Table I.6 outlines applications of the technique for the determination of metal ions in a variety of sample matrices between 1991 and mid-1999. Figure I.8 shows the number of novel flow through CL-based determinations published during the 1990s for analytes

of environmental interest contained in natural waters. It is evident from a review of the literature that research efforts have focussed on developing the classical luminol reaction (Section I.4.3.1) for sensitive determinations of metal ions in seawater, using solid-phase chelating resins to achieve an effective separation. There is also a noticeable trend towards novel CL systems, primarily based on the oxidation of organic compounds that are more selective towards the analyte in question, despite often having lower CL quantum yields. The utilisation of reversed micelles and surfactant assemblies as suitable reaction media (e.g. Saitoh *et al.*, 1998) has improved the characteristics of many CL reactions, and weak emissions have been enhanced through non-radiative transfer to sensitizer molecules (e.g. Segawa *et al.*, 1994).

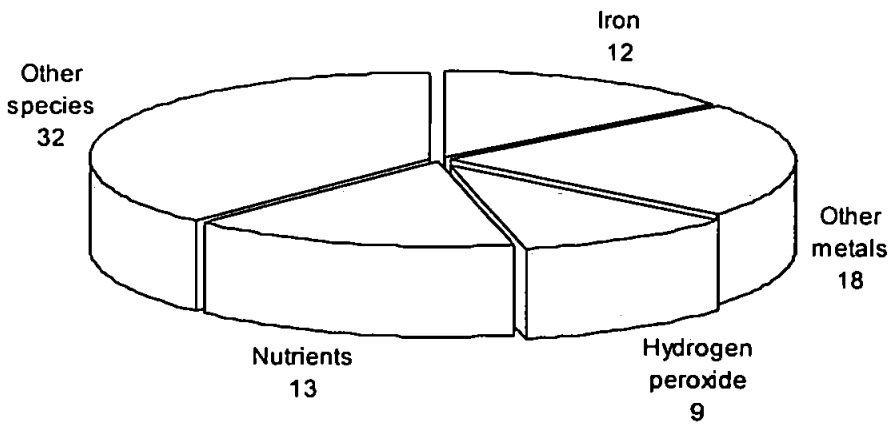

Figure I.8. Number of novel FI-CL methods published between 1990 and 1999 for the determination of a variety of species contained in natural water systems

Metal ion species	*CL reaction*	*Sample matrix*	*Limits of detection*	*Reference*
Al(III), Zn(II), Cd(II), In(III)	Formation of fluorescent compound by complexation of metal ion with *g*-hydroxyquinoline; excitation by reaction of bis(2,4,6-trichlorophenyl)oxalate and H_2O_2; use of 1,4-dioxane as organic solvent	Synthetic	20-70 ppb range[a]	Sato and Tanaka, 1996
Co(II)	Catalyzed oxidation of dibromoalizarin violet by H_2O_2 in alkaline solution; enhanced using cationic surfactant	Natural waters	68 pM	Chen *et al.*, 1994
Co(II)	Lophine - Co(II) – H_2O_2 reaction; enhanced in alkaline media by the addition of hydroxylammonium chloride	Eye lotions	45 nM	Nakashima *et al.*, 1997
Co(II)	Gallic acid – H_2O_2 reaction; preconcentration column containing 8-hydroxyquinoline immobilized on silica gel, fluoride containing metal alkoxide glass (8HQ-MAF)	Sea water	11 pM	Hirata *et al.*, 1996
Co(II), Mn(II)	Luminol oxidation by potassium periodate	Fresh, polluted waters, vitamin B_{12}	0.2 nM Co(II) 0.4 nM Mn(II)	Lin *et al.*, 1993
Co(II), Fe(II)	Decomposition of peroxymonosulfate; use of brilliant sulfoflavin sensitizer in micellar solution	Pepperbush, pond sediment	5.0 nM Co(II) 6.0 nM Fe(II)	Makita *et al.*, 1994
Co(II), Fe(II), $[VO]^{2+}$	Transition metal ion decompositions of peroxymonosulfate ion	Synthetic	10 nM Co(II) 0.2 μM Fe(II) 0.6 μM $[VO]^{2+}$	Makita *et al.*, 1993
Cu(II)	Oxidation of copper(II) - 1,10-phenanthroline chelates by H_2O_2 at alkaline pH	Sea water	0.05-0.10 nM	Sunda and Huntsman, 1991
Cu(II)	Oxidation of copper - 1,10-phenanthroline complex by H_2O_2; separation of copper from matrix on immobilized 8-hydroxyquinoline	Sea water	0.4 nM	Coale *et al.*, 1992
Cu(II)	Oxidation of 1,10-phenanthroline; copper complexation and ligand titration measurements	Seawater	0.1 nM	Zamzow *et al.*, 1998

Continued overleaf

Metal ion species	*CL reaction*	*Sample matrix*	*Limits of detection*	*Reference*
Cu(II)	Fluorescein - hydroxylamine - OH^- system; potassium fluoride acts as masking agent for Fe(II,III) and Co(II)	Serum	7.9 nM	Lin and Hobo, 1995
Cr(III)	Luminol - H_2O_2 system	Distilled, drinking, mineral, waste waters, food samples	0.2 nM	Escobar *et al.*, 1993
Cr(III)	Oxidation of pyrogallol with periodate at neutral pH; increased intensity with 3-(N- morpholino) propanesulphonic acid	Synthetic	19 nM	Nakano *et al.*, 1993
Cr(III)	Catalysed luminol oxidation by H_2O_2; using rate of binding to inhibitory ligand (EDTA) to gain specificity	Urine, blood serum, hair	0.2 nM	Escobar *et al.*, 1998
Cr(III), Cr(IV)	Separation by cation-exchange column; reduction of Cr(IV) by potassium sulfite; detection by luminol - H_2O_2 system	Synthetic	9.6 nM	Gammelgaard *et al.*, 1992
Cr(III), Cr(IV)	Separation by anion-exchange column; reduction by sulfur dioxide solution; detection by luminol oxidation	Fresh water	1.0 nM Cr(III) 1.9 nM Cr(IV)	Beere and Jones, 1994
Cr(III), Cr(VI)	Cr(III)-catalyzed oxidation of luminol by H_2O_2; Cr(VI) reduction using H_2O_2 in acidic medium	Waste water	<1.0 nM	Escobar *et al.*, 1995
Au(III)	Tetrachloroaurate(III) - luminol system in reversed micellar system	Chloroform	51 pM	Imdadullah *et al.*, 1991
Au(III)	Luminol in reversed micellar medium after solvent extraction	Industrial samples of silver-based alloy	Not reported	Imdadullah *et al.*, 1993
Au(III)	Tetrachloroaurate(III) with luminol in reversed micellar medium	Silver based alloy	0.05 fM	Imdadullah, 1994
Fe(II)	Rates and mechanisms of Fe(II) oxidation at nanomolar levels	Sea water	Not reported	King *et al.*, 1995
Fe(II)	Oxidation kinetics; luminol – dissolved oxygen reaction; time resolution <1 s	Lake water	Not reported	Emmenegger *et al.*, 1998
Fe(II), H_2O_2	Reaction of oxygen with bis(2,4,6-trichlorophenyl)oxalate (TCPO) in the presence of Fe(II); mechanistic investigation	Atmospheric liquid water	<0.1 μM Fe(II); not reported for H_2O_2	Quass and Klockow, 1995

Continued overleaf

Metal ion species	*CL reaction*	*Sample matrix*	*Limits of detection*	*Reference*
Fe(II), Fe(III)	Reaction of luminol – H_2O_2 –Fe(III)oxine complex; enhancement using reversed micellar solution (CTAC) in chloroform-cyclohexane; on-line solvent extraction; reversed FI manifold	Synthetic	90 nM	Kyaw *et al.*, 1998
Fe(II), total dissolved Fe	Brilliant sulfoflavin - H_2O_2 in neutral medium; preconcentration on 8-hydroxyquinoline column	Sea water	0.5 nM	Elrod *et al.*, 1991
Fe(II), total Fe	Luminol – H_2O_2 reaction; use of citric acid as activating and masking agent; micelle enhancement using cationic surfactant; silver reductant column	Human hair, natural waters	5 nM	Saitoh *et al.*, 1998
Fe(II), total dissolved Fe, Mn(II), total dissolved Mn	Catalysed luminol oxidation using potassium periodate; reversed FI manifold; *in-situ* monitoring	Underground water treatment, drinking water	54 pM Fe(II) 91 pM Mn(II)	Zhou and Zhu, 1997
Fe(III)	Luminol - aqueous ammonia - H_2O_2 reaction; selective column extraction using 8-HQ chelating resin; natural oxidation of sample to measure dissolved Fe	Sea water	50 pM	Obata *et al.*, 1993
Fe(III)	1,10-phenanthroline - H_2O_2 – sodium hydroxide system; enhancement using cationic surfactant (zephiramine)	Synthetic	1.8 nM	Watanabe *et al.*, 1996
Fe(II+III)	Luminol – dissolved oxygen – Fe(II) reaction; in-line matrix elimination and preconcentration on 8-hydroxyquinoline column; Fe(III) reduction using sulphite; shipboard analysis	Sea water	40 pM	Bowie *et al.*, 1998
Fe(III)	Luminol chemistry; in-line preconcentration; shipboard analysis	Sea water	21 pM	de Jong *et al.*, 1998
Fe(II+III)	Luminol chemistry; 8-hydroxyquinoline preconcentration column; sodium hydrogen sulphite reduction	Sea water	Not reported	Powell *et al.*, 1995
Fe(III)	Luminol – H_2O_2 – ammonia reaction; improved manifold; chemical speciation; particle leaching; effects of organic complexing agents	Seawater	10 pM	Obata *et al.*, 1997

Continued overleaf

Metal ion species	*CL reaction*	*Sample matrix*	*Limits of detection*	*Reference*
Mn(II)	Oxidation of 7,7,8,8-tetracyanoquinodimethane in alkaline solution; preconcentration on immobilized 8-hydroxyquinoline	Sea water	0.1 nM	Chapin *et al.*, 1991
Mn(II)	Oxidation of 7,7,8,8-tetracyanoquinodimethane in alkaline solution; eosin Y sensitization in surfactant bilayer vesicles	Raw, processed water	82 nM	Bowie *et al.*, 1995
Mn(II)	Luminol – H_2O_2 reaction; removal of Fe interference using 8-hydroxyquinoline column	Sea water	29 pM	Okamura *et al.*, 1998
Mn(II)	Kinetic study of the oxidation of Mn(II) at nanomolar concentrations; reaction of 7,7,8,8-tetracyanoquinodimethane in alkaline solution	Sea water	Not reported	von Langen *et al.*, 1998
Mn(II)	Electrostatic reagent immobilisation on anion-exchange resin; luminol – IO_4^- - Mn(II) reaction; column elution using Na_3PO_4	Waters	18 nM	Lu and Zhang, 1995
Rh(III)	Oxidation of luminol by dissolved oxygen in reverse micellar medium	Chloroform	0.5 μM	Imdadullah *et al.*, 1994
Ag(I)	Hydrophilic cation-exchange resin; detection based on oxidation by luminol with peroxodisulfate	Synthetic	4.6 nM	Jones and Beere, 1995
Ti(IV)	Reaction of Ti(III) with carbonate buffer; on-line Jones reductor column	Synthetic	1.0 μM	Alwarthan *et al.*, 1991
V(V)	Immobilisation of luminol and hexacyanoferrate(III) on anion-exchange column; elution using phosphoric acid; elimination of interferents using cation-exchange column	Geochemical samples, human hair	0.1 nM	Qin *et al.*, 1997
Zn(II)	Micellar enhanced chemiluminescence of 1,10-phenanthroline using trimethylstearylammonium chloride (TSAC)	Synthetic	23 nM	Watanabe *et al.*, 1999
rare earth metals	Reaction of analyte - EDTA complex with H_2O_2 in alkaline solution to produce reactive oxygen; detection by 1,10-phenanthroline CL; enhanced by surfactant and dye-sensitizer	Coal fly ash	e.g. 20 nM Eu(III)	Ishii *et al.*, 1992

[8] *Limits of detection as specified in the original paper*

Table I.6. FI-CL applications for metal ion species published between 1991 and mid-1999 (updated from Bowie *et al.*, 1995)

I.4.3 Chemiluminescence Reactions for the Determination of Iron

I.4.3.1 Luminol

The sensitivity of chemiluminescence methods for the determination of trace metals is well known (Seitz and Hercules, 1973; Kricka and Thrope, 1983). Most such methods are based on the catalysis or inhibition of reactions involving the oxidation of luminol (5-amino-2,3-dihydrophthalazine-1,4-dione), an acyl hydrazide, in basic solution (pH 10-11). This aqueous phase CL reaction was first documented by Albrecht (1928), and the predicted mechanism (Figure I.9) reported by Merényi *et al.* (1990) is believed to involve two steps; firstly, a nucleophilic addition to the carbonyl group, followed by breakdown of the formed α-hydroxy hydroperoxide intermediate.

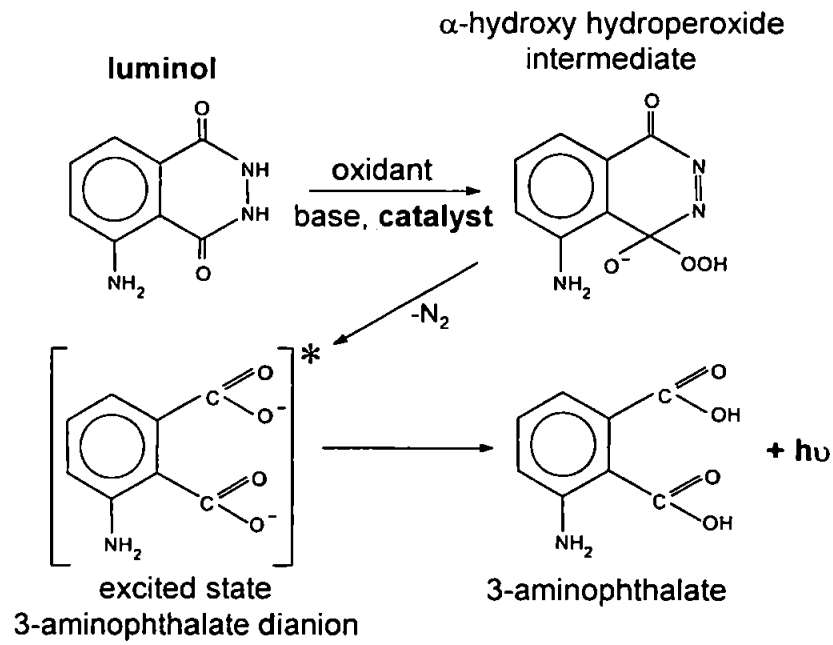

Figure I.9. Luminol CL reaction mechanism

The luminol CL reaction allows the determination of either the oxidising species (e.g. peroxides), organic compounds which can generate the oxidising species (e.g. haeme-containing enzymes, peroxidase), the catalyst (e.g. certain transition metal ions, hexacyanoferrate(III)), luminol itself), or species which quantitatively suppress the CL emission (e.g. ammonia); Table I.7.

Condition	*Specific agent*
1. Oxidant alone	O_2, O_3, H_2O_2, O_2^-, OCl^-, KO_2, $K_2S_2O_8$, NIO_4, NOCl, DMSO, OsO_4, BO_4^-
2. Catalyst + O_2	Fe^{2+}, Co^{2+}, *t*-butoxide, Br_2, I_2, $Fe(CN)_6^{3-}$, MnO_4^-, DMSO
3. Catalyst + H_2O_2/OH^- (pH 10-13)	
(a) free transition metal cations	Fe^{2+}, Fe^{3+}, Co^{2+}, Ni^{2+}, Cu^{2+}, Hg^{2+}, Cr^{3+}, Mn^{4+}, V^{4+}
(b) transition metal anion complexes	$Fe(CN)_6^{3-}$, MnO_4^-, $AuCl_4^-$, $SbCl_6^-$
(c) transition metal cation complexes	UO_2^{2+}, $Cu(NH_3)_6^{2+}$, VO_2^+
(d) free porphyrins	coproporphyrin
(e) porphyrin Fe^{3+}	protohaem, haematin, deutero-haematic, other modified haematin
(f) haemoproteins	haemoglobin, myoglobin, catalase, peroxidases, cytochrome c
(g) other Fe^{3+} proteins	ferritin
(h) corrins	vitamin-B_{12}
4. Enhancers	benzothiazoles (e.g. firefly luciferin on peroxidase), iodophenol at pH 8
5. Inhibitors	Ce^{4+}, Th, Zr^{2+}, cysteine, tris, CN^-, bicine, albumin, serum, EDTA

Table I.7. The triggering of luminol chemiluminescence (data from Campbell, 1988)

Luminol CL methods for Fe, Co, Mn and Cu have particularly low detection limits, at the low nanomolar level (Seitz and Hercules, 1972; Klopf and Nieman, 1983; Alwarthan and Townshend, 1987; Alwarthan *et al.*, 1990). The commonest oxidant has been alkaline hydrogen peroxide, but added oxidant is not always necessary. Seitz and Hercules (1972) determined Fe(II) by its catalysis of luminol chemiluminescence in the absence of added oxidant, the oxidant being assumed to be dissolved oxygen; the detection limit was 5 ng l^{-1}. Later, Klopf and Nieman (1983) found that Fe(II), Co(II), Mn(II) and Cu(II) stimulated chemiluminescent emission from luminol in a flow system in the absence of added oxidant, and Sarantonis and Townshend (1986) have reported a similar FI-CL system for Fe(II), Fe(III) and total Fe determinations by incorporating a silver reductor mini-column into the manifold. Recently, Saitoh *et al.* (1998) have enhanced the sensitivity of the luminol chemistry by adding tetradecyltrimethylammonium bromide (TTAB) as a cationic surfactant together with citric acid, and have reported a flow system for Fe(II) and total Fe determinations (detection limit 5.0 nM). All these methods have examined the luminol CL reaction using synthetic Fe standards,

although some have been successfully applied for analysis of Fe in certified reference materials. Applications of the luminol chemistry for Fe determinations in a seawater matrix were described in Section I.3.

I.4.3.2 Brilliant Sulfoflavin

Until recently, the luminol CL reaction system was not utilised widely in practice for chemical analysis, unlike other spectral methods. This was primarily due to its lack of selectivity. Yamada and co-workers therefore sought out novel CL systems for trace Cu(II) (Yamada and Suzuki, 1984; Yamada *et al.*, 1985a), Mn(II) (Yamada *et al.*, 1985b), Cr(III,IV) (Ohshima *et al.*, 1990; Yamada *et al.*, 1985c), Co(II) (Makita *et al.*, 1994) and Fe(II) (Yamada *et al.*, 1985c; Maikta *et al.*, 1994), incorporating the chemistry into a FI manifold. The brilliant sulfoflavin (BSF; sodium 4-amino-N-(p-tolyl)-naphthalimide-3-sulfonate; Figure I.10) – H_2O_2 - NaOH system (Yamada *et al.*, 1985c) was found to be highly selective towards Fe(II) species. The reaction was thought to be initiated by a Fenton-like reaction; that is, the CL is considered to be BSF-sensitized emission resulting from the energy transfer to BSF from singlet oxygen molecules produced through the reductive decomposition of H_2O_2 by Fe(II).

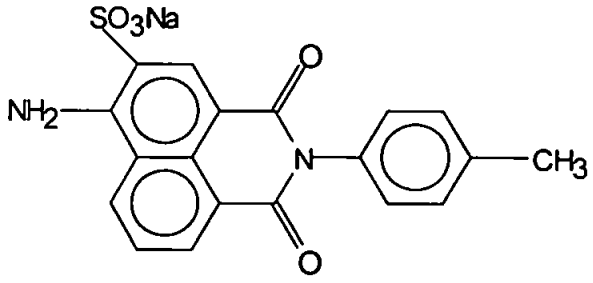

Figure I.10. Structure of brilliant sulfoflavin

The choice of the reaction media was deemed to be essential, and Yamada proposed that an aqueous CH_3CN solution provided the maximum CL signal. However, Elrod *et al.* (1991) investigated the reaction further and suggested the reaction was better performed in a phosphate buffer (pH 8.3). By coupling the CL system with an in-line preconcentration column containing the 8-hydroxyquinoline resin, a detection limit of 0.45 nM was achieved in a seawater matrix.

I.4.3.3 Other Reagents

Two other chemiluminescence systems have been investigated which allow the selective determination of Fe(II) species in solution. The first is based around the oxidation of 7,7,8,8-tetracyanoquinodimethane (TCNQ) by dissolved oxygen. This reaction was first utilised for the determination of Mn(II) (Yamada *et al.*, 1985b), using eosin-Y sensitizer and surfactant vesicles as the reaction media, however a further investigation of the interferences (Bowie *et al.*, 1995) suggests that Fe(II) produces a signal under this CL system large enough to allow its determination down to the micromolar level. The second CL system is based around the transition metal ion-catalysed decomposition of peroxymonosulfate (PMS, $KHSO_5$), which was found to be light emissive (Makita *et al.*, 1993, 1994). By use of a sensitiser in a micellar solution, the authors claimed the flow system allowed the selective determination of Fe(II) down to 6 nM. However, the very low Fe levels that are found in certain oceanic regions coupled with the poor reaction sensitivities precludes their use for analysing Fe in seawater. Such CL systems will only be beneficial to marine chemists if ways of increasing their sensitivity are found.

I.5 Flow Injection Analysis

The rapid and transient nature of solution-phase CL requires a means of rapid and reproducible mixing of sample and reagent streams. Luminescent detection systems have therefore received an increased interest since the advent of flow injection (FI), a powerful methodological innovation for sample handling that has been established over more than two decades of research. FI is characterised by its simple basis, relatively inexpensive equipment, ease of operation and great capacity for achieving results that are excellent in view of the rapidity, accuracy and precision with which they are obtained. Reported first by Ruzicka and Hansen in the 1970s, several texts discuss the theory, instrumentation and practice (Ruzicka and Hansen, 1988; Varcarcel and Luque de Castro, 1987; Karlberg and Pacey, 1989). FI constitutes the most advanced form of solution manipulation available to analytical chemists for mixing and transporting the reagents and products of a chemical reaction to the point of measurement.

The technique is essentially based on the injection of a highly precise liquid sample volume into an unsegmented liquid carrier stream. Following injection, the sample zone undergoes physical dispersion as it is pumped along a narrow-bore tube to a detector for measurement of a specific physico-chemical parameter as the solutions pass through a flow cell. The resulting transient signal is in the form of a narrow peak in which the height is usually proportional to the analyte concentration. A schematic representation of a simple, single channel FI manifold is given in Figure I.11(a), outlining the four basic components: the *propelling unit (P)*, the *injection system (S)*, the *reactor (R)*, and *flow-through detection unit (D)*. Such a low-pressure manifold commonly consists of narrow-bore (0.5-0.8 mm) PTFE tubing and fittings, peristaltic pumps, rotary injection valves, a flow cell and a detector to suit the application. Additional components include tightly wound mixing coils, 3-way switching valves to direct the flow, and/or solid phase preconcentration or reaction columns.

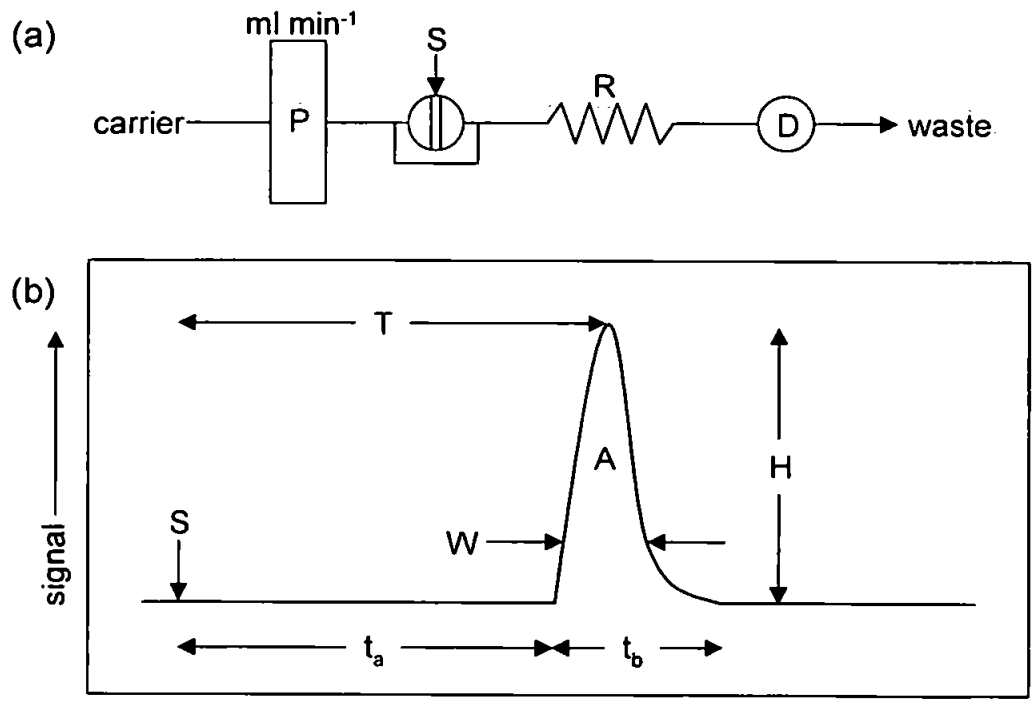

Figure I.11. (a) Schematic diagram of a single channel FI manifold; P=pump, S=sample injection valve, R=reactor, D=detector incorporating flow cell. (b) Single peak chart recorder output; S=sample injection, H=peak height, W=peak width, A=peak area, T=residence time, t_a=travel time, t_b=baseline-to-baseline time

A typical recorder output from a simple FI system is illustrated in Figure I.11(b). The response curve has the shape of a peak reflecting a continuum of concentrations or concentration

gradient. The *peak height (H), peak width (W)* and *peak area (A)* are all related to the analyte concentration. *Residence time (T)* during which chemical reaction takes place is defined as the time span between *sample injection (S)* and attainment of *maximum signal.* Other features include *travel time* (t_d), the period elapsed from injection to start of signal and *baseline-to-baseline time* (t_b), defined as the interval between the start of the signal and its return to the baseline. This parameter is dependant on the dispersion of the analyte.

Sample dispersion in FI is a highly reproducible process characterised by the dispersion coefficient (D):

$$D = C^0/C^{max}$$

where C^0 is the concentration of the analyte in the sample prior to dispersion and C^{max} is the maximum concentration in the dispersed sample zone at the time of detection. Dispersion is generally described as limited (D = 1-3), medium (D = 3-10) or large (D>10) (Valcarcel and Luque de Castro, 1988). The degree of dispersion can be controlled by adjusting the operating parameters, such as flow rate, injection volume, tubing length and diameter and manifold geometry. Variants on FI include the techniques of stopped flow, reverse FI, sequential injection and the continuous addition of reagent (Chapter IV).

I.6 IN-LINE ANALYTE PRECONCENTRATION

Many liquid-phase CL reactions suffer from poor selectivity. For example, the alkaline oxidation of luminol in the absence of H_2O_2 is known to be catalysed by several trace metal ions that are capable of existing in more than one valency state (e.g. Fe(II), Co(II), Cu(II), Mn(II); previous Table I.7; Klopf and Nieman, 1983; Campbell, 1988). In addition, the high ionic strength seawater matrix is likely to severely interfere with the quantitative relationship between Fe concentration and CL emission and its removal is essential to prevent precipitation prior to introduction of the alkaline CL reagents. To attain the sub-nanomolar detection limits required for the analysis of Fe in open-ocean samples, the analyte also requires preconcentration by up to an order of magnitude.

The concept of solid-phase extraction using chelating resins was first introduced over three decades ago using the Chelex-100 resin (Riley and Taylor, 1968), and similar methods have entertained extensive interest in recent years for the matrix removal and preconcentration of trace metals from seawater (Nickson *et al.*, 1995). The method of Landing *et al.* (1986) has been most commonly applied for the synthesis of a micro-column containing 8-hydroxyquinoline (8-HQ) on an inert resin support. 8-HQ is selective towards transition and heavy metal cations relative to alkali and alkaline-earth cations. Previous methods have involved the immobilisation of 8-HQ onto silica substrates, which offer the advantages of good mechanical strength, resistance to swelling and rapid overall exchange kinetics in column applications. Such immobilisations are, however, unstable at high pH. Landing *et al.* (1986) used the highly porous, chemically stable organic resin gel Toyopearl-TSK as the solid support. TSK-8HQ micro-columns have subsequently been incorporated in-line into several FI-CL manifolds for the determination of Fe (Elrod *et al.*, 1991; Powell *et al.*, 1995; Bowie *et al.*, 1998; de Jong *et al.*, 1998), Mn (Chapin *et al.*, 1991), Co (Sakamoto-Arnold and Johnson, 1987) and Cu (Coale *et al.*, 1992) in seawater.

I.7 RESEARCH OBJECTIVES

(i) To investigate chemiluminescence reaction chemistries for the determination of Fe(II) and Fe(III) species (Chapter I)

(ii) To design a flow injection manifold based on chemiluminescence detection of Fe (Chapter III)

(iii) To adapt the system for a seawater matrix and evaluate interferences (Chapter III)

(iv) To develop in-line preconcentration to lower detection limits and remove the sea-salt matrix (Chapter III)

(v) To investigate relative performances of photomultiplier tubes, solid-state photodiodes and charge-coupled cameras for chemiluminescence detection (Chapter II)

(vi) To automate the manifold and investigate CL data acquisition (Chapter II)

(vii) To investigate the kinetic effect of Fe on the luminol reaction using an alternative flow configuration, the continuous addition of reagent technique (Chapter IV)

(viii) To validate the FI-CL system in local field trials (Chapter V)

(ix) To deploy the system on-board oceanographic cruises of opportunity (Chapter V)

(x) To investigate the distribution of Fe in coastal seas and remote regions of the Atlantic Ocean and help unravel its complex cycling, speciation and biogeochemistry in seawater (Chapter V)

INSTRUMENTAL DEVELOPMENT

II.1 INTRODUCTION

This chapter discusses the instrumentation used during the research, and investigates the most appropriate instrumental components for the determination of iron (Fe) in a seawater matrix using flow injection (FI) analysis with chemiluminescence (CL) detection. Different components for each separate operation in a FI manifold are considered in detail and compared during the development work, in order to meet the analytical requirements for operation on-board a research vessel in a remote open-ocean environment (Table II.1). Different CL detection systems (photomultiplier tubes, photon counting heads, photodiodes, charge coupled devices) are presented. Automation of the FI manifold is detailed together with an investigation into data acquisition of the CL signals.

Parameter	*Requirement*
Sensitivity	High (LOD <0.1 nM)
Precision	<5%
Sample volumes required	Small (<100 ml)
Sample handling	Minimal
Sample throughput	Fast (ca. 6 h^{-1})
Operation	Automated
Detector	Robust
Cost	Inexpensive
Redox specific	Yes
Physical characteristics	Portable

Table II.1. Targets for a shipboard analytical monitor designed to determine Fe in the open-ocean

The fundamental principles, theory and applications of FI with CL detection were outlined in Chapter I and are detailed in Valcarcel and Luque de Castro (1987), Karlberg and Pacey (1989) and Campbell (1988). This section discusses the essential components of a FI manifold in greater detail (namely the propulsion system, the injection system, the flow cell and detector; see previous Figure I.11) and Table II.2 outlines current alternatives for the principal FI components.

Component	*Options*	*Description*
Propulsion system	Peristaltic pump	Set of rollers on a revolving drum, squeezing flexible tubing to produce constant pulsing flow
	Sinusoidal piston pump	Computerised cam-driven piston, producing bi-directional, variable pulseless flow
	Reciprocating pump	Piston pumping fluid through small chamber, with valves controlling movement through chamber; pulsing flow
	Gas pressure reservoir	Pressurised inlet gas vessel connected by flow regulator to each reagent or carrier stream, producing pulseless flow
	Solenoid miniature pump	Fixed displacement diaphragm, micro-dispensing, self priming, low voltage, pulsing
Injection system	Rotary valve	Six port unit containing sample loop; electrical or pneumatic operation
	Hydrodynamic	Selective starting and stopping of reagent pump; sample enters during stop and is carried through manifold on start-up; risk of cross-contamination
	Syringe	Manual injection via septum; poor analytical characteristics
	Multipositional selection	Electronic multi-port unit, allowing sequential selection of flow streams (sample, standard, reagents)
Flow cell	Flow-through cuvette	Allows beam of light to be directed through a narrow channel; used in spectrophotometry
	Spiral quartz glass	Flow passes through coil to ensure effective mixing of sample and reagents, one or two arm entry point, suited to CL
	Laminar flow	Elliptical orifice sandwiched between PTFE spacer and glass plates; flow enters at base and exits through outlet at top
	Fountain	Rectangular optical reaction zone; flow enters through central inlet, radiates into ring-shaped well and exits at edge
Detector	Optical	Spectrophotometry (UV-Vis, IR, solid state, diode array), fluorimetry, atomic spectrometry, chemiluminescence
	Electrochemical	Potentiometry (ion-selective and pH electrodes), conductimetry, amperometry, coulometry, voltammetry

Table II.2. Options for principle FI components

II.2 FI MANIFOLD COMPONENTS

II.2.1 Propulsion system

A FI manifold is fundamentally dependent on regular flow rates, allowing constant, reproducible dispersion (Ruzicka and Hansen, 1988). Peristaltic pumps (Figure II.1) are based upon multiple rollers on a revolving drum compressing flexible tubing against a bridge to produce a constant pulsing flow. Such devices have been proven to be reliable, simple, robust, relatively inexpensive and easily automated (Worsfold *et al.*, 1999). Models are often multi-channel allowing different streams in a FI manifold to operate with different flow rates, providing scope for independent channel operation. The major disadvantage in their use is the flow pulsing effect, which may adversely increases the noise generated by the reagents at the detector. The number of rollers and rotation rate of the pump determines the magnitude and frequency of pulsing. Tightly coiled manifold tubing can be incorporated into flow lines, however, to act as pulse dampeners. Other pumping systems, such as sinusoidal pistons or gas pressure reservoirs, are capable of producing a pulseless flow, although such units are limited in the amount of solution that may be delivered, they possess a contamination risk and are also less robust.

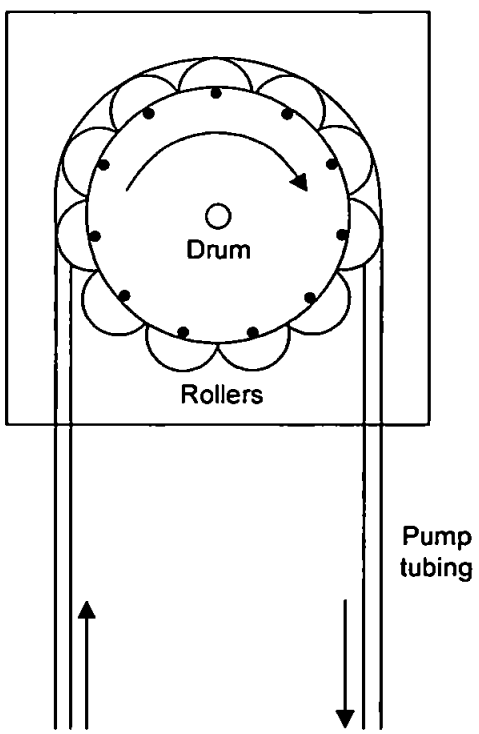

Figure II.1. Schematic diagram of a peristaltic pump

The FI-CL method developed during this research for the determination of Fe in seawater required three pumps:

- Pump A: Reagents pump,
- Pump B: Sample and buffer pump, and
- Pump C: Wash pump

The reagents pump delivered two flows to the detector, namely CL reagents and eluent carrier streams. The mixing of reagents through the manifold generated a background noise level caused by trace metal impurities in the solutions acting as catalysts for the luminol reaction. This baseline noise was dependent upon flow rates and pulsing. Hence analytical performance relied on a near pulseless flow for these two lines. A variable speed, 10-roller model (Gilson Minipuls 3, model MP4/HF) was chosen as the reagents pump to ensure smooth flow characteristics (peak-to-peak baseline noise <0.5 mV).

The sample and buffer pump delivered two flows to the injection system. For an FI-CL manifold incorporating a solid phase microcolumn within a sample injection valve, it was critical to deliver a precise volume of sample, standard or buffer, although the pulsing of the flow streams was not critical. Variable volumes resulted in reduced precision (RSD typically 8%) between replicates. A fixed speed, 8-roller unit (Ismatec Mini S 820) was employed for this task. High precision ("Accu-rated" polyvinyl chloride, PVC; or Tygon®, Elkay) pump tubing ensured the delivery of a precise volume of solution.

The wash pump contained only one flow line. Its function was to perform either UHP water rinses during the analytical cycle or to deliver an acid wash solution to the manifold for periodic cleaning of the solid phase column and the FI tubing of the system. Pulsing was not critical for this flow stream and a fixed speed, 8-roller model (Ismatec FIXO 4/820) was used.

II.2.2 Fluidics

FI is based upon the continuous, non-segmented flow of reagents and sample through several components (e.g. pumps, valves, columns, detectors) to waste. The ducting system functions to connect such components and allows for appropriate mixing and dispersion which is dependent on the manifold geometry and tubing internal diameter. Furthermore, the flow ducting must be constructed from robust and contamination free components.

II.2.2.1 Connecting Tubing

All FI manifold tubing was narrow bore Teflon® (polytetrafluoroethylene, PTFE, 0.75 mm i.d., Fisher), which is chemically inert and insensitive to temperature fluctuations.

II.2.2.2 Pump Tubing

Peristaltic pump tubing was selected for each flow line, depending on the type of solution and its function in the analytical cycle. Reagents, eluent carrier and wash solution streams required standard manifold PVC tubing which was suitable for dilute to medium (<10 %) concentration acids and alkalis, possessed an extended lifetime and was transparent for convenient flow monitoring. The sample and buffer flow lines, however, required accurate and consistent flow rates and hence "Accu-Rated" PVC tubing was used for this purpose. For fixed speed model peristaltic pumps, the flow rate can be adjusted by choosing pump tubing of appropriate i.d., signified by colour coded bridges. Care was taken not to over-tighten the pump tubing which would reduce its lifetime.

II.2.2.3 Connections

Several types of connectors were used in the FI system. Pump tubing could be directly sleeved to PTFE manifold tubing. Junctions between two ends of manifold flow lines and solid phase columns were constructed as a butt join using silicone bridges of ca. 10 mm in length. The reagent and carrier flow lines were merged within the light-tight detector housing using flanged PTFE tubing and a 3-way 'Hex'-connector (Omnifit, model 1003). A 3-way hexagonal valve 'Y'-piece (Omnifit, model 1102, Figure II.2) was used to merge sample and buffer lines. This

connector possessed open / closed switches to allow for selection of flow lines during method optimisation and solution blank contamination checks.

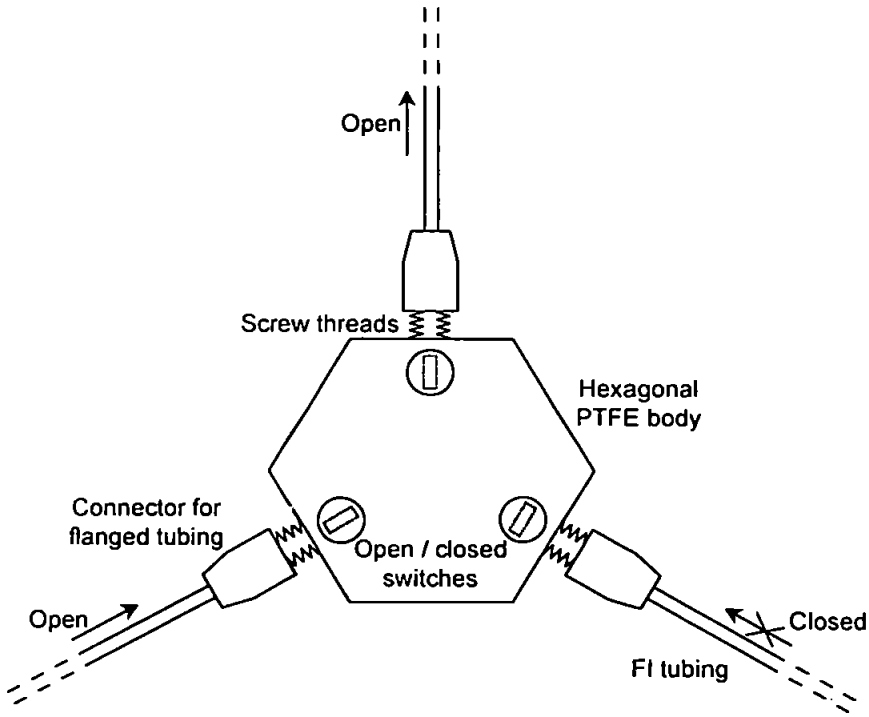

Figure II.2. Omnifit 3-way 'Y'-valve with switches

Three 3-way switching 'T'-valves were incorporated into the FI manifold in order to allow for choice of the appropriate solution during the analytical cycle. Two of these valves were used for selection of sample, sample plus one standard addition or sample plus two standard additions, and the third valve switched between the sample / buffer flow and wash pump flow. During method development, these switching valves were operated in manual mode using 3-way single key valves (Omnifit, model 1109 Figure II.3). The automated system used solenoid switching valves (Cole Palmer, model E-01367-72, Figure II.4) to control the flow of solutions.

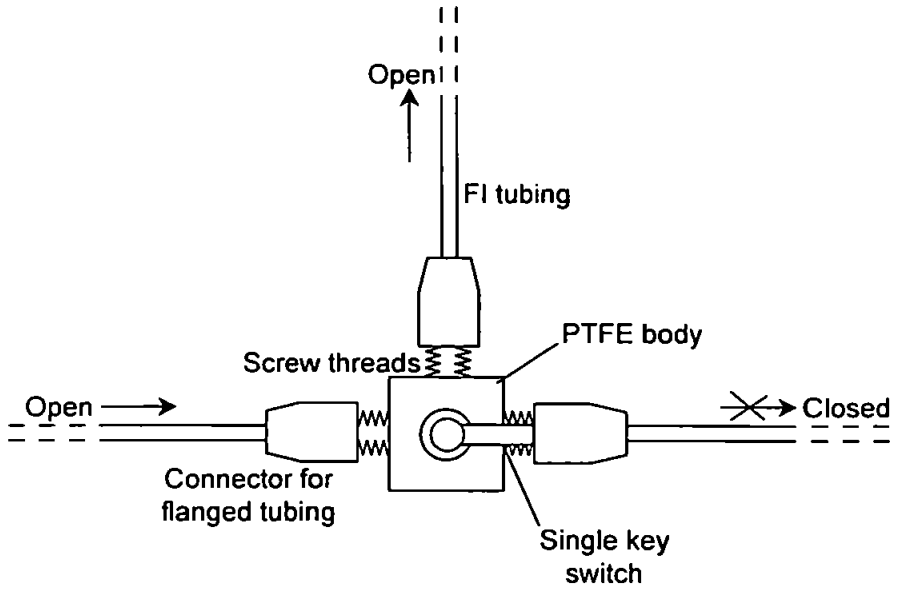

Figure II.3. Omnifit 3-way single key valve

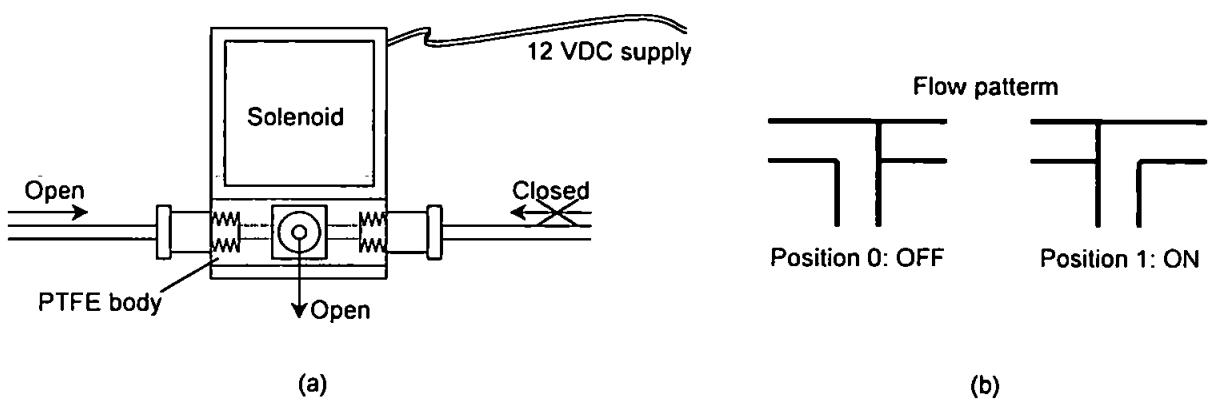

Figure II.4. (a) Cole Palmer solenoid switching valves, and
(b) Flow diagram of solutions during open / closed cycles

II.2.3 Injection Valves

The injection system in FI must be capable of inserting a fixed, precise volume of sample into a carrier stream. Two types of injection system were investigated during this work. The *rotary injection valve* (Rheodyne, model 5020) is based upon a six-port PTFE unit, incorporating a sample loop and/or solid phase column. The unit has two operating positions: the first for loading the loop (or column) with sample, and the second for eluting the sample from the loop into a carrier stream (Figure II.5). The valve is operated using a Universal Valve Switching

Module (Anachem) which may be controlled manually (push-button operation) or remotely (transistor-transistor logic (TTL) signal input). Rotary valves rely on a simple principle, are compact, operated rapidly (ca. 250 ms switching time), robust and easily automated. Alternative rotary injection valves (Valco, VICI) are now available which are manufactured from Cheminert® materials (a variety of inert composites, PFA, FEP, CTFE, PEEK) and hence have the added advantage of minimizing problems caused by acid solutions corroding the wetted parts of the valve and causing a contamination risk. These valves can be automated using micro-electric actuators and remotely controlled via contact closure, BCD 5V negative true input or RS-232 signals.

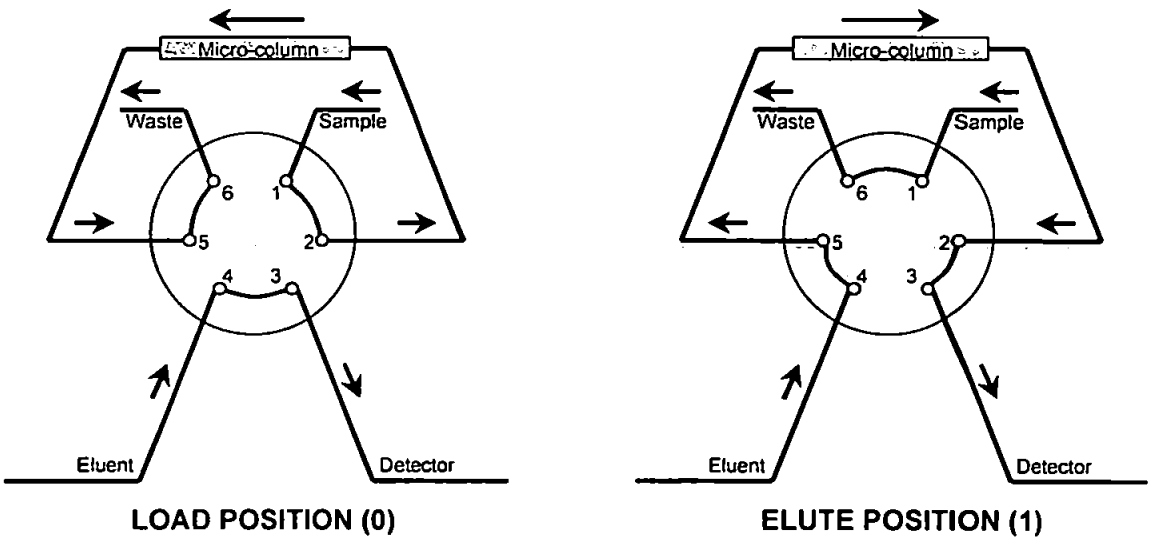

Figure II.5. Operation of a rotary injection valve

The second injection system was based upon a similar principle as the rotary injection valve, but incorporated four 3-way solenoid 'T'-valves in a sequence which allowed for sample load and elution cycles. The flow manifold for such a system is shown in Figure II.6. Automation of these valves would require 4 bits TTL input, compared to the single TTL input for the rotary valve and hence the former type of injection system was chosen for the duration of the research.

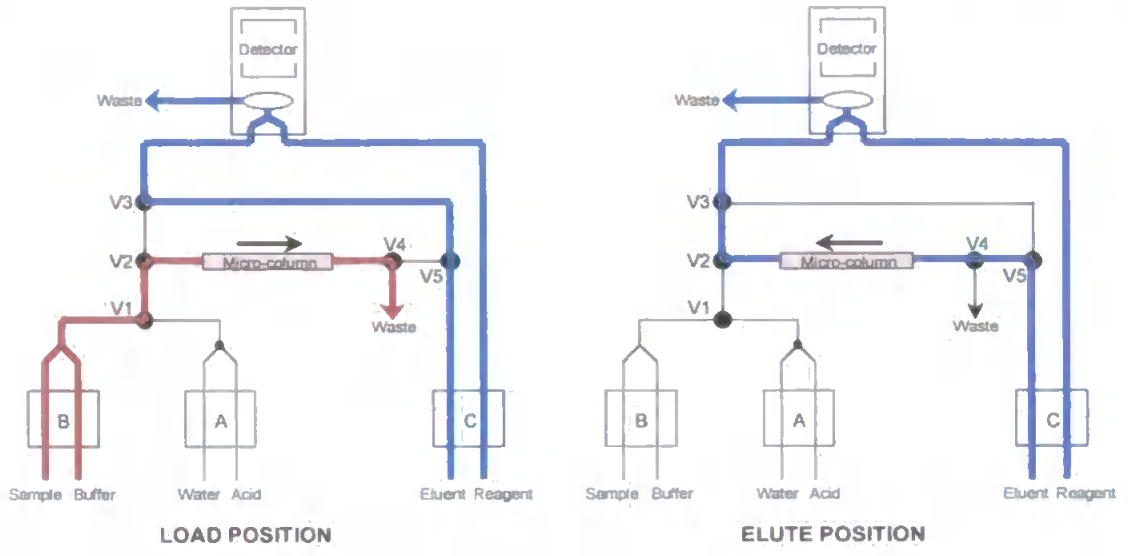

Figure II.6. Construction of an injection system using 3-way switching valves

II.2.4 Flow Cell

An essential component of a FI system, the flow cell is normally incorporated within the detector housing. This component should be inert, generate effective mixing and be designed to maximise a property of the analyte (e.g. CL emission) which is continuously monitored by the detector. A quartz glass spiral flow cell was designed so that the maximum of the CL emission occurred within the cell and hence was monitored by the detector through its end-window. The rapidity of CL reactions (typically 1-10 s) meant that solutions needed to enter the flow cell as soon as possible after mixing of sample and reagents. Two models were tested for their suitability in the FI manifold. Both types consisted of three turns of a tightly wound quartz glass spiral coil (tubing i.d. 1.1 mm; o.d. 3.0 mm; internal volume 130 µl; diameter 20 mm; Figure II.7). The first model (I) used only one inlet, whilst the second trial design (II) incorporated an extra arm in a 'V' design, so that the sample and reagents could actually mix inside the cell before passing to waste. The aim of design II was to maximise the signal by capturing the maximum of the CL signal generated during the fast (ms) luminol reaction. The flow cell was mounted behind a mirror contained within a light-tight housing, in front of the photosensitive window of the CL detector. Experiments with the 'V' flow cell, however, showed no improvement in sensitivity, and the more robust former design was therefore used in all further

work. The length of tubing between the point of merging the sample and reagent streams to the flow cell was minimised (12 mm) in order to allow the CL emission to occur within the coiled glass. In an optimised system (section III.3.2) reagents were pumped at a flow rate 3.2 ml min^{-1}, resulting in a delay time between confluence of sample and reagents and entry to the flow cell of 0.1 s. The residence time of the CL-emitting slug in the coiled glass flow cell was 2.4 s. Increasing the internal diameter of the quartz glass of the flow cell to 1.8 mm resulted in a longer residence time, but no apparent increase in sensitivity, due to less turbulence and therefore poorer mixing.

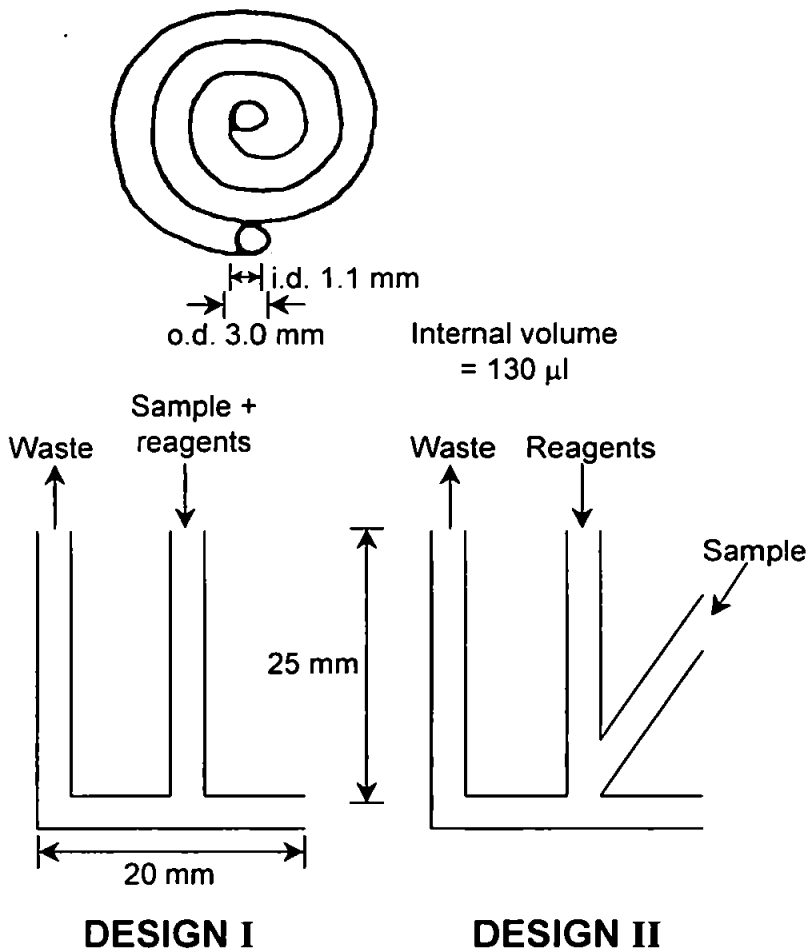

Figure II.7. Spiral quartz glass flow cell; one and two arm design

II.3 CHEMILUMINESCENCE DETECTION

The CL detector in a FI system must respond directly to light to produce an electrical signal that may be sent to a recorder. Three types of detection system are available which are capable of monitoring CL with low photon emission; namely photoelectric devices (e.g. photomultiplier tubes, photon counting modules), photoconductor devices (e.g. photodiodes) and charge transfer devices (e.g. charge coupled cameras). Table II.3 describes the properties of the three types of detectors, including a comparison between photomultiplier tubes and photon counting heads which incorporate the same detector but with different electronics. The quantum efficiency of the detector (the fraction of incident photons that yield electrons) is dependent on the cathode material (in photomultipliers) and is a strong function of wavelength. Quantum efficiencies for photomultipliers and photodiodes are generally poor. Care was taken to match the optical transmission properties of the flow cell with the λ_{max} of the CL reaction and the λ range of the detector (Figure II.8).

Property	*Photomultiplier*	*Photon Counting Head*	*Photo-conductor*	*Charge Coupled Device*
Manufacturer	Thorn EMI	Hamamatsu	Camspec CL1	Instruments SA
Sensor	Photomultiplier tube	Photomultiplier tube	Two photodiodes	Charge transfer
Physical characteristics	Fragile	Sturdy	Robust	Very fragile, liquid N_2 cooled
Power source	High voltage (1.1kV)	Low voltage (5 V)	Low voltage (15 V)	Mains voltage (240 V)
Size (lxwxh)	Medium (20x5x5 cm)	Miniature (8x2x5 cm)	Medium (30x10x20 cm)	Very large (60x60x40 cm)
Weight	Portable (0.6 kg)	Very light (0.2 g)	Light (1 kg)	Heavy (10 kg)
Cost	Expensive (£800)	Expensive (£400)	Cheap (£50)	Very expensive (£5000)
Spectral response	Very good, but low in red (λ_{max}~380 nm)	Very good (λ_{max}~470 nm)	Reasonable, but low in blue (λ_{max}~700 nm)	Poor, limited to 150 nm range; but two-dimensional
Response time	Very fast (100 ns)	Fast (ns range)	Medium (500 ns)	Very slow (ms)

Table II.3. A comparison of CL detection systems

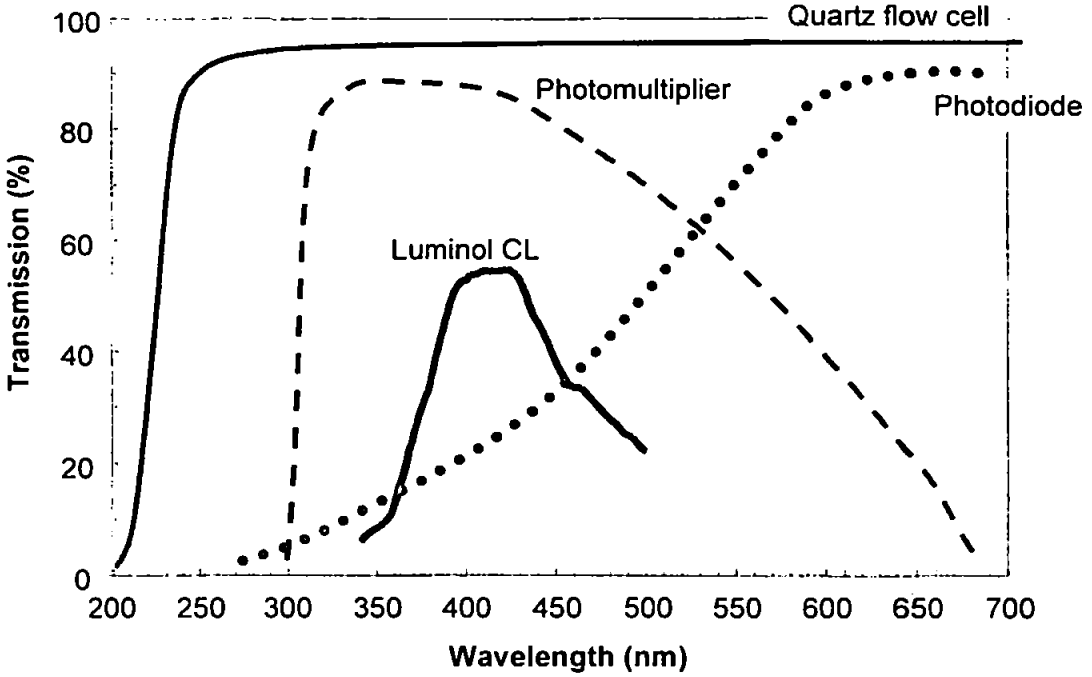

Figure II.8. Light / optical transmission properties of the flow cell, CL reaction and detector

II.3.1 Photomultiplier Tubes

II.3.1.1 Conventional Units

A photomultiplier tube (PMT; Figure II.9; Wayne, 1994) generates and multiplies electrons from incident photons and thereby enhances the signal. The PMT end-window (10 mm effective diameter, fused silica glass) detects a photon at the photocathode and emits an electron according to the photoelectric effect (primary emission). The electron is then electrostatically accelerated by a high voltage and focused to hit the first of the electron multiplier dynodes, which emits several electrons as a result of secondary emission. Each of these electrons is then accelerated and focused, and hit the second dynode, emitting more electrons. The amplification process is repeated up to 14 times before the resulting electrons are collected as a pulse of charge at the anode, which then outputs a current. The amplification typically takes less than 100 ns. The photomultiplier was equipped with a built-in current-to-voltage amplifier (C634), capable of four different settings ("A, B, C & D", x1, x10, 100 & x1000 factors respectively).

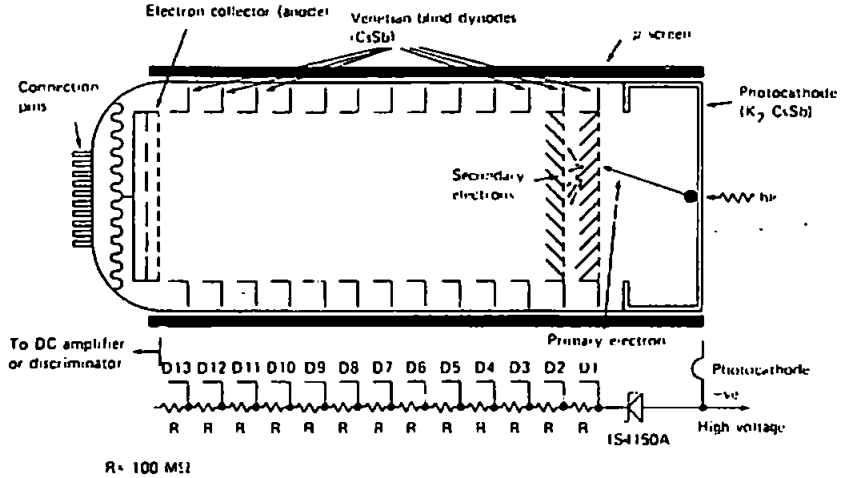

Figure II.9. Schematic diagram of a photomultiplier tube

II.3.1.2 Miniature Photon Counting Heads

A recent advance in photoelectric technology is a series of compact low power PMTs whose electronics is based on a single photon counting head. These devices comprise a low noise PMT, a high-speed amplifier, discriminator and a high voltage power supply circuits in one housing. The units require +5 VDC and a pulse counter of TTL input in order to be able to measure and acquire weak light signals. The present detector system, however, incorporated the larger photomultiplier tube (Thorn EMI, 9789QA) powered using a 1.1 kV supply (Thorn EMI, PM28B). This detector possessed similar sensitivity to the photon counting heads and had previously been used successfully in-house for similar CL applications (e.g. determination of H_2O_2; Price *et al.*, 1994).

II.3.1.3 Cooled Housings

Housings may be employed in luminescence applications to cool the photomultiplier tube and reduce the ambient dark current. Two types of cooled housing are commercially available: the forced air-cooled type and the liquid cooled type. The photocathode is set behind an evacuated, double-walled Pyrex insulating window. The PMT can be cooled to typically 50°C below the ambient temperature, with a 10-fold reduction in detector dark current signal reported at –20°C (Sakamoto-Arnold and Johnson, 1987). In the FI-CL system reported in this thesis, it was deemed unnecessary to cool the PMT unit since the baseline noise produced by the mixing of

reagents (ca. 0.5 mV) was over an order of magnitude greater than the background baseline generated by the detector at room temperature under dark conditions (ca. 0.04 mV) (Section III.3.1).

II.3.2 Solid-state Photodiodes

Photodiodes are based on the effect of light on the resistivity of the pn junction of a semiconductor (Campbell, 1988). A semiconductor, is a crystalline material with conductivity intermediate between that of a conductor and an insulator (Atkins, 1990). Silicon, a common semiconductor, is a Group IV element and in its crystalline form has four electrons localised in covalent bonding. The lack of free electrons implies silicon to be an insulator. However, an occasional electron is liberated by ambient thermal energy and moves through the crystal lattice and conducts electricity. This excitation now leaves a positively charged hole, associated with the silicon atom, which can move stepwise through the lattice. A bound electron from a neighbouring silicon atom jumps to the electron deficient region leaving another positive hole, and conduction continues with electrons passing in one direction, and positive holes in the other.

Semiconductors may be 'doped' by adding a tiny amount of impurities, such as Group V elements which add extra non-bonding electrons (n-type), or Group III elements which encourage more positive holes (p-type). A diode is formed by manufacturing adjacent n- and p-type regions within a single silicon crystal, called a pn junction.

Shining UV / visible light onto a pn junction under reverse bias (positive holes and negative electrons are drawn in opposite directions, away from the pn junction to form a depletion layer) generates additional electrons and holes which result in an increase in conductivity. This increase is directly proportional to the amount of radiant light. Photodiode based devices consist of either a single large incident area (ca. 1 cm^2) or an array of as many as 1000 diodes fabricated side-by-side on a single silicon chip, used to enhance sensitivity and to enable multi-wavelength monitoring.

During method development, the performance of a solid-state Camspec CL1 detector was evaluated. The unit employs two photodiodes and an amplifier combination, possessing negligible dark current. In experiments, however, the end-window Thorn EMI (model 9798QA) photomultiplier tube showed better performance characteristics for luminol CL, including a significant sensitivity improvement, and was hence selected for subsequent work. The blue light emission is very fast during the luminol CL reaction and PMTs are the fastest light detectors available (response time ca. 60 ns), with no delay or build-up of signal, low dark current (0.16 nA) and showing good spectral response to blue (420-450 nm) emissions. The poor response of the photodiode based system was attributed to two reasons. Firstly, the spectral response characteristics of the photodiode (λ_{max}~700 nm) are not compatible with the emission wavelength of the luminol reaction (λ_{max}~440 nm); and secondly, the recorder response time was not fast enough to monitor the emission as effectively as a PMT unit.

II.3.3 Charge Transfer Devices

Recent years have seen the development of charge transfer devices (CTDs), multi-channel solid state integrating photon detectors possessing high sensitivity and resolution (Earle *et al.*, 1993). A CTD camera incorporates a two-dimensional array of photosensitive metal oxide semiconductor capacitors arranged within a single, solid-state integrating circuit (Stanley, 1997). Signal information is accumulated as light strikes the detector film and stored as electrical charge. A CTD camera can measure variations in light intensity with wavelength and by appropriate alignment of fibre optic cables, multiple sources may be simultaneously determined using different regions of the array (Qiu *et al.*, 1995).

Two forms of CTD spectrometer exist. The first is based around **inter-cell** charge transfer, wherein the charge accumulated on the detector element is transferred to a serial register and then to a charge sensing amplifier (a *charge-coupled device* or *CCD*). The second involves **intra-cell** charge transfer, a shift of charge between two electrodes, generated by photons striking a pixel. This induces a voltage fluctuation, which is proportional to the intensity of light (a *charge-injection*

device or *CID*). CIDs have found use in wide dynamic range imaging applications in atomic spectroscopy, whereas CCDs are better suited to low intensity spectroscopy (e.g. Raman and fluorescence), as the on-chip amplification allows for excellent signal-to-noise output. CCDs have also found widespread use in spatial (e.g. astronomical) imaging.

CCD detectors are sensitive through the UV to near IR radiation range (200 – 1100 nm) and are capable of high wavelength resolution. Units must be liquid nitrogen cooled (-130°C) to reduce detector dark current (<1 electron / pixel / hour). Pixels are typically 22 x 22 μm in size, and arrays may be ordered as 578 x 385 pixels. CCD spectrometers offer mechanical simplicity, reliability and full spectrum data acquisition. However, their poor sensitivity (compared to photomultipliers), large size, fragility, and high capital & operational costs precludes their use as a shipboard CL detector, although CCD cameras are useful for fundamental laboratory studies.

A simple continuous flow – chemiluminescence manifold was constructed and coupled to a detection system consisting of a two-dimensional CCD spectrometer equipped with fibre optic probes (Figure II.10). The CCD array consisted of 256 x 1024 pixels in 27.6 x 7.0 mm grid of 27 μm square pixels in combination with 270M imaging spectrograph (Instruments S.A.) and Spectramax version 1.1d software (Jobin Yvon Optics and Spectroscopy). A silica core, fluorine doped silica clad fibre optic cable (1000 μm diameter) was attached to the spectrograph and focussed onto the spiral flow cell. A mercury / argon lamp was used to calibrate the wavelength scale. Luminol and Fe(II) standards were prepared as outlined in Section III.2.1. A 5.0 mM solution of hydrogen peroxide was prepared by serial dilution of a 30 % (v/v) stock with UHP water. Under this instrumental configuration, a spectrum of the Fe(II)-catalysed luminol CL reaction was obtained (Figure II.11), confirming the intense blue (λ_{max} 410-450 nm) emission. The calibrated CCD-CL system was linear up to 10.7 μM with a limit of detection of 95 nM. The poor sensitivity of the system precluded its further use for the CL-based analysis of trace levels of Fe in seawater.

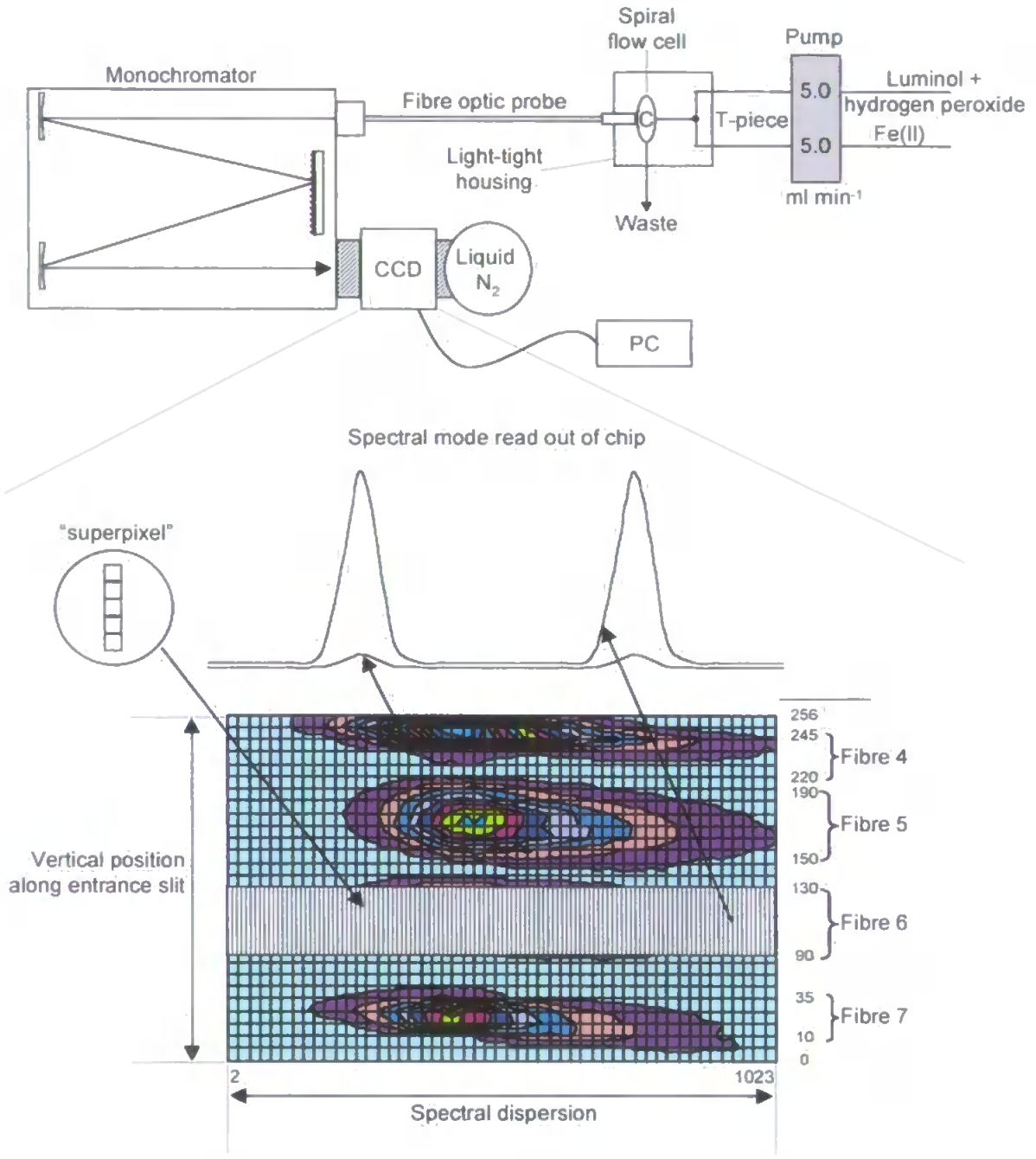

Figure II.10. Schematic diagram of a CCD spectrometer and the projection of four fibres onto a 2D pixel grid using artificial light sticks (peroxyoxalate CL reaction) as source (figure reproduced from Segura *et al.*, 1999; courtesy of Antonio Segura, University of Granada, Spain)

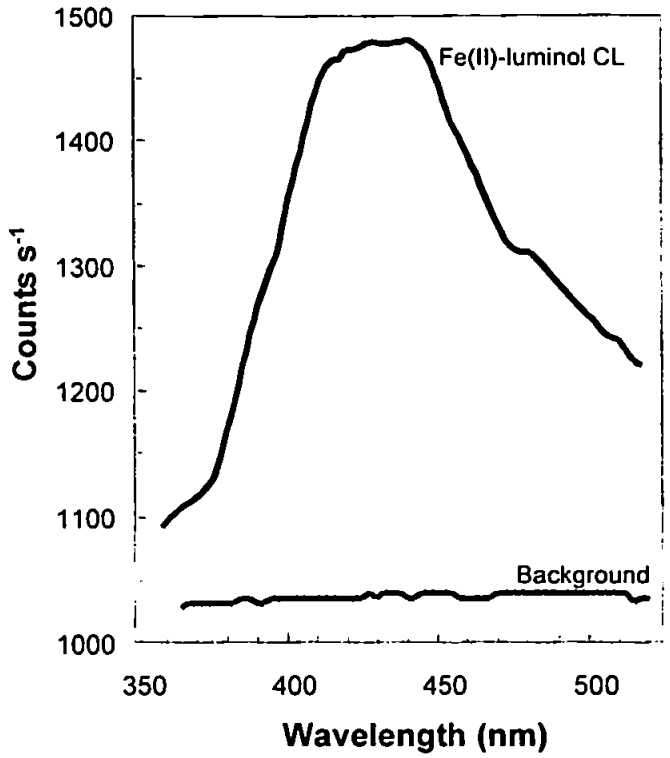

Figure II.11. Spectrum of the Fe(II)-luminol reaction. Experimental conditions: [Fe(II)] = 9.0 μM; [luminol] = 2.0 mM; [H_2O_2] = 5.0 mM, pH = 10.8; reagents and sample flow rates = 5 ml min^{-1}. Instrumental conditions: vertical binning=40 pixels; horizontal binning = 28 pixels; integration time = 2.0 s; accumulations = 2.

II.4 AUTOMATION

In order to be able to perform repeated shipboard analyses, the manual FI-CL manifold used during method development required full automation of all component parts, to provide the following advantages:

- improved precision
- reduced chance of human error (especially at sea during continual analyses)
- reduced analysis time and increased sample throughput
- free up analyst time for other tasks.

The manual FI system included three peristaltic pumps, three 3-way switching valves and one injection valve. Each of these components needed to be PC controlled via an interface digital-to-analogue converter (A/D) card. A block diagram of the FI-CL system illustrating solution flow, automated remote control and data acquisition connections is shown in Figure II.12. The development and optimisation of this manifold is described fully in Chapter III.

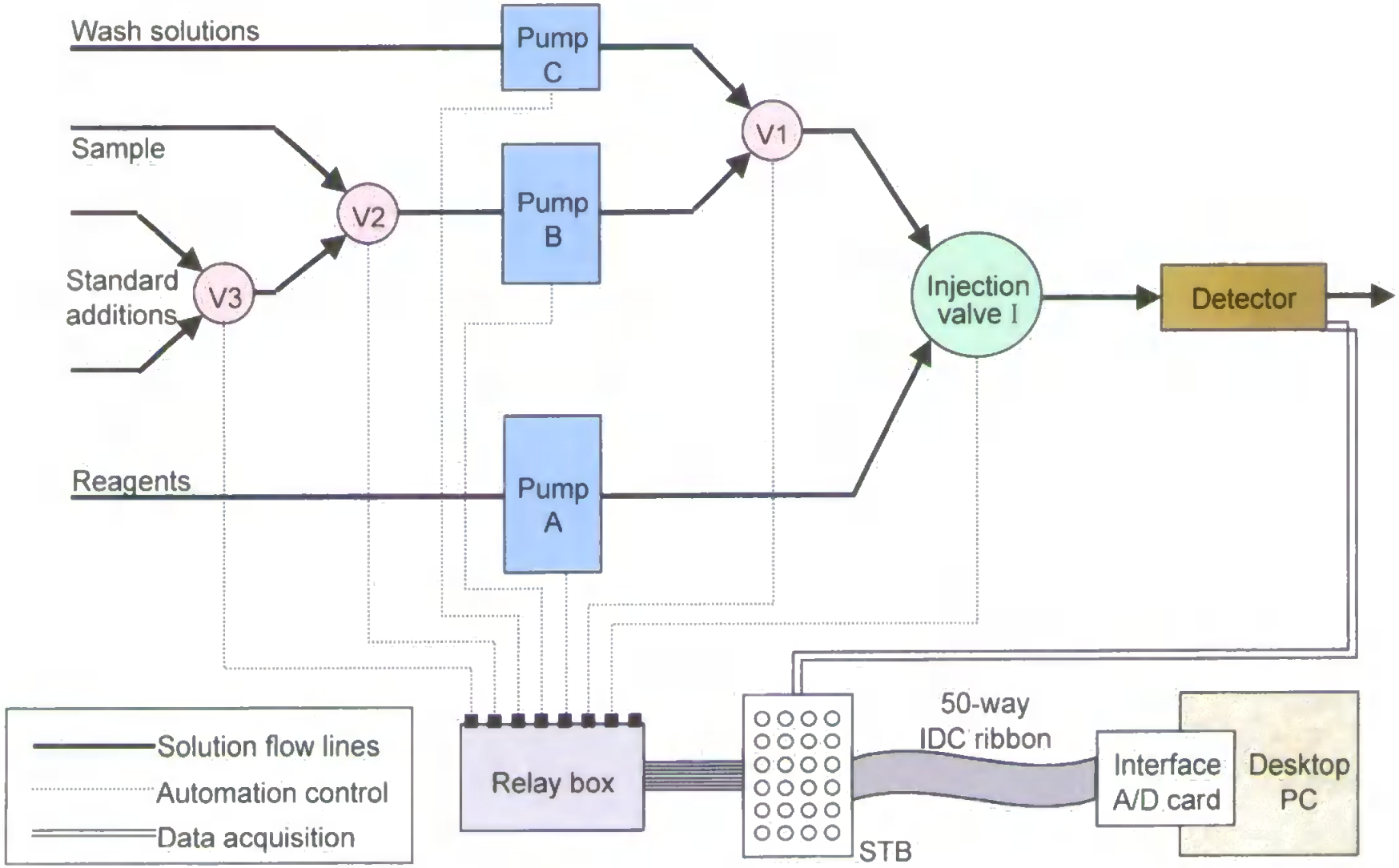

Figure II.12. Diagram showing movement of solutions and input / output communications links in the FI manifold; STB=screw terminal board

II.4.1 PC Interface Card

A 12 bit analogue interface device control and data acquisition card (Brainboxes®, model PC AD 1211L) housed in a desktop PC (Viglen 486 DX-66) was used to control the FI monitor. The full specifications of the A/D card are given in Table II.4.

Model	*PC AD1211L*
Analogue Input	12 bit
Channels type (jumper selectable)	16 single ended OR 8 differential OR 16 pseudo differential
Channels select	Programmable
Bipolar input	±10 V, ±5 V, ±2.5 V
Unipolar input	0-10 V, 0-5 V
INTERRUPTS	
A/D done IRQs	Yes
Analogue Output	Two 12 bit DACs
Bipolar output	±10 V, ±5 V, ±2.5 V
Unipolar output	0-10 V, 0-5 V
Throughput	100 kHz per DAC
DIGITAL I/O	
TTL output	8 bit
TTL input	8 bit
Throughput	1 MHz
Pacer Clock	0.005 Hz – 600 kHz
External clock	Yes (to 1 MHz)
External trigger	Yes (-ve edge)
A/D throughput	30 kHz
Programmable Gain Input	1-10-100-1000 (low level)
DMA Capabilities	None

Table II.4. Brainboxes® PC AD1211L technical specifications

An analogue screw terminal board (STB, Brainboxes®) was used to access the input / output lines of the AD1211 card. Terminals on the board are logically grouped according to one of four distinct functions (Figure II.13). The analogue STB provided 85 screw terminals, each of which accepted 0.6 mm cable (RS Components) from a relay box (Section II.4.3). A standard

50-way IDC ribbon cable was used to enable direct connection from the A/D card in the PC to the screw terminal board.

AD Chan 0	1	2	Ch8 / Ch0 Rtn
AD Chan 1	3	4	Ch9 / Ch1 Rtn
AD Chan 2	5	6	Ch10 / Ch2 Rtn
AD Chan 3	7	8	Ch11 / Ch3 Rtn
AD Chan 4	9	10	Ch12 / Ch4 Rtn
AD Chan 5	11	12	Ch13 / Ch5 Rtn
AD Chan 6	13	14	Ch14 / Ch6 Rtn
AD Chan 7	15	16	Ch15 / Ch7 Rtn
Analog Gnd	17	18	Amp Low
+12 V Out	19	20	-12 V Out
Power Gnd	21	22	DAC0 Output
DAC0 Gnd	23	24	DAC1 Output
DAC1 Gnd	25	26	Digital Gnd
Digital Gnd	27	28	Dig Input 0
Dig Input 1	29	30	Dig Input 2
Dig Input 3	31	32	Digital Gnd
Dig Input 4	33	34	Dig Input 5
Dig Input 6	35	36	Dig Input 7
Digital Gnd	37	38	Dig Output 0
Dig Output 1	39	40	Dig Output 2
Dig Output 3	41	42	Digital Gnd
Dig Output 4	43	44	Dig Output 5
Dig Output 6	45	46	Dig Output 7
Digital Gnd	47	48	Digital Gnd
Ext Trig In	49	50	Ext Clk In

Figure II.13. Pinout connections from the PC AD1211L card via the screw terminal board

II.4.2 Relay Box

The A/D card provided 8 bits of TTL output. Each bit was used to control one component of the FI manifold, each component being capable of accepting differing voltage input signals (Table II.5). Therefore, a relay box containing an integrated circuit of five Darlington pairs (Figure II.14) was constructed in-house as an interface between the PC and FI components, in order to convert the TTL voltage signals into either 12 VDC or mains 240 V for the switching valves and Ismatec peristaltic pumps, respectively. A schematic diagram of the relax box i/o connections is shown in Figure II.15.

Component	*Model*	*Input signal*	*Hexadecimal code*
Peristaltic pump	Gilson Minipuls 3	TTL direct	0 ON 1 OFF
	Ismatec Mini S 820	Mains 240 V	16 ON
	Ismatec FIXO 4/820	Mains 240 V	8 ON
Injection valve	Rheodyne 5020 (via Universal Valve Switching Module, Anachem)	TTL direct	2 SWITCH POSITION
3-way switching valves	Cole Palmer E-01367-72	12 VDC	128 Valve1 ON 64 Valve2 ON 32 Valve3 ON

Table II.5. Type of input signal required for remote operation of FI components

II.4.3 Software Design

II.4.3.1 Operating Code

Software routines for the PC AD1211L card were written in Microsoft™ Quick BASIC version 4.5, and were operated through a Windows 3.1 environment. The Quick BASIC code was designed around a sample program, "Quanta", supplied by the manufacturer (Brainboxes®). A total of 14 different routines were composed, each corresponding to a specific sequence of operations of the FI manifold (Table II.6). Each operating routine was initiated by selection of the appropriate icon from an "Iron FI-CL Operating System" window (Figure II.16).

II.4.3.2 Driver Files

Three files, present in the Quick BASIC sub-directory, were required to integrate the software routines with Quick BASIC.

- **AD1200Q.QLB**

  Quick Library. This provides access to the full range of Quanta driver routines from within the Quick BASIC environment.

- **AD1200Q.LIB**

  Quanta Medium Model Library with calling conventions suitable for Quick BASIC. This contains all the Quanta Driver routines for use when compiling stand alone .EXE files and when compiling from the DOS command line.

- **AD1200.INC**

  Include file defining the syntax and parameters for each of the Quanta routines contained in the AD1200Q.QLB and the AD1200Q.LIB libraries. The information in the include files also provides the on-line help.

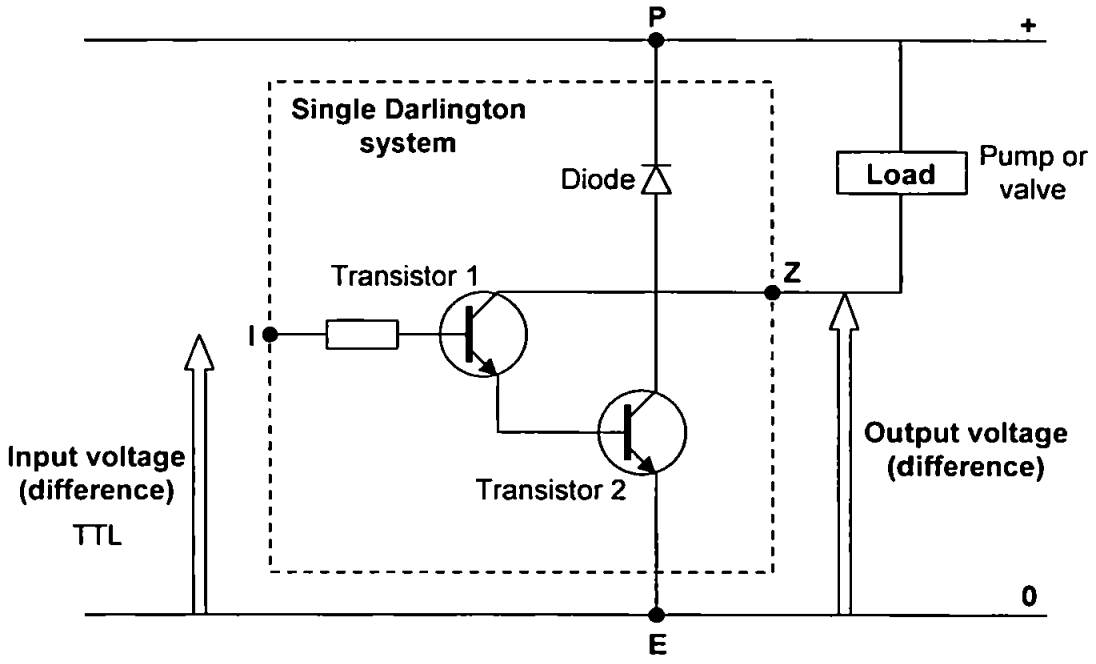

Figure II.14. A single Darlington pair system designed for controlling currents generated during the step-up conversion of TTL signals into 12 and 240 V (I = input; Z = output; P = positive; E = earth)

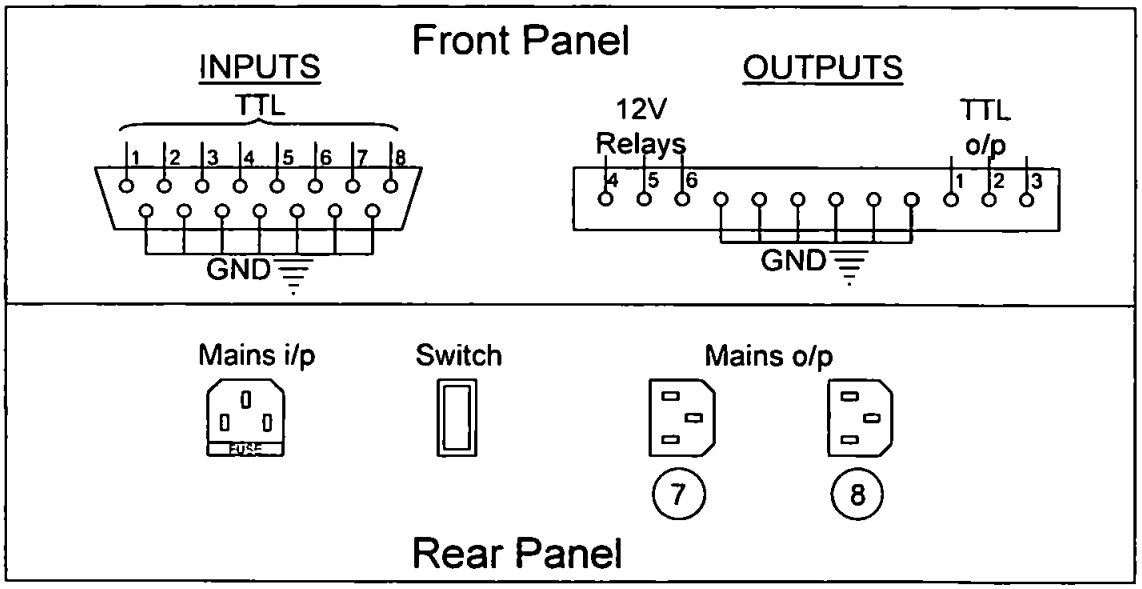

Figure II.15. Input and output connections on the relay box

Operation Name	*Description*	*Execution Filename*	*QBASIC Code Filename*
STOP FI-CL SYSTEM	Switches OFF all instrumentation and stops flows	STOP.exe	QB_STOP.bat
REAGENT PUMP (60 S)	Switches reagents pump ON for a 60 s period	RGNTS1.exe	QB_RGNT1.bat
WASH PUMP (60 S)	Switches wash pump ON (UHP water / acid) for a 60 s period	WASH1.exe	QB_WSH1.bat
WASH PUMP (120 S)	Switches wash pump ON (UHP water / acid) for a 120 s period	WASH2.exe	QB_WSH2.bat
COLUMN BLANK	Sequence to determine preconcentration column blank (no loading)	COLBLANK.exe	QB_COLBK.bat
UHP WATER WASH AND ELUTION	Sequence to determine UHP water blank, verify contamination free flow lines and measure baseline noise level (column loading)	WSHELUT.exe	QB_WSHEL.bat
SWITCH INJECTION VALVE	Switches injection valve between load and elute positions	SWCH.exe	QB_SWCH.bat
SIGNAL ONLY	Monitors CL signal without any flow of solutions	SIGNAL.exe	QB_SIG.bat
FLUSH SW_ONLY LINE	Flushes "sample only" flow line with solution	SW_ONLY.exe	QB_SW0.bat
FLUSH SW_1ST LINE	Flushes "sample plus 1st standard addition" flow line with solution	SW_1st.exe	QB_SW1.bat
FLUSH SW_2ND LINE	Flushes "sample plus 2nd standard addition" flow line with solution	SW_2nd.exe	QB_SW2.bat
ANALYSE SW SAMPLE CYCLE	Sequence to analyse seawater sample, including four replicates and two standard additions	ANALY1.exe	QB_ANA1.bat
ANALYSE SW SAMPLE CYCLE (NO SAMPLE EXCHANGE)	Sequence to analyse seawater sample, without any flushing of flow lines from previous analysis	ANALY2.exe	QB_ANA2.bat
ANALYSE SW SAMPLE CYCLE (WITH DATA ACQUISITION)	Sequence to analyse seawater sample, including replicates, standard additions and acquisition of CL signals	CYCLE6.exe	QB_CYL6.bat

Table II.6. Software routines used to control the FI-CL manifold

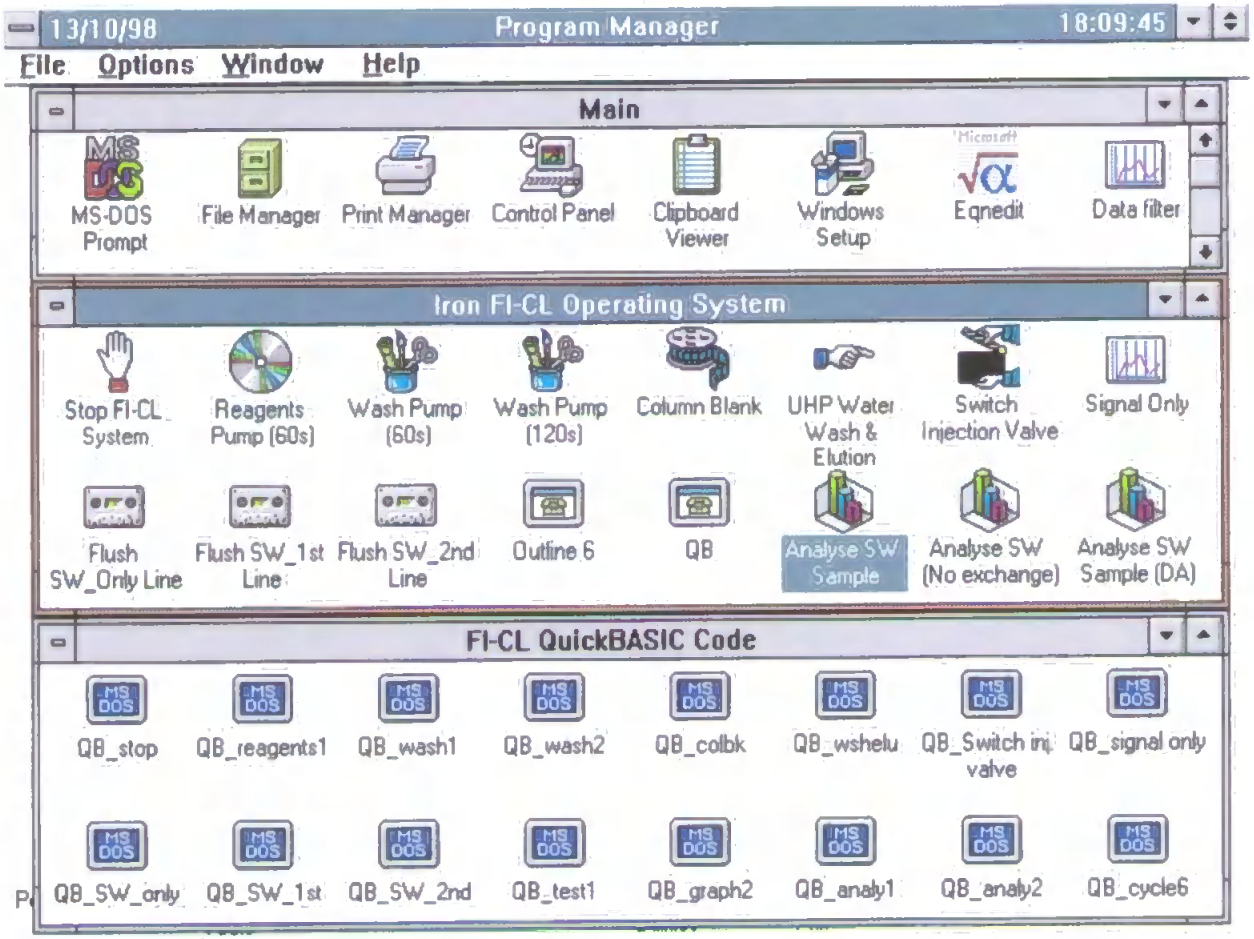

Figure II.16. Screen display of "Iron FI-CL Operating System" icons and associated Quick BASIC code windows; the "Analyse SW Sample" icon is highlighted

II.4.3.3 Compilation

Programs were developed and immediately verified within the Quick BASIC environment. In order to use the Quanta software driver, it was necessary to specify the following syntax on the command line when Quick BASIC was loaded:

- QB ANALY1 /l AD1200Q.QLB

when editing the BASIC program ANALY1, for example. In addition, the beginning of each BASIC program contained a meta command for AD1200 include file library definitions:

- REM $INCLUDE:'AD1200.INC'.

Stand alone .EXE programs were produced from .BAS source code using the pull-down Run menu within the Quick BASIC environment. Quick BASIC compilation invokes the BC command line compiler and the output from this compiler has to be linked with the routines in the AD1200Q.LIB library.

II.4.4 System Operation

Operation and states of FI components during one cycle of the analysis routine ("Analyse SW Sample") is illustrated in Figure II.17 and associated timing parameters and hexadecimal code are shown in Figure II.18. Appendix A contains full, annotated Quick BASIC software code for the "Analyse SW Sample" cycle (Filename: ANALY1.BAS). This software code includes no replicate injections of each sample solution, and the programming subroutines written for initialisation of the screens used for the data acquisition is incorporated.

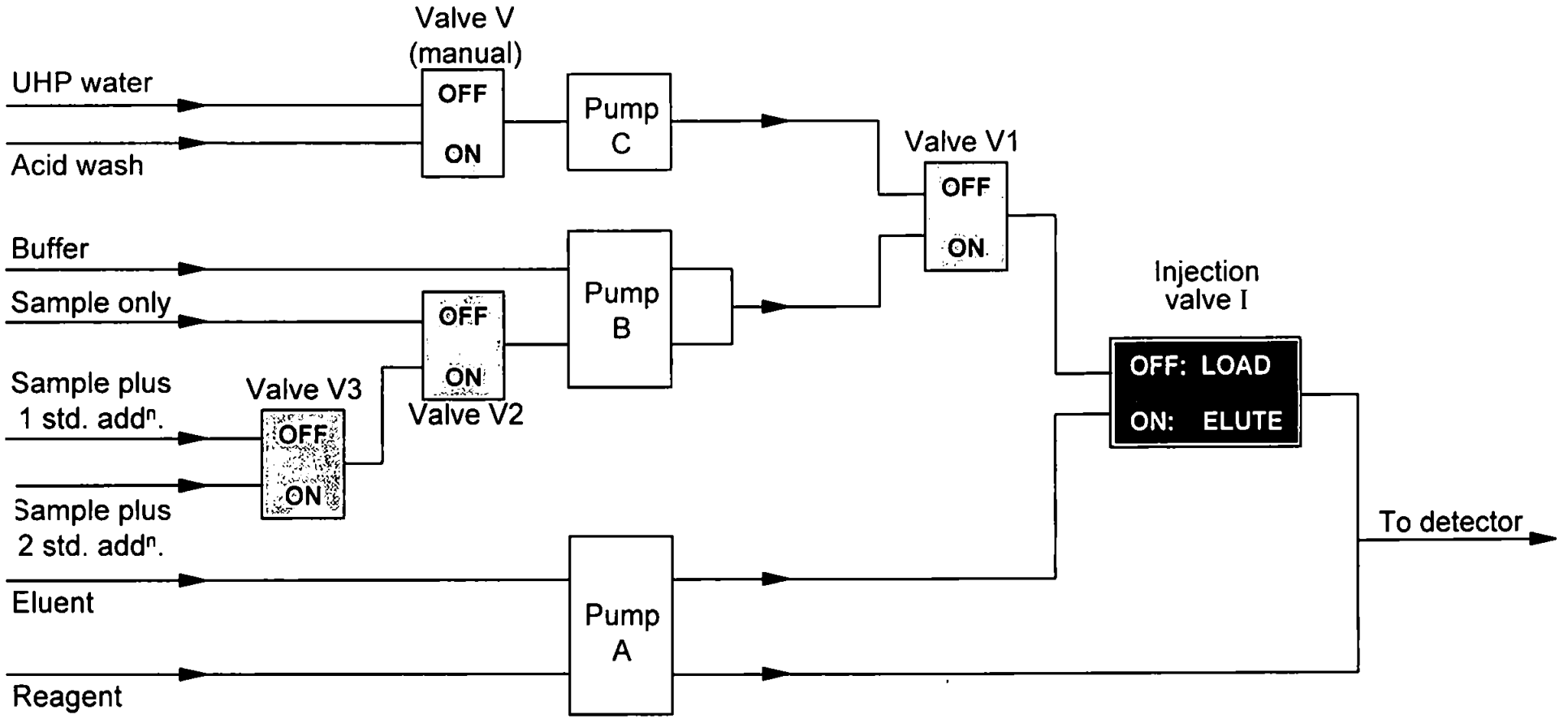

Figure II.17. Logic state of components during analytical cycle

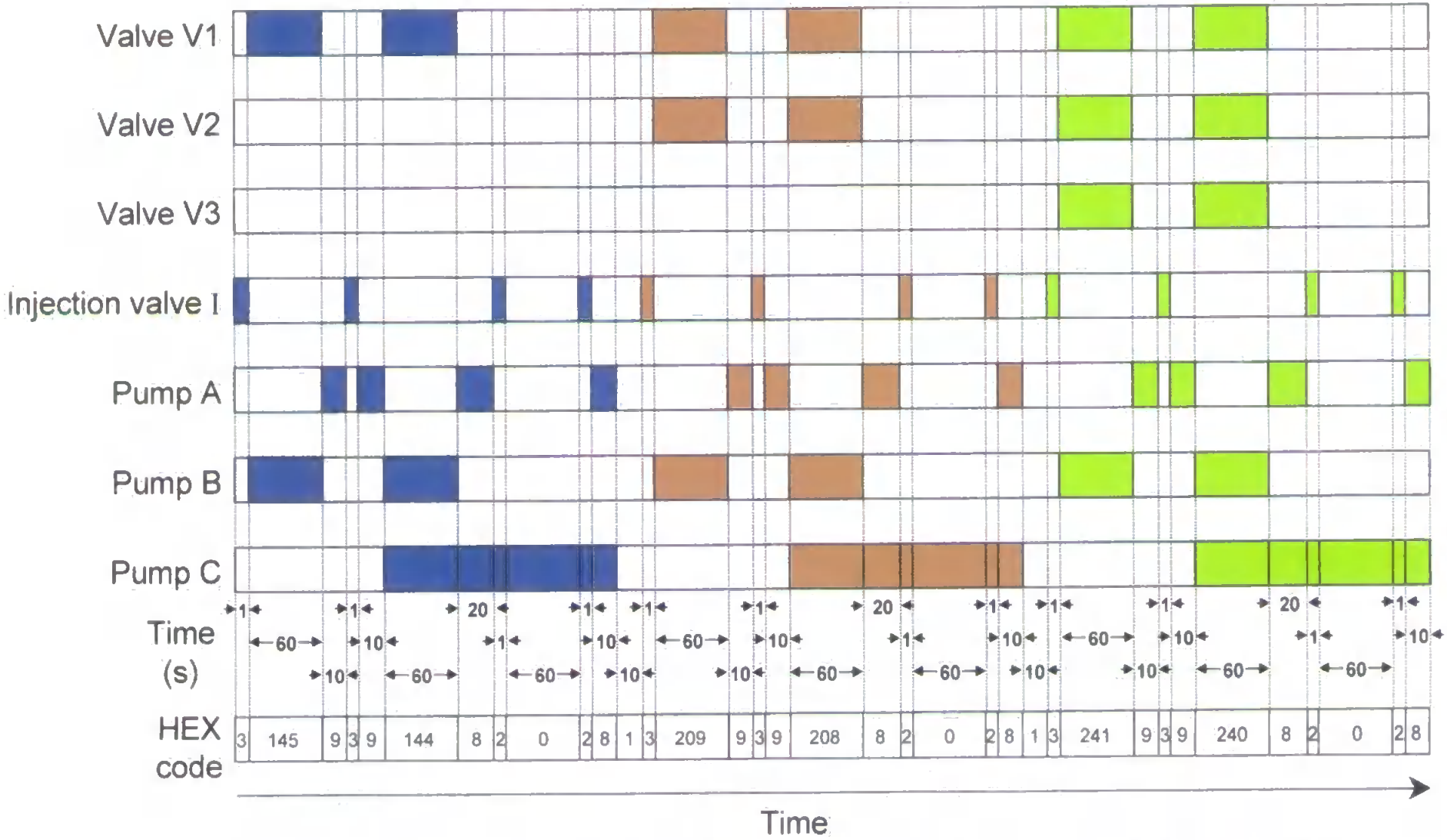

Figure II.18. Timing sequence during one analytical cycle of the FI manifold; no replicate injections of each sample solution are shown

II.5 DATA ACQUISITION

Acquisition of data under computer control provides a general and versatile method for recording data as digital information after conversion using an analogue-to-digital (A/D) card from the analogue photomultiplier input. Information about the timing of signals may also be recorded. The data obtained may be processed numerically immediately and may also be stored as files for subsequent recall and manipulation. The PC AD1211L A/D card possessed 16 single ended or 8 differential input channels of 12-bit analogue-to-digital input. Signals were sent directly from the +ve and –ve outputs of the photomultiplier to the AD Channel 0 and Analogue Ground of the A/D card (via the STB) respectively. All cables were shielded using aluminium foil. The PC A/D card possessed an single channel throughput equivalence of 30 kHz, although the frequency response was mediated at 50 Hz, defined in the software routine running through the Windows operating system.

II.5.1 Software Code

Two software routines were written in Quick BASIC for the acquisition and storage of luminescence signals. The first (filename: SIGNAL.BAS) contained no program code for the automated operation of pumps and valves in the FI system, and was simply used during the development of a data acquisition system. Pumps and valves were manually operated to generate CL signals using the Fe FI manifold. In the second routine (filename: CYCLE6.BAS), the automated analytical cycle routine for Fe determinations was incorporated into the data acquisition code.

II.5.2 Instrumental Development

During development work, a low voltage power supply was used in place of the PMT detector in Figure II.12, in order to simulate variable millivolt signals which would be sent to the A/D card. Successful acquisition of the signals from the low voltage supply was achieved using both the SIGNAL.BAS and CYCLE6.BAS routines (Figure II.19). These signals were stored on disk and subsequently interpreted (peak height, peak area, peak width at half height, elution time) using a data manipulation software package (e.g. WinFAAS).

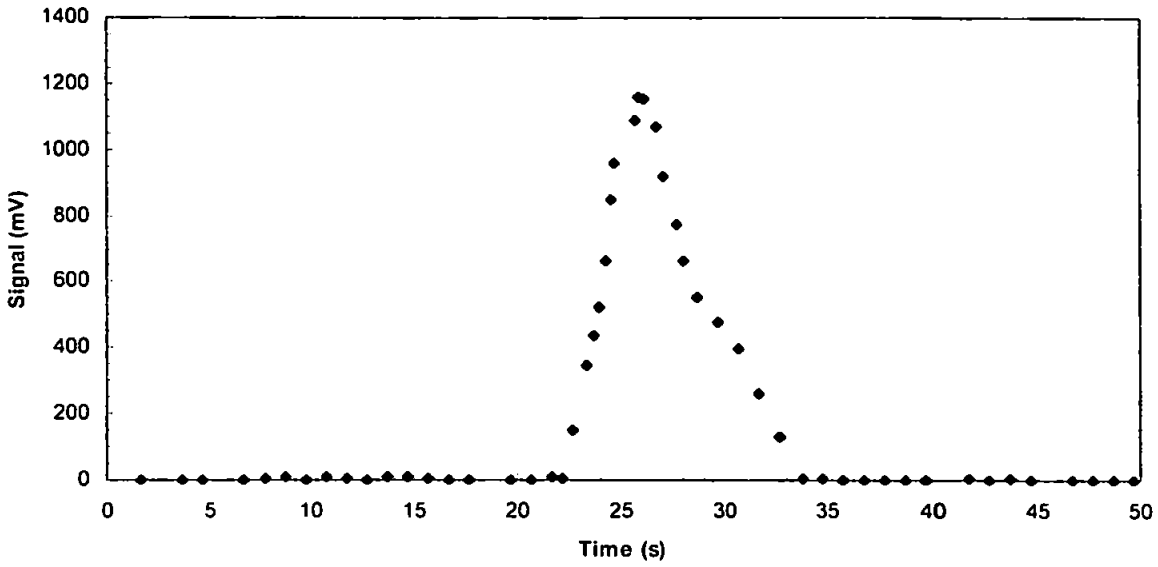

Figure II.19. Voltage signals acquired from a low voltage supply using the A/D card

II.5.3 Problems

For the next series of experiments, the power supply was replaced by the photomultiplier tube of the FI system. However, problems were experienced when attempting to acquire the CL signals generated during an analytical cycle. A noisy baseline was observed containing very large irreproducible spikes, often greater than 500 mV (Figure II.20). Furthermore, on elution of a CL peak, the quantity and magnitude of the spikes increased and a smooth FI peak as measured on a chart recorder was not acquired using the A/D card. The source of these problems was believed to be the photomultiplier tube itself. The unit is powered using a high voltage supply (1.1 kV). Typical CL signals generated during the analysis of Fe in open-ocean seawater by FI-CL are of the order of 100 mV and blank levels and less than 5 mV. Hence, the spikes were thought to be due to stray voltages from the power supply (or feedback from the PMT) interfering with the low voltage signals sent from the PMT to the A/D card. Better shielding on the cabling would help to minimise these spikes. Investigations into the use of data averaging, filtering and transform methods to distinguish between a true CL signal and noise spikes would also help in the acquisition of spectra. Due to time limitations during the course of this work, however, no further attempts were made to resolve these difficulties and signals were monitored using a flat-bed chart recorder. It is envisaged that the new generation of low power photon counting heads (as discussed in Section II.3.2.2), coupled with advanced software and A/D

cards (LabVIEW, NI-DAQ, National Instruments), will simplify the task of acquiring weak light signals using an A/D card.

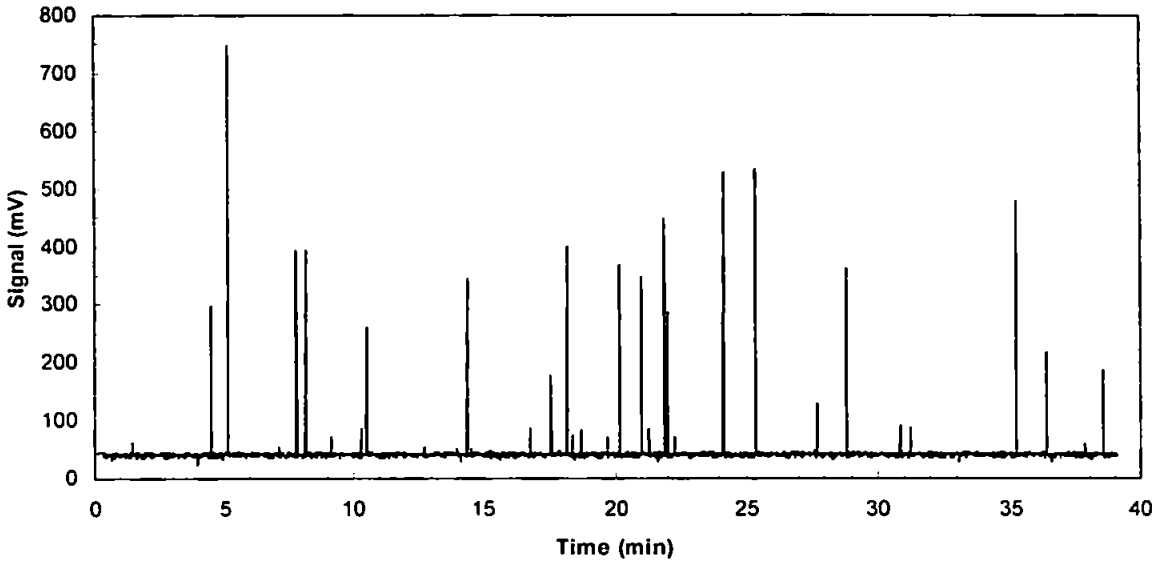

Figure II.20. Example of baseline and noise spikes acquired from the PMT using A/D card during operation of the FI-CL monitor

II.6 CONCLUSIONS

Conclusions from the evaluation of FI instrumentation needed for the shipboard CL-based determination of Fe in seawater are:

1. The use of peristaltic pumps, 0.75 mm i.d. PTFE manifold tubing, 3-way solenoid switching valves and a six port rotary injection valve for the movement of solutions.
2. Optical matching of detection system and CL emission using a spiral quartz glass flow cell mounted in front of a high voltage photomultiplier tube.
3. Laboratory-based use of CCD camera to confirm an intense blue (λ_{max}=410-450 nm) luminol CL emission.
4. Automation of the FI manifold using a commercially available analogue/digital interface card, a transformer relay box and desktop PC running Quick BASIC operated through a Windows 3.1 environment.
5. Acquisition of CL signals using the A/D interface card and data interpretation software; problems due to the inability to measure and differentiate CL peaks from baseline noise spikes have yet to be resolved.

A FLOW INJECTION – CHEMILUMINESCENCE PROCEDURE FOR THE DETERMINATION OF IRON IN SEAWATER

III.1 INTRODUCTION

This chapter describes the optimisation and validation of a flow injection – chemiluminescence (FI-CL) procedure for the determination of Fe in a seawater matrix (Bowie *et al.*, 1998). The principal objective was in the development of an automated, transportable system capable of measuring Fe at sub-nanomolar levels at sea on–board research vessels.

III.2 EXPERIMENTAL

III.2.1 Reagents and Standards

All plasticware was cleaned by first soaking in hot 5% (v/v) micro detergent (DECON®; Merck BDH) for 24 h, followed by 1 week in 50% (v/v) hydrochloric acid (HCl, AnalaR; Merck BDH) and 1 week in 50% (v/v) nitric acid (HNO_3, AnalaR; Merck BDH). Labware was thoroughly rinsed with ultra high purity (UHP) de-ionised water (18.2 MΩ cm^{-1}, Elgastat Maxima). All reagents and standards were of analytical grade, supplied by Merck BDH, unless stated otherwise, and prepared in UHP water.

III.2.1.1 Iron Standards

A 0.01 M Fe(II) standard was prepared by dissolving 0.3921 g of *di*-ammonium ferrous sulphate hexahydrate ($Fe(NH_4)_2(SO_4)_2.6H_2O$) in 100 ml of a 0.1 M quartz sub-boiling distilled hydrochloric acid (Q-HCl) solution. This stock was prepared monthly. Other standards were prepared daily in 0.01 M Q-HCl by serial dilution. Fe(II) standards were pre-purged with nitrogen (N_2) immediately before use to avoid oxidation. Fe(III) working standards were prepared by dilution of a 1000 ppm (17.9 mM) Fe(III) atomic absorption standard solution ($Fe(NO_3)_3.9H_20$) in 0.5 M nitric acid (SpectrosoL). These Fe(III) solutions were prepared in low Fe seawater (LISW; Section III.2.1.8) and kept at pH 8 for at least 1 h to oxidise any Fe(II) present in the stock solution and then acidified to pH 1 with Q-HCl (9 M). These conditions ensured the integrity of the redox state of the Fe standards.

III.2.1.2 Luminol / Carbonate Buffer

A 0.1 M sodium carbonate (Na_2CO_3) buffer was prepared by dissolving 5.3 g in 500 ml of UHP water. A stock solution of ca. 2 M sodium hydroxide (NaOH) was prepared by dissolving 8 g in 100 ml of UHP water. Luminol (5-amino-2,3-dihydro-1,4-phthalazinedione, Fluka) was used as received. A stock solution of luminol (0.01 M) was prepared by dissolving 0.1772 g in 100 ml of Na_2CO_3 followed by sonicating for 30 min. A working luminol reagent solution ($1x10^{-5}$ M) was prepared by diluting 0.5 ml of the stock solution in 500 ml of 0.1 M Na_2CO_3 and adjusting to pH 12.2 with the NaOH solution. This reagent was passed through a column containing the Chelex-100 chelating resin just prior to use in order to reduce the baseline noise generated by trace Fe impurities in the reagents (Section III.2.3.4). On mixing with the HCl eluent stream in the FI manifold, an effluent pH of 10.4 allowed optimum chemiluminescent emission. Luminol solutions provided maximum and stable sensitivity after a storage period of 24 h and therefore were prepared a minimum of 1 day in advance (Section III.3.2.3). Luminol solutions were stable for at least 1 month.

III.2.1.3 Acids / Ammonia

Purified hydrochloric acid (Q-HCl, 9 M) and purified acetic acid (Q-acetic acid, 17.5 M) were prepared by a single distillation of the analytical grade acids in a quartz-finger, sub-boiling distillation apparatus (Section III.2.3.1). An ammonia solution (Q-NH_3, ca. 6 M) was purified using isothermal distillation (Section III.2.3.2) and nitric acid (HNO_3, Aristar; Merck BDH, 15.5 M) was used as received.

III.2.1.4 Ammonium Acetate Buffer

Ammonium acetate (NH_4-O-Ac) stock solution (2 M) was prepared by adding 22.2 ml of Q-acetic acid to 90 ml of Q-ammonia solution and diluting to 200 ml with UHP water. A working sample buffer (0.4 M) for in-line pH adjustment of the sample was prepared by diluting 20 ml stock to 100 ml with UHP water, and adjusting to pH 5.5 with Q-acetic acid. In the FI manifold, this buffer was cleaned in-line using two 8-HQ columns (Section III.2.3.3) in series.

III.2.1.5 Reducing Reagent

A stock solution (0.04 M) of reducing reagent for Fe(III) was prepared by dissolving 0.1008 g of sodium sulphite (Na_2SO_3, S(IV), extra pure; Merck BDH) in 15 ml of UHP water, adding 5 ml of 0.4 M NH_4-O-Ac buffer (pH 5.5) and sonicating for 10 min. This stock reagent was cleaned by passing the solution through two sequential 8-HQ columns (Section III.2.3.3) just prior to use. 2.5 µl aliquots were added per ml of acidified seawater to achieve a final sulphite concentration of 100 µM in the sample. The reducing reagent was allowed to react with the acidified sample for at least 8 h.

III.2.1.6 HCl Carrier

The eluent solution (0.09 M) was prepared by diluting 5 ml of Q-HCl (9 M) to 500 ml with UHP water.

III.2.1.7 Acid Wash

An acid wash solution (0.6 M Q-HCl / 0.16 M HNO_3) was prepared by diluting 7 ml of Q-HCl (9 M) and 1 ml of HNO_3 (15.5 M) to 100 ml with UHP water.

III.2.1.8 Low Iron Seawater (LISW)

Seawater used to optimise the FI-CL manifold and perform matrix interference experiments was collected from the English Channel (near Eddystone Rocks) in a 20 l high density polyethylene (HDPE) container. After a 2 month storage period, it was transferred to a 10 l HDPE container and acidified to pH 2 using Q-HCl. The seawater was then buffered to pH 5 via the addition of 2.5 ml of 2 M NH_4-O-Ac buffer (pH 5.5) per 100 ml of seawater. The water was passed through two sequential 8-HQ columns (Section III.2.3.3) at ca. 1 ml min^{-1} in order to remove Fe from the matrix. The eluent seawater was once again acidified to pH 2 with Q-HCl and stored in the dark.

III.2.2 Clean Techniques

Contamination of samples and reagents by aerosol particles is a severe problem in ultratrace analysis. The analysis of Fe requires strict protocols in order to avoid contamination which may result in erroneous results. All measurements required patience and careful monitoring of FI-CL signals generated during operation. Wherever possible, experimental work was carried out in a class-100 laminar flow bench (Bassaire model A3VB) contained in a class-1000 clean air room. Special body suits (Tyvek®) and poly-latex boots were worn at all times in the clean room, and all sample and reagent handling was carried out with the user wearing polythene gloves. Samples and reagents bottles and flasks were always closed and doubly sealed within plastic bags, except when solutions were being manipulated. For shipboard analyses, reagents and samples were contained within a sealed perspex cabinet unit (350 x 345 x 380 mm), and PTFE tubing was used to transfer the solutions to the FI analyser which was positioned in the ship's laboratory.

III.2.3 Reagent Clean-up Procedures

The success of trace analysis procedures is dependent on the purity of the reagents. Certain commercially available chemicals were found to contain quantities of Fe impurities which may adversely affect the analytical figures of merit of the method and prevent accurate determinations at very low Fe concentrations. Furthermore, the mixing of the two reagent streams in front of the PMT end-window generated a continuous background CL emission. This was due to trace levels of Fe present in either the buffered luminol CL reagent or the acid eluent. An elevated background would seriously degrade the detection limit of the technique. Four reagent clean-up procedures were therefore employed. The resulting molarity of acid and ammonia solutions which were purified using distillation methods was ascertained through standard titration techniques.

III.2.3.1 Quartz Sub-boiling Distillation Still

A quartz finger, sub-boiling distillation still was utilised for the purification of the following materials: hydrochloric acid, nitric acid and acetic acid (Howard and Statham, 1993). A

schematic diagram of the still is shown in Figure III.1. Commercially available HCl (11.3M), HNO_3 (15.5M) and acetic acid (17.5M) (all AnalaR, Merck BDH) were each cleaned using the distillation still. The stock acids were introduced into the unit until the surface of the liquid touched the rim of the outlet tube. The purification is based upon the vaporisation of the liquid by radiative heating of the surface of the liquid to prevent boiling. The violent boiling action typical of a conventional distillation apparatus leads to a significant carry-over of raw solvent with the distillate. The surface evaporation process does not generate such a spray or droplets and the condensate is therefore of higher purity.

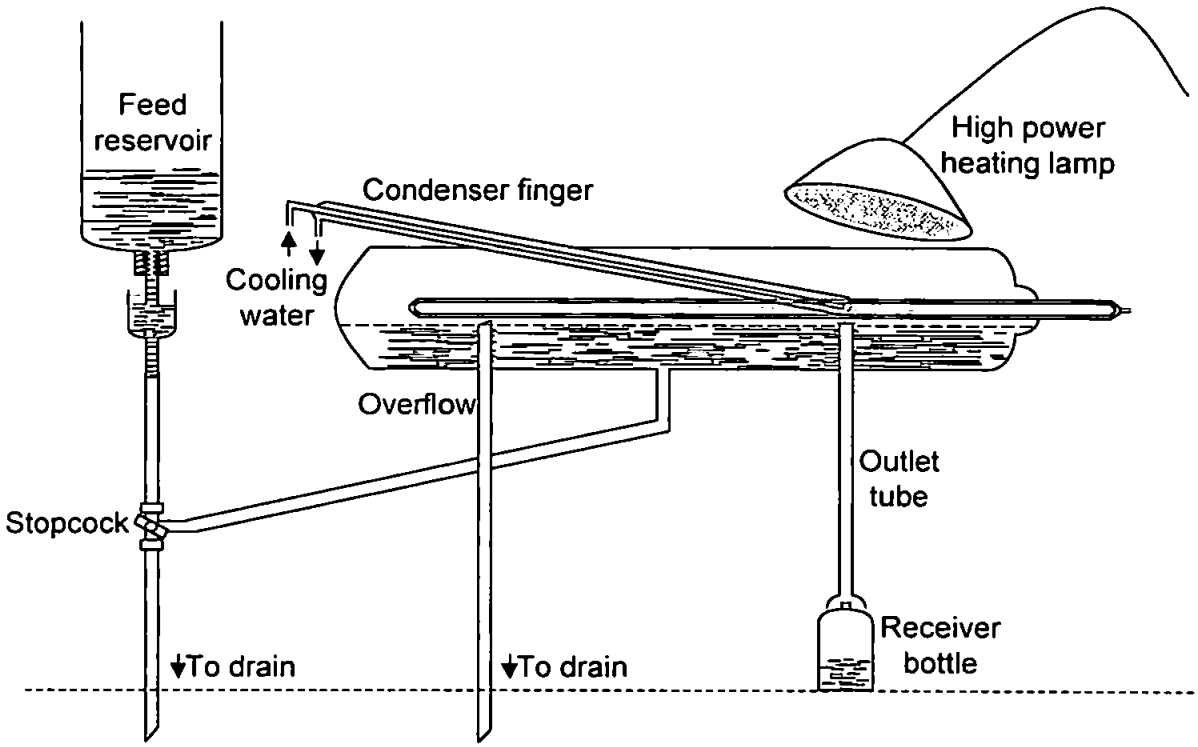

Figure III.1. Schematic diagram of apparatus for sub-boiling distillation

Heating was carried out by means of a high power infra-red lamp (250 W), directed onto the surface of the liquid. Care was taken to prevent the stock acids from becoming too hot and starting to boil. An inclined, water cooled cold finger condensed the acid vapour and led the condensate into a pre-cleaned collecting bottle outside the still. A constant head device was used to feed the still reservoir, which was periodically flushed with fresh acid to prevent the build-up of contaminants. The distillation still was in continual operation and the typical rate for

purification of hydrochloric acid was 250 ml d^{-1}. Titration of the purified acids resulted in concentrations of Q-HCl (9.2 M), Q-HNO_3 (~12 M) and Q-acetic acid (~17 M).

III.2.3.2 Isothermal Distillation

Isothermal (or isopiestic) distillation is a very simple procedure suitable for materials (e.g. ammonia) which possess a high vapour pressure at room temperature. High purity NH_4OH was prepared from 30% NH_4OH (specific gravity 0.88, AnalaR, Merck BDH) by isothermal distillation. As illustrated in Figure III.2, two wide-mouth 1 l HDPE bottles each containing ca. 800 ml of UHP water were placed in a 5 l wide mouth keg containing ca. 2.5 l of the analytical grade ammonia solution. The keg was sealed and left for 5 days at room temperature, with a single daily stir, allowing the ammonia to equilibrate between the two aqueous solutions. During this period, the ammonia transfers to the UHP water, leaving the involatile trace elements behind and generating a high purity ammonia solution (ca. 5-6 M).

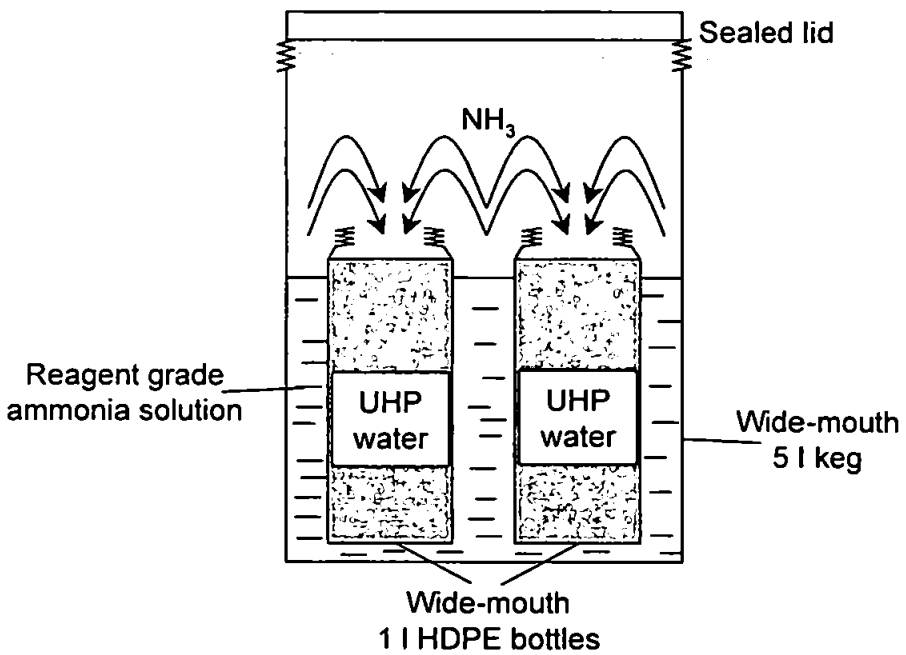

Figure III.2. Purification of ammonia solution by isothermal distillation

III.2.3.3 8-Hydroxyquinoline Micro-column

The chelating properties of 8-hydroxyquinoline (8-HQ) and its preference for transition and heavy metal cations (e.g. Fe, Co, Mn, Cu, Al, Zn, Cd, Ni, Pb) relative to alkali and alkaline earth

metals has been previously reported (Landing *et al.*, 1986; Nickson *et al.*, 1995). A chelating resin of 8-HQ immobilised on a hydrophilic vinyl co-polymer (TSK gel, Toyopearl HW-75F, 30-60 micron, fine, TosoHaas Co., supplied through Anachem) was prepared according to a modified procedure of Landing *et al.* (1986; and subsequent personal communication, 1996), described in full in Section III.3.4. The micro-columns were constructed from 2.4 mm i.d. PTFE tubing, as illustrated in Figure III.3. The column ends were fabricated using 0.89 mm i.d. Tygon pump tubing, which was connected to the 0.75 mm i.d. PTFE manifold tubing. A plug of quartz wool was placed at either end in order to retain the resin inside the column. The columns were cleaned with 0.5 M Q-HCl for at least 4 h, followed by UHP water for 24 h prior to use.

Two successive 8-HQ columns were used for in-line purification of the 0.4 M NH_4-O-Ac sample buffer with a flow rate of 0.2 ml min^{-1}. The Fe(III) reducing reagent was also cleaned using the 8-HQ resin prior to analysis. 0.04 M S(IV) was buffered to pH 5.5 via the addition of 5 ml of 0.4 M NH_4-O-Ac buffer per 20 ml reducing reagent, and the resulting solution passed through two 8-HQ columns at a rate of 0.7 ml min^{-1}.

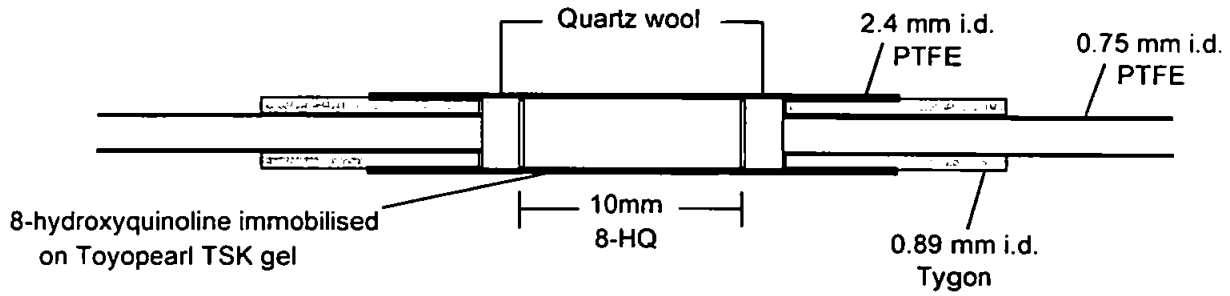

Figure III.3. Micro-column containing 8-HQ resin used for sample reagent purification

III.2.3.4 Chelex-100 Column

Chelex-100 is a macroporous polystyrene divinylbenzene polymer containing paired iminodiacetic acid (IDA, Figure III.4) ions, which act as chelating groups in binding polyvalent metal ions. The main advantage is its selectivity for polyvalent metals over commonly occurring monovalent cations, such as alkali metals Na^+ and K^+. The material is therefore widely used in applications which involve removing or concentrating trace metals in natural waters (Riley and

Taylor, 1968). The quantity of metal cations retained is a function of pH. Below pH 2, the resin acts as an ion exchanger and no metals cations are chelated; conversely, effective adsorption occurs in the pH range 4 - 14, when the metal cations replace an equivalent amount of resin cations, e.g. NH_4^+. The most effective eluting agents are mineral acids.

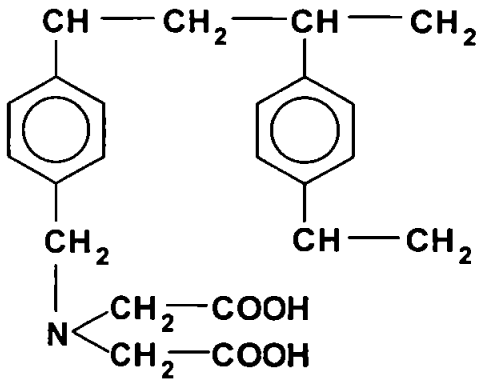

Figure III.4. Structure of iminodiacetic acid (IDA)

Chelex-100 possesses better stability than 8-hydroxyquinoline resins at high pH, despite its tendency to swell. Furthermore, large volumes of buffered luminol CL reagent need to be purified and because of the limited capacity of the 8-HQ columns, the iminodiacetic acid chelating column was chosen for the clean-up of the luminol / Na_2CO_3 / NaOH reagent. The Chelex-100 column, illustrated in Figure III.5, was prepared as follows. A glass column (12 mm i.d., 380 mm length) was soaked in hot 5% (v/v) micro detergent (DECON®; Merck BDH) for 24 h, followed by 24 h in 10% (v/v) hydrochloric acid (AnalaR; Merck BDH) and thoroughly rinsed with UHP water. The lower end of the column was plugged with quartz wool. Chelex-100 resin (ligand: iminodiacetic acid, sodium form, 50 - 100 mesh, Sigma) was poured into the column until a depth of ca. 80 mm was achieved. The resin was washed with 3 x 50 ml 10 % (v/v) HCl followed by UHP water until the effluent was neutral, and then with 50ml 10 % (v/v) ammonia solution (to convert the resin into its ammonium form) followed by UHP water until the effluent was neutral. Approximately 250 ml of the luminol reagent solution was passed through the column, the initial 50 ml being discarded. After reagent clean-up, the resin was

re-conditioned using ca. 50 ml of 10 % (v/v) HCl, followed by ca. 200 ml UHP water until the effluent was once again neutral. No deterioration in the performance of the column was found over a continuous usage period of one month.

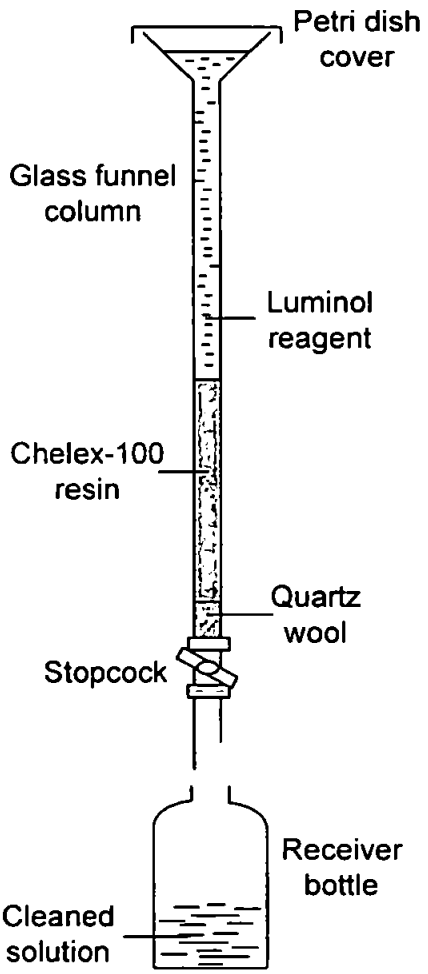

Figure III.5. Chelex-100 column used for clean-up of luminol / Na_2CO_3 CL reagent

III.2.4 Instrumentation

A detailed description of the individual components of the FI-CL system is contained in Chapter 2. Figure III.6 shows a schematic manifold of the assembled FI-CL monitor. Three peristaltic pumps (Pump A: Ismatec FIXO 4/820, Pump B: Ismatec Mini-S 820, Pump C: Gilson Minipuls 3) were used to deliver the wash solutions, sample / buffer and reagents solutions, respectively, to the injection valve, preconcentration column and CL detector. All manifold tubing was PTFE (0.75 mm i.d., Fisher) except for the peristaltic pump tubing, which

was flow-rated PVC ("Accu-rated", Elkay) and the 8-HQ columns. A six-port rotary injection valve (Rheodyne, model 5020, HPLC technology) operated by a Universal Valve Switching Module (Anachem) was used to transport the sample to the detector. Three 3-way PTFE solenoid switching valves V1, V2 & V3 (Cole Palmer, model E-01367-72) enabled sample, sample plus standard addition(s), UHP water and acid wash solutions to pass sequentially through the 8-HQ preconcentration column. The load, wash and inject cycles of the FI monitor were computer controlled using a device control and data acquisition card (Brainboxes, model PC AD 1211L) housed in a PC (Viglen 486 DX-66).

A quartz glass spiral flow cell C (1.1 mm i.d., 130 µl internal volume) positioned behind a mirror in a light-tight housing enabled the CL reaction to be monitored. The detection system consisted of an end-window photomultiplier tube (Thorn EMI, 9789QA) contained in a µ-metal shield for magnetic insulation (MS52D), a built-in current-to-voltage amplifier (C634, setting "C", x100), an ambient temperature rf shielded housing (B2F/RFI) and a 1.1 kV power supply (Thorn EMI, PM28B). The amplifier was supplied with 15 V from an independent power supply (BBH products). Once powered, the PMT detection system remained switched on and took <1 h to stabilise and give low dark current and voltage signals. Peak detection and quantification was achieved using a flat-bed chart recorder (Kipp and Zonen, BD111).

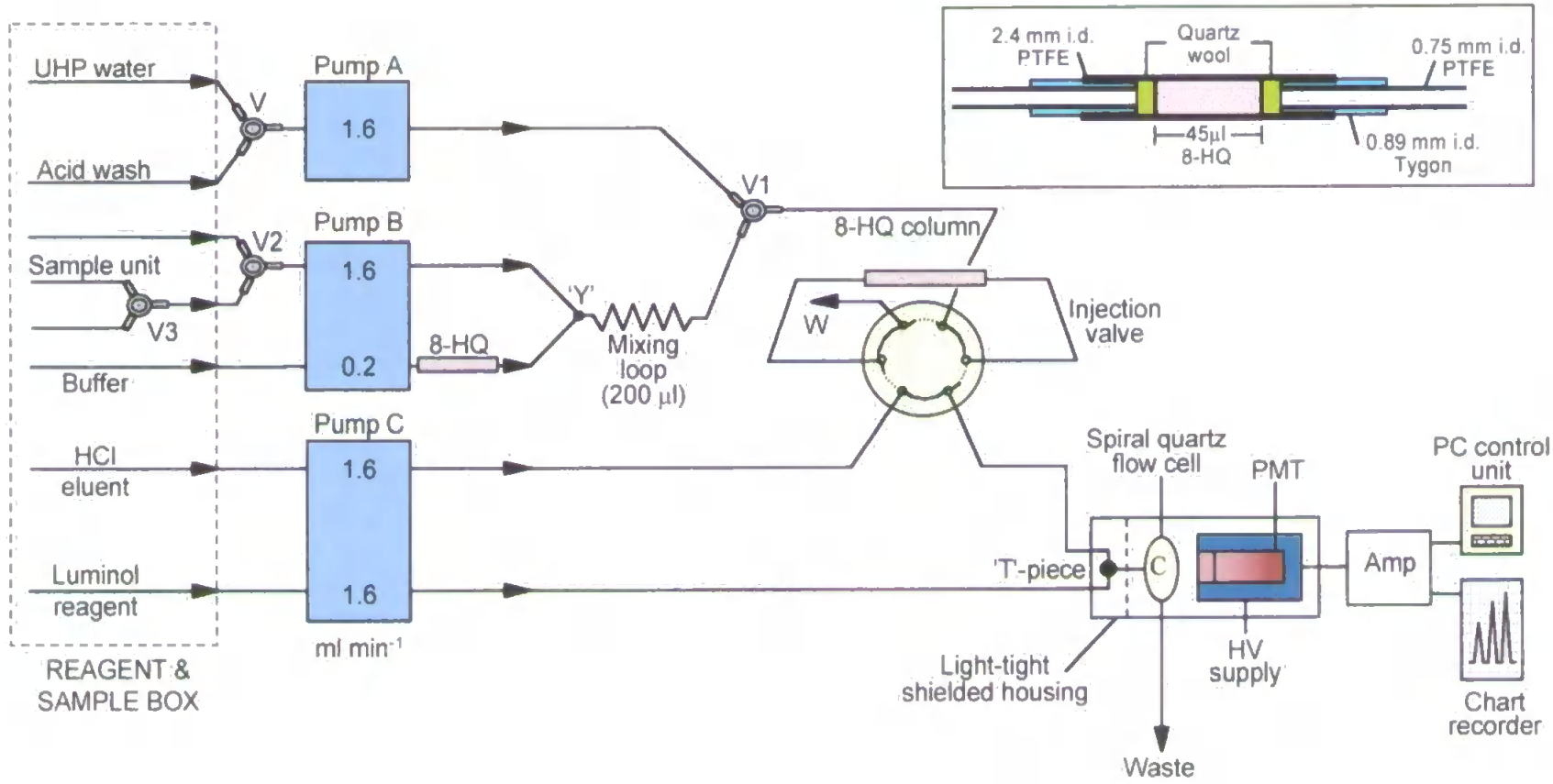

Figure III.6. Flow injection manifold used for the chemiluminescence based determination of Fe in seawater; inset shows expanded structure of column
PMT = photomultiplier tube, C = flow cell, V1, V2 and V3 = switching valves, A = wash pump, B = sample pump, A = reagents pump

III.2.5 Standard Procedures

The CL detection system remained on throughout method development and shipboard analyses. After the stabilisation period, the PMT and amplifier gave low dark current (0.16 nA, quoted by Thorn EMI) and dark voltage (<0.1 mV) signals. Background electronic noise was minimised using high quality leads and a low noise PMT and was typically 0.04 mV (peak-to-peak). Reagent solutions and the FI-CL system were kept at 20 °C in the clean air laboratory in order to prevent the generation of air bubbles in the FI tubing and to maintain a steady baseline from the PMT detection unit.

Injection of a Fe(II) standard or spiked sample into the FI-CL resulted in a sharp, repeatable CL peak superimposed on the background CL emission. The signals were sent to a flat-bed chart recorder and the peaks measured manually with a ruler. For each standard or sample, four replicates were obtained and the average, standard deviation and other statistical measurements calculated using an Excel 7.0 spreadsheet (see Figure V.8).

Due to the nature of the analytical method, it is imperative to ensure high accuracy and precision in the preparation of reagent, standard and sample solutions. High precision variable volume micropipettes (Eppendorf Research 3110; 10-100 µl, 100-1000 µl and 500-5000 µl) were used throughout the work. These pipettes contain a ceramic piston and possess a minimum of metallic parts. They were regularly re-calibrated using a five-figure analytical balance (Sartorius A 200 S). A unique pipette tip was retained exclusively for each solution, stored in 25 ml sterilin vials or plastic bags and changed if memory effects were noted or if the volume setting was adjusted. pH measurements were performed on a HANNA Instruments HI 9021 meter, calibrated in the pH 4-7 or pH 7–10 ranges using standard buffer solutions (Colourkey, BDH Merck), as required.

Prior to use, the FI manifold, the PTFE flow lines, fittings and connectors were cleaned with 0.5 M Q-HCl and UHP water for several hours. The pump tubing was suitable for one week of near continuous shipboard analyses, after which all channels were changed. Over a one month

cruise period, the use of one 8-HQ resin column for preconcentration of Fe from open-ocean seawater showed no deterioration in performance or reduction in chelating ability.

The accuracy of the FI-CL measurements was ascertained by analysing seawater certified reference materials (NASS-4, CASS-2, National Research Council of Canada, Marine Analytical Chemistry Standards Programme) during method development and shipboard analyses. Furthermore, a contamination check was regularly made by re-analysis of Fe in a South Atlantic reference seawater sample, which had previously been found to contain 0.72 ± 0.09 nM (n=5). To verify the flow tubes were free from contamination and the CL reagents generated a low, steady baseline noise, a simple UHP water wash and elution cycle was employed at regular period during the analysis, as outlined in Table II.6. The Fe content in the sample reagents was confirmed *via* the addition of 2 or 3 times the normal reagent concentrations to a UHP water blank.

III.2.6 Blank Procedures

The analytical blank for a calibration curve is defined as: "the signal generated by a solution containing no deliberately added analyte, but containing the sample reagent additions as the other test samples and also subjected to exactly the same sequence of analytical procedures" (Miller and Miller, 1993). All seawater samples were analysed by the method of standard additions. This technique relies in principle on a blank solution giving zero signal at zero Fe concentration. Despite the stringent reagent clean-up procedures described above, it was not possible to obtain a blank solution that contained no residual Fe. Furthermore, UHP water was found to contain a low Fe content (ca. 150 pM), even after 8-HQ column clean-up procedures. Therefore, to obtain a reliable blank level, two solutions were prepared:

BLANK B1: 100 μM S(IV) in UHP water (20 ml)

BLANK B2: 0.01 M Q-HCl + 200 μM S(IV) in UHP water (20 ml).

Hence, by subtraction, B2 – B1 gives the CL signal generated by any residual Fe in the reagents which are added to a seawater sample. This value should be subtracted from the signal generated by each sample or sample plus standard addition solution to give a resulting accurate standard additions calibration line. Typical Fe contributions to blank levels from each of the sample reagents, as measured by shipboard FI-CL, were as follows:

BLANK B1: 170 pM

BLANK B2: 350 pM

$\therefore$ B2 – B1: 180 pM

NH_4OAc buffer: 12 pM

It should be noted that the NH_4OAc sample buffer contribution was deemed negligible.

III.2.7 Operating Procedures

A schematic flow chart showing the analytical procedure used for the determination of Fe in seawater by FI-CL is given in Figure III.7. One analytical cycle was completed in 2 min 42 s. Firstly, the seawater sample was flushed through the manifold for 60 s to remove the previous solution from the flow lines. The seawater was next pumped through the sample line where it was buffered in-line to pH 5.0 as it passed through the 0.45 m (200 µl) knitted mixing coil. The combined flow then passed through the 8-HQ column at a rate of 1.8 ml min^{-1} for typically 60 s, during which time the Fe was preconcentrated from its sea-salt matrix. Longer load times could be used to increase the sensitivity of the system. By switching the solenoid valve V3, UHP water was subsequently passed through the column (20 s) to remove any residual sea-salt matrix ions present. The injection valve was then switched to the elute position and 0.09 M Q-HCl flowed through the column in a reverse direction (60 s) carrying the Fe to the detection system where it mixed with the buffered reagent stream and generated a CL peak. The injection valve was then returned to the load position and washed with UHP water (20 s) to remove residual hydrochloric acid before the next load sequence commenced. The analysis of one sample in triplicate with two standard additions each in triplicate could be completed within 28 min. This

time could be reduced to <20 min by using only one standard addition for calibration. All responses were blank corrected for reagent impurities using the response for UHP water, as outlined in Section III.2.6.

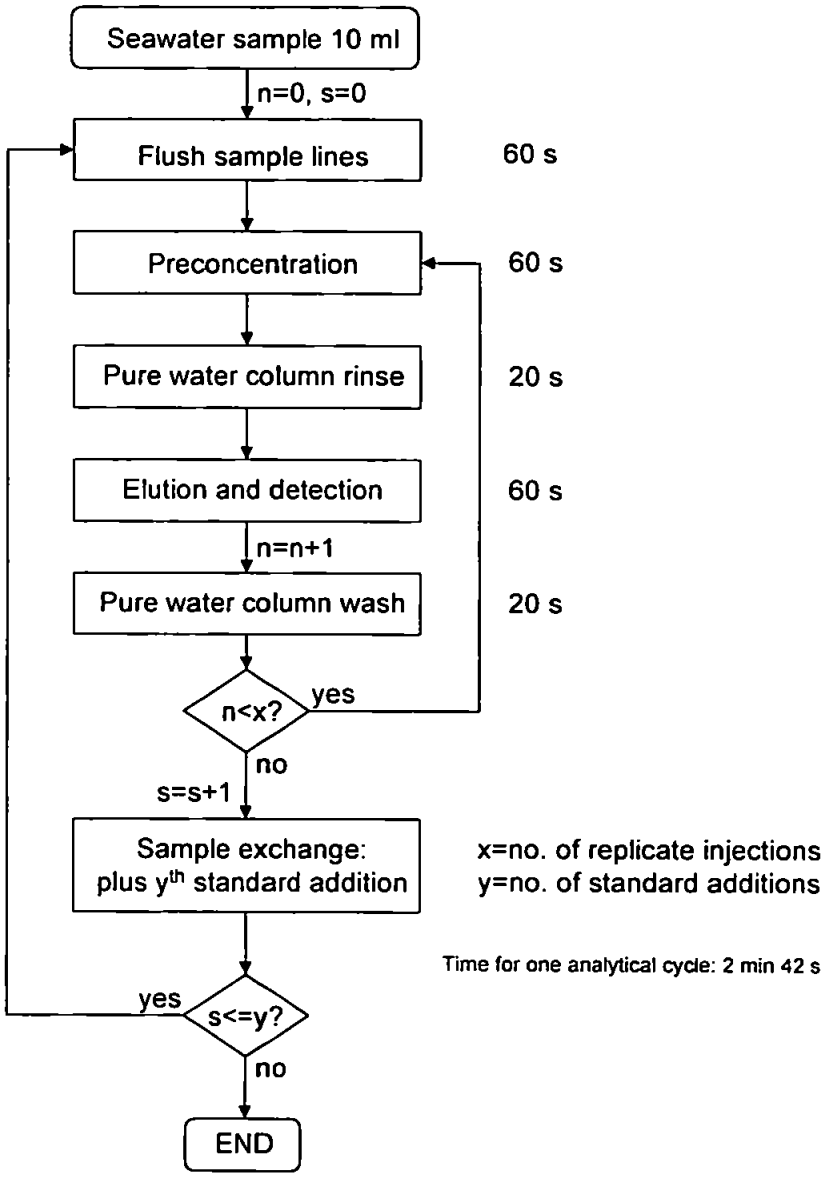

Figure III.7. Flow chart of the analytical procedure used for the determination of Fe in seawater using FI-CL

A typical detector output for a series of four replicates of the analytical cycle using a South Atlantic seawater sample is shown in Figure III.8(a). The peak shapes can be described as follows. Firstly, on reagent start-up, a small rise was noted as the baseline shifted from that generated by the PMT electronic noise to an increased level produced by impurities contained in the reagents. This reagent noise was steady whilst the 8-HQ column underwent the UHP wash

and sample load preconcentration cycle. On elution of Fe(II), a small negative dip was noted as ca. 0.03 ml of residual UHP water in the dead volume of the 8-HQ column temporarily replaced the Q-HCl eluent stream and reduced Fe impurities in the reagent baseline. Fe ions were next eluted from the column and a sharp, narrow positive peak resulted (ca. 8-10 s at half height, Figure III.8(b)). The elution volume was approximately 0.38 ml, resulting in a theoretical concentration factor of ca. 5. Occasionally, after the elution period, the CL peak did not return smoothly to the baseline, which was only restored after switching the injection valve back to the load position. One explanation for such an effect was that additional binding sites were created on the 8-HQ column due to adsorption of organics from seawater samples. Rinsing the 8-HQ column with the acid wash solution (0.6 M HCl / 0.16 M HNO_3, 60 s) followed by UHP water (60 s) was effective in eliminating this small tail, which did not adversely affect the precision of the method.

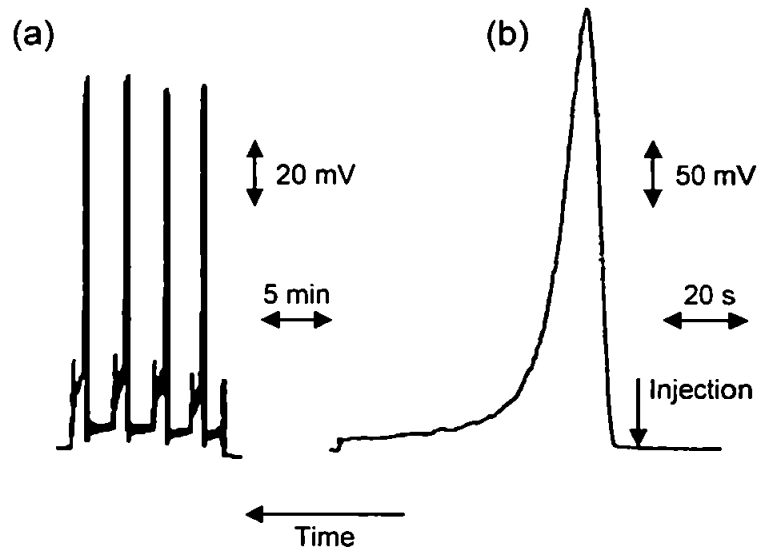

Figure III.8. (a) Detector output for a series of four replicate load, rinse, elute and wash steps using a South Atlantic seawater sample (TD-Fe = 0.48 nM); (b) Expanded single peak showing CL emission generated on elution

III.3 RESULTS AND DISCUSSION

III.3.1 Background Chemiluminescence

The mixing of reagent solutions through the manifold generated a background emission. Figure III.9(a) illustrates the stabilisation of the PMT baseline (ca. 0.04 mV, peak-to-peak) after installation on a ship's laboratory, and Figure III.9(b) shows the background CL emission and noise produced by the reagent flow during four injection sequences (with loading of no sample solution onto the preconcentration column). After reagent clean-up procedures discussed in Section III.2.3, the CL emission was minimised to 0.75 mV and a stable baseline noise (peak-to-peak) of 0.5 mV achieved. The baseline noise was much reduced when UHP water only passed through the flow cell, due to the absence of CL reagent. Previously studies (Price, 1995) noted that an increase in CL emission with air temperature may occur due to the release of thermally generated electrons from the photocathode, which consequentially increases the detector dark current. Furthermore, a change in temperature may alter the sensitivity of the CL reagent system. It was concluded, however, that thermostating of the reagents was not necessary for the following reasons:

(i) long-term optimisation experiments were performed during a period of temperature stability or within a regulated (20°C) clean air laboratory, and

(ii) during shipboard determinations, the laboratory was temperature regulated and a rapid standard addition procedure was adopted for Fe quantification.

Occasionally, a small quantity of air bubbles were noted in the waste line downstream of the flow cell, probably the by-products of the luminol CL reaction. These were not deemed to be a problem and upstream of the flow cell a smooth continuous flow was maintained.

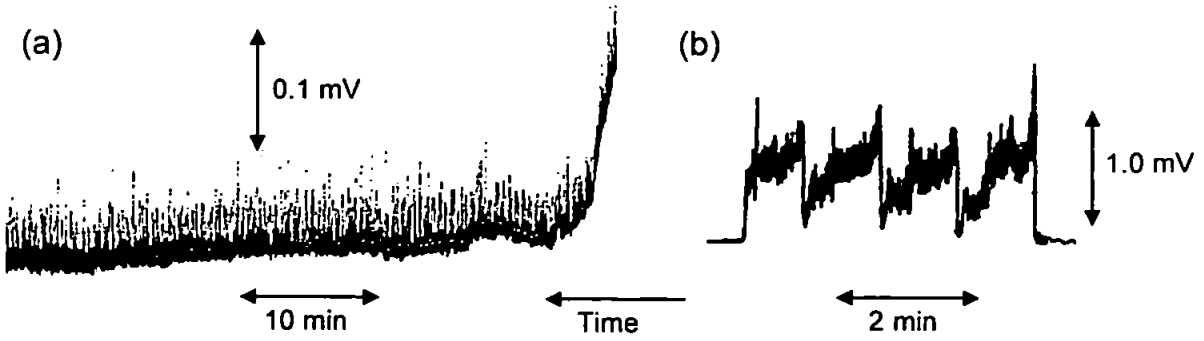

Figure III.9. (a) Stabilisation of PMT baseline after detector power-up; (b) Background CL emission and reagent baseline noise through four injection steps (no sample load)

III.3.2 CL Reaction System

III.3.2.1 Simplex Optimisation

Simplex optimisation is a multivariate optimisation technique designed to locate the summit of the response surface defined by the system variables. The Fe(II)-catalysed chemiluminescence emission from luminol oxidation in the absence of added oxidant has been well documented (Seitz and Hercules, 1972; Klopf and Nieman, 1983; Sarantonis and Townshend, 1986). Key variables, namely reagent flow rate, sample load volume, luminol concentration, reaction pH and PMT voltage, were evaluated using a modified simplex algorithm written in-house. For these studies no preconcentration of the analyte was performed and the 8-HQ column shown in Figure III.6 earlier was replaced by a sample loop consisting of a short length of PTFE tubing (internal volume 120 µl), as illustrated in a schematic diagram of the manual FI-CL system (Figure III.10). The distance between the point of merging sample and reagents was kept as short as physically possible (1 cm length, 0.08 s residence time) to ensure a rapid passage of solutions into the flow cell. Standards prepared in 0.01 M Q-HCl were used throughout.

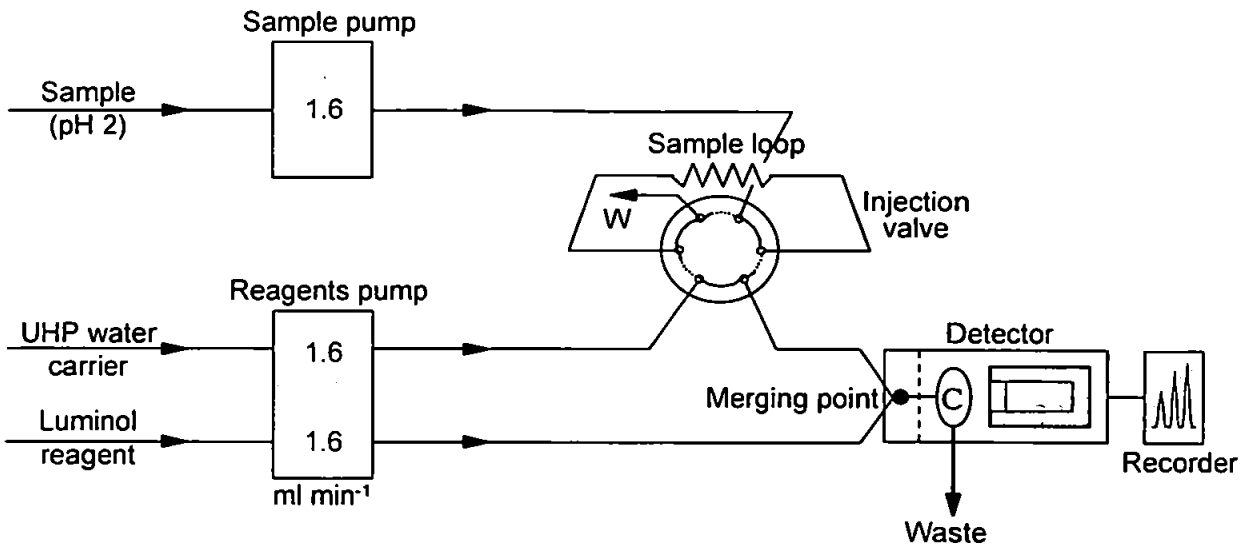

Figure III.10. Manual FI-CL manifold used during initial optimisation work

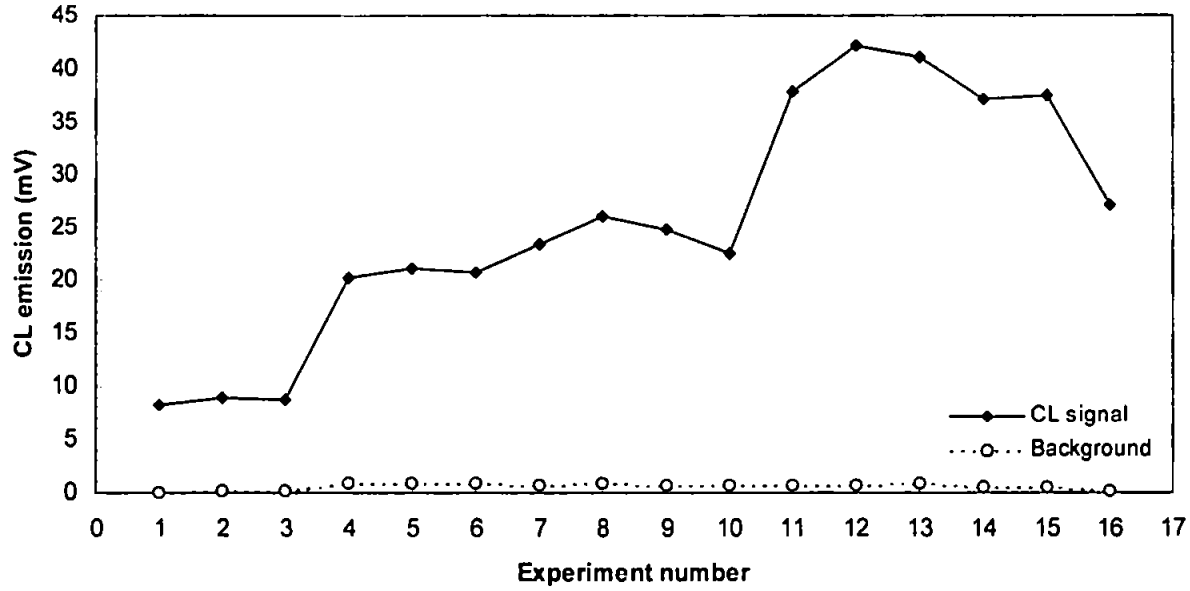

Figure III.11. Simplex history for initial optimisation ([Fe(II)]=20 nM)

Variable	*Unit*	*Range*	*Step size*	*Starting conditions*	*Optimum conditions*
Flow rate[a]	ml min^{-1}	0.8 - 3.3	0.1	1.3	3.0
Sample load volume[a]	ml	25 - 400	25	100	120
[Luminol]	M	10^{-7} - 10^{-3}	variable	10^{-7}	10^{-5}
Reaction pH[b]	-	8 - 12.5	0.2	11.8	10.4
PMT voltage	kV	0.8 - 1.2	0.05	1.0	1.1

[a]No preconcentration column was used for the initial optimisation of the CL reaction system; hence these conditions are not optimal for a manifold containing an 8-HQ column
b UHP water used as carrier stream; pH = 12.2 is the optimum when 0.09 M Q-HCl used as eluent (effluent pH ca. 10)

Table III.1. Results from the simplex optimisation of the FI-CL method for Fe(II) standards (10nM - 1μM) prepared in UHP water

The variables, conditions and optimum results for the simplex optimisation are shown in Table III.1 and the simplex history for an initial optimisation using a 20 nM Fe(II) standard is shown in Figure III.11. These conditions were valid for Fe(II) standards ranging from 10 nM to 1 μM prepared in UHP water, and were reached after 12 iterations of the simplex. The history suggests the starting conditions were near the optimum values. The large increase between experiments 3 & 4 was attributed to an increased flow rate and the rise between experiments 10 & 11 was due to a reaction pH change. Subsequent experiments used these optimum conditions. However, under a system containing an 8-HQ preconcentration column, variables such as flow rates and sample load volume required re-optimisation. These experiments confirmed that the reaction is highly pH dependant and requires a strongly alkaline (ca. pH 10.4) buffered reagent for maximum sensitivity.

III.3.2.2 Univariate Optimisation

Each of the key variables identified above was univariately optimised to investigate its effect on the FI-CL method and to determine the allowed ranges. One variable was varied whilst the others were set at their optimum values given in Table III.1. Fe(II) standards of varying concentration were used.

FLOW RATE

A CL emission versus flow rate curve is shown in Figure III.12. The flow in a CL detection system requires careful monitoring because the speed of the CL reaction and the time from mixing of the Fe(II) solution and reagents in the spiral flow cell must be matched as closely as possible. The entire emission versus time profile is not observed and the CL intensity detected in a flowing stream is the integrated portion of the emission profile that occurs during the time interval intersected by the observation cell. Reagent and carrier flow rates were kept identical to ensure reproducible mixing at the 'T'-piece merging point.

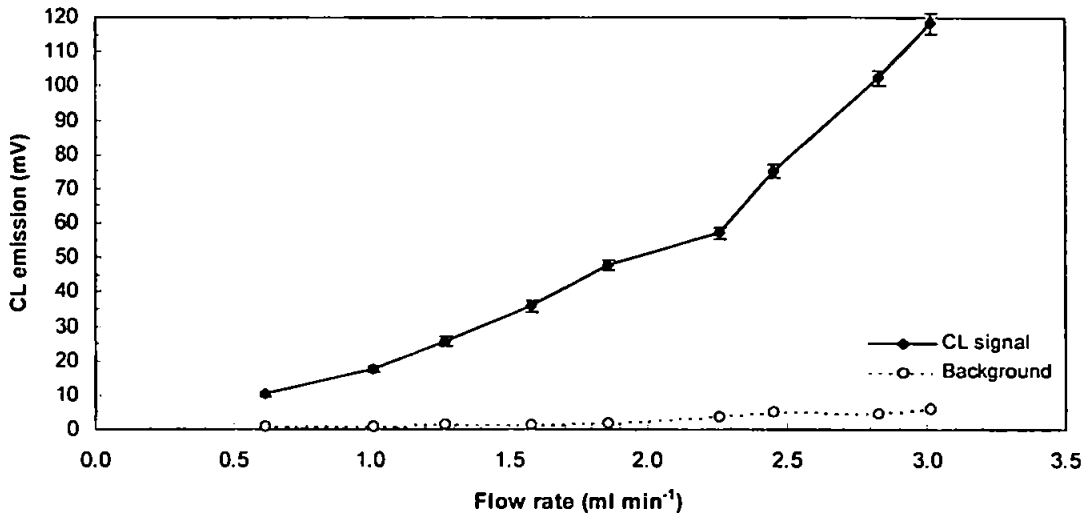

Figure III.12. Effect of reagents flow rate on CL emission

Signals continued to increase with increasing flow rate, consistent with a very rapid Fe(II) – dissolved oxygen – luminol reaction rate. The increased emission was attributed to the increased amount of turbulence within the flow cell, the reduced time before the CL reaction passed through the flow cell and hence the increased number of molecules reacting in front of the detector end-window. For method development, an operating flow rate of 3.0 ml min^{-1} was selected as a compromise between signal intensity, pump tubing integrity and reagent consumption.

Sample Loop Volume

The univariate optimisation for sample volume is shown in Figure III.13. The highest CL emission was achieved with a loop of 120 µl. A plateau was reached at higher values. This loop size maintained a balance between increased emission and low repeatability values. Lower sample volumes increased the dilution of the sample zone, whilst higher volumes increased the sample dispersion in the CL system and resulted in higher random errors reducing the precision of replicate injections.

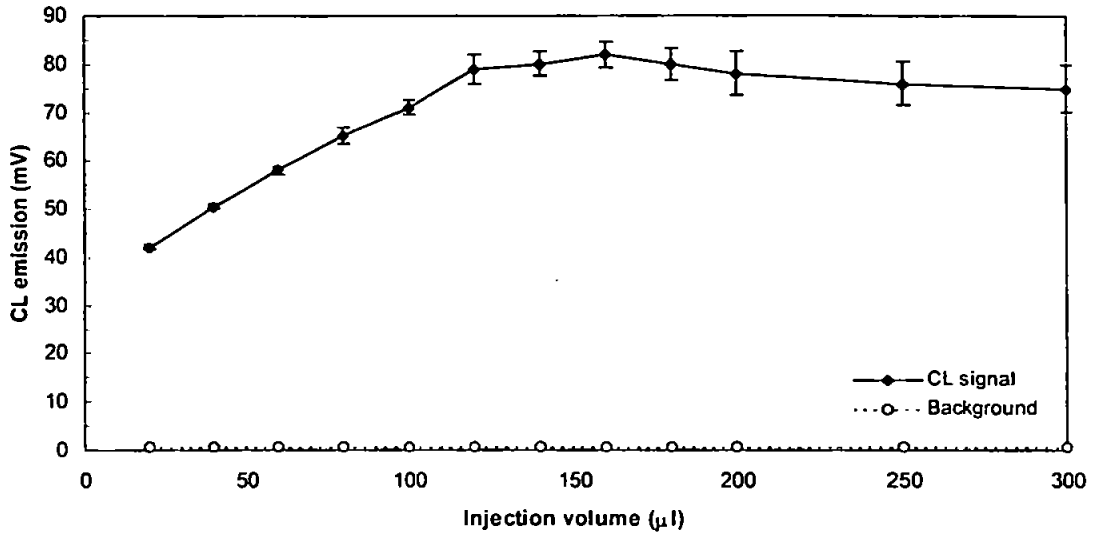

Figure III.13. Effect of injection loop volume on CL emission

LUMINOL CONCENTRATION

The luminol concentration optimum is shown in Figure III.14. High reagent concentrations increased the CL emission, but also cause an increase in the background emission, and hence a concentration of $1x10^{-5}$ M luminol was chosen to maintain a balance. The slight decrease in light at the highest luminol concentrations may be due to Fe(II) complexing with luminol or with the aminophthalate product of luminol oxidation. Self-quenching of the light may also occur at higher reagent concentrations.

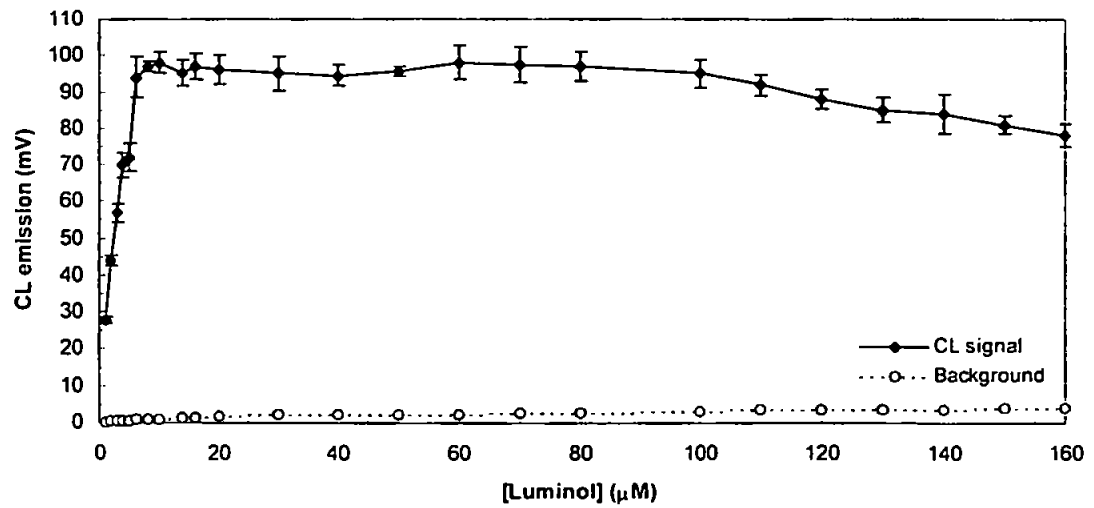

Figure III.14. Effect of luminol concentration on CL emission

REACTION pH

The effect of buffer, and hence reaction pH, on the CL emission is shown in Figure III.15. The catalytic effect of Fe ions on the oxidation of luminol is highly pH specific. Previous methods have reported a reaction pH of 10.5-11.0 (Seitz and Hercules, 1972), 10.3 (Klopf and Nieman, 1983), 11.4 (Sarantonis and Townshend, 1986) and 10.4 (Alwarthan and Townshend, 1987). This work found the optimum CL reaction to occur at pH 10.4.

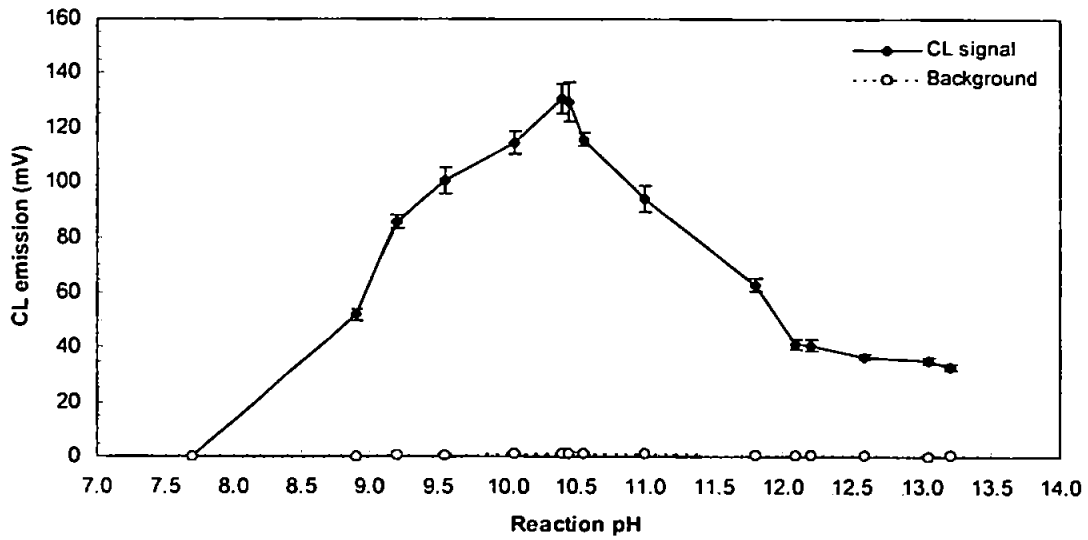

Figure III.15. Effect of reaction pH on CL emission

III.3.2.3 Variation of Luminol Sensitivity over Time

In order to assess stability of luminol reagent over time, and hence determine when the solution was at its most sensitive, the signal obtained by a 20 nM Fe(II) standard was monitored over a period of 4 d. Optimum reaction conditions were used; the luminol concentration was $1x10^{-5}$ M in 0.1 M carbonate buffer with a reaction pH = 10.4. Figure III.16 indicates that the luminol working solution was most active ca. 24 – 45 h after preparation. All working solutions were freshly prepared 1 d prior to use.

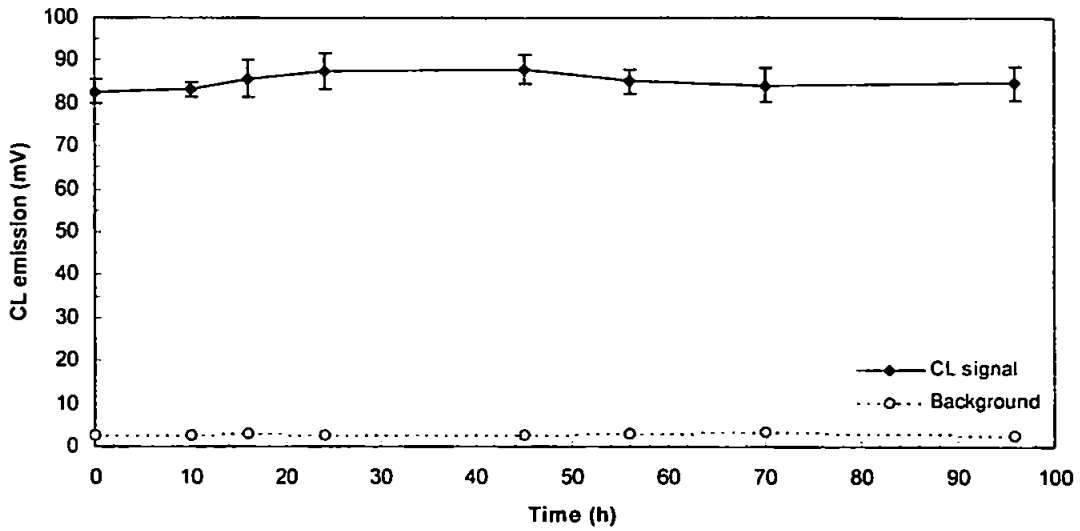

Figure III.16. Variation in sensitivity of luminol reagent with time

III.3.2.4 Degassing of Reagents

The present system is based around the catalytic effect of Fe(II) ions on the oxidation of luminol in basic aqueous solution, giving rise to a characteristic blue emission (λ_{max}~440 nm; previous Figure II.11), the oxidant being assumed to be dissolved oxygen. In order to investigate this in more detail, the luminol reagent and Q-HCl carrier stream were purged for 30 minutes with helium gas, in order remove dissolved oxygen. The CL signal was reduced to 6 % of its original value, although some residual chemiluminescence remained. This may be due to the diffusion of oxygen through the PTFE tubing of the flow system or the reagent solution re-absorbing oxygen from the atmosphere. The luminol reagent was next treated by pure oxygen bubbling for 10 min. The signal using this reagent was 150 % of the value obtained for the ordinary reagent solution open to the air. Dissolved oxygen therefore seems to be one of the reactants in the CL system. Seitz and Hercules (1972) used pure oxygen to stir the reaction cell and consequently obtained a lower detection limit. Since oxygen was also one of the reactants, the sensitivity was naturally improved using oxygen as the stirring gas.

III.3.3 Fe(III) Reduction

Experiments were performed with various reducing agents. Ascorbic acid concentrations as low as 1 μM resulted in total suppression of the luminol CL emission. Additions of

hydroxylammonium hydrochloride also reduced the signals and generated poor, irreproducible FI peaks which did not return to the baseline. Sulphite (Na_2SO_3; S(IV)) produced the best results with no interference to the analytical method. A complete study of the reduction kinetics of Fe(III) by sulphite in natural waters has been reported by Millero *et al.* (1995b). The rates of reduction of Fe(III) with S(IV) can be represented by:

$$Fe(III) + S(IV) \xrightarrow{k} products$$

giving an overall rate equation:

$$\frac{d[Fe(III)]}{dt} = -k[Fe(III)]^a[(S(IV)]^b$$

where a and b are the order of the reactions with respect to Fe(III) and S(IV). The removal of Fe(III) can be expressed as:

$$[Fe(III)]_t = [Fe(III)]_{t0} - [Fe(II)]_t$$

where the subscripts denote the initial concentration (t_0) and concentration of Fe(III) and Fe(II) ions at time t respectively. Hence, the rate constant can be determined by measuring the percentage reduction of Fe(III) under pseudo first order conditions with an excess of S(IV), simplifying the rate equation to:

$$\frac{d[Fe(III)]}{dt} = -k'[Fe(III)]$$

where:

$$k' = k[S(IV)]^b .$$

This relationship is illustrated by measuring the Fe(II) formed during Fe(III) reduction by S(IV), as shown in the concentration versus time profiles in Figure III.18. Figure III.19(a) and (b) displays ln ($[Fe(III)]_0/[Fe(III)]$) versus time for the reduction of Fe(III) at varying S(IV) concentrations ($[Fe(III)]_0$ = 10 nM, S = 35, pH 2.2, T = 20 °C), enabling ln k' to be evaluated (Table III.2). Furthermore, a plot of ln k' as a function of ln [S(IV)] (Figure III.20) yields a least squares line of 0.9772, validating the first order disappearance of Fe(III) with an excess initial level of S(IV). This data results in an overall rate constant ln k = 4.30 in seawater under the given conditions ([S(IV)] = 100 µM, S=35, pH = 2.2, T=20 °C), and hence a half-life $t_{1/2}$ = 94 min.

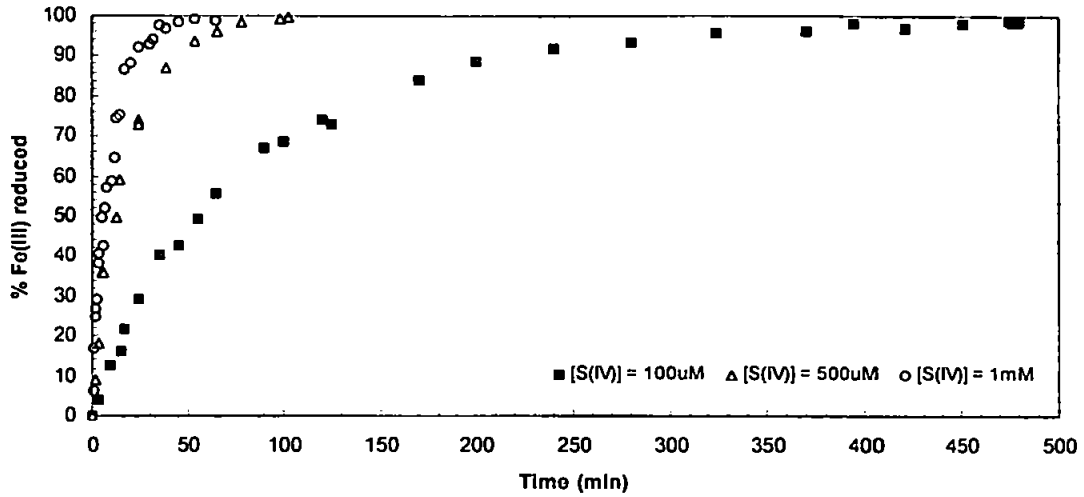

Figure III.18. Plot illustrating time course of Fe(II) formation resulting from the reduction of Fe(III) by S(IV) in seawater ($[Fe(III)]_0$=10 nM, $[S(IV)]_0$=varying concentration, S=35 psu, T=20°C, pH=2.2)

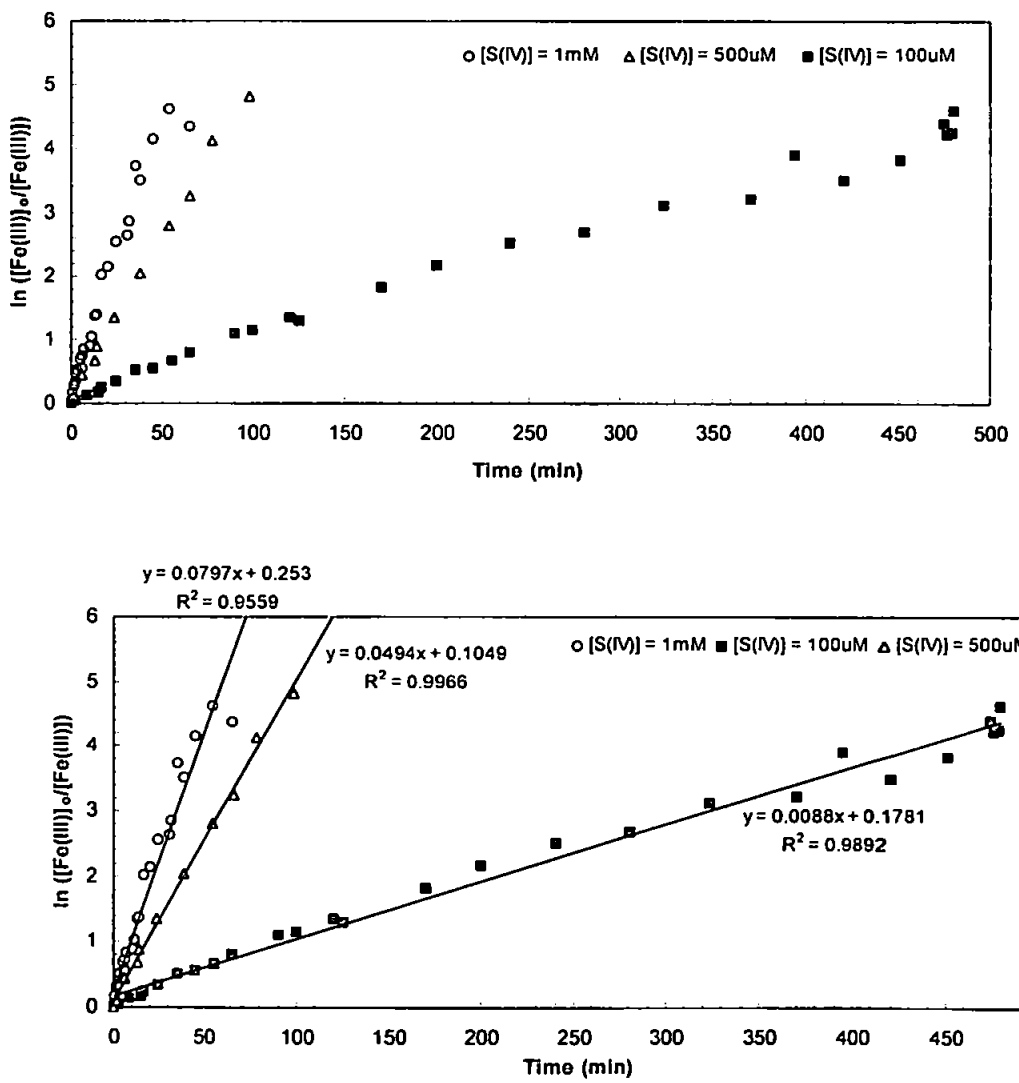

Figure III.19. Plots of ln ($[Fe(III)]_0/[Fe(III)]$) versus time for the reduction of Fe(III) by S(IV) in seawater ($[Fe(III)]_0$ = 10 nM, S = 35 psu, T = 20°C, pH 2.2); (a) data points, (b) regression

[S(IV)] (M)	*k' (min^{-1})*	*ln S(IV)*	*ln k'*
1.00E-04	0.0088	-9.2103	-4.7330
5.00E-04	0.0494	-7.6009	-3.0078
1.00E-03	0.0797	-6.9078	-2.5295

Table III.2. Logarithmic values of S(IV) and k'

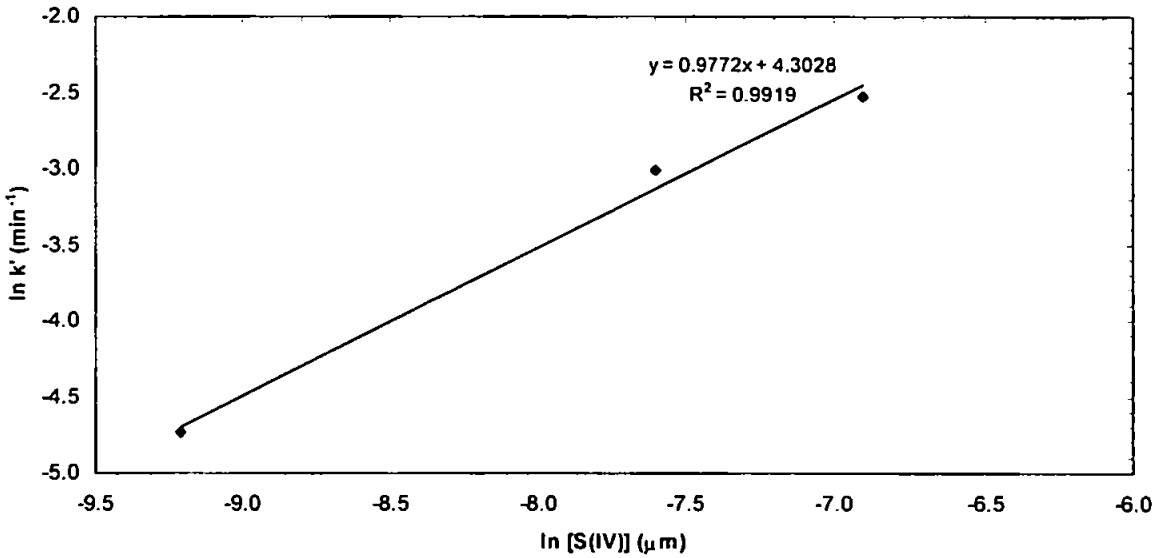

Figure III.20. Plot of ln k' versus ln [S(IV)] for the reduction of Fe(III) by S(IV) in seawater ($[Fe(III)]_0$ = 10 nM, S = 35 psu, T = 20°C, pH 2.2)

Appendix B contains a spreadsheet representation of half-life data for the reduction of Fe(III) using S(IV) in natural waters with respect to temperature, pH, [S(IV)] and ionic strength. Using the constants given in Millero *et al.* (1995b), the reduction of Fe(III) species in seawater (S = 35) has a half-life $t_{1/2}$ = 65 min at pH 2.2 ([S(IV)] = 100 μM, T = 25 °C). Furthermore, in seawater at pH 2.0, Millero *et al.* (1995b) reported a half-life $t_{1/2}$ = 12 min ([S(IV)] = 1 mM, T = 25 °C). In our experiments, Fe(III) standards and samples were treated with reducing reagent ([S(IV)] = 100 μM, S = 35, pH = 2.2, T = 20 °C) for 8 h prior to analysis. Greater than 98% reduction of Fe(III) species was observed after 8 h, and standard additions to seawater samples containing Fe(II) and Fe(III) showed no significant difference in calibration gradient up to a Fe concentration of 10 nM.

III.3.4 Matrix Elimination and Preconcentration

III.3.4.1 Overview

Solution chemiluminescence reactions generally suffer from poor selectivity and, in addition to Fe(II), several transition metal cations (e.g. Co(II), Cu(II), Mn(II), Cr(III), Ni(II), Zn(II)) and anions (e.g. Br^-, Cl^-, SO_4^{2-}) are known to catalyse the luminol – dissolved oxygen system and their application has been widely reported (e.g. Seitz and Hercules, 1972; Klopf and Nieman, 1983). These interfering species act to alter the apparent quantitative relationship between observed luminescent power and analyte concentration. The effect of trace metal ions on the FI-CL system will be studied in detail in Section III.3.5. Here, the focus is on interference problems generated by the sea-salt matrix.

The six major components of seawater, which make up >99 % by weight, were shown previously in Table I.2. To investigate the interference of seawater matrix ions, solutions of various different salts were prepared in UHP water at their oceanic concentration (Table III.3) and cleaned to remove heavy metal impurities using a Chelex-100 column, as described in Section III.2.3.4. These solutions were acidified to pH 2.2 with Q-HCl. 100 nM Fe(II) was added to each solution and any change in CL emission noted between these standards and a 100 nM Fe(II) standard with no addition.

Ion	*Concentration (M)*[a]
Chloride (Cl^-)	0.56
Sodium (Na^+)	0.47
Magnesium (Mg^{2+})	0.05
Calcium (Ca^{2+})	0.01
Potassium (K^+)	0.01
Sulphate (SO_4^{2-})	0.028

[a] Data from Kester *et al.*, 1967; S = 35

Table III.3. Concentrations of major ions in seawater

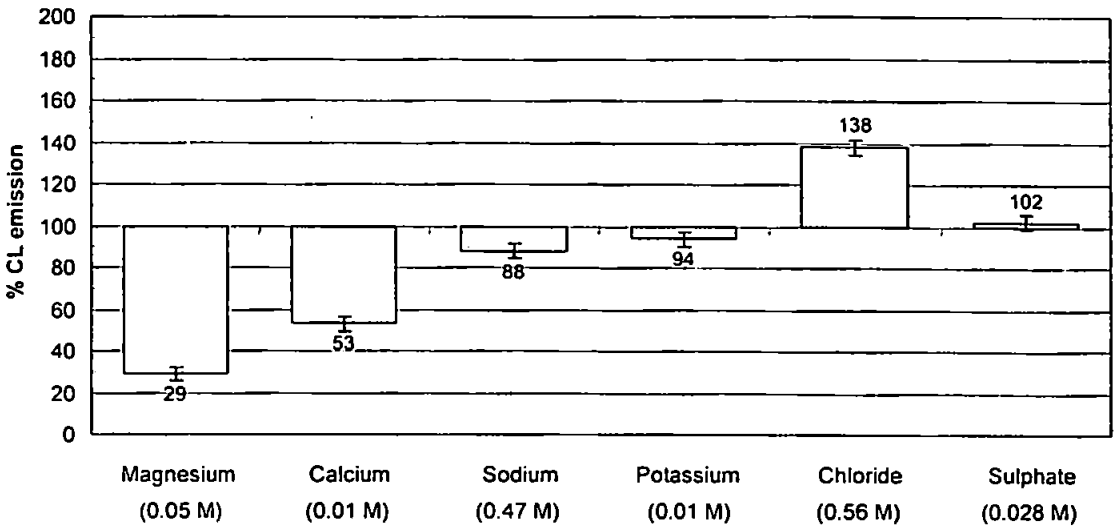

Figure III.21. The interference effect of sea-salt matrix ions ([Fe(II)$_0$=100 nM, pH=2.2, T=20 °C)

Figure III.21 presents the results of the measurement of a 100 nM Fe(II) standard prepared in salt solutions (Mg^{2+}, Ca^{2+}, Na^+, K^+, Cl^-, SO_4^{2-}) at natural seawater concentrations. The signals are normalised to the Fe(II) measurement after the standard addition and are corrected for their blank. Hence, 100% emission is the signal given by a 100 nM Fe(II) standard solution prepared in UHP water.

These studies showed that generally more than 70% of the CL signal was suppressed in standards prepared in solutions containing Ca^{2+} and Mg^{2+} ions at their typical seawater concentrations, compared to UHP water standards. This common effect for solution chemiluminescence methods in a seawater matrix has been previously reported for the luminol reaction (Seitz *et al.*, 1972; Chang *et al.*, 1980). Both groups observed no quenching of the CL emission if the Mg^{2+} concentration was below a certain level. In addition, synthetic UHP solutions containing halide ions showed significant increases in the CL signal (e.g. >30 % enhancement on addition of 0.56 M Cl^-). An enhancement of the luminol reaction by halide ions has previously been published (Bause and Patterson, 1979; Chang *et al.*, 1980; Chang and Patterson, 1980), using Cr(III), Co(II), Fe(II) and Ni(II) as catalysts in the luminol reaction. This halide enhancement effect ($Br^- > Cl^- > F^-$) remained relatively constant at different metal concentrations, but varied according to the reaction pH. Bromide ions were reported to give a five-fold signal increase for the Fe(II) – luminol – peroxide CL system (Chang and Patterson,

1980). The proposed mechanism for this CL enhancement was an interaction of the halide ions with a metal – O_2 – luminol complex, causing an increase in CL emission. The halide ions were reported to increase the CL efficiency by increasing the rate constant for the CL pathway. This was achieved through a catalytic cleavage of an activated molecular complex, producing more excited aminophthalate ions.

Furthermore, elimination of the sea-salt matrix prior to introduction of the buffered CL reagent is necessary to prevent any precipitation of $Mg(OH)_2$ and $Ca(OH)_2$ such sea-salt ions in the FI manifold at the reaction pH (ca.10.4). Fe(II) ions must also be separated from other heavy metals and concentrated to achieve the picomolar detection limits required for remote open-ocean analyses.

III.3.4.2 Selection of Chelating Resin

A popular method of matrix removal employs solid phase extraction, where the seawater sample is passed over a solid support containing functional groups, the analyte is retained on the support, usually by adsorptive and chelating processes, and the unwanted matrix components are passed to waste. The retained analytes may then be desorbed from the chelating agent, usually by a weak acid solution. This technique is readily amenable to flow injection methods, whereby the extraction and elution of the ions may be carried out in-line.

Important requirements in the selection of a chelating agent are:

(i) an adequate exchange capacity,

(ii) little swelling or contraction of the resin on sample load / elution,

(iii) low metal blank contamination, and

(iv) most importantly in a pH specific alkaline CL reaction, ease of elution with a weakly acidic solution.

Previous FI-CL methods for Fe measurements have used the following chelating methods: 8-HQ immobilised on Toyopearl (formerly Fractogel) TSK (Elrod *et al.*, 1991; Measures *et al.*,

1995; Powell *et al.*, 1995; Bowie *et al.*, 1998; de Jong *et al.*, 1998), 8-HQ and derivatives immobilised on silica gel (Obata *et al.*, 1993, 1997) and 8-HQ immobilised on controlled pore glass (Alwarthan *et al.*, 1990). In addition, numerous FI - spectrophotometric methods have employed the following chelating columns as a means of separating the analyte from the seawater matrix.: C_{18} phase columns (Okumura *et al.*, 1997), some impregnated with reagent(s) (King *et al.*, 1991; Blain and Tréguer, 1995), melamine - formaldehyde resins (Filik *et al.*, 1997), chelation of ferrozine complex with poly-(chlorotrifluoroethylene) resin (Zhang and Terada, 1994), fibrous cellulose sorbents which contain functional groups (Kolotyrkina *et al.*, 1995), solvent soluble membrane filters (Taguchi *et al.*, 1994; Gu and Zhou, 1996), and Chelex-100 micro-columns (Rubi *et al.*, 1996).

A chelating resin of 8-hydroxyquinoline (8-quinolinol, Figure III.22) immobilised on a solid support (TSK gel, Toyopearl HW-75F, 32-63 micron, fine, TosoHaas Co., supplied through Anachem) was prepared according to a modified procedure of Landing *et al.* (1986; and subsequent personal communication, 1996), outlined in Section III.3.4.3. Toyopearl TSK is a semi-rigid spherical gel, synthesised by a copolymerisation of ethylene glycol and methacrylate type polymers. The intertwined vinyl polymer agglomerates offer high porosity, mechanical and chemical stability and a high hydrophilicity due to the presence of ether linkages and hydroxyl groups. TSK beads are small and uniform, and show no signs of swelling at high pH values. The numerous surface hydroxyl groups enable relatively simple chemical modification, which is used in the immobilisation of ligand such as 8-hydroxyquinoline *via* phenyl-azo linkages. The polymer solid support itself shows no cation exchange capacity and does not concentrate dissolved humic or fluvic acids. 8-HQ is known to be highly selective. for transition metal cations relative to alkali and alkaline-earth metals, especially at pH < 6.

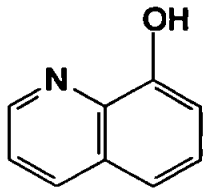

Figure III.22. Structure of 8-hydroxyquinoline (8-HQ)

Landing *et al.* (1986) reported TSK-8HQ to be relatively stable in acid solutions (2.0 M HCl / 0.1 M HNO_3). For example, during the preconcentration of Cu(II), the resin preserved 88.2% of its original capacity after 240 h of acid treatment. After 48 h base treatment (0.5 M NaOH), a decrease in breakthrough capacity of 32% was observed. The base catalyses the hydrolysis of the resin benzoyl-ester linkages. In comparison, 8-HQ immobilised on silica gel shows a decrease of 38% of its total exchange capacity after 24 h at pH 12 (ca. 0.01 M NaOH), due to the extensive hydrolysis of the silica support (Marshall and Motolla, 1983).

III.3.4.3 Resin Synthesis

Toyopearl TSK HW-75F is the precursor for the benzoylation reaction, whereby *p*-nitrobenzoylchloride is attached to the resin. The nitrogroup is then reduced to an amino group, which is diazotised. By preservation of the two nitrogen atoms, 8-HQ is attached. Figure III.23 illustrates the reaction scheme for the 8-HQ immobilisation.

All reagent solutions were filtered (0.45 µm pore size, 47 mm diameter, polycarbonate; Nucleopore) to remove contaminant particles which may end up in the modified resin. All steps were performed in a laminar flow hood in order to reduce any particulate contamination which would result in high resin column blanks. Figure III.24 shows a flow chart of the resin synthesis procedure. Total net preparation time was 25 h. The synthesis provided enough resin slurry to pack more than 200 columns.

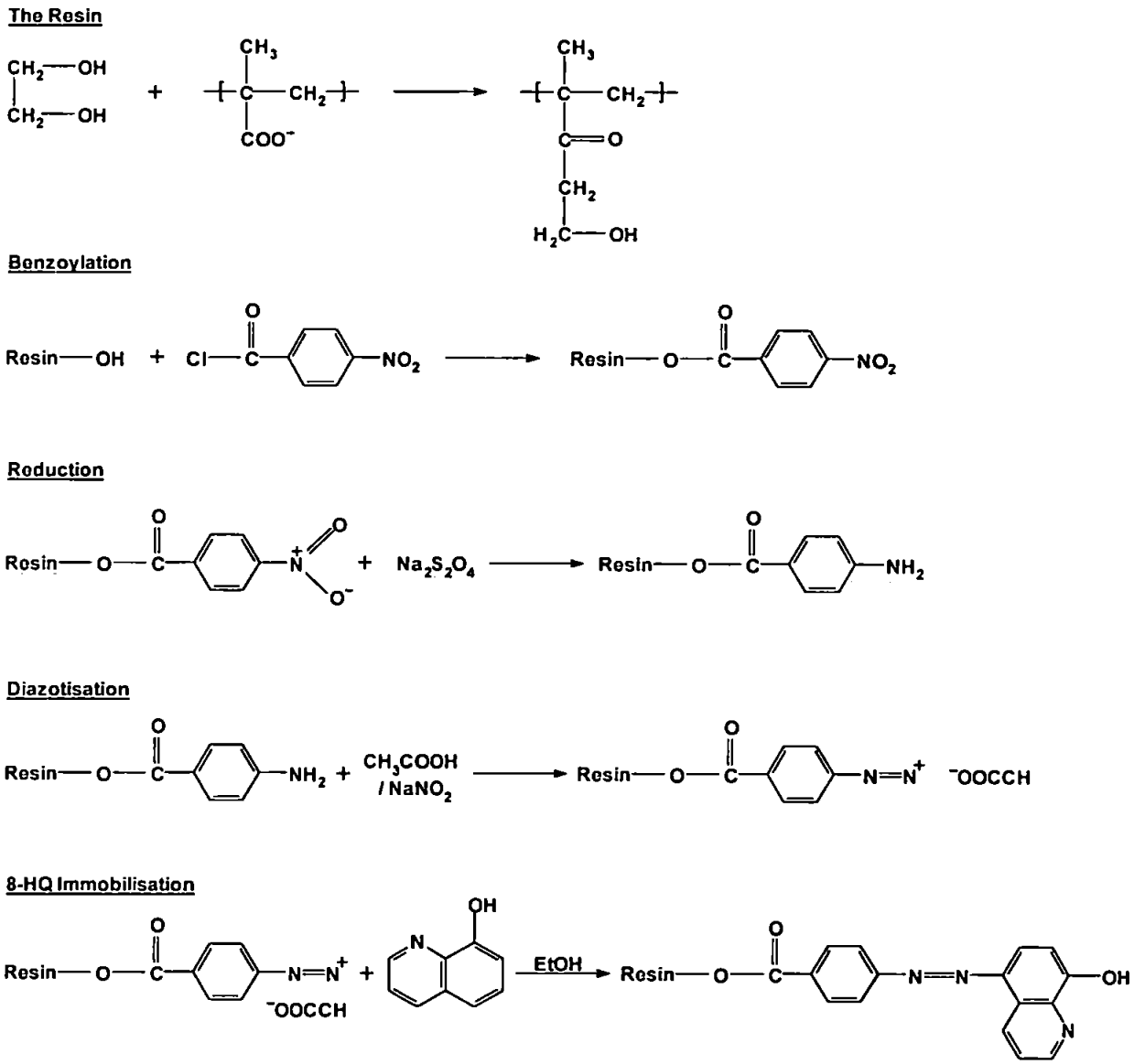

Figure III.23. Reaction scheme for the immobilisation of 8-HQ

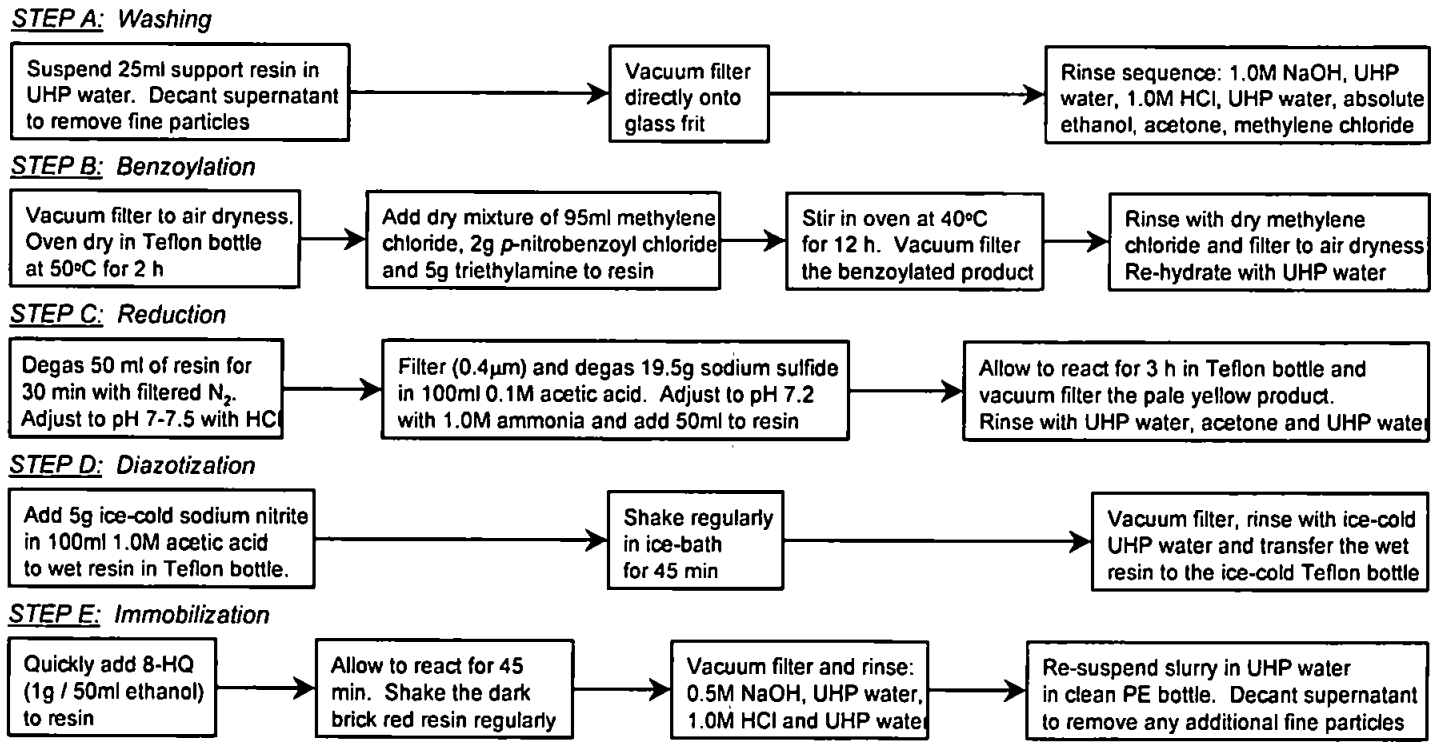

Figure III.24. Flow chart illustrating the synthesis of Toyopearl TSK - 8-hydroxyquinoline resin

III.3.4.4 Optimisation

The complexation of Fe by the chelating resin is influenced by many parameters. 8-HQ complexes strongly with Fe(II) and Fe(III) ions, with stability constants (log K_1) of 8.71 and 13.69, respectively (Sillén, 1964). In a dynamic flow injection system, however, the exchange times are much reduced and the reaction may not reach equilibrium, although the localised microenvironment may enhance the chelation of Fe. Therefore, the experimental parameters of sample pH, column internal diameter and length and eluent concentration need to be optimised for maximum chelating efficiency. The sample, wash solution and reagent flow rates were also optimised once again after insertion of the 8-HQ column in the manifold, in order to maintain adequate loading rates without excessive back pressures.

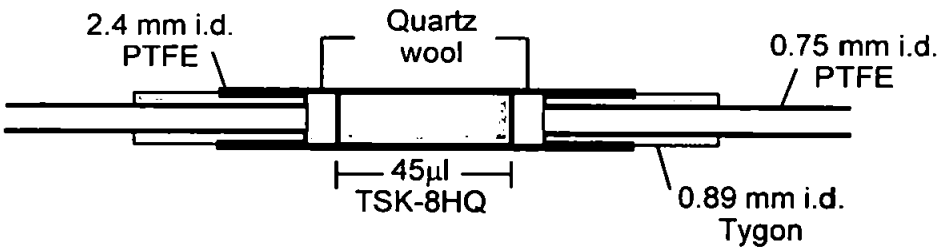

Figure III.25. Preconcentration and matrix elimination micro-column containing TSK-8HQ resin

COLUMN CONSTRUCTION

Various columns were constructed with a range of lengths and diameters. Initially, PTFE tubing of 1.5 mm i.d. was used to pack the resin. Such a narrow diameter resulted in increased back-pressure in the FI manifold and a reduced flow rate for loading sample was necessary, increasing the overall analysis time. Increasing the column to lengths greater than 30 mm showed no improvement in sensitivity and resulted in increased dead volumes and back-pressures and less reproducible peaks. Columns were therefore constructed from 2.4 mm i.d. PTFE tubing and a 10 mm length of resin was used (volume of resin = 45 µl), as illustrated in Figure III.25. The column ends were fabricated using 0.89 mm i.d. Tygon pump tubing, which was connected to the 0.75 mm i.d. PTFE manifold tubing. A plug of quartz wool was placed at either end in order to retain the resin inside the column. Prior to packing the columns, the 8-HQ slurry was stirred in order to form a homogenous suspension. A flow line was connected from the PTFE column direct to the resin reservoir. Narrow bore pump tubing was attached downstream of

the column and the resin drawn up at low pressure using a peristaltic pump (ca. 0.4 ml min^{-1}). The low concentration of Fe ions in the sample, coupled with high stability constants, explains why such a small volume of resin can be used. The columns were cleaned with 1.0 M Q-HCl for at least 12 h, followed by UHP water for 12 h prior to use. The 8-HQ columns were also used for in-line purification of the ammonium acetate buffer and Fe(III) reducing reagent prior to analysis, as described in Section III.2.3.3.

SAMPLE pH

Figure III.26 illustrates the retention of Fe(II) ions on a 8-HQ column as a function of sample pH. Fe(II) was quantitatively retained from seawater in the pH range 4.5 - 8.0, consistent with a theoretical treatment for the effect of pH on metal – 8HQ complexes (Zueklhe and Kester, 1985; Sohrin *et al.*, 1998). High sample pH values result in solutions in which the analyte becomes unstable, Fe(II) oxidation takes place and precipitation may occur. Indeed, Fe(II) analyte loss was noted within 1 h from seawater samples which were buffered to pH 4.5 - 5.0 prior to analysis. Therefore, during all further work, samples were acidified to pH 2.0 (0.01 M Q-HCl), and the pH was only adjusted in-line using ammonium acetate buffered at pH 5.5 immediately prior to adsorption onto the 8-HQ column. This resulted in a final sample pH of ca. 5.0, which maintained a balance between loading efficiency and Fe(II) oxidation rates.

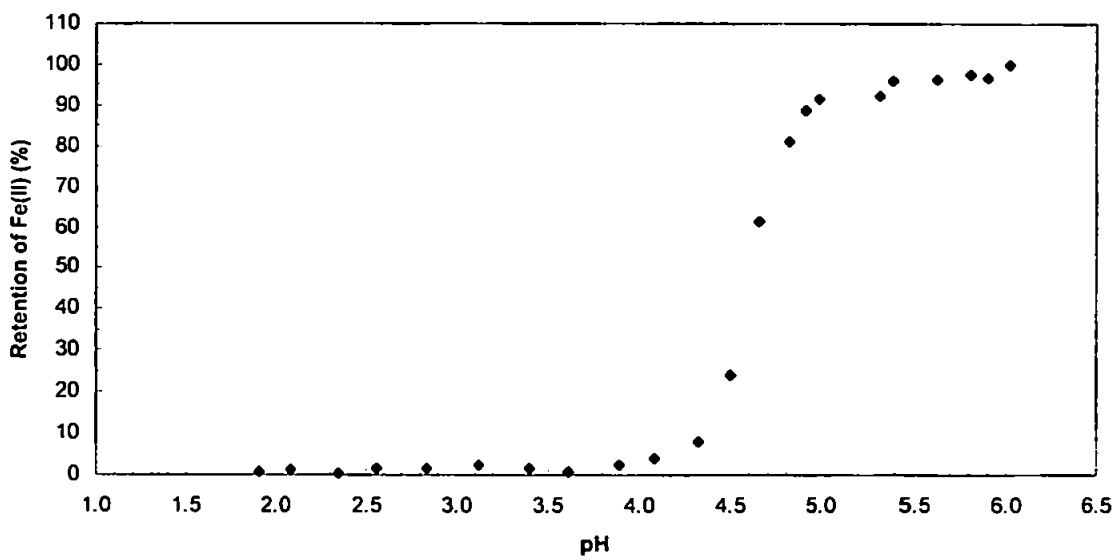

Figure III.26. Retention of Fe(II) ions on an 8-HQ column as a function of pH ([Fe(II)]=2.5 nM)

ELUTION

The acidic eluent must be sufficiently strong to rapidly desorb the Fe from the 8-HQ resin, but mild enough not to suppress the highly pH dependent CL reaction, and therefore 0.09 M Q-HCl was used. On elution of Fe(II), a small negative dip in the signal was noted prior to a sharp positive emission. This was due to a pH change in the solution transported to the CL cell, produced by the mixing of UHP water in the dead volume of the 8-HQ column with the luminol reagent. After such a dip, Fe(II) ions contained in the acidic eluent reached the detector and produced the measured signal.

III.3.4.5 Column Breakthrough Capacity

In a dynamic column operation, the breakthrough capacity is the most useful method of characterising the column. This parameter is defined as the maximum amount of metal ion that can be chelated per unit mass of solid under the existing operating conditions, before the analyte is detected in the column eluent. A modified flow injection manifold (Figure III.27) was used to measure the capacity of the column. Operating conditions are as outlined in the manifold and given in Table III.4. A fresh TSK-8HQ column (internal volume = 45 µl) was attached directly in-line with the detector and acidified seawater (pH 2.0) containing 10 µM Fe(II) was buffered in-line (pH 5.0) and passed continuously through the column. Initially, the CL reading was at the baseline, indicating the effective complexation of the Fe ions onto the resin. As the analyte began to break through the column and mixed with the luminol reagent, the signal increased until a plateau was reached, indicating that chelating sites on the TSK-8HQ column were saturated.

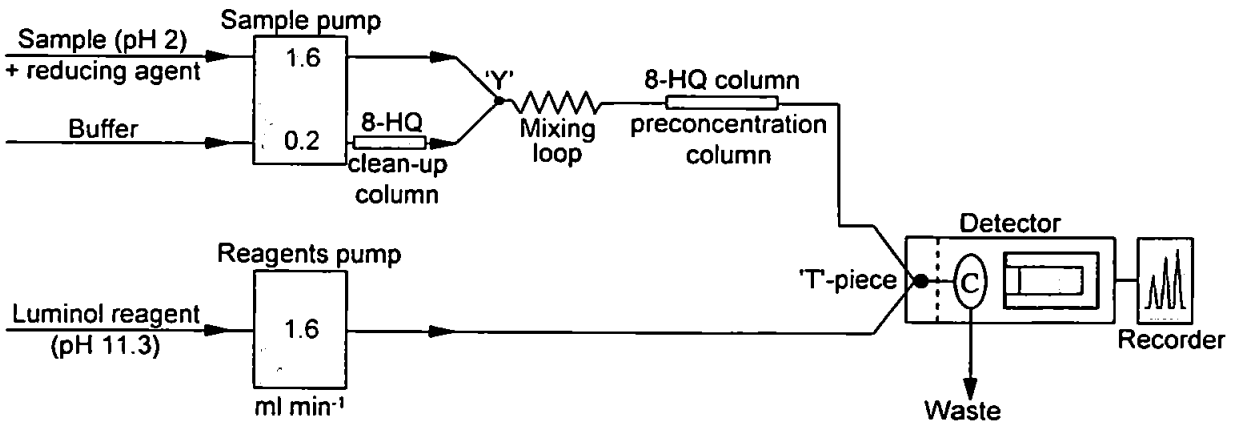

Figure III.27. Modified FI-CL manifold used for the breakthrough capacity experiment

Variable	Solution	Concentration	pH
Sample	Fe(II)	10 μM	2.0
Reducing agent	S(IV)	100 μM	n/a
Sample buffer	Ammonium acetate	0.4 M	5.5
CL reagent	Luminol	10 μM	n/a
Reagent buffer	Sodium carbonate	0.1 M	11.3

Table III.4. Operating conditions used for breakthrough capacity experiment

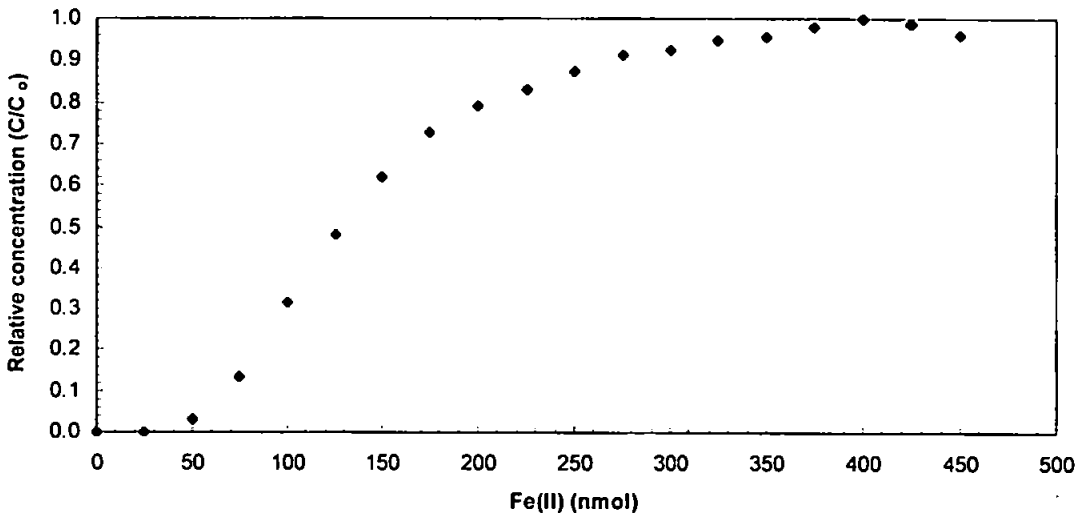

Figure III.28. Fe(II) breakthrough curve for a 45 μl TSK-8HQ column; C/C_o is the effluent / influent concentration ratio ([Fe(II)]=10 μM, [S(IV)]=100 μM, pH=2, flow rate=1.6 ml min^{-1})

An Fe(II) breakthrough curve is shown in Figure III.28. The breakthrough capacity of the column can be interpolated from the curve, based on the ratio of the concentration in the effluent (C) over the total concentration in the sample (C_o), at the point where $C/C_o = 0.05$ (Landing *et al.*, 1986). At breakthrough, the column retained 56 nmol (3.1 μg) of Fe(II), which is significantly higher than the 1 - 2 pmol of Fe recovered from loading a 1.6 ml sample containing 1.0 nM Fe, typical of ocean waters. Since the dry mass of the resin contained in a 45 μl TSK-8HQ column was 54.7 mg, this represents a total capacity of 1.02 μmol of Fe(II) / g of resin.

III.3.5 Interference Studies

Experiments were conducted in seawater at pH 2 with Fe(II) concentrations of 1.0 nM. Individual metal ions were added at 1, 10 and 100 times the Fe(II) concentration and the change in CL emission was compared to the signal for 1.0 nM Fe(II) only. Possible interfering metal

ions investigated were Co(II), Cr(III), Ni(II), Mn(II), Cu(II), Ag(I), Pb(II) and Zn(II), and the results are presented in Table III.5.

With the exception of Co(II), none of the elements exhibited a significant interference at any of the concentrations tested, when loaded onto the 8-HQ column at pH 5.0, but problems were encountered above this level at ambient seawater pH, presumably due to the partial adsorption of other metals (e.g. Mn(II)) onto the column at pH values above 6 (Sohrin *et al.*, 1998). Co(II) showed a strong positive interference at all concentrations, and is known to be an efficient catalyst for the luminol CL system (Klopf and Nieman, 1983). However, maximum Co(II) concentrations in open-ocean waters typically range between 100-300 pM (Sakamoto-Arnold and Johnson, 1987) and, in additional experiments, no interference to the analytical method was noted at concentrations up to 500 pM Co(II). The addition of 1000 pM of Co(II) to a 1.0 nM Fe(II) standard yielded a 28 % increase in CL signal.

III.3.6 Calibration

III.3.6.1 Analytical Figures of Merit

Calibration graphs for the optimised system are shown in Figures III.29. The curves illustrate a greater sensitivity for standards prepared in UHP water compared with those in LISW (calibration slopes = 39.2 and 25.9, respectively; Figure III.29(b)). Figure III.29(c) validates the complete reduction of Fe(III) species by sulphite. The calibration for Fe in the optimised system was linear in the concentration range 0.04-10 nM (r^2 = 0.9974), and the relative standard deviation was 3.2% (n=5) for a 1.0 nM Fe(II) standard. The limit of detection in low Fe seawater (three times the standard deviation) was 40 pM for a preconcentration time of 1 min. This could be improved by increasing the loading time, although this would require further purification of the sample buffer, UHP water and reducing reagents, in order to reduce the blank signal. The sample throughput for complete analyses in triplicate including standard additions was 3 h^{-1}.

Ratio	*Metal conc$^{n.}$ (nM)*	*Co(II)*	*Cr(III)*	*Ni(II)*	*Mn(II)*	*Cu(II)*	*Ag(I)*	*Pb(II)*	*Zn(II)*
1x	1.0	128 ± 4	101 ± 3	102 ± 2	104 ± 5	102 ± 5	100 ± 3	97 ± 4	99 ± 2
10x	10.0	244 ± 5	99 ± 2	101 ± 4	98 ± 6	97 ± 5	105 ± 4	101 ± 4	97 ± 1
100x	100.0	398 ± 4	99 ± 3	103 ± 4	94 ± 7	98 ± 6	104 ± 5	101 ± 3	100 ± 1

[d]The data values are percent signal intensity relative to the signal intensity of 1.0 nM Fe(II) in the absence of other added metals. Uncertainties represent two standard deviations (95% confidence) for n=4

Table III.5. Responses for interfering metal ions in the presence of 1.0 nM Fe(II) in seawater, normalised to the response for 1.0 nM Fe(II) in seawater[d]

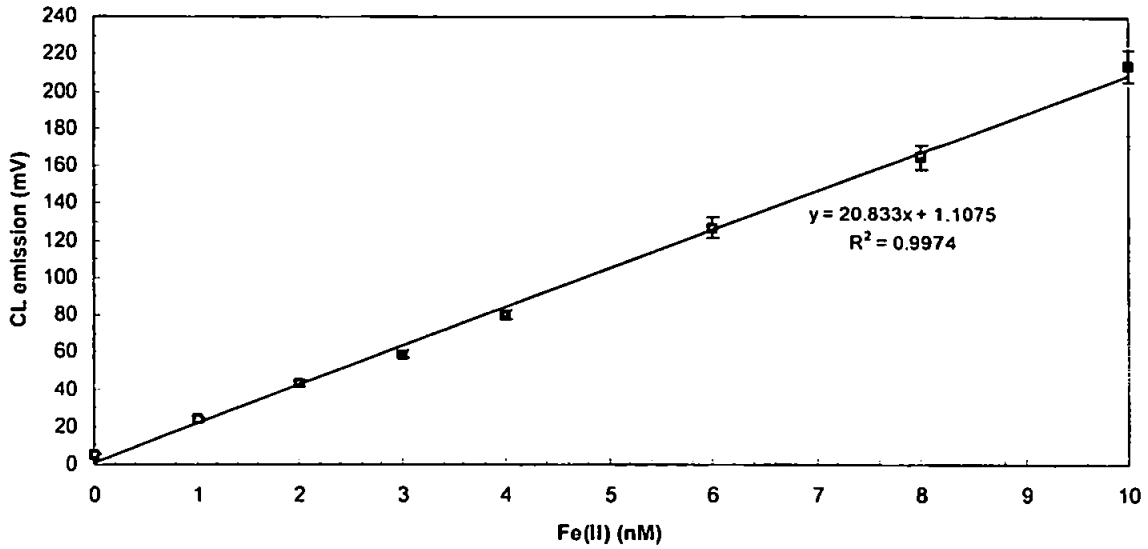

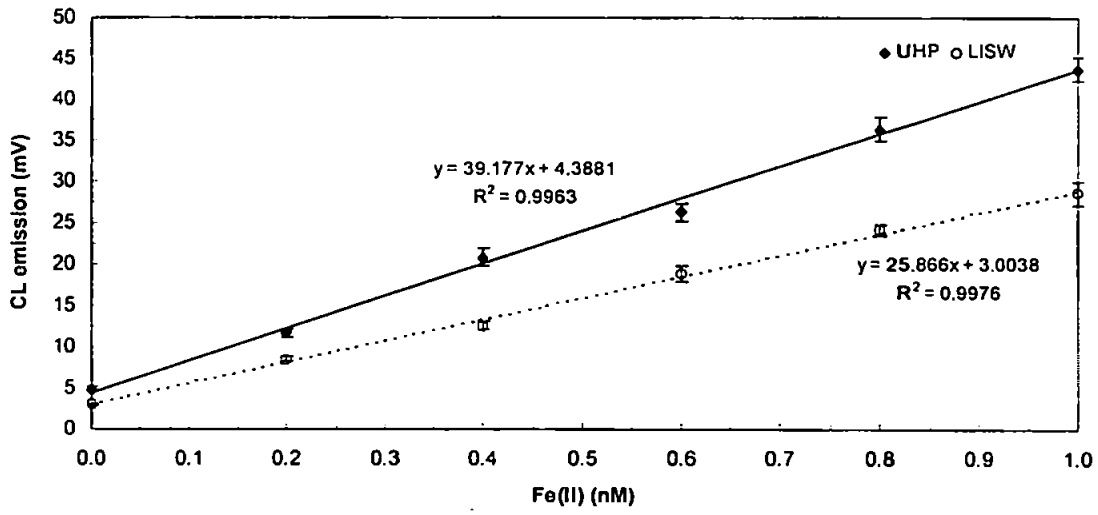

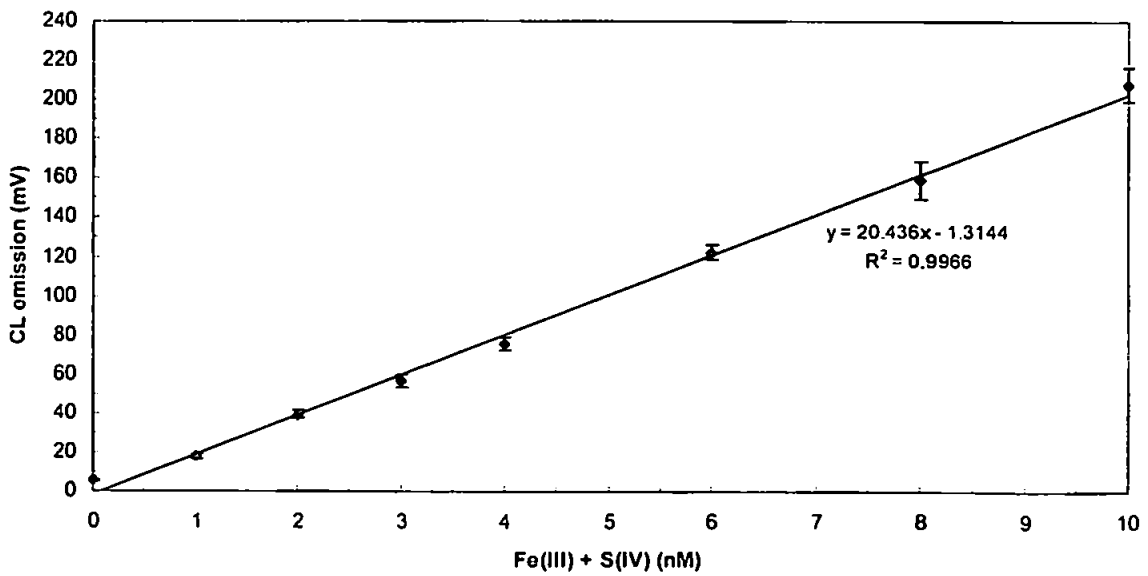

Figure III.29. Calibration graphs: (a) Fe(II) ions in LISW over the range 0-10 nM; (b) Fe(II) ions in LISW and UHP water over the range 0-1.0 nM; (c) Fe(III) ions reduced by S(IV) in LISW over the range 0-10 nM

III.3.6.2 Certified Reference Materials

The accuracy of the flow injection - chemiluminescence technique was ascertained by analysing seawater certified reference materials obtained from the National Research Council of Canada, Marine Analytical Chemistry Standards Programme. The results for North Atlantic Surface Seawater (NASS-4) and Coastal Atlantic Surface Seawater (CASS-2) are shown in Table III.6.

Standard solution	Fe concentration (nM)	
	Certified[a]	FI-CL[a]
NASS-4	1.88 ± 0.29	2.01 ± 0.12
CASS-2	21.49 ± 2.15	23.61 ± 0.94

[a] Uncertainties represent 95% confidence interval for an individual sub-sample

Table III.6. CRM results for dissolved Fe(II+III) for trace metal certified seawater solutions[e]

A *t*-test can be used to check whether the two data sets for open-ocean seawater (NASS-4) differ significantly. The null hypothesis adopted is that the means of the results given by the two methods are equal. The pooled value of the standard deviation is given by:

$$s^2 = \frac{\{(n_1 - 1)s_1^2 + (n_2 - 1)s_2^2\}}{(n_1 + n_2 - 2)}$$

where $\bar{x}_1$ and $\bar{x}_2$ are the two sample means, s_1 and s_2 their corresponding standard deviations and n_1 and n_2 the number of measurements. Hence, in our case,

$$s^2 = \frac{(2 \times 0.29^2 + 4 \times 0.12^2)}{6} = 0.0376$$

$$\therefore s = 0.194$$

The value of t is then given by:

$$t = \frac{(\bar{x}_1 - \bar{x}_2)}{s\sqrt{(1/n_1 + 1/n_2)}}$$

where t has $n_1 + n_2 - 2$ degrees of freedom. So,

$$t = \frac{(1.88 - 2.01)}{0.194\sqrt{(1/3 + 1/5)}} = -0.92$$

Appendix A.1 reference data (Miller and Miller, 1993) gives the critical value of $|t|$ (P=0.05) at 8 degrees of freedom of 2.45. Since the experimental value of $|t|$ is less than the reference value, the difference between the two results is insignificant at the 5% level and the null hypothesis is

accepted, confirming the good agreement between experiment results by FI-CL and certified values.

III.4 CONCLUSIONS

The development of a highly sensitive system for the shipboard determination of dissolved Fe at the sub-nanomolar level was presented, based on a flow injection technique coupled with luminol chemiluminescence detection. Meticulous care was taken to minimise contamination risks during all development work and four reagent clean-up procedures were adopted. The chemical and instrumental parameters were investigated using a univariate optimisation protocol. Dissolved Fe(II+III) levels were determined after Fe(III) reduction using sodium sulphite. A chelating resin was synthesised *via* the immobilisation of 8-hydroxyquinoline onto a solid support (Toyopearl TSK) and a micro-column constructed for in-line matrix elimination and preconcentration. This permitted the selective determination of Fe with a practical limit of detection (3s) of 40 pM when 1.6 ml of sample was loaded onto the column, and a relative standard deviation of 3.2 % (n = 5) for a 1.0 nM Fe sample. One analytical cycle (incorporating load, wash and rinse steps) could be completed within 3 min. The automated method was validated by determining Fe in NASS-4 and CASS-2 certified reference materials.

THE KINETIC EFFECT OF IRON ON LUMINOL CHEMILUMINESCENCE USING THE CONTINUOUS ADDITION OF REAGENT

IV.1 INTRODUCTION

IV.1.1 Luminol Chemiluminescence

Chemiluminescence (CL) reaction systems for the determination of trace metals possess excellent sensitivity (Seitz and Hercules, 1973; Kricka and Thorpe, 1983), as discussed in Section I.4.2. Many methods are based on the catalysis or inhibition of reactions involving the oxidation of luminol (5-amino-2,3-dihydrophthalazine-1,4-dione). Iron (Fe) has been determined using the luminol chemistry in the presence of an oxidant, usually hydrogen peroxide or dissolved oxygen, with low nanomolar detection limits reported for synthetic Fe standards (Seitz and Hercules, 1972; Klopf and Nieman, 1983; Sarantonis and Townshend, 1986; Alwarthan and Townshend, 1987; Alwarthan *et al.*, 1990) . More recently, several CL methods have been reported for the determination of Fe in a seawater matrix using the luminol reagent (Obata *et al.*, 1993, 1997; O' Sullivan *et al.*, 1995; Powell *et al.*, 1995; Bowie *et al.*, 1998; de Jong *et al.*, 1998) or brilliant sulfoflavin (Elrod *et al.*, 1991), whilst other workers used similar analytical systems to monitor Fe(II) oxidation rates (King *et al.*, 1995; Emmenegger *et al.*, 1998). Flow injection manifolds were used in most cases for rapid and reproducible sample and reagent handling.

IV.1.2 Continuous Addition of Reagent

The continuous addition of reagent (CAR) technique was first developed a decade ago (Marquez *et al.*, 1988; Marquez *et al.*, 1990a) , in order to improve the analytical figures of merit from very fast CL reactions, where imprecise measurements often arise due to irreproducible mixing of sample and reagents. Currently, flow injection (Sarantonis and Townshend, 1986; Alwarthan and Townshend, 1987; Alwarthan *et al.*, 1990) and stopped-flow (Gonzalez-Robledo *et al.*, 1989; Gaikwad *et al.*, 1994; Gaikwad *et al.*, 1995) techniques exist as popular alternatives to discrete sampling vessels, the latter possessing the advantage that full CL intensity versus time profiles can be recorded. CAR also allows the whole transient signal to be monitored, and thus CL reaction rates can be related to analyte concentrations, improving precision and selectivity in comparison to classical measurement parameters, such as peak height or area calculations. Recent review articles suggest that monitoring growth and decay curves on time resolved CL

measurements will widen the analytical application of many classical reactions (Soper *et al.*, 1998).

The theoretical foundation of the CAR technique (Velasco *et al.*, 1992) has allowed its applicability to be demonstrated in a number of clinical (Carmona *et al.*, 1992; Cepas *et al.*, 1993), pharmaceutical (Marquez *et al.*, 1990b; Pérez-Bendito *et al.*, 1996; Blasco *et al.*, 1997) and environmental analyses (Quintero *et al.*, 1991; Cobo *et al.*, 1997; Jimenez-Prieto and Silva, 1998). In addition, the kinetic approach of the CAR technique has proved to be an effective tool for resolving non-linear multicomponent systems using computational neural networks (Ventura *et al.*, 1997; Hervas *et al.*, 1998; Jimenez-Prieto and Silva, 1999). Characteristics of CAR determinations include:

(a) reproducible mixing of sample and reagents,

(b) recording of the whole CL response profile, including a wide linear portion on which reaction rates can be measured,

(c) adjustment (e.g. reduction) in the rate of a given reaction, due to the second-order nature of the reaction, and

(d) the ability to suppress background reagent emission (e.g. peroxyoxalate CL; Cepas *et al.*, 1994)

Hence, the CL reaction can be recorded *via* a simple data acquisition system which can perform accurate calculations on the CL emission versus time curve.

IV.1.3 Kinetic Determination of Iron using a CAR Manifold

The initial aims of this work were to investigate the classical luminol CL system using a CAR manifold. The reaction was based on the oxidation of luminol, which was catalysed by Fe(II) ions in the presence of dissolved oxygen and under alkaline conditions. Luminescence was recorded as the emission of blue light (λ_{max} ~440nm). Initial efforts, therefore, were focused on the quantitative aspects of the system, re-evaluating the reaction chemistry, optimising the instrumental parameters and investigating possible interferents. Secondly, the analytical characteristics of the CAR system for the determination of Fe were compared with existing

instrumental methods (batch, stopped flow, flow injection), a study into the reduction characteristics of Fe(III) species with sulphite was performed, and attempts made to apply the technique to real samples.

IV.2 EXPERIMENTAL

All labware was thoroughly cleaned by first soaking it in 5% micro-detergent (DECON, Merck, España) for several hours, followed by an approximately 10% hydrochloric acid (HCl) rinse for 24 h. Items were doubly rinsed with high purity de-ionised water (Milli-Q system, Millipore, 18.2 MΩ cm^{-1}). All reagents and standards were analytical grade, supplied by Merck unless otherwise stated, and prepared in MQ water.

IV.2.1 Reagents

A 0.2 M carbonate buffer was prepared by dissolving 5.3 g Na_2CO_3 in 250 ml MQ. The buffer was adjusted to pH 11.5 by the addition of NaOH. Luminol (5-amino-2,3-dihydro-1,4-phthalazinedione, Sigma) was used as received to prepare a 0.01 M stock by dissolving 0.1772 g in 100 ml of 0.1 M Na_2CO_3 buffer. A $5x10^{-4}$ M working solution was prepared from this stock by adding 12.5 ml to 250 ml of 0.2 M carbonate buffer. A 0.1 M stock solution of sulphite Fe(III) reducing reagent was prepared by dissolving 1.324 g Na_2SO_3 in 100 ml MQ.

IV.2.2 Standards

A 0.01 M Fe(II) standard was prepared by dissolving 0.3921 g $Fe(NH_4)_2(SO_4)_2.6H_2O$ in 100 ml of a 0.1 M HCl solution. This stock was prepared weekly and was found to be stable over this period. Other standards were freshly prepared in 0.01 M HCl by serial dilution. Similarly, a 0.01 M Fe(III) standard was prepared by dissolving 0.4822 g $(NH_4)Fe(SO_4)_2.12H_2O$ in 100 ml of 0.1 M HCl, and standards subsequently prepared in 0.01 M HCl by serial dilution.

IV.2.3 Instrumentation

The apparatus used to implement the CAR technique for CL determinations (Figure IV.1) consisted of an autoburette (Metrohm Dosimat 665) which was connected to a

spectrofluorimeter (Perkin-Elmer 650-10 s). The fluorimeter was operated in its energy mode (λ_{em} 440 nm, PM gain high) and contained a mini-reaction vessel (total internal volume 10 ml) equipped with stirrer which was positioned between a reflecting mirror and the emission end-window. The band width of the emission monochromator was set at 20 nm. Light signals were sent from the fluorimeter to a data acquisition and processing system consisting of a PC micro-computer (Mitac PC-AT 12MHz) equipped with PC-Multilab PCL-711 ADC software developed in-house for the application of reaction rate methods to CL determinations. A QuickBASIC™ software routine performed the calculation of maximum reaction rate and maximum CL intensity (traditionally the peak height measurement), together with calibration plots using both measured parameters. The automated CAR-CL system was controlled by a QuickBASIC™ program.

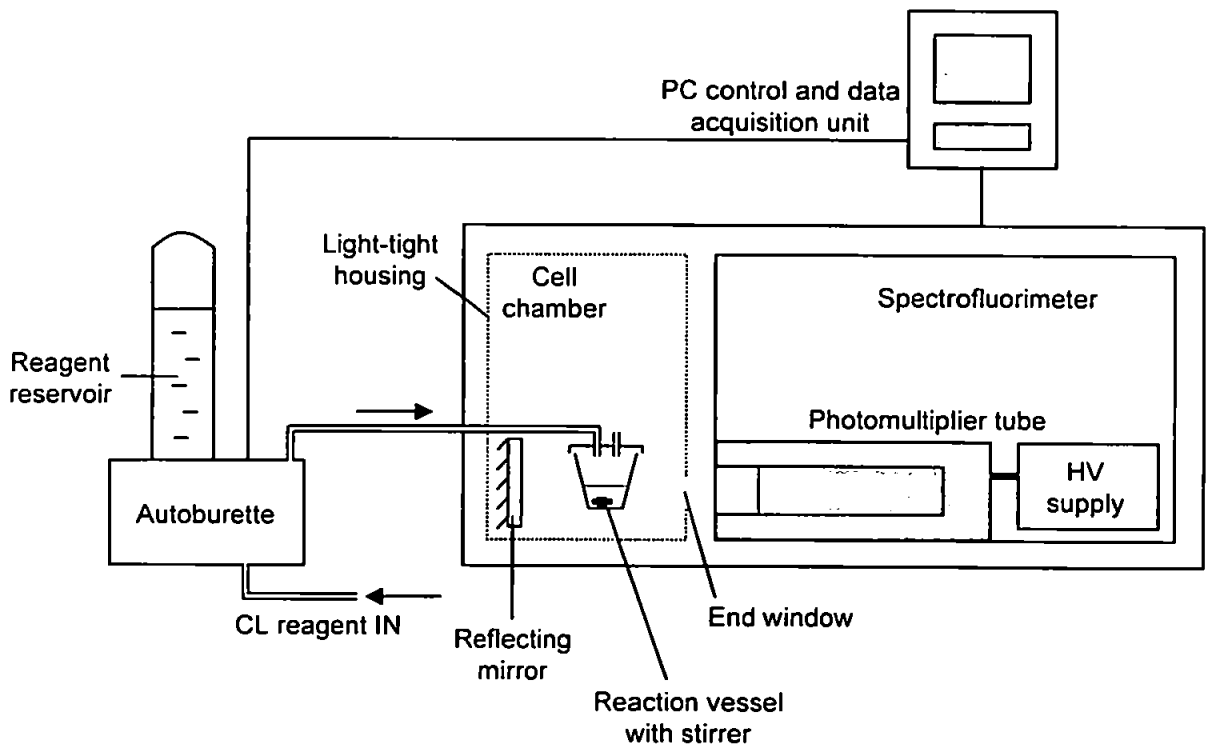

Figure IV.1. Schematic diagram of the instrumentation used for the continuous addition of reagent - chemiluminescence technique

IV.2.4 Operating Procedures

The reaction vessel was initially filled with a 1.0 ml volume of the acidified Fe(II) standard solution, the concentration ranging between 10 nM and 10 μM. Initially, the standard solution

in the vessel measured pH 2.4. The stirrer was switched on and the reaction initiated by adding luminol solution ($5x10^{-4}$ M) contained in 0.2 M carbonate buffer from the autoburette at a rate of 10 ml min^{-1}. Under these conditions, the initial reagent pH was 11.5 and the final pH in the reaction vessel after 5 s of reagent addition was 10.9. The CL output of the reaction was monitored by the photomultiplier tube of the spectrofluorimeter at an emission wavelength of 440 nm, and signals sent to the data acquisition unit. The full CL emission versus time profile was immediately recorded on the PC, and the two measured parameters (maximum reaction rate and maximum peak intensity) calculated from the initial rise of the curve. A typical CL emission versus time profile obtained under the CAR-CL system is shown in Figure IV.2. The linear rise zone of the CL response - time curve is used to calculate the formation or maximum reaction rate by simple linear regression.

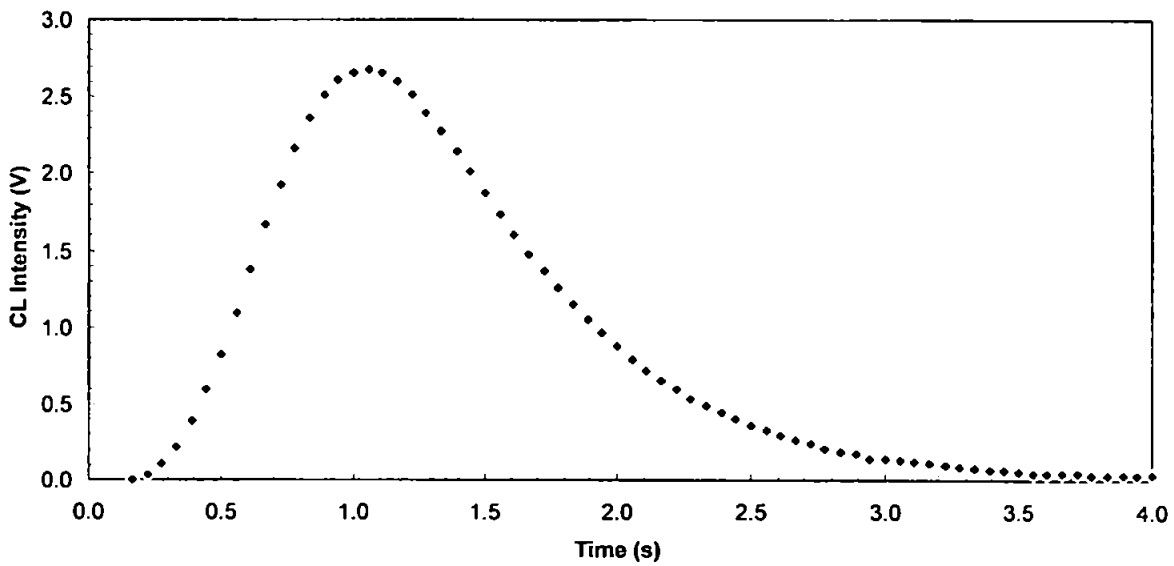

Figure IV.2. CAR-CL intensity vs. time profile; [Fe(II)]=450 nM; optimum conditions (see Table IV.1)

IV.2.5 Ion-exchange Column

An anion-exchange column was constructed from Dowex 1 (ionic form: chloride, cross-linkage: 40%, dry mesh: 50-100; Sigma). 500 mg of the resin was first conditioned for several hours with 6 M HCl. The resin was next packed into a column (length 5.2 cm, 3.2 mm i.d.) constructed from PTFE tubing and plugged at each end with glass wool. This column was incorporated into

a flow manifold attached to a peristaltic pump (Gilson Minipuls 3). The flow rate through the column ranged between 0.08 - 2.0 ml min^{-1}.

IV.3 Results and Discussion

IV.3.1 Optimisation

Each of the key variables was univariately optimised to investigate their effect on the CAR-CL method and to identify the allowed ranges. One parameter was adjusted whilst the others were set at their optimum values, which are given in Table IV.1. All changes in variables could be monitored using both reaction rate and peak height measurement parameters. Due to the complex speciation of Fe and rapid oxidation and precipitation kinetics in alkaline aqueous media, care had to be taken when preparing standards. A stock Fe(II) solutions (1 μM) was freshly prepared daily and all standards used throughout the optimisation experiments were acidified using 0.01 M HCl.

Luminol CL occurs in a strongly basic medium, and therefore the effect of adding the alkaline reagent to the acidic standard in the reaction vessel was first studied. Preliminary experiments showed that it was necessary for the reagent to be added to the reaction vessel rapidly in order to raise the pH to the level for optimum CL emission and prevent analyte losses due to Fe(II) oxidation. As shown by Figure IV.2, the CL reaction was generally developed in a very short time (completion achieved within 5 s). Slower addition rates resulted in longer reaction times since the CAR technique is capable of controlling the speed of the reaction; however, such curves were imperfectly formed and the maximum peak intensity below optimum (see Section IV.3.1.6).

Variable	Optimum value
[Luminol] reagent	$5x10^{-4}$ M
[Na_2CO_3] buffer	0.2 M
Addition rate	10 ml min^{-1}
Initial cell volume	1.0 ml
Reagent pH	11.5
Sample pH	2.4
Final pH in reaction vessel	10.9
Fluorimeter senistivity	30 (fine)
PC data acquisition range	+/- 5.0 V

Table IV.1. Optimum experimental conditions for Fe(II) determinations

IV.3.1.1 Buffer Molarity

The effect of changing the concentration of Na_2CO_3 buffer contained in the autoburette with respect to addition rate is illustrated in Figure IV.3. A more concentrated buffer allowed the pH in the reaction vessel to increase towards the reaction optimum in a shorter time period and hence reduce the residence time (T_{max}) of the CL peak. This effect was more pronounced at slower addition rates, where the CL curve took the form of a broader, shallower peak. In order maintain minimum reagent consumption, and not to increase the speed of the reaction to a point where the precision in maximum reaction rate and peak height measurements become unworkable, a 0.2 M Na_2CO_3 buffer was chosen as the matrix for the luminol reagent, and used for all subsequent work.

IV.3.1.2 Luminol Concentration

The influence of the concentration of the luminol reagent added from the autoburette was studied over the range $5x10^{-6}$ M to $1.17x10^{-3}$ M (Figure IV.4). Both measured parameters increased sharply up to a concentration of $2x10^{-4}$ M, whereupon the increase was more gradual. Other instrumental techniques suffer from the disadvantage that high reagent concentrations increase the background emission. CAR is free from such constraints, however solubilisation problems in the reservoir of the autoburette did occur with luminol concentrations above $5x10^{-4}$M, and therefore this value was chosen as an optimum for further determinations. Luminol solutions are known to be most sensitive approximately 24 h after preparation

(Gonzalez-Robledo *et al.*, 1989; Bowie *et al.*, 1998) after which they remain stable for several weeks. The reagent was therefore prepared 1 day prior to analysis.

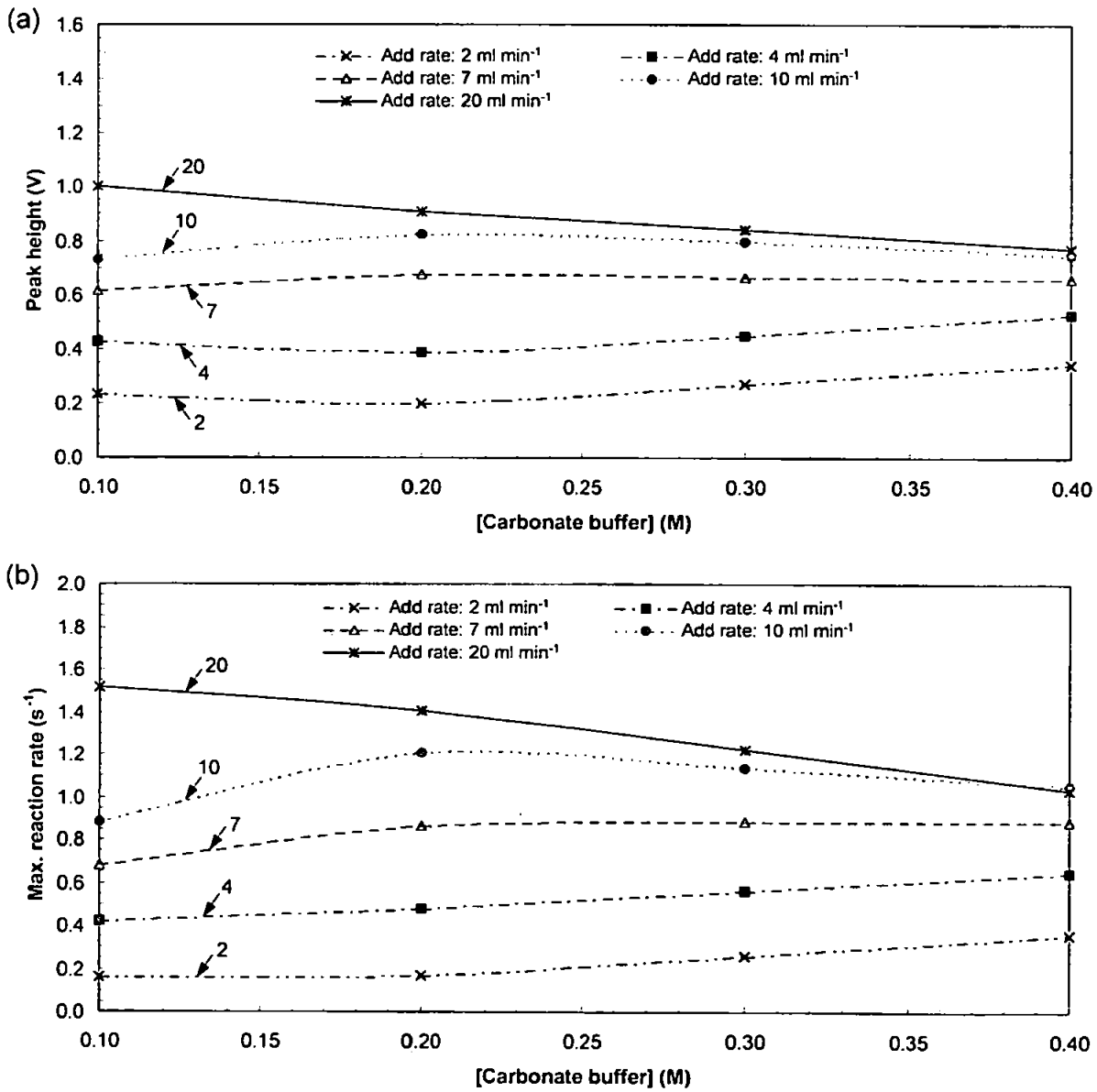

Figure IV.3. Effect of carbonate buffer concentration under different addition rates (arrows show addition rates (ml min^{-1}): (a) peak height; (b) maximum reaction rate parameters

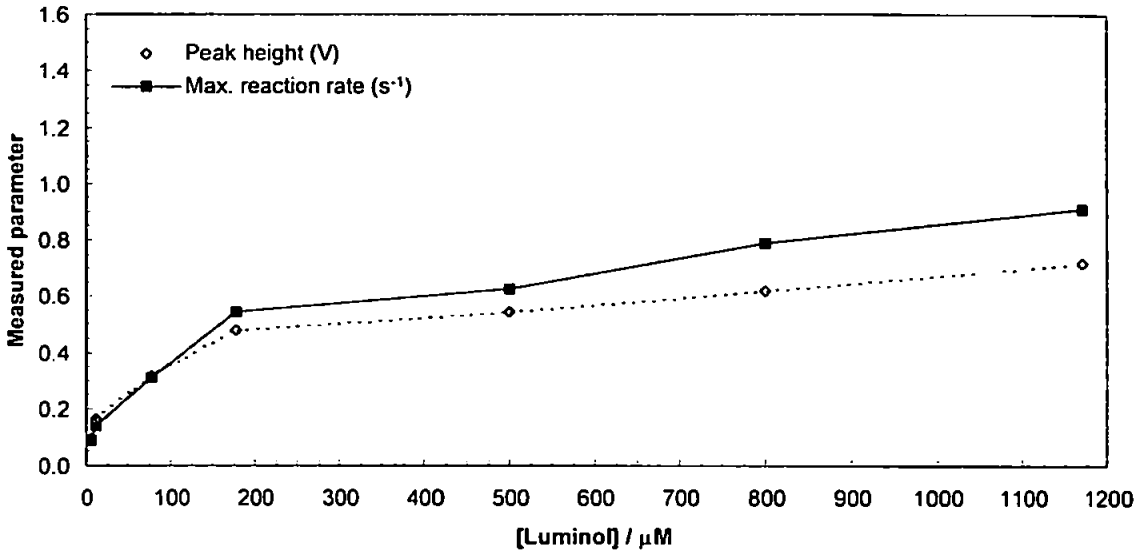

Figure IV.4. Effect of luminol concentration on the measured parameters

IV.3.1.3 Initial Cell Volume

The initial sample volume (V_0) is a key instrumental variable in the CAR technique. The effects of changing this variable across differing addition rates is shown in Figure IV.5. Results clearly showed that at all addition rates tested, the optimum cell volume was 1.0-1.5 ml for peak height data, and 1.0 ml for reaction rate measurements. Lower volume resulted in reduced precision, whilst volumes above 1.0 ml gave CL signals of reduced sensitivity, particularly in terms of reaction rate measurements. It should be noted that above an addition rate of 8 ml min^{-1}, varying V_0 affected peak height measurements more markedly than reaction rates, and indeed maximum CL peak intensities were similar between initial cell volumes of 1-5 ml. Differences between the two measured parameters can be ascribed to the different relative contributions of the formation (maximum reaction) and decay rate to the peak height of the CL signal.

IV.3.1.4 Reagent pH

The effect of buffer and hence reaction pH on the CL emission is shown in Figure IV.6. The catalytic effect of Fe(II) ions on the oxidation of luminol is highly pH dependent, with the reaction favouring alkaline conditions (>pH 10; Seitz and Hercules, 1972). Experiments performed during this work found a broad optimum, with CL signals at their most intense when

the reagent was maintained at pH 11.5, resulting in a final pH in the reaction vessel of approximately 10.9.

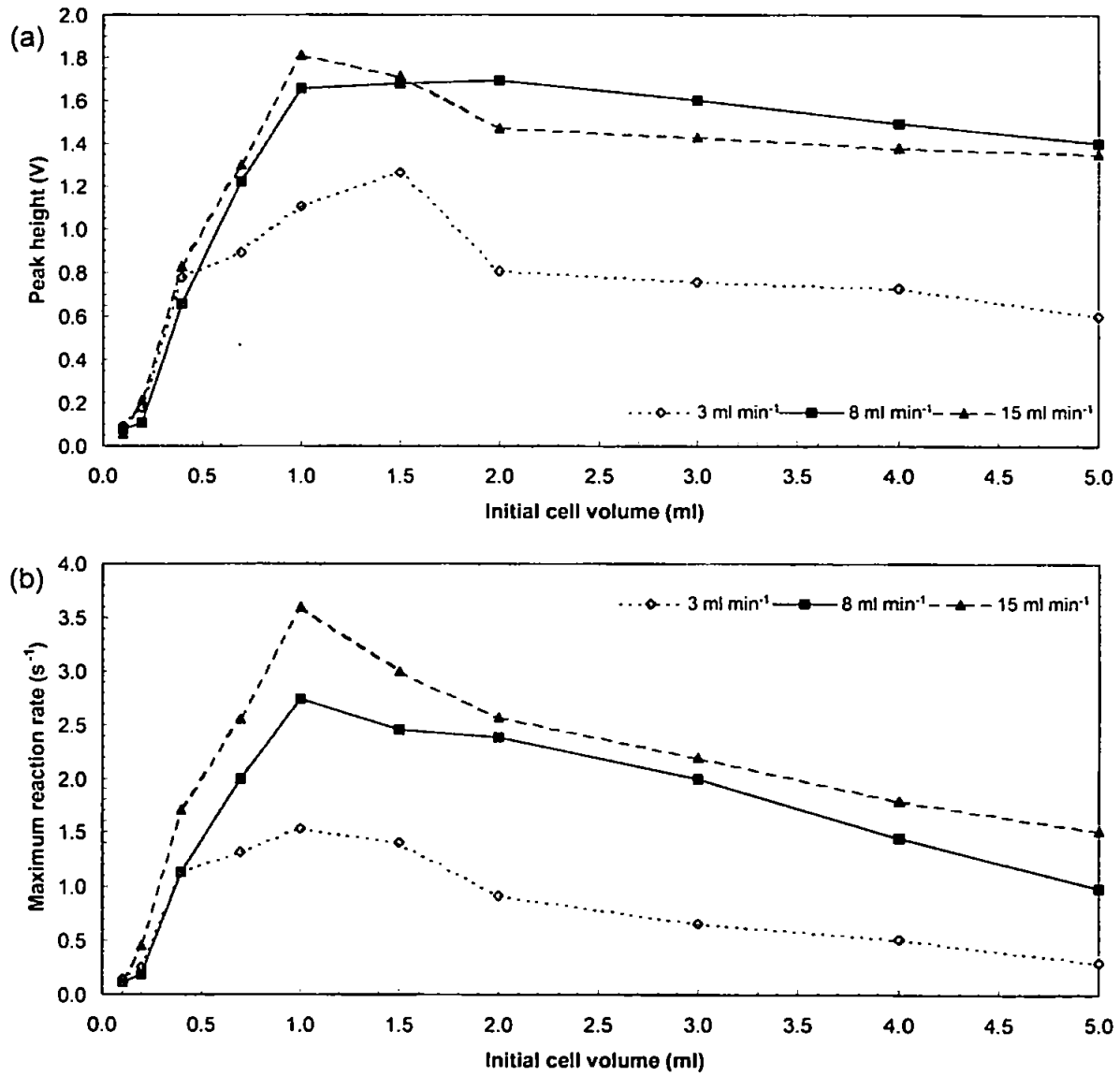

Figure IV.5. Effect of the initial cell volume on the CAR-CL reaction: (a) peak height data; (b) maximum reaction rate measurements

IV.3.1.5 Sample pH

An investigation into the effect of changing the pH of Fe(II) standards contained in the reaction vessel prior to addition was carried out to ascertain the optimum and range for future analyses. This data would provide vital information regarding sample handling and digestion procedures if the CAR-CL method was applied to real matrices. Figure IV.7 shows that an optimum value of pH 2.6 provided a balance between Fe(II) oxidation rates ($t_{1/2} \geq 1$ day) and analyte stability, whilst creating an environment where the solution pH is high enough to obtain a satisfactory CAR-CL curve. Furthermore, it is clearly noted that as the initial sample pH is increased, the residence time (T_{max}) is reduced, as the solution in the reaction vessel reaches optimum pH for luminol CL. Under the conditions listed in Table 1, T_{max} at maximum peak height occurs after 1.22 s.

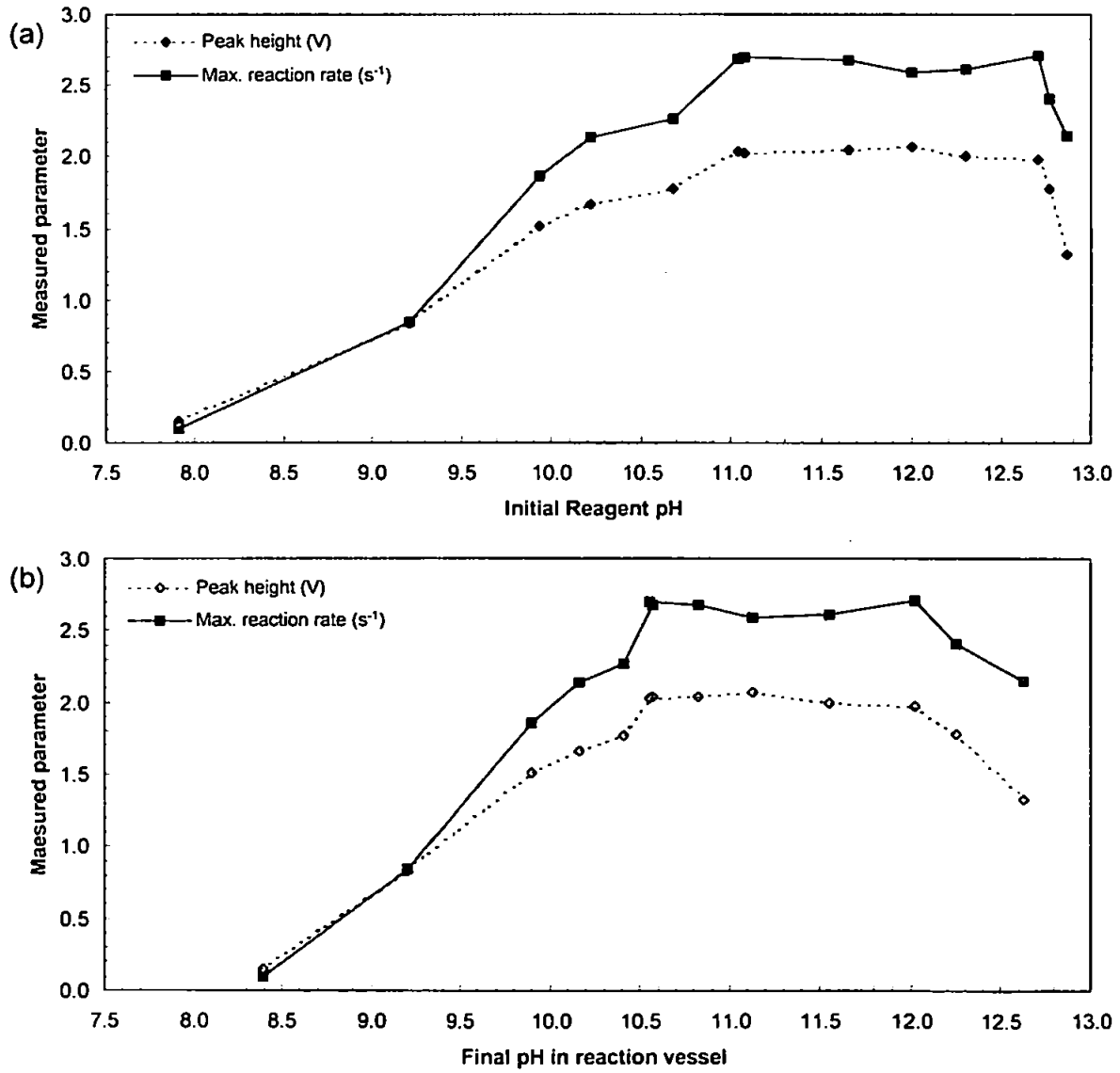

Figure IV.6. Effect of reagent pH on the CAR-CL reaction: (a) initial reagent pH in autoburette; (b) final pH in reaction vessel

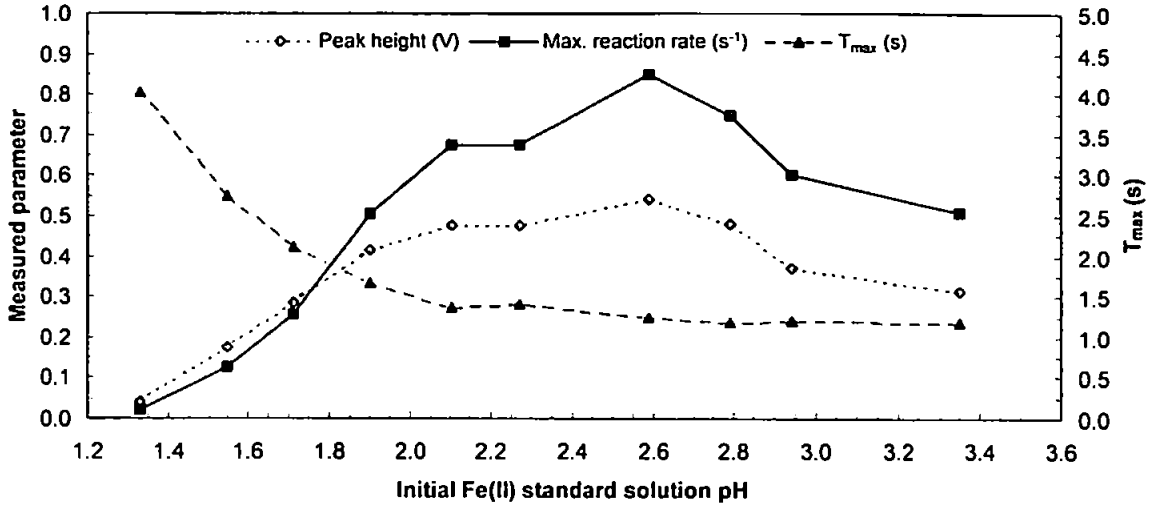

Figure IV.7. Effect of initial sample pH on the CAR-CL reaction

IV.3.1.6 Addition Rate

The effect of luminol reagent addition rates was assessed over a wide range (between 0.1 and 20 ml min^{-1}). Rates below 1 ml min^{-1} resulted in very weak CL signals that could not be differentiated from the detector noise, and hence poor CAR curves. The CL intensity versus time curves obtained behaved similarly towards maximum reaction rate and peak height measurements over a range of buffer molarities, as shown in Figure IV.8, although the effect of changes were more pronounced for reaction rate data above an addition rate of 10 ml min^{-1}. Figure IV.9 shows a plot of maximum reaction rate versus square root of addition rate, under the optimum condition shown in Table IV.1. This plot is consistent with the theoretical postulates of the CAR technique (Velasco *et al.*, 1992) with a linear dependence observed up to an addition rate of 10 ml min^{-1}. This value was selected as a compromise between system sensitivity and reduced reagent consumption. Figure IV.10 illustrates the effect changing the addition rate on the CAR-CL emission versus time profiles. Faster addition rates reduced reaction times (T_{max} varying between 4.30 s and 1.06 s) and provided increased CL intensities up to a value of 15 ml min^{-1}.

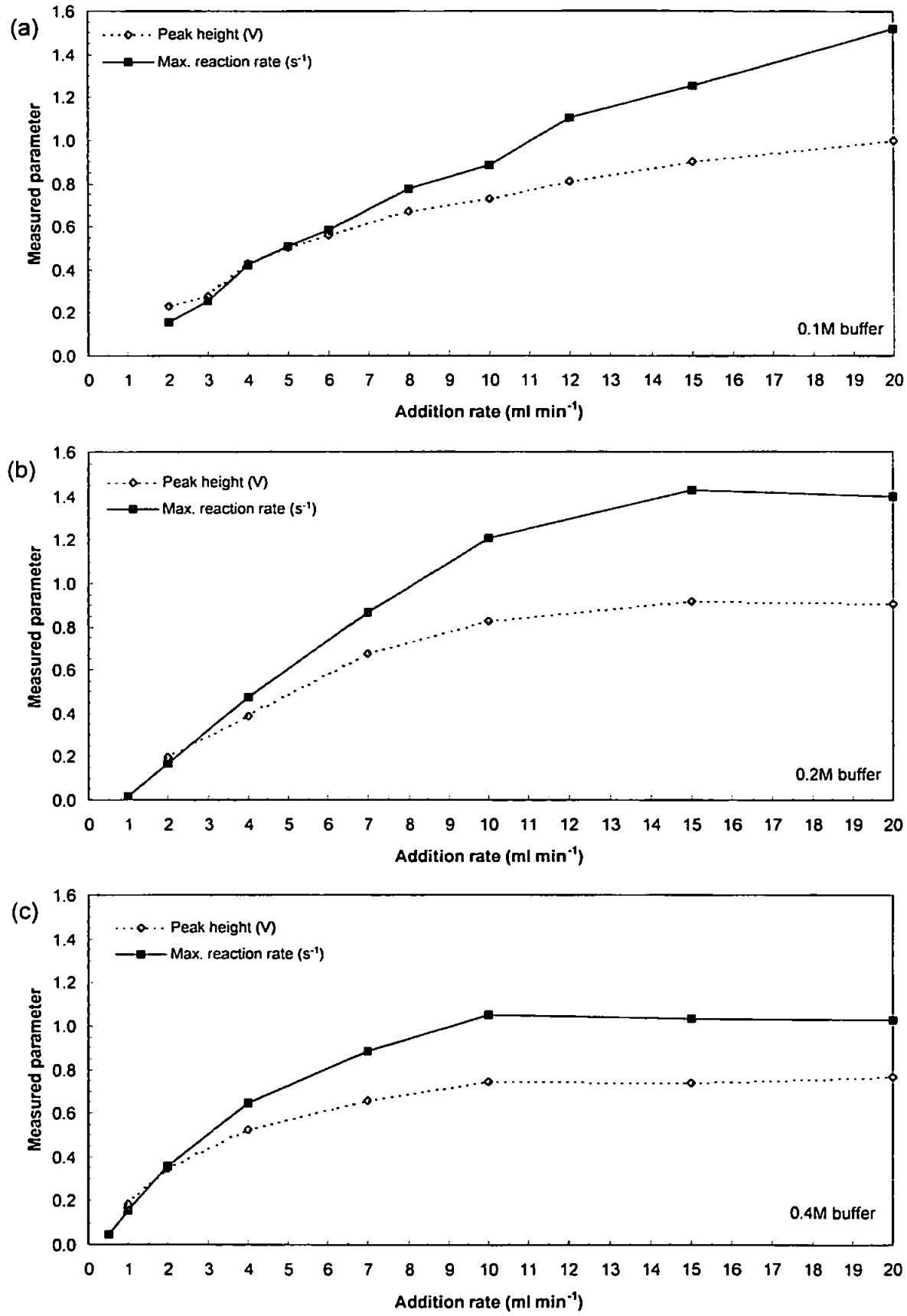

Figure IV.8. Effect of the addition rate on the measured parameters under the CAR-CL manifold: (a) 0.1 M buffer; (b) 0.2 M buffer; (c) 0.4 M buffer

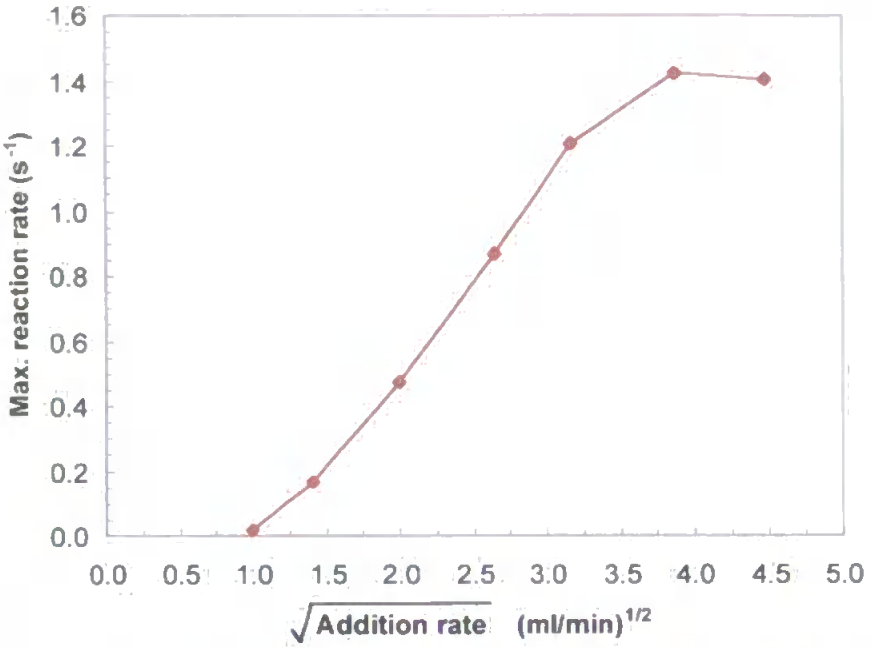

Figure IV.9. Plot of maximum reaction rate vs. square root of addition rate

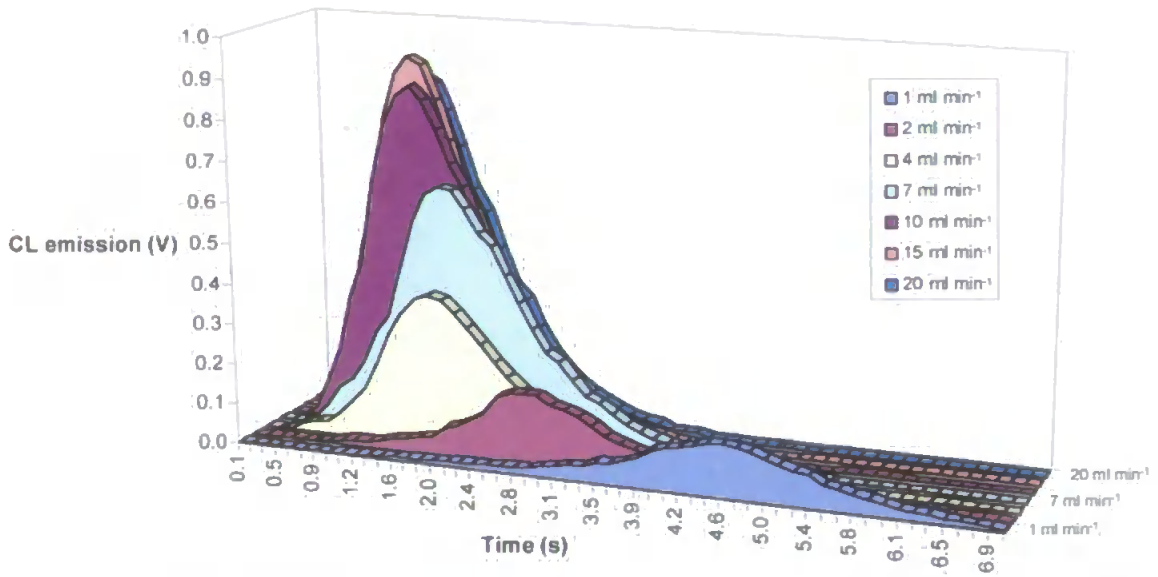

Figure IV.10. Schematic illustration of the effect changing the addition rate on T_{max} and the CAR-CL emission vs. time profiles

IV.3.2 Interferences

Two experiments were performed to ascertain the effect of a variety of interfering ions on the luminol chemistry operated using a CAR manifold. The first investigated the effect of transition metal ions on the CL signal, whilst the second focused on potential interference problems

generated by modifying the ionic strength of the reaction medium; for example, *via* the addition of major sea-salt matrix ions.

IV.3.2.1 Transition Metal Cations

For evaluation of selectivity in the present FI-CL system, individual metal ions were added to acidified 100 nM Fe(II) standard solutions prepared in MQ water at 1, 10 and 100 times the Fe(II) concentration (i.e. at 0.1, 1 and 10 μM level). The change in CL emission was compared to the signal in their absence. Further experiments at lower interferent concentrations were performed if interference was noted at the 0.1 μM concentration level.

Table IV.2 presents the results from treatments of potentially interfering metal concentrations at multiples of the Fe(II) concentration. Values are percent signal intensity relative to the signal intensity of 100 nM Fe(II) in the absence of the other added metals. The average ± standard deviation of three replicate analyses is given. Interference levels are given for both reaction rate and peak height measurements. The shaded boxes indicate the tolerance limit to each foreign species, taken as the largest concentration yielding an error less than ±5% in the determination of 100 nM Fe(II).

As can be seen from Table IV.2, it is impossible to differentiate between the selectivities provided by the two different measurement parameters. Furthermore, the metal ions tested showed similar interference levels under a CAR manifold to those determined under a FI manifold with no preconcentration column (Bowie, unpublished data). Studies show that neither Zn(II), Ni(II), Pb(I), Ag(I) or Hg(II) exhibited a significant interference at any of the concentrations tested. Cr(III) exhibited an increasing quenching effect, whilst Fe(III) caused an enhancement of the signal at 10x and 100x the Fe(II) concentration. Co(II) showed a strong positive interference across the range. The severity of Co(II) interference to the CL system has previously been reported (Sarantonis and Townshend, 1986), and the ability of the metal to catalyse the reaction has been used for its determination (Boyle *et al.*, 1987). Both Mn(II) and Cu(II) showed marked signal reductions. Similar effects were reported by Seitz and Hercules

(1972) and Sarantonis and Townshend (1986), and attributed to the oxidation of Fe(II) *via* a path that does not result in CL emission. At the pH of the reaction, Cu(II) and MnO_2 can oxidise Fe(II) to Fe(III):

$$Cu(II) + Fe(II) \rightarrow Cu(I) + Fe(III)$$
$$MnO_2 + 4H^+ + 2Fe(II) \rightarrow Mn(II) + 2Fe(III) + 2H_2O$$

The Mn(II) and Cu(I) formed are oxidised by O_2 at the reaction pH causing the catalytic oxidation of Fe(II) without involving luminol. This explanation is supported with the observation that the signal reduction is more pronounced at higher Mn(II) and Cu(II) concentrations, while at increased luminol concentrations, the quenching of the signal is less as luminol can now compete more effectively with the alternative Fe(II) oxidation pathway.

IV.3.2.2 Seawater Matrix Ions

The six major components of seawater, namely Cl^-, Na^+, Mg^{2+}, Ca^{2+}, K^+ and SO_4^{2-} make up >99% by weight of sea-salts (Table I.2). To investigate the interference of these major matrix anions and cations, solutions of various different salts were prepared in acidified MQ water, 100 nM Fe(II) added to each and any change in CL emission noted between these standards and a 100 nM Fe(II) standard with no addition.

Figure IV.11 shows the results of the measurement of 100 nM Fe(II) in the various salt solutions. Sodium (0.47 M), magnesium (0.05 M), calcium (0.01 M), potassium (0.01 M), chloride (0.56 M) and sulphate (0.028 M) ions were tested at concentrations found in natural seawater (previous Table III.3) following the method of Kester *et al.* (1967) for the preparation of artificial seawater solutions. The signals are normalised to the Fe(II) measurement after the standard addition and are corrected for their blank. The interference ratio for each species tested was consistently higher for maximum reaction rate measurements compared to peak height data. This is due to the fact that each major interfering sea-salt ion caused a decrease in the residence time (T_{max}) and hence resulted in a faster reaction in comparison to the CAR-CL curve obtained for the Fe(II) standard prepared in MQ water only.

Treatment	Metal add^n / μM		Cr(III)	Zn(II)	Co(II)	Cu(II)	Mn(II)	Fe(III)	Ni(II)	Pb(I)	Ag(I)	Hg(II)
0.01x	0.001	Peak height			105±6							
		Reaction rate			104±5							
0.05x	0.005	Peak height			122±3		102±6					
		Reaction rate			124±4		100±2					
0.1x	0.01	Peak height			168±4	98±3	82±5	96±3				
		Reaction rate			169±5	100±5	83±6	98±6				
0.5x	0.05	Peak height			244±4	49±3	42±2	102±2				
		Reaction rate			242±2	55±5	44±3	101±2				
1x	0.1	Peak height	99±6	104±6	377±8	31±2	23±1	106±2	101±2	103±5	104±6	100±2
		Reaction rate	99±7	103±5	384±5	33±4	27±5	105±3	100±2	105±6	105±5	100±2
10x	1	Peak height	66±4	103±2	926±8	23±3	2±0	128±10	99±1	105±5	107±9	101±3
		Reaction rate	68±6	98±3	879±9	20±1	3±0	127±10	98±2	104±6	107±7	100±2
100x	10	Peak height	10±2	94±9	607±7	9±1	0±0	237±6	103±4	101±4	99±4	101±2
		Reaction rate	10±2	94±9	666±5	8±0	0±0	245±8	102±5	100±5	98±5	102±2

Table IV.2. Summary of metal interference levels; shaded boxes indicate the tolerance limit to each foreign species; no preconcentration step; mean ± standard deviation (n=3)

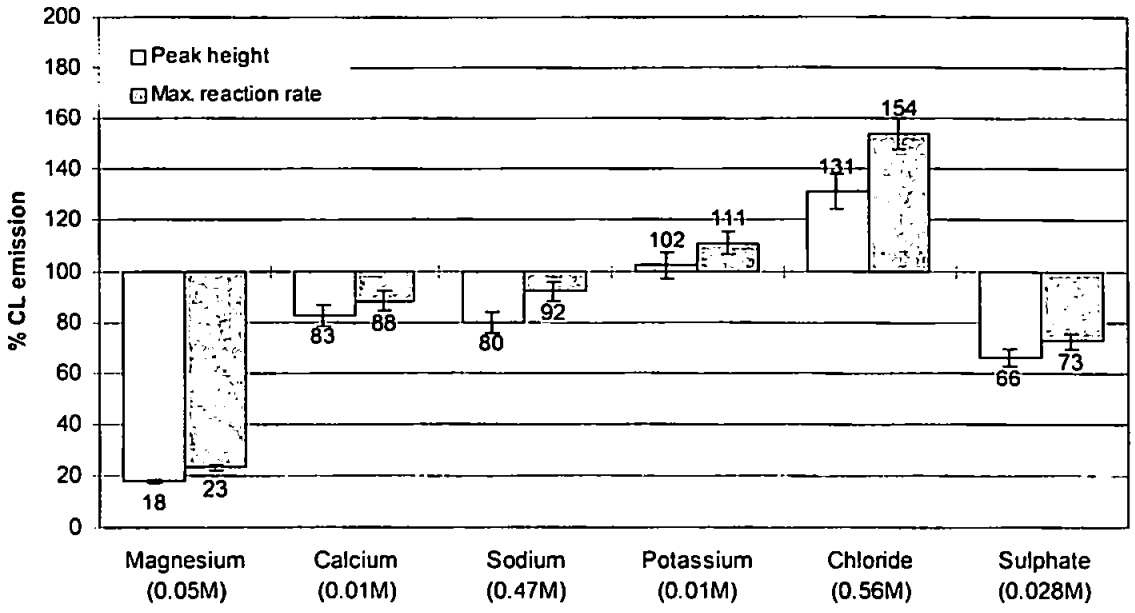

Figure IV.11. Interfering effect of changing matrix composition on the CAR-CL determination of Fe(II)

Results show that the alkali and alkaline-earth metals, particularly Mg^{2+}, suppress the luminol CL signal, consistent with observations using a FI manifold (Section III.3.4) and batch systems (Seitz *et al.*, 1972; Chang and Patterson, 1980). In our experiments, Cl^- anions enhanced the CL intensity. A similar observation for halide ions has been published elsewhere (Bause and Patterson, 1979; Chang and Patterson, 1980; Chang *et al.*, 1980). The proposed mechanism for this CL enhancement was an interaction of the halide ions with a metal-O_2-luminol complex, causing an increase in CL emission. The results of the CAR study are, once again, similar to those for a FI manifold (Section III.3.4.1), although Ca^{2+} ions appear as less of a quencher, whilst SO_4^{2-} ions may prove a greater interference problem.

IV.3.3 Fe(III) Reduction

In order to enable total Fe determinations to be made on real sample matrices, an investigation into the reduction characteristics of Fe(III) → Fe(II) species was carried out. Screening experiments were performed with various reducing agents. As observed in Section III.3.3, ascorbic acid additions resulted in total quenching of the CL signal. Hydroxylamine hydrochloride concentrations up to 100 µM were ineffective in reducing the Fe(III) standards, whilst 1 mM additions partially suppressed the CAR-CL emission. Sulphite (Na_2SO_3) generated the best Fe(III) reduction characteristics. A full theoretical treatment of the reduction of Fe(III)

species using sulphite was reported in Section III.3.3 and the reaction kinetics in natural waters has been reported elsewhere (Millero *et al.*, 1995b). The rate is first order with respect to Fe(III) and S(IV):

$$\frac{d[Fe(III)]}{dt} = -k[Fe(III)][S(IV)]$$

A Fe(III) reduction versus time curve obtained using the CAR-CL system is given in Figure IV.12. Appendix B contains a spreadsheet representation of half-life data for the reaction in natural waters with respect to various parameters (temperature, pH, [S(IV)], ionic strength). Using constants given in Millero *et al.* (1995b), in a zero ionic strength medium (e.g. MQ pure water) the half-life for the reduction of Fe(III) species is 6.6 s at pH 3.5 ([S(IV)]=400 µM, T=25 °C). During the CAR-CL experiments, samples at pH 2.4 were treated with Fe(III) reducing reagent ([S(IV)]=400 µM , T=25 °C, MQ matrix) and allowed to react for at least 1 h. System response from standards additions using both Fe(II) or Fe(III) ions was not statistically different up to an initial concentration of 200 nM, consistent with the complete reduction of Fe(III) by sulphite. Under the stated conditions after a 1 h reaction time, greater than 96% of Fe(III) ions were effectively reduced. Above the 200 nM Fe level and for samples of different pH, greater S(IV) concentrations and/or reaction times should be applied.

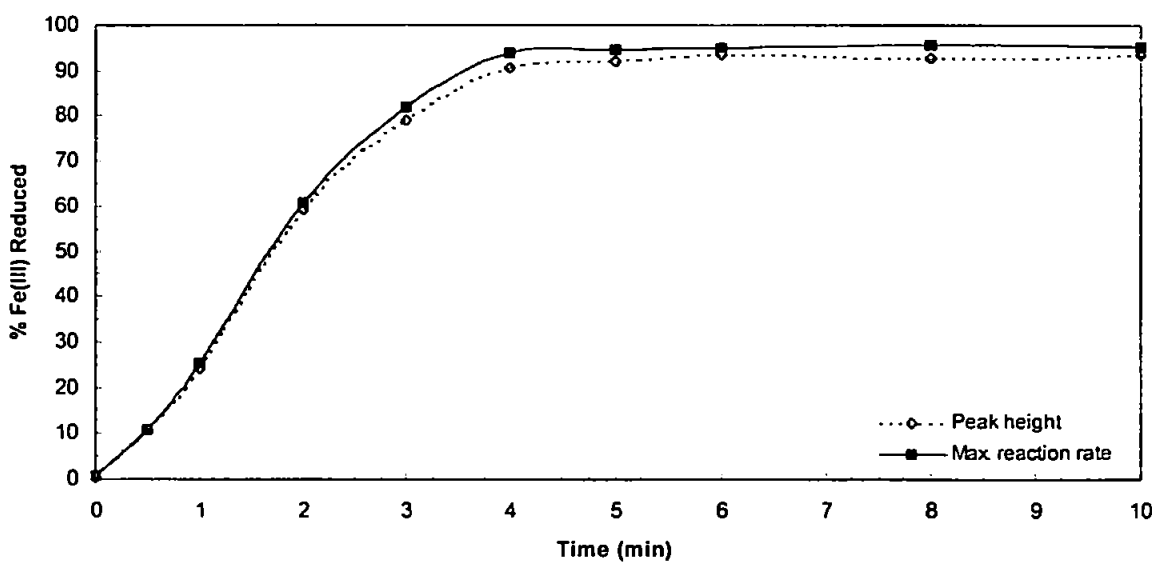

Figure IV.12. Percentage of Fe(III) species reduced by sulphite vs. time ([Fe(III)]=100 nM, [S(IV)]=400 µM, T=25°C, pH=2.4, matrix=MQ pure water)

IV.3.4 Calibration

The response of the optimised system to solutions containing varying concentrations of Fe(II) ions was monitored *via* both reaction rate and peak height measurements. A working calibration curve is shown in Figure IV.13, whilst the analytical figures of merit are given in Table IV.3 and Figure IV.14 displays the CAR-CL intensity versus time profiles over the working range. The limit of detection was calculated as the Fe(II) concentration giving a signal equal to the blank plus three times its standard deviation, the precision was measured at two differing Fe(II) concentrations within the linear range, and the sample throughput estimated from the time taken to perform three replicate analyses, including sample changeover in the CAR system. As shown, both measured parameters can be used for the CAR-CL determination of Fe in synthetic samples.

Parameter	*Peak height measurement*	*Maximum reaction rate measurement*
Linear dynamic range	1.0×10^{-8} - 1.0×10^{-6} M	1.0×10^{-8} - 1.0×10^{-6} M
Limit of detection (3s)	1.1×10^{-8} M or 0.61 ng ml^{-1}	1.6×10^{-8} M or 0.89 ng ml^{-1}
Limit of determination (10s)	2.2×10^{-8} M	3.8×10^{-8} M
Correlation coefficient, r^2	0.9933	0.9956
Sensitivity	$(y = 3\times10^{6}x + 0.0701)$ V nM^{-1}	$(y = 5\times10^{6}x + 0.0578)$ $(s\ nM)^{-1}$
Relative standard deviation (n=5)	3.6%[a]; 6.1%[b]	3.7%[a]; 4.9%[b]
Sampling rate (h^{-1})	48	53

[a] [Fe(II)]=20nM, [b] [Fe(II)]=600nM

Table IV.3. Analytical figures of merit for the CAR-CL technique

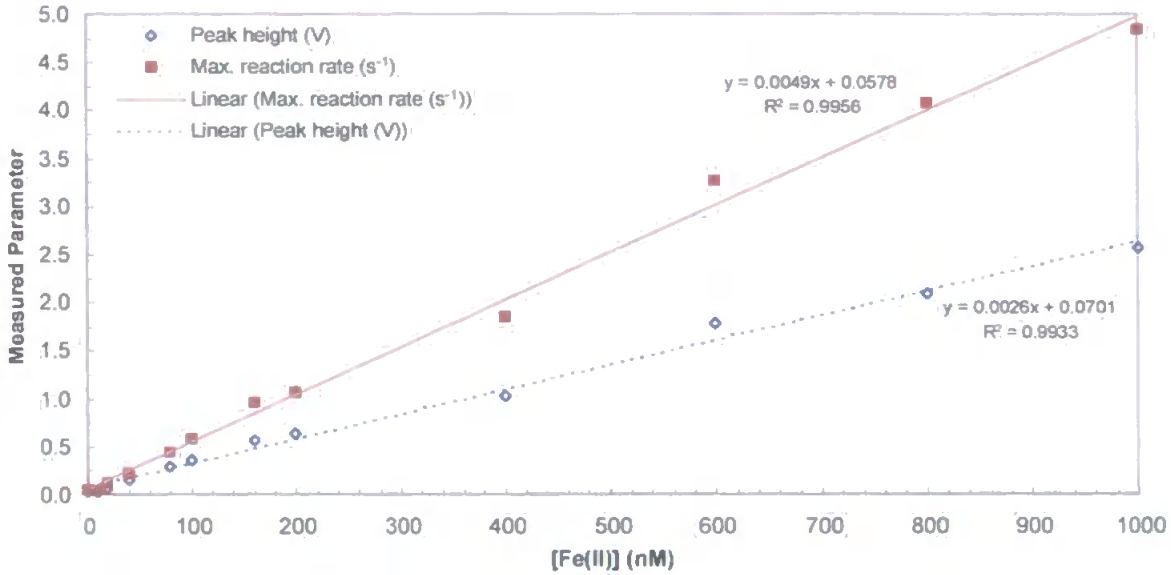

Figure IV.13. Calibration of the CAR-CL system for the determination of Fe(II) species

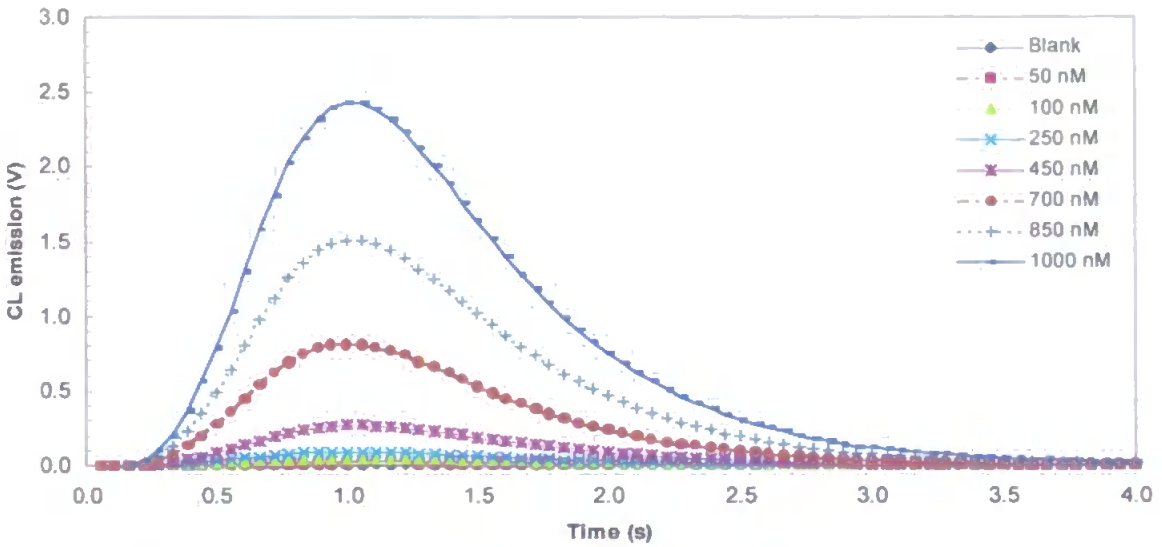

Figure IV.14. CL intensity vs. time curves over the linear calibration range

IV.3.5 Comparison of Techniques

The proposed CAR method was compared with other recently reported methods based on similar CL determinations for Fe species. The results in Table IV.4 illustrate that the CAR method is a useful alternative for the determination of Fe(II) and total Fe(II+III).

CL system	*Limit of detection*[a]	*Linear dynamic range*[a]	*Observations*	*Ref.*
Luminol / O_2	0.005 μg l^{-1}	0.005 - 50 μg l^{-1}	Batch reaction cell; bisulphite reduction	1
Luminol / O_2	$5.0x10^{-10}$ M	$1x10^{-9}$ – $1x10^{-6}$ M	FI manifold; silver reductor mini-column	2
Luminol / H_2O_2	$1x10^{-13}$ M	10 -70 ng ml^{-1}	8-Hydroxyquinoline on CPG preconcentration column	3
Luminol / H_2O_2	$5x10^{-11}$ M	$9x10^{-11}$ - $1.8x10^{-9}$ M	FI manifold; Fe(III) direct analysis; 8-HQ separation column	4
Luminol / O_2	0.06 nmol kg^{-1}	0.25 - 200 nmol kg^{-1}	Stopped flow manifold; sulphite reduction	5
Luminol / O_2	$4x10^{-11}$ M	$1x10^{-10}$ - $1x10^{-8}$ M	FI manifold; 8-HQ preconcentration column; sulphite reduction	6
Luminol / O_2	$1.1x10^{-8}$ M	$1x10^{-8}$ - $1x10^{-6}$ M	CAR manifold; sulphite reduction	7

References
1. Seitz and Hercules, 1972
2. Sarantonis and Townshend, 1986
3. Alwarthan *et al.*, 1990
4. Obata *et al.*, 1993
5. O'Sullivan *et al.*, 1995
6. Bowie *et al.*, 1998
7. This study

[a] Detection limits and linear ranges as reported in the original papers

Table IV.4. Comparison of the CAR technique with other reported Fe CL methods

IV.3.6 Determination of Iron in Non-fat Milk Powder by CAR-CL

IV.3.6.1 Procedure

The CAR-CL method was applied in order to determine the content of Fe in a non-fat milk powder (National Bureau of Standards, SRM 1549). Approximately 1 g of the powder was weighed into a clean crucible, placed in a furnace and the temperature gradually increased to 600°C for approximately 2 h. The ashed solid was then dissolved in 1.0 M HCl. The resulting solution was subsequently diluted in 0.01 M HCl, in order to allow the Fe concentration in the sample to lie within the linear range of the CAR method. The Fe(III) reducing reagent was added and allowed to react for 1 h.

However, when the sample solution was introduced into the CAR-CL manifold, no peak was obtainable in the range T_{max} = 0.8-1.4, the normal elution time for Fe(II) species, and hence neither reaction rate nor peak height measurements were possible. Major constituents of the

SRM, such as calcium, magnesium or phosphate ions, were postulated to be severely interfering with the analytical method.

IV.3.6.2 Ion-exchange Separation

An anion-exchange column (Dowex 1, chloride form) was used to treat the SRM prior to introduction to the analytical method, in order to separate the Fe(III) ions from the matrix of the SRM. The ashed solid was dissolved in 6.0 M HCl and passed through the column at 0.08 ml min^{-1}, retaining the negatively charged Fe chloro-complexes ($FeCl_3^-$, $FeCl_4^{2-}$, $FeCl_6^{4-}$). Elution was then performed using 10 ml of 0.01 M HCl in the reverse direction at a flow rate of 0.2 ml min^{-1}, shifting the equilibrium and disassociating Fe from the column. The collected eluent solution was next raised to pH 2.4 using additions of 1.0 M ammonia solution, before the Fe(III) reducing reagent was added and allowed to react for 1 h. The sample solution was then introduced into the CAR-CL manifold in the usual manner. Quantification of the Fe content in the SRM could be achieved using either calibration or standard addition methods. Despite the separation, no CL peak was achieved using the CAR manifold. Unfortunately, time restraints prevented any further investigation into: (i) other interferents to the method, (ii) retention of Fe complexes onto the anion-exchange column, or (iii) the catalytic effect of the Fe in the column eluent on the luminol reaction.

IV.4 CONCLUSIONS

The analytical characteristics reported here testify to the reliability of CAR technique for monitoring fast (<1 ms) CL reactions. Both maximum reaction rate and peak height measurements can be applied to transient CL intensity versus time profiles for the quantification of Fe(II), or total Fe after Fe(III) reduction, in sample solutions (limit of detection 11 nM). The method is perhaps more advantageous for the determination of Fe in biological and clinical samples where the Fe content is higher than in seawater, which has been the most common matrix for environmental applications based upon luminol CL.

Proposed future work includes adaptation of the CAR analytical system in order for the sample solution to be automatically introduced into the reaction vessel before the addition of reagent allows the CL intensity versus time profile to be recorded. The sample and reagent solutions could then be drained from the cell, followed by a MQ wash prior to the introduction of the next sample. Such modifications would undoubtedly improve the sample throughput, reduce any possible contamination problems and enable the CAR-CL system to function in a fully automated process environment.

IRON DISTRIBUTIONS IN SURFACE WATERS OF THE ATLANTIC OCEAN

V.1 INTRODUCTION

V.1.1 Overview

This chapter discusses the shipboard validation of a flow injection – chemiluminescence (FI-CL) technique for the determination of iron (Fe) in seawater and subsequent deployment on a research cruise in the North and South Atlantic Ocean. The comprehensive dataset for Fe obtained compared favourably with previously reported oceanic distributions. Additional data acquired during the CCMS-PML Atlantic Meridional Transect programme allowed for a detailed investigation into marine biogeochemical processes occurring in the upper water column, which controlled Fe and other trace metal concentrations and fluxes in the surface Atlantic Ocean.

V.1.2 Atlantic Ocean

The Atlantic Ocean is a narrow basin, relative to the Pacific, connecting the Arctic and Southern Oceans (Figure V.1). Relatively shallow, averaging 3,310 m deep, the Atlantic Ocean has wide continental margins, the Mid-Atlantic Ridge, several semi-isolated seas, receives large amount of water and sediments from riverine runoff and large areas underlie a path of strong aerosol deposition. Its upper water circulation is dominated on a gross scale by two large anticyclonic gyres, a counter-clockwise one in the South Atlantic and a clockwise one in the North Atlantic. A plethora of water mass types and associated internal circulations can be found in the Atlantic Ocean, full details of which are provided by Pickard and Emery (1990) and outlined in Section V.3.3.

V.1.3 Atlantic Meridional Transect

V.1.3.1 Background

The Atlantic Meridional Transect (AMT[1]; Robins and Aiken 1996) was conceived as a means of acquiring a time series of oceanographic, biological, chemical and optical data over large latitudinal ranges (50°N to 50°S). The 15,000 km transect of the Atlantic Ocean crosses through a number of contrasting global-scale oceanic provinces, where environmental conditions vary

[1] http://www1.npm.ac.uk:80/amt/

from polar to tropical, from eutrophic shelf seas to oligotrophic mid-ocean gyres and from polluted to pristine. Core AMT scientific objectives involve refinement of our understanding of the role of ocean biota in biogeochemical processes, carbon fluxes and ultimately global climate and the development of remotely sensed measurements of global primary production.

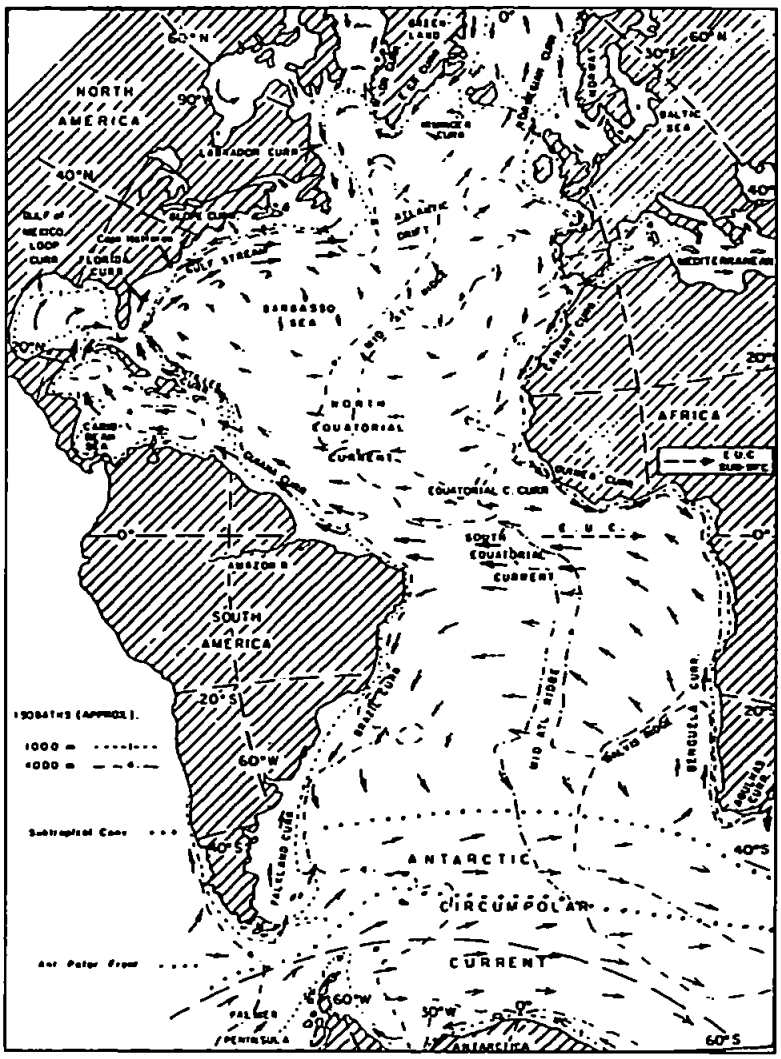

Figure V.1. Atlantic Ocean: surface circulation patterns (including 1000 and 4000 m isobaths; reproduced from Pickard and Emery, 1990)

The AMT project voyages take advantage of the twice yearly passage of the National Environmental Research Council (NERC) vessel, the *RRS James Clark Ross*, operated by the British Antarctic Survey (BAS) during its passage to and from Antarctica each year. The research ship serves as an ideal platform to conduct oceanographic research on the responses of distinct ecosystems and the coupled marine atmosphere to natural and anthropogenically forced environmental change. The cruise track provides an excellent opportunity to elucidate surface distributions and upper water column vertical profiles for trace elements through regions of

diverse input (e.g. continental runoff, shelf regeneration, atmospheric deposition, precipitation, upwelling systems) and removal (e.g. biological uptake, particle scavenging, biogenic export) mechanisms. A berth of opportunity was obtained on AMT-3 (autumn 1996), the third Atlantic transect in the current series.

R.R.S James Clark Ross (JCR; Figure V.2) is a fully equipped multi-role scientific research vessel. Commissioned in May 1991, 90 m in length, the ship has ice-breaking capabilities and can endure 55 days continuous operation in Antarctic waters.

Figure V.2. *RRS James Clark Ross* on passage through waters off the Antarctic Peninsula

V.1.3.2 Cruise Track

AMT-3 left Grimsby (UK) on 20th September 1996 and sailed for Portsmouth to load aviation fuel. Eighteen scientific personnel were on-board. Thereafter, a course *via* the Western Approaches was taken towards the first major waypoint at 47°N, 20°W (Figure V.3). The course was next altered in a due south direction remaining on the 20°W line of longitude, only minor deviations made to remain outside territorial waters near Madeira, Africa and the Cape Verde Islands. At a latitude of 10°N, the ship altered to a south-westerly course heading for the Rio de

la Plata entrance in Uruguay, arriving on October 17th. Departing Montevideo six days later, a generally southerly course was taken, arriving in Port Stanley (Falkland Islands) on 25th October 1996.

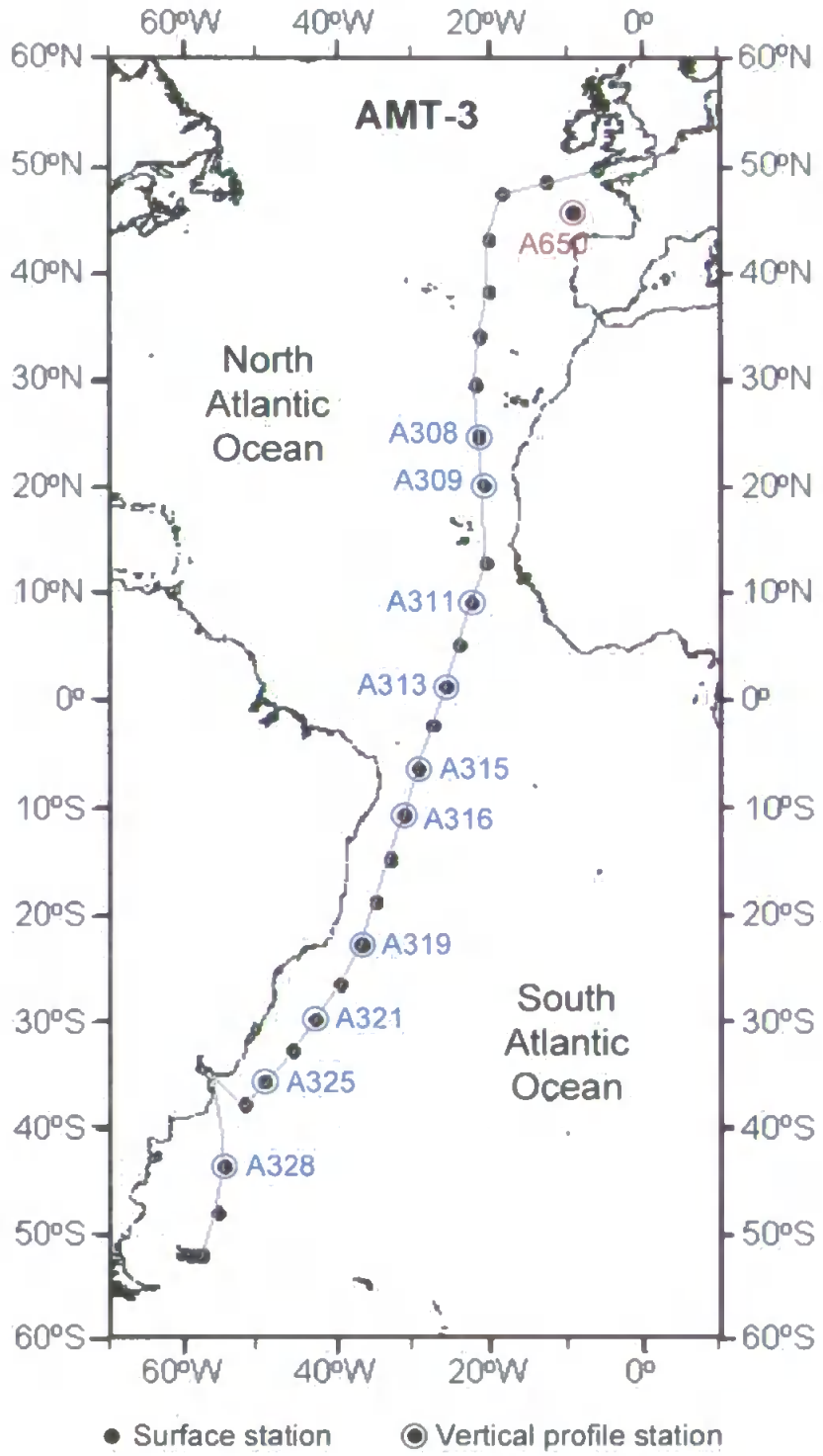

Figure V.3. Ship's track and stations during cruise AMT-3 (Mercator projection)

V.1.3.3 Biogeochemical Oceanic Provinces

Five main biogeochemical provinces along AMT were defined by Longhurst *et al.* (1995): (1) the North Atlantic Drift (NADR, 60°-40°N); (2) the North Atlantic Subtropical Gyre (NAST, 40°–25°N); (3) the North Atlantic Tropical Gyre (NATR, 25°-10°N); (4) the Western Tropical Atlantic (WTRA, 10°N-5°S); and (5) the South Atlantic Tropical Gyre (SATL, 5°-40°S). The distribution of temperature, salinity, trace metal and nutrient data from this study, in combination with recent satellite remote sensing images (e.g. CSCZ[2], SeaWiFS[3], Figure V.4) allows for a refinement of the provinces named above, and an identification of typical oceanographic regimes encountered during the AMT-3 expedition (Table V.1). Each province represents an area of similar chemical, biological and/or physical oceanography, the features of which are discussed in more detail below (Section V.3.4.3). The assignment of province boundaries shows small-scale variation with season and each region may encompass more than one water mass. However, provinces defined in September and October 1996 during AMT-3 are broadly typical in comparison with other AMT or similar Atlantic Ocean cruises (e.g. Rutgers van der Loeff *et al.*, 1997).

Type of Oceanographic Region	*Biogeochemical Province*	*Acronym*	*Latitudinal Range*
Continental shelf	South-west Approaches	SW App	50°N to 47°N
Open-ocean gyre	North-east Atlantic Oligotrophic Gyre	NEAOG	43°N to 24°N
Open-ocean upwelling	North-west Africa Upwelling	NWAUp	20°N
North Equatorial region	South of Upwelling / North of Equator	SUp/NEq	17°N to 3°N
Equatorial upwelling	Equator	Eq	2°N to –3°S
Open-ocean gyre	South Atlantic Oligotrophic Gyre	SAOG	-6°S to –30°S
SW Atlantic mixing zone	Brazil and Falkland Currents Confluence	BFCC	-32°S to –48°S
Coastal shelf	East Falkland Shelf	EFS	-52°S

Table V.1. Biogeochemical provinces assigned during AMT-3 cruise

[2] Coastal Zone Color Scanner; http://daac.gsfc.nasa.gov/data/dataset/CZCS/

[3] Sea-viewing Wide Field-of-view Sensor; http://daac.gsfc.nasa.gov/data/dataset/SEAWIFS/

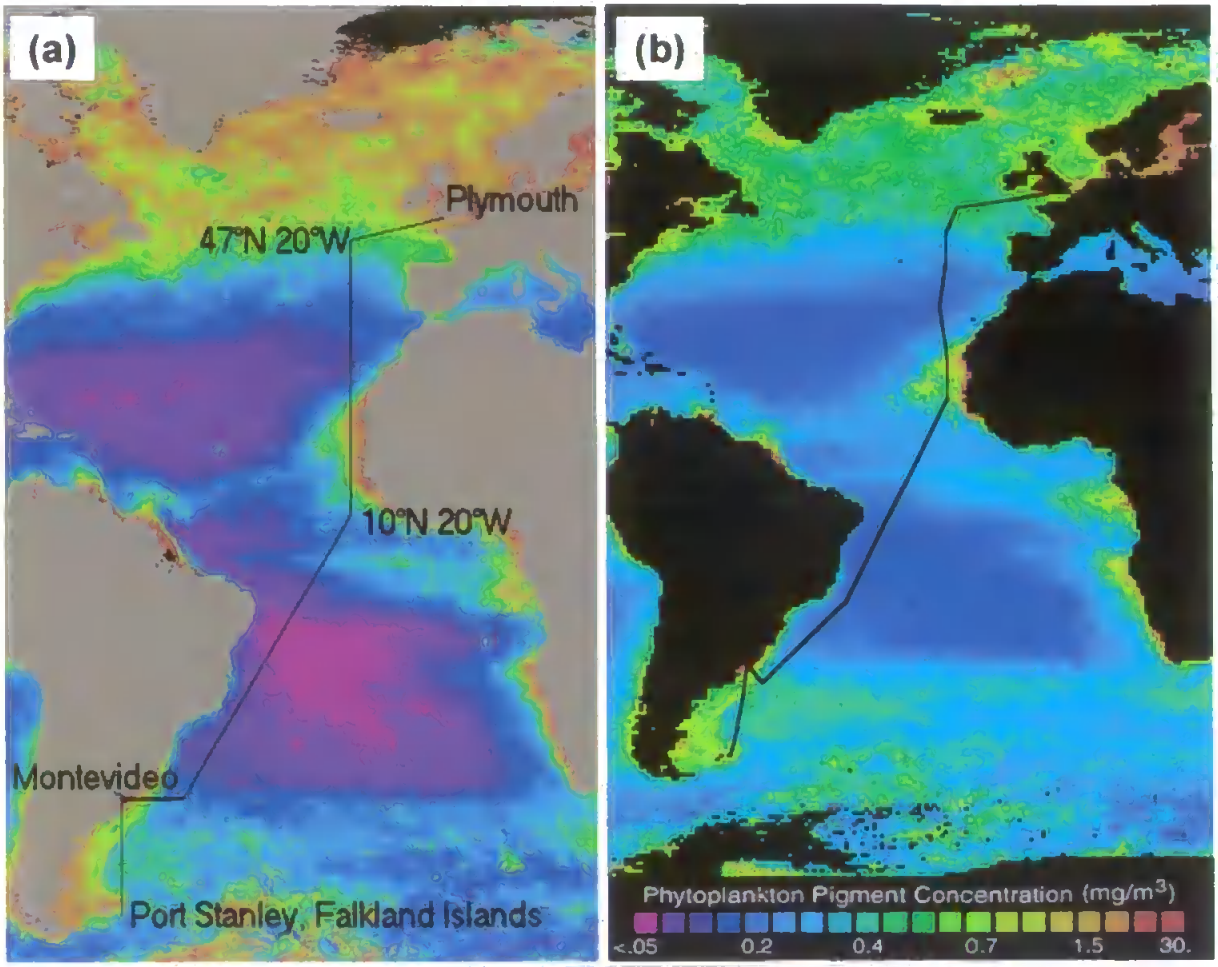

Figure V.4. (a) Ocean colour background, CSCZ chlorophyll composite for 1993. Zones of common colour represent distinct physical or biological provinces (high chlorophyll: yellow, orange and red, low chlorophyll: blue and mauve; reproduced courtesy of NASA/CSCZ)
(b) AMT-3 cruise track over SeaWiFS 1998 yearly composite image for the Atlantic Ocean (reproduced from NASA/GSFC SeaWiFS level-3 chlorophyll *a* browser)

V.1.3.4 Iron Analysis Objectives

1. To map underway Fe levels along the complete transect using FI-CL technology for sub-nanomolar determinations
2. To investigate the vertical structure of Fe in the upper water column through contrasting biogeochemical provinces *via* daily Go-Flo casts, correlating fluctuations with hydrography and biological activity
3. To fingerprint Fe input mechanisms along the transect (e.g. atmospheric dusts and rain, sedimentary regeneration, upwelling waters, frontal systems, riverine plumes) using the sampling strategy outlined in objectives 1 and 2, through sub-sample elemental analysis (objective 4) and *via* cross-correlation with hydrographic data and other AMT shipboard measurements (e.g. nutrients, chlorophyll, production)

4. To correlate Fe with other trace metal profiles (Al, Co, Ni) *via* laboratory analyses on selected asset preserved sub-samples
5. To focus specifically on the extent of Saharan fallout across the Atlantic and investigate the direct contribution of such aerosols to Fe levels in the water column (i.e. solubility, mobility, reactivity).

V.1.4 Historical Trace Metal Data for the World's Oceans

A better understanding of Fe distributions and trace element cycling in oceanic surface waters can only be achieved through high quality trace metal measurements made in combination with high resolution biological and physical oceanographic information. Such data is scarce. Synoptic field studies are needed to provide valuable information on the relative importance of various input and removal mechanisms to the surface layers (0-200 m) of the World's oceans.

Previously reported oceanic trace metal distributions are summarised in Table V.2. Long distance surface water transects for Fe and aluminium (Al) have been performed in the Atlantic Ocean (Powell *et al.*, 1995; Helmers and Rutgers van der Loeff, 1993), revealing both elements to be spatially and seasonally variable. The vertical distribution of Fe has been investigated in all oceanic basins (except the South Atlantic), and recent data show consistency in deep waters, approaching a mean value of 0.7 nM, as discussed by Johnson *et al.* (1997). Data for Al, cobalt (Co) and nickel (Ni) is more sparse and previous studies have focussed on the North Atlantic. Al concentrations show significant fluctuation through differing water masses, whilst Co values average 20-40 pM away from surface layers. Ni displays no inter-ocean fractionation in surface layers, revealing a nutrient (or recycled) vertical structure in deeper waters.

Region	Fe (nM)			Al (nM)			Co (pM)			Ni (nM)		
	Surface	Deep	Ref.	Surface	Deep	Ref.	Surface	Deep	Ref.	Surface	Deep	Ref.
SW Approaches		n.o.		100-350	n.o.	*12*	50-170	30-190	*18*	4.0-5.0	n.o.	*23*
				50-120	n.o.	*13*				3.8	3.8	*18*
NE Atlantic	0.2	0.6	*1*	10-15	20-40	*14*	20-40	20-40	*19*	1.7-3.0	3.5-4.0	*24*
	1.0	3.9	*2*							2.4-2.5	3.8	*23,2*
NW Atlantic	0.2-0.6	0.7-0.9	*3*		n.o.			n.o.			n.o.	
South Atlantic		n.o.		11.4-12.2	2.3-15	*15*		n.o.		2.5	4.0-5.0	*25*
Atlantic Ocean[a]	0.5-10[b]	n.o.	*4*	0.2-86	10-25	*15*		n.o.			n.o.	
				1.2-79[b]	n.o.	*16,17*						
North Pacific	0.1	0.7	*5*		n.o.		170	25	*20*		n.o.	
	0.05	0.7	*6*									
Equatorial Pacific	0.05	0.4	*7,8*		n.o.		10-24	n.o.	*21*	2.0-2.9	n.o.	*21*
South Pacific	0.1	0.7	*5*		n.o.			n.o.			n.o.	
Indian Ocean	0.3	1.0	*9*		n.o.			n.o.		2.1	6.0-8.0	*24*
Southern Ocean	0.3-0.5	0.6-1.1	*10*		n.o.		30-40	20	*22*	6.0	7.0-8.0	*22*
	0.2-0.6[b]	0.4-1.2[b]	*11*									

References

1. Martin *et al.* (1993)
2. Danielsson *et al.* (1985)
3. Wu and Luther (1994)
4. Powell *et al.* (1995)
5. Landing and Bruland (1987)
6. Martin et al (1989)
7. Gordon et al (1997)
8. Johnson *et al.* (1997)
9. Saager *et al.* (1989)
10. Löscher *et al.* (1997)
11. Sedwick *et al.* (1997)
12. Kremling (1985)
13. Kremling and Hydes (1988)
14. Hydes *et al.* (1986)
15. Measures (1995)
16. Rutgers van der Loeff *et al.* (1997)
17. Helmers and Rutgers van der Loeff (1993)
18. Tappin *et al.* (1993)
19. Landing *et al.* (1995)
20. Knauer *et al.* (1982)
21. Gordon *et al.* (1998)
22. Westerlund and Öhman (1991)
23. Kremling and Pohl (1989)
24. Saager *et al.* (1997)
25. Yeats *et al.* (1995)
24. Morley *et al.* (1993)

n.o.: no observations [a] Surface water latitudinal transect All dissolved values, except [b] (unfiltered, total dissolvable TD)

Table V.2. Abundance of trace metals (Fe, Al, Co, Ni) in the World's oceans; table shows selection of typically reported values

V.2 EXPERIMENTAL

V.2.1 Shipboard Procedures

All reagents and standards were prepared on-board ship from pre-weighed solid stocks and pre-cleaned solutions, as outlined in Section III.2.1. Clean techniques were strictly observed and all sample and reagent handling performed within a specially designed clean area constructed within the ship's laboratory. The FI-CL analyser (manifold shown previously in Figure III.6) was used for all analyses and operated using the procedures described in detail in Chapter 3. Spare components were taken to sea in case of instrumentation breakdown, together with ancillary fieldwork equipment and a comprehensive set of consumables and sample bottles as a contingency for complete system failure. Instrumentation was transported and housed in a specially designed wooden box modified for trace metal analysis and containing a sealed Perspex® cube enclosure for reagents and samples (Figure V.5). Equipment was securely tied down or fixed to the benches of the ship's laboratory prior to departure.

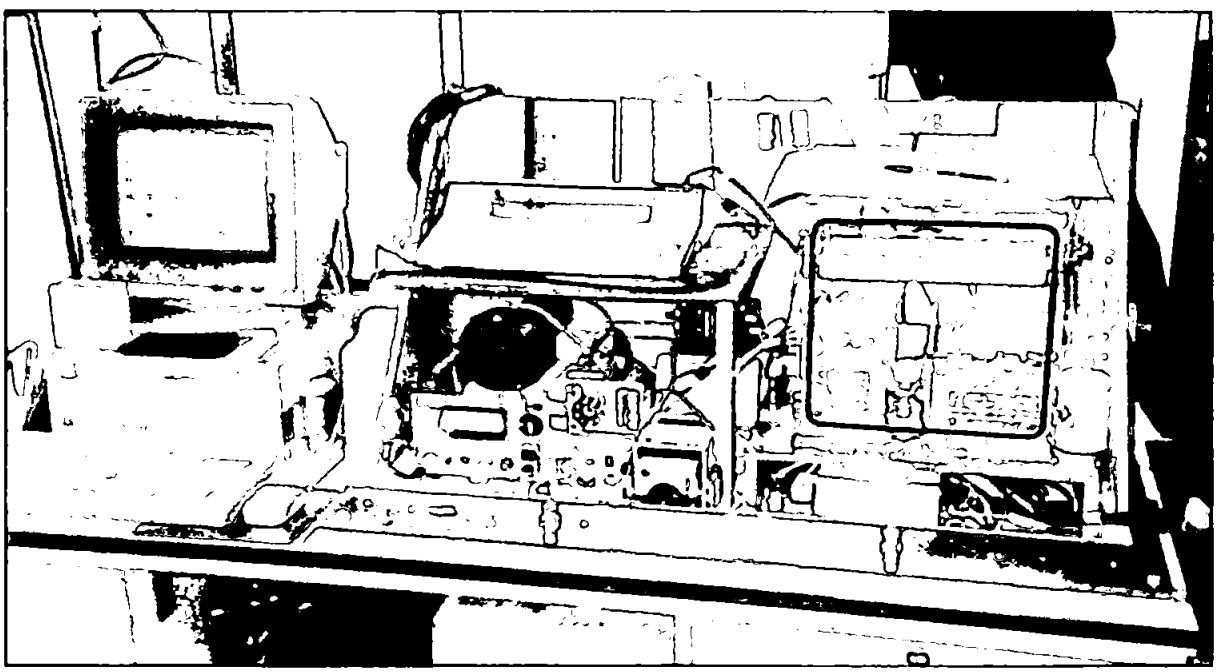

Figure V.5. FI-CL instrumentation in operation on AMT-3

250 ml HDPE sample bottles were cleaned using standard procedures for all plasticware: 5% hot micro-detergent for 24 h, followed by 1 week in 50% (v/v) hydrochloric acid and 1 week in 50% (v/v) nitric acid, with a thorough UHP rinse between each step. Sample bottles were stored under 0.01 M Q-HCl prior to use and doubly sealed within plastic bags at all times except

during sampling and analysis. The efficiency of the acid washing procedure was assessed through the analysis of Fe in sub-aliquots taken randomly from 5 sample bottles. The concentration in all measurements of the acidified UHP water was not statistically different from the level found in a blank solution prepared in an identical manner in a PTFE bottle (30 ml) which, through continuous use, had been shown to be free from contamination. This indicated that the acid washing procedure was satisfactory for trace metal studies.

V.2.2 Sampling

V.2.2.1 Local Field Trials

The macrotidal Tamar Estuary acts as a filter and effectively traps elevated riverine concentrations of metals, resulting from large property gradients (salinity, pH, turbidity) which exist at the land – sea interface (Millward, 1995). In order to assess the practicality of shipboard operation of the FI-CL analyser and to validate the analytical method for samples containing relatively high (>1.0 nM) and variable Fe concentrations, three trials were performed locally in the Tamar Estuary (Figure V.6), south-west Devon (UK). Trials I and II were axial transects from Plymouth Sound (seawater end-member) north to Calstock (riverine end-member) and were performed on-board the *R.V. Tamaris*, a flat-bottomed fibre-glass research vessel operated by Plymouth Marine Laboratory (PML). Trial III was a land-based expedition, performed remotely in a mobile laboratory situated on the bank of the Tamar Estuary, near Halton Quay. These surveys were designed to field test the instrumentation and investigate changes in dissolved Fe concentrations in the estuary.

TAMAR ESTUARY TRANSECTS

Trial I was performed on 13th February 1996, Trial II on 22nd May 1996. Samples were collected by hand at the bow of the *R.V. Tamaris*, with the user wearing arm-length clean gloves and taking care to minimise contamination. These samples were filtered at sea through acid cleaned (0.05 M Q-HCl, 24 h) 0.45µm, 47 mm polycarbonate membranes (Nucleopore) mounted between Teflon supports (diss-Fe). Analyses were carried out in near-real time on-board ship. A standard addition procedure allowed for variations in the sensitivity of the calibration due to

large salinity changes. Ancillary shipboard data (temperature, salinity, pH, dissolved oxygen, turbidity) was obtained *via* an on-board data logging system.

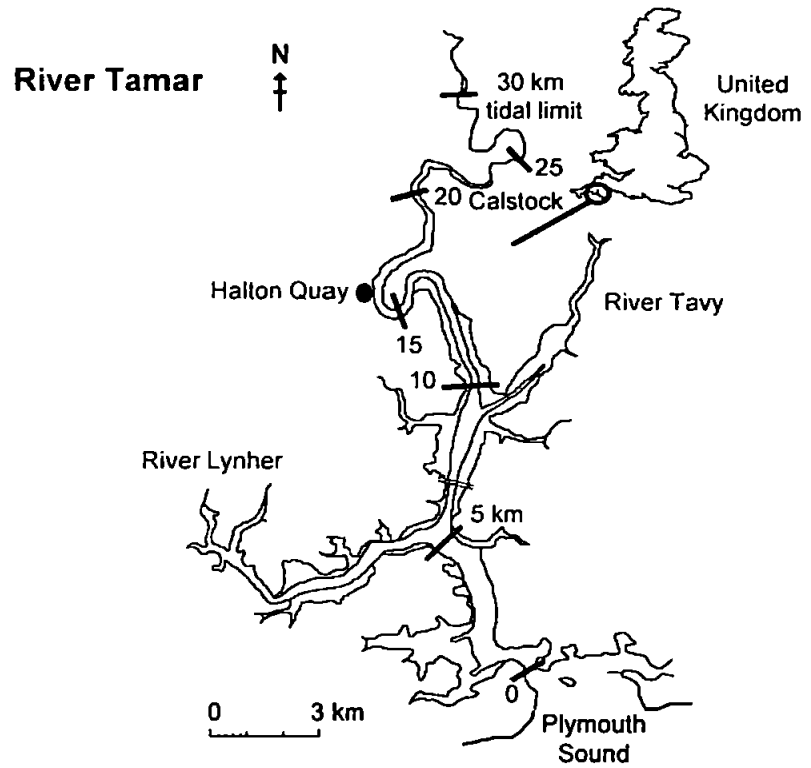

Figure V.6. Map of the Tamar Estuary, southwest England. Distances shown from reference point in Plymouth Sound

TAMAR ESTUARY TIDAL CYCLE

Trial III investigated changes in dissolved Fe during a 14 h tidal cycle of the Tamar Estuary (28th January 1997). Labile and dissolved copper (Cu) and zinc (Zn) analyses were performed by David Whitworth (University of Plymouth, UoP), using cathodic stripping voltammetric (CSV) techniques (Achterberg and van den Berg, 1996). *In situ* salinity measurements were interpolated from data obtained from a pHOX 52E conductivity meter and dissolved oxygen was measured using a Yellow Springs Industries meter (model number 5739). The concentration of suspended particulate matter (SPM) in samples was determined by the weight of particulate material collected on a pre-weighed 0.45 μm porosity cellulose acetate filter from a known volume (usually ~250 ml) of water. The filters were dried overnight at 45 °C and re-weighed on a 5 decimal place precision balance. Samples were collected from 0.5 m below the surface using an on-line pumping system (Whitworth *et al.*, 1998). A tangential filtration device (Figure V.7) was designed in order to remove suspended particulate matter on-line prior to introduction into the

FI manifold. Analytical instruments were operated within a mobile laboratory and powered using a petrol generator.

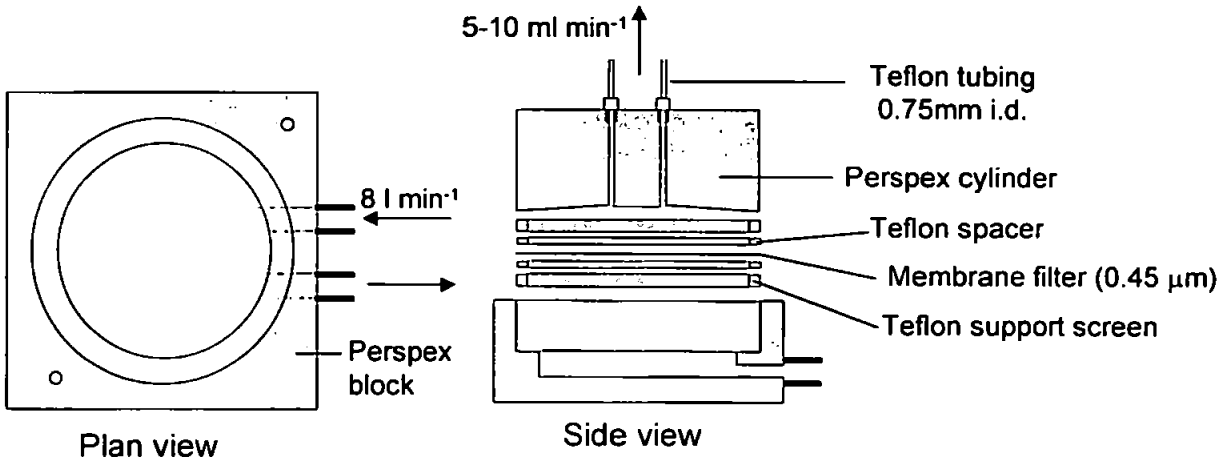

Figure V.7. On-line tangential filtration unit for the removal of suspended particulate matter from estuarine samples (modified from Morris *et al.*, 1978). Sample water was pumped through the lower section of the unit at ca. 8 l min^{-1}, and pulled across a polycarbonate membrane (0.45 µm pore size, 47 mm diameter, Nucleopore) mounted in a Teflon sandwich. Filtered water was collected through two output channels at 5-10 ml min^{-1}. All other fittings were chemically inert.

V.2.2.2 Atlantic Meridional Transect

All sample collection was performed following the same procedures. 10 l Go-Flo Teflon® lined poly(vinyl) chloride sampling bottles (property of Research Vessel Systems, RVS) modified for trace metal work were mounted on an epoxy-paint coated rosette frame, deployed on a plastic-coated steel hydrowire. Go-Flo samplers contained silicone 'O'-rings, seals and external silicone closures. Each bottle was thoroughly washed prior to use using the following protocol: 5% micro-detergent (DECON®; Merck BDH), UHP water, 5% HCl (several hours), UHP water and finally with copious seawater. The open Go-Flo samplers were tripped electronically at pre-selected depths between –2 m to -200 m in the upper water column. In order to minimise the time each sample was in the Go-Flo bottle, seawater for Fe analysis was taken immediately on retrieval of the samplers. Two tests were employed to ensure the integrity of the sample water. Firstly, the Fe concentration in samples taken from the Go-Flo bottle tripped at the –7 m depth were compared to sample water taken from the all-Teflon underway supply available on the *R.R.S. James Clark Ross*, which has its intake at the –7 m depth. Secondly, Fe concentrations in seawater taken from Go-Flo samplers fired at identical depths were compared and any outlier Go-Flo bottles cleaned once again. Results are presented in Section V.3.1.4.

Sub-sample aliquots were taken from 10 l Go-Flo sampling bottles, rinsed three times, filled, closed and re-sealed within the plastic bags. All samples were unfiltered in order to minimise potential sample contamination from the filtration procedure. The majority of samples were collected from open-ocean environments, remote from continental land masses and hence contained a low SPM concentration. The validity of this strategy is discussed in Section V.3.2. Sampling was conducted on a daily station basis at 10:00 to 10:30 local time, approximately 4° latitudinal intervals apart during the north-to-south AMT cruise 3. Table V.3 contains the full station data for AMT-3 cruise.

V.2.3 Sample Pre-treatment

Samples were immediately transferred to a dedicated clean area within the ship's laboratory and acidified to pH 2.0 with 250 µl of sub-boiling, quartz-distilled HCl (Q-HCl, 9.0 M) per 250 ml of sample. Samples collected for subsequent land-based analysis were also acidified and stored in the dark for transport to UoP. A Fe(III) reducing reagent (Na_2SO_3) was added to acidified samples collected for shipboard analysis (final concentration 100 µM) and allowed to react for at least 12 h.

V.2.4 Quantification

The samples were analysed and calibration performed using the method of standard additions. Three 10 ml aliquots of reduced sample were transferred to pre-cleaned 25 ml polystyrene screw-capped vials (Sterilin, Merck BDH). Sub-sample 1 was left alone, whilst sub-samples 2 and 3 were spiked with a small volume (20 - 50 µl) of Fe(II) standard (variable concentration) to achieve standard additions ranging from 0.2 to 5.0 nM. The sub-samples were mixed and analysed in order of increasing concentration. Since it was not possible to obtain a "zero" blank (i.e. a blank solution that contained no residual Fe) the signal generated by a blank solution was subtracted from the signal generated by each sample or sample plus standard addition solution, as outlined in Section III.2.6.

Station	*Go-Flo*	*CTD*	*Date*	*Day*	*GMT*	*Latitude (°)*	*Longitude (°)*
A301	A3-01	none	22/9/96	266	08:00	49 40.5N	05 41.4W
A302	A3-02	none	23/9	267	09:30	48 24.7	12 30.0
A303	A3-03	1	24/9	268	10:30	47 22.0	18 12.7
A304	A3-04	2	25/9	269	10:30	42 54.0	19 59.5
A305	A3-05	3	26/9	270	11:25	38 10.1	20 00.8
A306	A3-06	4	27/9	271	11:25	34 02.0	21 15.5
A307	A3-07	5	28/9	272	11:25	29 29.6	21 48.5
A308	A3-08	6	29/9	273	11:25	24 40.6	21 24.1
A309	A3-09	7	30/9	274	10:55	20 05.1	20 37.7
		No hydrographic station due to EEZ restrictions					
A310	A3-10	8	2/10	276	10:55	12 45.6	20 32.7
A311	A3-11	9	3/10	277	10:55	09 03.1	22 16.6
A312	A3-12	10	4/10	278	10:55	05 10.2	24 01.0
A313	A3-13	11	5/10	279	10:55	01 17.4	25 46.9
A314	A3-14	12	6/10	280	10:55	02 23.4S	27 27.3
A315	A3-15	13	7/10	281	10:55	06 29.0	29 16.2
A316	A3-16	14	8/10	282	11:55	10 46.8	31 14.5
A317	A3-17	15	9/10	283	12:15	14 53.4	33 07.3
A318	A3-18	16	10/10	284	11:55	18 51.9	35 02.8
A319	A3-19	17	11/10	285a	11:55	22 55.9	36 57.3
A320			11/10	285b	16:13	23 20.9	37 10.4
A321	A3-20	18	12/10	286a	11:55	26 36.9	39 36.0
A322			12/10	286b	16:00	27 00.1	40 00.8
A323	A3-21	19	13/10	287	12:00	29 51.0	42 54.7
A324	A3-22	20	14/10	288	12:00	32 48.0	46 07.0
A325	A3-23	21	15/10	289a	12:30	35 42.7	49 34.0
A326			15/10	289b	17:10	36 05.4	50 03.4
A327	A3-24	22	16/10	290	11:50	37 48.4	52 11.6
			Montevideo port-call				
A328	A3-25	23	23/10	297	12:55	43 34.7	55 01.4
A329	A3-26	24	24/10	298	12:55	48 00.1	55 52.8
A330	A3-27	25	25/10	299	11:00	51 55.9	57 53.6

Table V.3. AMT-3 full station list

The time for one analytical cycle was 3 min and hence a seawater sample could be quantified within 28 min, using two standard additions and analysing each solution in triplicate. Clearly, this time could be reduced if only one standard addition was employed. Typical peaks from a series of standard additions solutions added to a South Atlantic seawater sample are shown in Figure V.8. All CL signal data was recorded and entered into an Excel 97 spreadsheet specially designed for calculation of linear regression and sample concentration, plus gradient, intercept and concentration errors (Figure V.9).

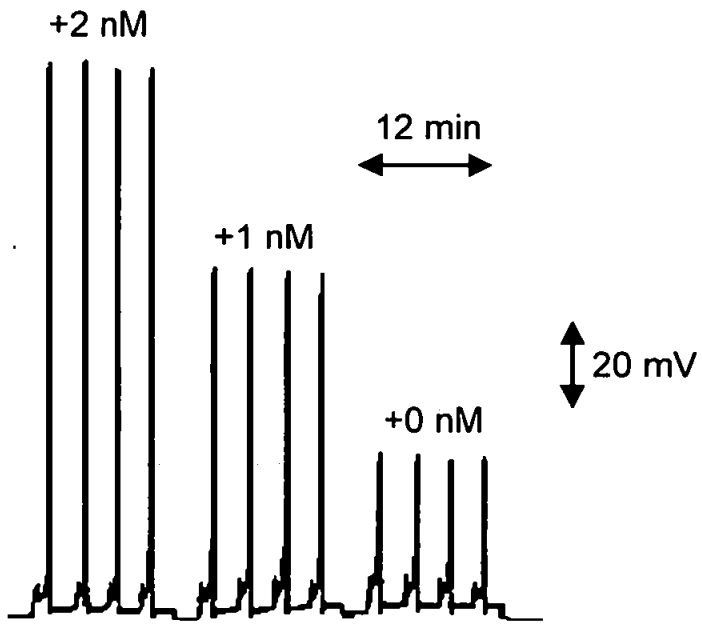

Figure V.9. Detector output from a series of standard additions of Fe to a South Atlantic seawater sample (AMT-3 station A3-15, SDY 281, 07/10/96, 10:55 GMT, 06°29.0'S, 29°16.2'W, depth=-200 m, [TD-Fe]=0.48 nM)

V.2.5 Ancillary Measurements

V.2.5.1 Sub-sample Trace Metals

IRON, COBALT AND NICKEL ANALYSIS

In order to complete objectives (3) and (4) outlined in Section V.1.3.4 and assist in the interpretation of shipboard iron ($TD\text{-}Fe_{ship}$) distributions, additional replicate sub-samples were collected for every surface sample taken along the latitudinal transect, together with vertical profile samples from five selected station casts. These samples were subsequently analysed at the UoP after an acidification (pH 2.0) and ca. 16 month storage period. All sample preparation and analysis was performed under a class-100 laminar flow unit contained in a class-1000 clean room facility.

IRON ANALYSIS DATASHEET													
Underway	n/a		SDY	281		Sample bottle	1		[TD-Fe] (nM)	0.48		
Station	15		Date	07/10/96		Filter cartridge	n/a		r squared	0.9983		
Go-Flo	15		Time (GMT)	10:55		Sterilins	A					
Go-Flo bottle	1		Lat.	S 06o29.02'		Filename	A3-15.dat		Notes			
CTD	13		Long.	W 29o16.23'		Preparation time	11:15					
Depth (m)	-200					Reduction time	11:15					
Cast	1/2					Analysis time	19:30					
SPREADSHEET USED TO ENTER REPLICATES												
Fe (nM)	f.s.d. (V)	Peak height (mm)				Average	Std. dev.	R.S.D. (%)	CL (mV)	CL emission (mV)		
Blank B1	0.02	17.5	17	18.5	19	18.00	0.91	5.07	1.80	(after blank subtraction)		
Blank B2	0.02	38	41	42	41	40.50	1.73	4.28	4.05			
Net Blank									2.25			
0	0.2	28.5	29	30.5	27	29.00	1.47	5.08	29.00	26.75		
1	0.2	78.5	79	75	79.5	78.00	2.04	2.62	78.00	75.75		
2	0.2	137	133	132.5	136	134.63	2.21	1.64	134.63	132.38		
CALCULATION OF LINEAR REGRESSION, ANALYTE CONCENTRATION, AND GRADIENT, INTERCEPT AND CONCENTRATION ERRORS												
x	y	x-x'	(X-X')^2	y-y'	(y-y')^2	(x-x')(y-y')	x^2	y'	y-y'	(y-y')^2		
0	26.75	-1	1	-51.54	2656.54	51.54	0	25.48	1.27	1.62		
1	75.75	0	0	-2.54	6.46	0.00	1	78.29	-2.54	6.46		
2	132.38	1	1	54.08	2925.01	54.08	4	131.10	1.27	1.62		
3	234.88	0	2	0	5588.01	105.63	5	234.88	0.00	9.69		
No. (x,y)	3		Gradient (m)	52.813		S(y/x)	3.11		Confidence Intervals:			
Mean x (x')	1		Intercept (c)	25.479		S(m)	2.20		t-test value (n-2)	12.71		
Mean y (y')	78.29		r	0.9991		S(c)	2.84		Gradient (m)	27.98		
						S(x extr.)	0.07		Intercept (c)	36.12		
									Analyte concentration	0.90		
SUMMARY OUTPUT												
Regression Statistics												
Multiple R	0.9992532											
R Square	0.998507							[TD-Fe] (nM)	0.48			
Adjusted R Square	0.9970141											
Standard Error	2.9598001											
Observations	3											
ANOVA												
	df	*SS*	*MS*	*F*	*Significance F*							
Regression	1	5859.03125	5859.03125	668.80737	0.024604429							
Residual	1	8.760416667	8.760416667									
Total	2	5867.791667										
	Coefficients	*Standard Error*	*t Stat*	*P-value*	*Lower 95%*	*Upper 95%*	*Lower 95.0%*	*Upper 95.0%*				
Intercept	13.396667	2.701915473	4.95821087	0.1266974	-20.93427743	47.72761076	-20.934277	47.7276108				
X Variable 1	54.125	2.092894726	25.86131033	0.0246044	27.53236505	80.71763495	27.5323651	80.7176349				

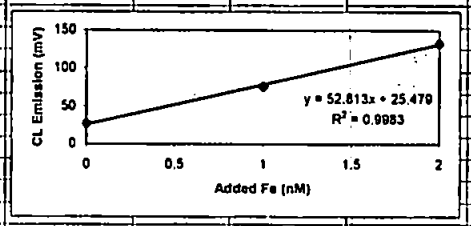

Figure V.8. Illustration of spreadsheet used for data collection and calculation of analyte concentration, regression and statistical errors

Land-based iron (TD-Fe_{land}) analysis was performed using the FI-CL method described in Chapter 3 after a reduction step in the shore-based laboratory. TD-Co and TD-Ni analyses were performed by David Whitworth (UoP) using adsorptive cathodic stripping voltammtery (AdCSV, Achterberg and van den Berg, 1997; Vega and van den Berg, 1997). In order to avoid interferences to the voltammetric method from dissolved organic compounds and to liberate complexed metal species, sub-aliquots of Co and Ni samples were exposed to UV irradiation prior to analysis, following the method of Achterberg and van den Berg (1994). Full details of Co and Ni analyses are described elsewhere (Whitworth, 1999). Replicate (n=3) Co and Ni analyses on identical sub-samples were performed on ca. every fifth sample. The analytical figures of merit for each method used for the sub-sample trace metal analysis are summarised in Table V.4.

Element	*Limit of detection*	*Typical RSD (%)*	*Linear range*	*Sensitivity*	*Correlation coefficient*
Fe (nM)	0.04	3.2 (n=5)	0.04 - 10	18.8 mV / nM	0.9974
Al (nM)	6.3	1.8 (n=5)	6.3 – 2040	0.16 f.u. / nM	0.9991
Co (pM)	15	0.74 (n=10)	15 – 200	152 nA / pM	n/a
Ni (nM)	0.19	1.5 (n=10)	0.2 - 10	9.41 nA / nM	n/a

f.u.: fluorescence units

Table V.4. AMT-3 trace metal analysis figures of merit

ALUMINIUM ANALYSIS

Total dissolvable aluminium (TD-Al) determinations were undertaken using a modified spectrofluorimetric method, based upon formation of an aluminium - lumogallion complex (λ_{max}=568 nm), first reported by Nishikawa *et al.* (1967) and developed for natural waters by Hydes and Liss (1976). The method determines Al in solution as dissolved species, weakly adsorbed onto or extracted from particulates during acidification of the unfiltered sample. Calibration was performed *via* the addition of an internal standard in order to control matrix effects in the samples. The analysis of replicate (n=3) sub-samples of the same AMT sample also resulted in good reproducibility (<10%).

Due to the expected low concentrations of Al to be found in the open-ocean AMT samples, great care was taken in preparation of all solutions. All sample handling was performed within a class-100 laminar flow hood. The pH of stored, acidified samples was raised to pH 5.0±0.1 using a sodium acetate – acetic acid buffer in combination with a small aliquot of Q-ammonia solution. Results were compensated for natural fluorescence of the sample, instrumental blank, as well as blank contribution from the acidification, buffering and lumogallion addition stages. The lumogallion and buffer solutions were the greatest contributors to the reagent blank, which consequently determined the limit of detection of the method. All measurements were performed on a Hitachi F-4500 fluorescence spectrometer. Figure V.10 illustrates emission spectra and corresponding calibration graph (blank corrected) for the Al - lumogallion fluorimetric method.

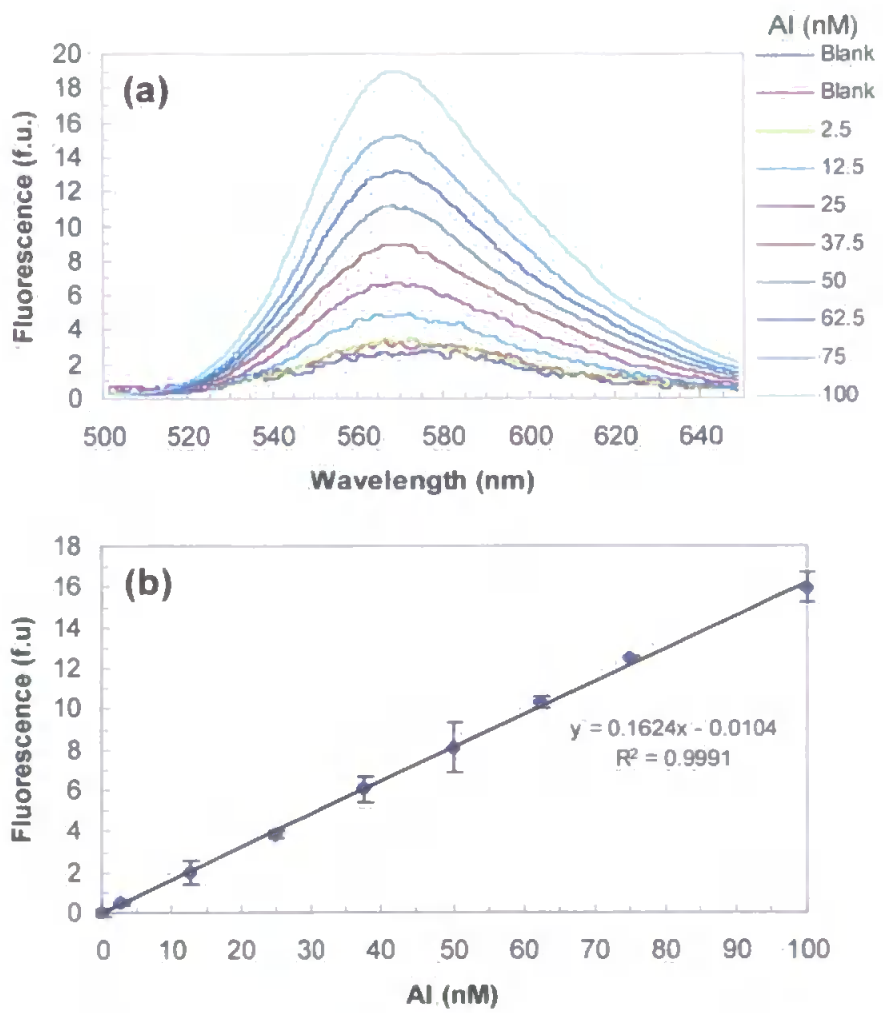

Figure V.10. (a) Emission spectra and (b) calibration graph for the determination of Al using the lumogallion fluorimetric method

V.2.5.2 Inorganic Macro-nutrients

Dissolved nitrate (NO_3^-), nitrite (NO_2^-), phosphate (PO_4^{3-}) and silicate ($Si(OH)_4$) were determined on-board ship in water taken from Go-Flo bottle samples. The analyses were performed by Colin Griffiths and Tony Bale and data digitised and processed by Malcolm Woodward (all PML). Nutrient concentrations were measured colorimetrically using a 4-channel, Technicon auto-analyser using standard methodologies (Grashoff *et al.*, 1983; modified by Woodward *et al.*, 1999). Limits of detection were 0.07, 0.07, 0.37 and 0.05 μM for NO_3^-, NO_2^-, PO_4^{3-} and $Si(OH)_4$, respectively. Due to the limited sensitivities of the techniques, surface water nutrient concentrations were only detectable in the shelf waters of the Western Approaches and through the Falkland Current.

V.2.5.3 Phytoplankton Abundance and Pigments

On-board chlorophyll analysis and sample collection for carotenoid biomarker pigment determinations was performed by Ray Barlow (PML). For chlorophyll analysis, 0.25 l of seawater taken from Go-Flo bottles fired at typically 5 depths at each station was filtered through GF/F filters, immediately extracted for 12-18 hours in 90% acetone and the chlorophyll fluorescence measured with an Turner Designs 10-AU fluorimeter (calibrated using chlorophyll *a* standards, Sigma), using the non-acidification method of Welschmeyer (1994). To determine the concentrations of a range of light-harvesting and light protecting chlorophylls, carotenoids and phaeopigments, a 2.1 l sample was drawn from each of 9 depths through the upper water column. Samples were filtered through GF/F filters and stored frozen in liquid nitrogen for subsequent transport to PML for reverse-phase HPLC analysis.

V.2.5.4 Phytoplankton Composition and Production

Phytoplankton stock and rate measurements were conducted on water samples collected from typically 7 depths at each station; experiments were performed by Emilio Marañón (Southampton Oceanography Centre) and Beatriz Mouriño (Universidad de Vigo, Spain). Size-fractionated chlorophyll *a* concentrations were determined fluorimetrically, as described in Section V.2.5.3. Vertical profiles of size-fractionated primary production were obtained from

^{14}C incubations conducted using an on-deck incubator provided with a range of 10 irradiances from 97% to 1% of the surface irradiance level (I_0). After a 7-8 h incubation period, samples were sequentially filtered through 20 μm, 2 μm and 0.2 μm polycarbonate filters and the radioactivity of each fraction determined on a Beckman liquid scintillation counter. Photosynthesis-irradiance (P-I) experiments were carried out on water from 3 depths at each station (surface, deep chlorophyll maximum (DCM) and an intermediate depth). Filtered (0.2 μm) samples were decontaminated and counted as described above.

V.2.5.5 Particle Size and Numbers

Particle numbers in the range 1.9-60 μm were measured in surface samples taken from the ship's underway pumped supply whilst on-station using a standard Coulter multisizer fitted with a 100 μm orifice. Calibration of the instrument was checked using 14.02 μm latex spheres and the manometer flow time was calibrated relative to the siphon volume so that the particle numbers could be calculated from the sampling time interval (typically 30 s). Data was provided courtesy of Tony Bale (PML).

V.2.5.6 Microbial Web Studies and Bacterial Dynamics

Studies of the microbial web were performed by Mike Zubkov (University of Southampton). Experiments included quantification of the activity of two general groups (bacteria and nanoplaktonic flagellates) in terms of vertical distribution, size structure, bacterivory and control of bacterial numbers by protozoa. Samples were collected from typically 10 depths at each daily station.

V.2.5.7 Hydrographic Data

Underway measurements, including salinity, temperature, fluorescence and photosynthetically available radiation (PAR), were obtained using flow-through sensors connected to the underway pumped supply from a nominal depth of –7 m. All sensors were interfaced to the ship's Ocean Logger. Conductivity, salinity and temperature were measured through vertical profiles using Neil Brown sensors deployed on a CTD unit (Mk IIIB, Instrument Systems, Inc.) whilst the

ship was stationary. The precision of the underway Sea-Bird thermosalinograph and the on-station CTD sensors were checked with reference to values obtained from salinity bottles using a Guildline "Autosal" salinometer, and with certified, ISO reversing digital thermometers. Vertical fluorescence distributions were obtained using a PML (Aiken, 1981) fluorimeter fitted to the CTD unit. All hydrographic data was processed by Nigel Rees (PML).

V.3 Results and Discussion

V.3.1 Analytical Performance

V.3.1.1 Instrumentation Operation

Local Field Trials

The robust nature of the instrumentation was thoroughly tested during the local field trials. The Fe monitor operated successfully during both axial river transects (Trials I & II). No major instrumentation problems were experienced despite harsh weather conditions and the only difficulties encountered were de-frosting of the reagents and filtration of estuarine samples containing a high particulate load. Samples were diluted with UHP water where necessary in order to bring them within the linear range of the analytical method. Figure V.11 shows the results from Trial II, which mapped the distribution of diss-Fe, turbidity and salinity against distance from Plymouth Sound, a reference point at the seawater end of the Tamar Estuary.

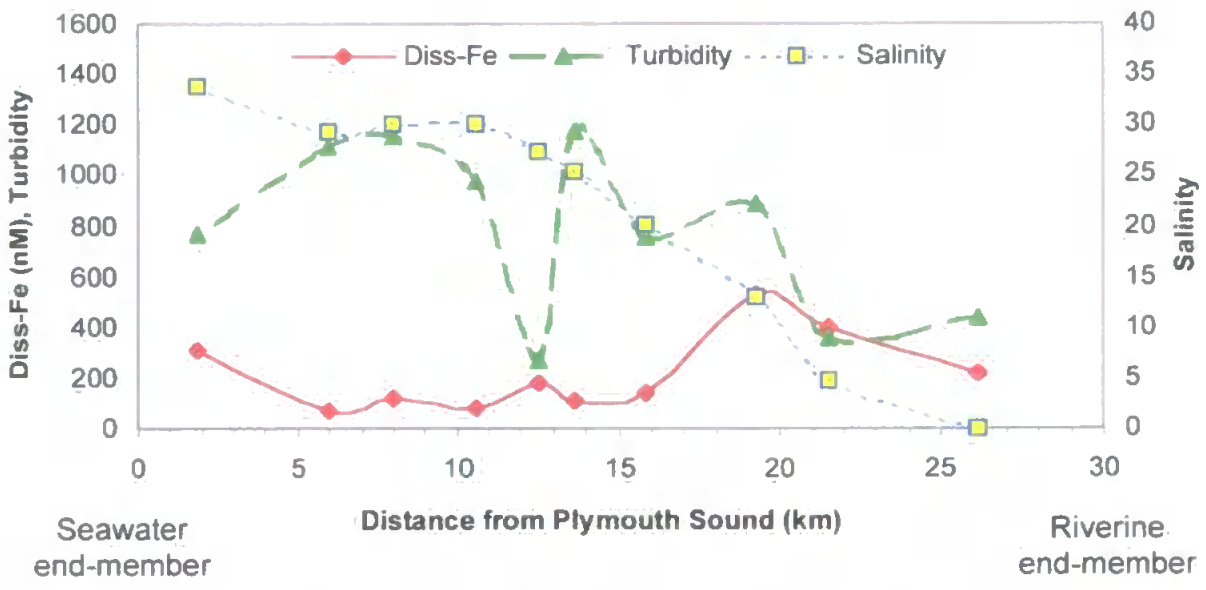

Figure V.11. Diss-Fe, turbidity and salinity versus distance along an axial transect of the Tamar Estuary, May 1996

Problems were encountered during the tidal cycle (Trial III) and the survey was carried out with limited success. However, difficulties were not associated with malfunctioning of system components, but were caused by blank contamination problems associated with the UHP water system which were difficult to eliminate in the field. Nevertheless, 10 samples were successfully analysed for diss-Fe in a shore-based clean laboratory. Figure V.12 shows the results for diss-Fe, labile Cu, SPM and salinity against sampling time. The Fe data is consistent with previously reported studies in the Tamar Estuary (Morris *et al.*, 1986), demonstrating a non-conservative mixing process, in part due to the flocculation of organic matter and aggregation of colloids when salinity increased (Sholkovitz, 1978; Hunter and Leonard, 1988; L'Herroux *et al.*, 1998). The purpose of this study was principally to assess the feasibility of remote operation of the FI-CL monitor and the full dataset and interpretation will be reported elsewhere.

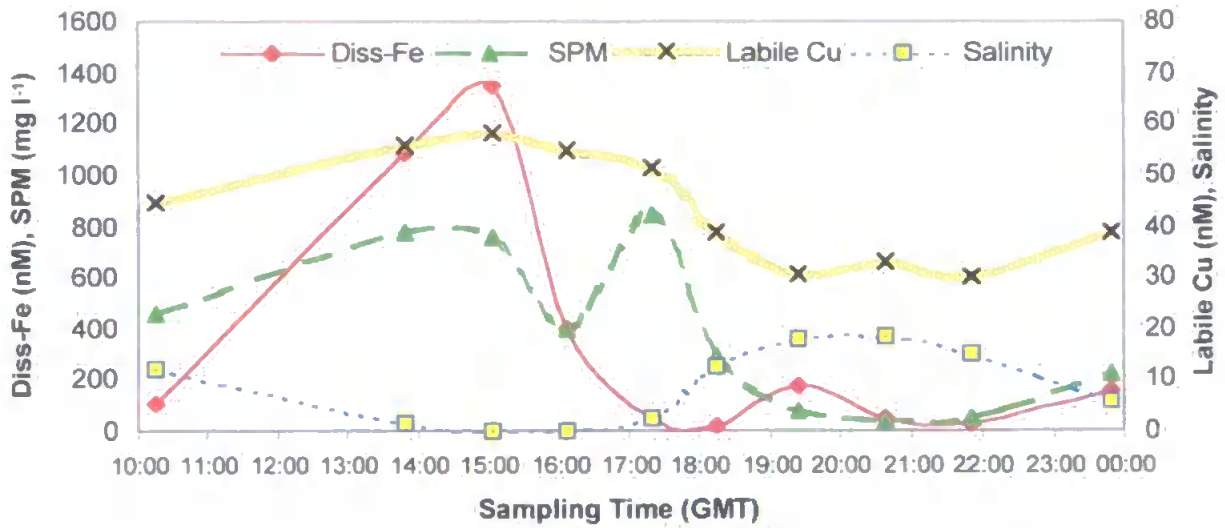

Figure V.12. Diss-Fe, labile Cu, SPM and salinity versus sampling time during a 14 h tidal cycle of the Tamar Estuary, January 1997

ATLANTIC MERIDIONAL TRANSECT

The overall performance of the FI-CL analytical system during shipboard AMT deployment was considered to be excellent. No significant problems were encountered. The total down-time of the system during the AMT cruise was ca. 2 hours, where the injection valve was not rotating satisfactorily. Initially, an 8-HQ micro-column was poorly packed causing flow problems and needed replacing. Contamination problems within the FI tubing were swiftly resolved using a weak acid rinse cycle, as outlined in Section III.2.5. The need for rigorous acid washing of the

Go-Flo sampling bottles prior to use prevented reliable Fe vertical profiling during early station work.

V.3.1.2 Quality Control Procedures

A total of 163 samples were analysed on-board ship during AMT-3. 12 samples were suspected to be contaminated for Fe (7% of the total). Whilst recognising that this is a controversial practice, these values have been removed from the dataset used for interpretation and are indicated by square brackets [ ] in Appendix C, part (iv). Rejection was based upon either a lack of acceptable precision for replicate analyses of a single sample (>15%), or lack of oceanographic consistency when compared to the vertical structure of other trace metals (Al, Co, Ni) which have better characterised distributions. It was believed that the source of the contamination was either from the Go-Flo samplong bottle or the HDPE collection bottle. In either case, the Go-Flo sampler was once again subjected to the acid washing procedures outlined in Section V.2.2.2 and the collection bottle discarded. During land-based sub-sample analysis, 3 collection bottles were suspected to be contaminated. Contaminated samples typically represented isolated outliers that occurred randomly in the dataset and were inconsistent with other oceanographic data.

V.3.1.3 Certified Reference Material

In order to verify the accuracy of shipboard Fe measurements using the FI-CL technique, the North Atlantic Surface Seawater certified reference material (NASS-4) was analysed on five separate occasions whilst at sea. In addition, the trace metal content of the NASS-4 solution was measured prior to the land-based sub-sample trace metal determinations. Results (Table V.5) show good agreement with certified values for Fe, Co and Ni values, and are not statistically different under a *t*-test comparison of the different methods of analysis at 95% confidence interval. Al is not certified in NASS-4; however, the quality of the measurements was checked by repetitive analysis of this standard solution. Results were reproducible throughout the analysis period: [Al]=59.4±4.3.

Standard solution	*NASS-4*	
Element	**Certified**	**Observed**
Fe (nM)	1.88±0.29	2.01±0.12[a]; 1.95±0.14[b]
Al (nM)	Not certified	59.4±4.3
Co (pM)	150±17	158±7
Ni (nM)	3.9±1.5	4.1±0.2

[a] Land-based analysis
[b] Shipboard analysis

Table V.5. CRM results for land-based and shipboard analyses of trace metals in North Atlantic standard seawater solution; values show ± 95% confidence interval for an individual sub-sample

V.3.1.4 Sampling System Validation

After thorough cleaning of the Go-Flo sampling bottles (described in Section V.2.2.2), their integrity was ascertained by implementing two types of sampling comparison methods periodically during the cruise. Firstly, on five separate occasions, a sample was taken from the Go-Flo bottle fired at the surface (-7 m), and within 40 min of departure from the station, a sample was collected from the all-Teflon pumped underway supply at –7 m below the surface. The TD-Fe concentration in each sample was determined. Table V.6 summarises the results and Figure V.13 contains a plot of the TD-Fe concentrations in samples taken from the underway supply versus samples from Go-Flo bottles. A good correlation is noted where the slope (=0.94) of the best-fit line is not significantly different from 1.

Sample[a]	*Go-Flo cast*	*GMT*	*Date*	*Day*	*Latitude*	*Longitude*	*TD-Fe (nM)*
Station 8	A3-08	11:25	29 Sept	273	24.67°N	-21.40°W	1.21
Underway	n/a	12:00	1996		24.68°N	-21.41°W	1.03
Station 9	A3-09	10:55	30 Sept	274	20.08°N	-20.56°W	2.46
Underway	n/a	11:15	1996		20.07°N	-20.57°W	2.32
Station 11	A3-11	10:55	03 Oct	277	09.05°N	-22.28°W	0.32
Underway	n/a	11:17	1996		09.05°N	-22.28°W	0.23
Station 16	A3-16	11:55	08 Oct	282	-10.77°S	-31.24°W	0.76
Underway	n/a	12:06	1996		-10.78°S	-31.24°W	0.88
Station 21	A3-20	11:55	12 Oct	286	-26.60°S	-39.60°W	0.96
Underway	n/a	12:12	1996		-26.62°S	-39.60°W	0.87

[a] Station sample taken from daily Go-Flo cast at –7 m depth; underway sample taken while ship steaming, shortly after moving off station, allowing time for flushing of pumped supply system, also at -7 m depth

Table V.6. Comparison of [TD-Fe] in samples collected from Go-Flo bottles versus samples taken from underway supply

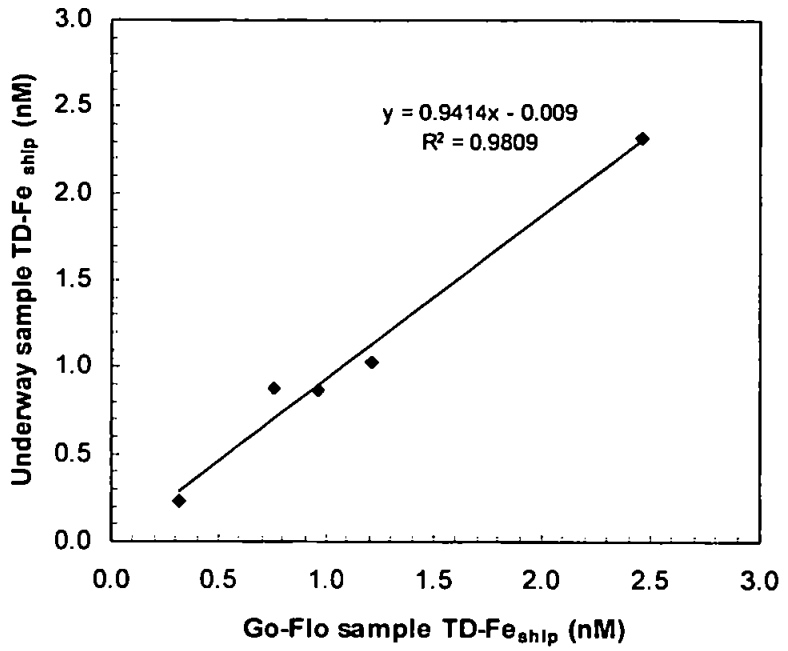

Figure V.13. [TD-Fe] in samples collected from underway supply versus Go-Flo bottles

Sample location	*GMT*	*Date Day*	*Latitude Longitude*	*Go-Flo bottle*	*Depth (m)*	*TD-Fe (nM)*	*Notes*
Station A311	10:55	03 Oct 1996	09.05°N	11	-7	0.30	Surface
Go-Flo A3-11		SDY 277	-22.28°W	12	-7	0.34	seawater
Station A312	10:55	04 Oct 1996	05.17°N	5	-70	0.30	Chlorophyll
Go-Flo A3-12		SDY 278	-24.02°W	6	-70	0.35	maximum
Station A325	12:30	15 Oct 1996	-35.70°S	7	-30	2.49	Chlorophyll
Go-Flo A3-23		SDY 289	-49.57°W	8	-30	2.17	maximum
Station A330	11:00	25 Oct 1996	-51.90°S	4	-40	2.77	Coastal shelf
Go-Flo A3-27		SDY 299	-57.89°W	5	-40	3.01	seawater

Table V.7. Comparison of [TD-Fe] in samples taken from different Go-Flo bottles fired at identical depths on the same cast

Furthermore, on four separate occasions, samples from two Go-Flo bottles fired at identical depths on the same cast were analysed for their TD-Fe content. Results for the analysis of samples taken from these replicate Go-Flo bottles, contained in Table V.7, were compared using a paired *t*-test. Adopting the null hypothesis that there is no significant difference in the concentration of TD-Fe measured in each of the two Go-Flo samplers, one can test whether the mean of the differences differs significantly from zero. For the pairs of values, the differences are –0.04, -0.05, 0.32, -0.24. The mean difference ($\bar{x}_d$) is –0.0025 and the standard deviation of the differences (s_d) is 0.23. Therefore, $t = \bar{x}_d \sqrt{n / s_d}$ = -0.01 where t has (n-1) degrees of freedom. The critical value of $|t|$ is 3.18 (P=0.05, 95% confidence interval; Miller and Miller,

1993) and since the calculated value is less than this, the null hypothesis is retained and the two sampling methods do not give significantly different values for the TD-Fe concentration.

V.3.1.5 Replicate Sub-sample Analyses

Table V.8(a) shows the results for the analysis of TD-Fe_{ship} in sub-aliquots taken from the same Go-Flo sampling bottle. Table V.8(b) contains data for the shore-based determinations of TD-Fe_{land} in sub-aliquots taken from the same HDPE collection bottle. Reproducibility between replicate measurements was found to be between 4.3 and 11.9%, with the poorest precision in the region of the chlorophyll maximum.

ANALYSIS	SHIPBOARD[a]			LAND-BASED[b]		
Station	11	21	24	9	Underway	21
Go-Flo cast	A3-11	A3-20	A3-22	A3-09	n/a	A3-20
GMT	10:55	11:55	12:00	10:55	00:45	11:55
Day	277	286	288	274	284	286
Date	03 Oct 1996	12 Oct 1996	14 Oct 1996	30 Sept 1996	10 Oct 1996	12 Oct 1996
Latitude	09.05°N	-26.60°S	-32.80°S	20.08°N	-16.80°S	-26.60°S
Longitude	-22.28°W	-39.60°W	-46.12°W	-20.63°W	-34.01°W	-39.60°W
Go-Flo bottle	6	11	1	11	n/a	11
Depth (m)	-50	-7	-200	-7	-7	-7
TD-Fe (nM)						
Replicates 1.	0.41	1.00	2.14	7.86	1.00	2.70
2.	0.53	0.96	2.24	7.70	0.87	2.94
3.	0.47	0.90	2.39	6.59	0.91	2.82
4.	0.41	1.09	2.57			
5.	0.51	0.97	2.37			
Mean	0.47	0.96	2.34	7.38	0.93	2.82
Standard deviation	0.06	0.09	0.16	0.69	0.07	0.12
R.S.D. (%)	11.9	9.0	7.0	9.4	7.2	4.3
Notes	Chlorophyll maximum	Surface seawater	Deep seawater	Surface seawater	Underway seawater	Surface seawater

[a] Replicate shipboard analysis of identical samples taken from the same Go-Flo bottle, but stored in different HDPE sample bottles
[b] Replicate land-based analysis of identical samples taken from the same Go-Flo bottle and stored in the same HDPE sample bottle

Table V.8. Results from AMT-3 analysis of TD-Fe in replicate sub-samples

V.3.2 Nature of the Trace Metal Measurements

Due to the low particulate matter concentrations in the open-ocean and the risk of contamination, samples were not filtered prior to acidification and analysis. The chemical nature

of Fe and other trace metals (Al, Co, Ni) in these samples is therefore somewhat uncertain. Under these conditions, it was expected that dissolved (including the majority of organically bound), colloidal and labile exchangeable (leachable at pH 2) particulate Fe would become amenable to the acidification (0.01 M Q-HCl), reduction (100 µM S(IV), >12 h) and preconcentration (TSK-8HQ resin) steps of the FI-CL analytical method. Only acid-resistant forms, including matrix bound aluminosilicate Fe and very unreactive crystalline Fe phases would not be determined. Land-based analyses would consequentially determine an increased fraction of particulate Fe that had become solubilised during the storage period (16 months). Al, Co, and Ni analyses would similarly detect the dissolved fraction plus any particulate bound metal released during the acidification and storage period. Thus, all metal measurements performed during this study are termed "total dissolvable" (TD), dissolved plus exchangeable particulate fractions.

The validity of this strategy is supported by similar expeditions (Powell *et al.*, 1995; Rutgers van der Loeff *et al.*, 1997; Yeats *et al.*, 1995; Kremling, 1985) which analysed trace metals in unfiltered samples. Westerlund and Öhman (1991) reported that no significant difference was noted between analyses of Co, Ni, Cu, Pb and Zn in filtered and unfiltered samples taken from the Weddell Sea, Antarctica. Furthermore, in a trace metal study in the Eastern central and South Atlantic, Yeats *et al.* (1995) concluded that filtered and unfiltered samples were not significantly different for Cd or Ni, but may be slightly higher in the surface layer for Cu. No observations were made for Fe, Al or Co. However, Powell *et al.* (1995) reported that 40-60% of Fe in near-surface suspended material collected in similar Atlantic Ocean waters during 1990 was dissolved after 4 h of room temperature treatment with a dilute (2 M Q-HCl / 1 M Q-HNO_3) acid mixture. Buat-Ménard and Chesselet (1979) estimated atmospheric particulate fluxes over the open Atlantic Ocean and reasoned that such deposition would have a significant effect on trace elemental chemistry, particularly for metals associated with aluminosilicate minerals, such as Fe and Al. As noted in the following discussion, enhanced atmospheric particulate material depositions were encountered in a number of oceanic regions during the AMT-3 cruise, which may not have been observed by other workers in different open ocean regimes. A significant

contribution from metals bound to particulate matter (either biogenic or lithogenic of origin) cannot therefore be generally neglected in coastal waters, productive areas or regions subjected to a high atmospheric flux and hence with enhanced suspended particulate matter (SPM) concentrations. During this study, the majority of particles in open-ocean environments were of biogenic origin, an observation consistent with the findings of Helmers (1996). This is illustrated along AMT-3 by the good relationship between Coulter suspended particle number and chlorophyll *a* concentrations in surface waters (Figure V.14). One would therefore expect the presence of such particles to have a significant effect on the distributions of micro-nutrient metals (esp. Fe, Co) through the euphotic zone.

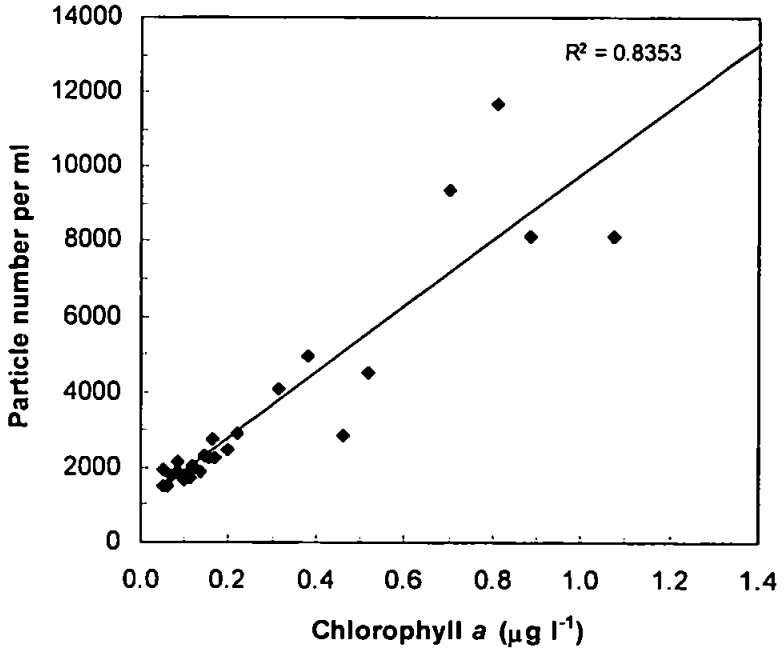

Figure V.14. Relationship between surface chlorophyll *a* and particle number along AMT-3

The strong relationship in Figure V.14 (r^2=0.84, n=25) even holds up at on day 274 at 20°N, despite intensified mineral aerosol deposition noted at this latitude. This may be coincidental since elevated chlorophyll *a* concentrations at this station were possible due to nutrient enrichment through the strong Mauritanian upwelling system. In a similar transect of the Atlantic Ocean, Helmers (1996), using a continuous flow centrifuge technique, recorded an overall average SPM concentration of 27 µg l^{-1}, with a range between 1 µg l^{-1} in the south-west Atlantic to a maximum of 115 µg l^{-1} in the open-ocean off West Africa.

V.3.3 Water Column Structure

V.3.3.1 Literature Data

Emery and Meincke (1986) have presented a revised table of water masses and sets of (temperature – salinity) T-S curves for the Atlantic Ocean. Their report was based on the compilation of many oceanographic observations between 1936 and 1982, and updated the work of Sverdrup *et al.* (1942). Four dominant upper (0-500 m) waters were identified for the Atlantic, underlain by five intermediate waters of varying salinities originating from a wide range of latitudes. AMT-3 passed through two of these upper waters masses (Eastern North Atlantic Central Water, ENACW; South Atlantic Central Water, SACW), together with Sub-Antarctic Surface Water (SASW) which forms part of circumpolar waters in the Southern Ocean. Their temperature and salinity characteristics are described in Table V.9 and a geographical distribution shown in Figure V.15.

In the eastern basin, the main upper waters consist of Eastern North Atlantic Central Water (ENACW). The differentiation with waters to the west expresses the physical characteristics of the northern subtropical gyre circulation, which is dominated by the Gulf stream system and the isopycnals are correspondingly deeper it the eastern basin. ENACW is more saline than its western counterpart due to winter convection transferring salt from the surface layer into central water, together with the influence of Mediterranean Outflow Water (MOW). ENACW transits into South Atlantic Central Water (SACW) at about 15°N, with similar temperatures but marginally lower salinities. The non-symmetrical geographic boundaries in the Atlantic contribute to strong Equatorial surface water exchange. Sub-antarctic Surface Water (SASW), which has its origin all along the area just north of the Sub-antarctic Front, penetrates into the eastern South Atlantic at about 35°S, discussed in detail in Section V.3.4.3.

Water Mass	*Acronym*	*Temperature (°C)*	*Salinity*
Eastern North Atlantic Central Water	ENACW	8.0-18.0	35.2-36.7
South Atlantic Central Water	SACW	5.0-18.0	34.3-35.8
Sub-Antarctic Surface Water	SASW	3.2-15.0	34.0-35.5

Table V.9. Temperature and salinity characteristics of upper (<500 m) water masses along AMT-3

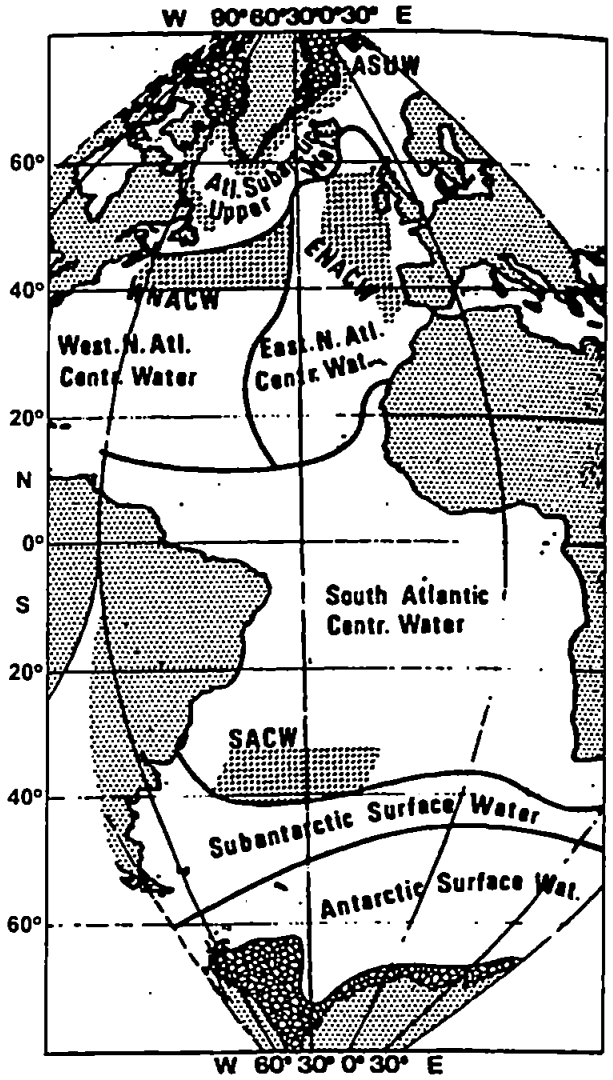

Figure V.15. Distribution of upper waters (0-500 m) of the Atlantic Ocean. Water masses are labelled in abbreviated form with their boundaries indicated by solid lines. Formation of these water masses are marked by cross hatching and labelled with the corresponding acronym title (reproduced from Emery and Meincke, 1986)

V.3.3.2 AMT-3 Temperature and Salinity Distributions

The latitudinal distributions of temperature and salinity from 50°N to 50°S reflect the changes in the structure of the water column along the transect (Figure V.16). During AMT-3, the upper water column of the temperate North Atlantic demonstrated weak thermal stratification, whilst waters in the South Atlantic central gyre were well-mixed. An outcropping of isotherms, and subsequent reduction in the thickness of the upper mixed layer was observed around 20°N and across the Equator, indicating a presence of cooler upwelled sub-surface waters. The thermocline in the northern subtropical gyre was clearly shallower than its southern counterpart, a feature also reflected in the nutrient structure. Figure V.17 illustrates the temperature versus

salinity (T-S) characteristics, partitioned into upper water mass types described above, for data recorded at every station along AMT-3 transect.

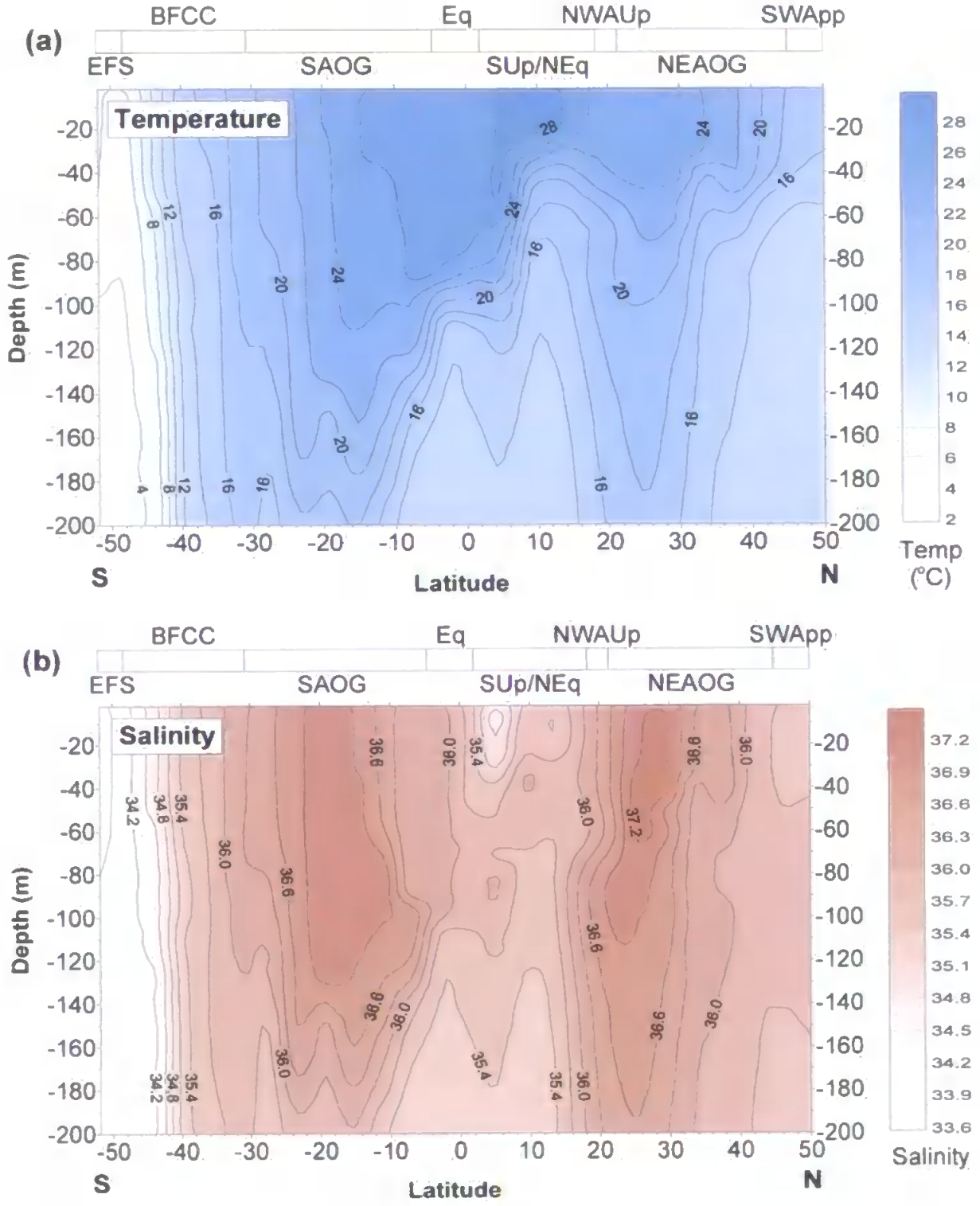

Figure V.16. Latitudinal distribution of (a) temperature and (b) salinity in the upper water column of the Atlantic Ocean during September / October 1996 (AMT-3)

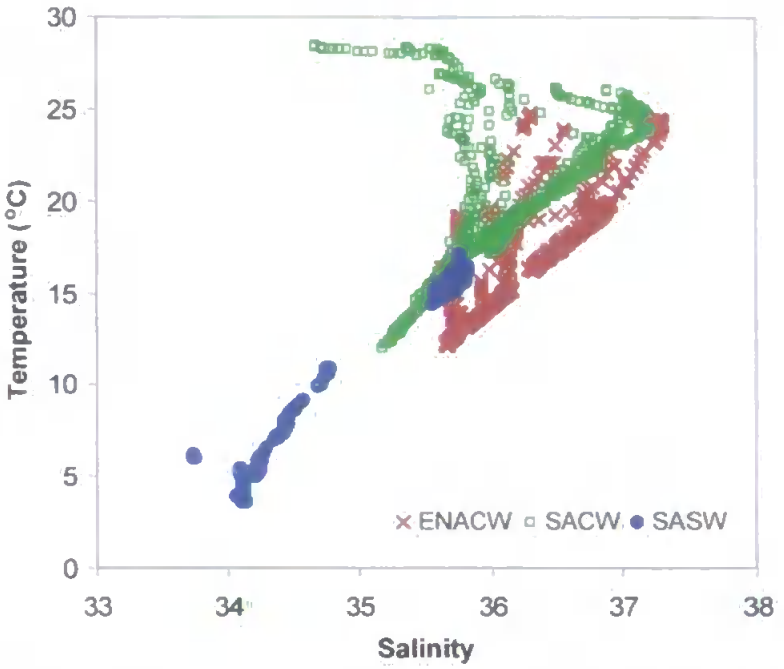

Figure V.17. T-S plot for water masses experienced in the upper 200 m at all stations along AMT-3

V.3.4 Latitudinal Surface Water Trace Metal Distributions

V.3.4.1 Overview

The surface (~7 m depth) concentrations of total dissolvable iron (TD-Fe_{ship}) measured on-board the AMT-3 expedition are shown in Figure V.18(a). Figure V.18(b) illustrates variations in surface water chlorophyll *a* concentrations and photosynthetic activity, Figure V.18(c) Coulter particle number distribution and Figures V.18(d) & (e) show surface water classical nutrient levels along the transect. Total dissolvable trace metal (TD-Fe_{land}, TD-Al, TD-Co, TD-Ni) concentrations measured in land-based sub-sample analyses are shown in Figures V.19(a) & (b). Hydrographic data (temperature, salinity) is contained in Figure V.19(c), whilst a temperature – salinity (T-S) plot describes the surface water masses (Figure V.19(d)).

V.3.4.2 Results

The latitudinal distribution of TD-Fe_{ship} showed significant spatial variability, consisting of a series of distinct enrichments superimposed on a baseline concentration ranging between 0.3-1.0 nM. Highest TD-Fe_{ship} levels were noted at the start of the transect in European shelf waters. Fe levels decreased rapidly to 1.1 nM in the north-east Atlantic gyre between 30° and 24°N. A pronounced TD-Fe_{ship} maximum of 2.5 nM, the highest recorded open-ocean

concentration, was observed at 20°N off the west coast of Africa. Low TD-Fe_{ship} was observed in tropical waters between the Equator and 10°N and also in the South Atlantic gyre through the Brazilian Basin. A small increase in Fe content was observed across the Equator and a maximum of 1.7 nM was noted towards Uruguay at 35°S. Further south, TD-Fe_{ship} tended towards baseline values, with an increase (2.7 nM) observed in the shelf waters off East Falkland.

Land based analyses for TD-Fe_{land}, TD-Al and TD-Co showed similar trends in surface water distributions compared to the shipboard results. Surface TD-Fe_{land} concentrations ranged between 0.7 nM, found in the remote waters of the Brazilian Basin, to 7.4 nM, observed to the west of Africa. Generally speaking, these values were in very good agreement with the only other surface Fe dataset for the Atlantic Ocean which employed similar sampling, storage and analytical procedures (Powell *et al.*, 1995; TD-Fe range: 0.5 – 10 nM). The wide concentration range for TD-Al (14-79 nM) demonstrated that atmospheric inputs influenced Al surface water concentrations. Partial dissolution of sporadic aeolian dust fluxes is an important source of this element for the surface ocean (Measures and Edmond, 1990). AMT-3 measurements for Al were again consistent with literature data (0.2-86 nM, Measures, 1995; 0.9-79 nM, Helmers and Rutgers van der Loeff, 1993). TD-Co concentrations ranged from 20 pM (southern oligotrophic gyre) to 110 pM (near the African continent).

In northern temperate latitudes, total dissolvable TD-Fe_{land}, TD-Al and TD-Co concentrations were relatively low, showing small fluctuations around baseline values of 1.5 nM, 17 nM and 30 pM respectively. Elevated TD-Fe_{land}, TD-Al and TD-Co were observed in tropical waters, with marked maxima of 7.4 nM, 79 nM and 110 pM respectively occurring at 20°N, superimposed on broader enrichments in this region. TD-Fe_{land} showed a broad minimum of 1.0 nM between the Equator and 16°S and values fluctuated between 2.0-3.0 nM in temperate south Atlantic waters. TD-Al and TD-Co concentrations exhibited uniform lower values in the sub-tropical and temperate waters of the south Atlantic (20 nM and 32 pM, respectively). Small TD-Fe_{land} and TD-Al maxima were observed at 48°S (TD-Fe_{land}=4.5 nM, TD-Al=50 nM),

whereas TD-Co showed a trend of surface water enrichment in the south-west Atlantic, increasing linearly to 73 pM with increasing degree of latitude south.

The surface water latitudinal distribution of TD-Ni was very different to those of Fe, Co and Al. Values ranged from 1.4 nM, observed in the region SUp/NEq, to 6.8 nM measured on the shelf off the Falkland Islands. No maximum was observed for Ni in the tropical north Atlantic. Ni demonstrated no inter-province fractionation, except for the region in the south-west Atlantic below 38°S, and a baseline average value of 2.3±0.5 nM was observed across the whole transect. In the south-west Atlantic (35° – 52°S), Ni demonstrated a similar profile to Co, with a linear increase ($TD\text{-}Ni_{max}$=6.8 nM) towards the southernmost sampling station.

V.3.4.3 Characterisation of Biogeochemical Provinces

As discussed in Section V.1.3.3, the transect along AMT-3 was partitioned into distinct biogeochemical provinces which demonstrated similar chemical, biological and/or physical oceanographic properties. High evaporation, resulting in high surface water salinities, experienced in the subtropical gyres contrasted with the low salinities through the Inter-Tropical Convergence Zone (ITCZ) associated with increased precipitation. High SPM and chlorophyll *a* concentrations coupled with elevated NO_3^- and PO_4^{3-} were indicative of coastal influences or upwelled waters. Enhanced TD-Fe and TD-Al concentrations fingerprinted a source of continental particles delivered through aerosol deposition. Enhanced TD-Fe concentrations coupled with TD-Co and/or TD-Ni signified a freshwater source of these metals in terms of coastal riverine runoff, or from below *via* shelf regeneration or upwelling events. Another explanation for such coupling was the release of matrix-bound metals from particles of similar elemental composition.

Table V.10 contains a summary of mean upper water column data (<200 m) for $TD\text{-}Fe_{ship}$ and other shipboard data obtained for each oceanographic province. In addition, Table V.11 presents the mean province results for the land-based sub-sample analysis of trace metals (Fe, Al, Co, Ni). Variations between the provinces are shown schematically in Figure V.20.

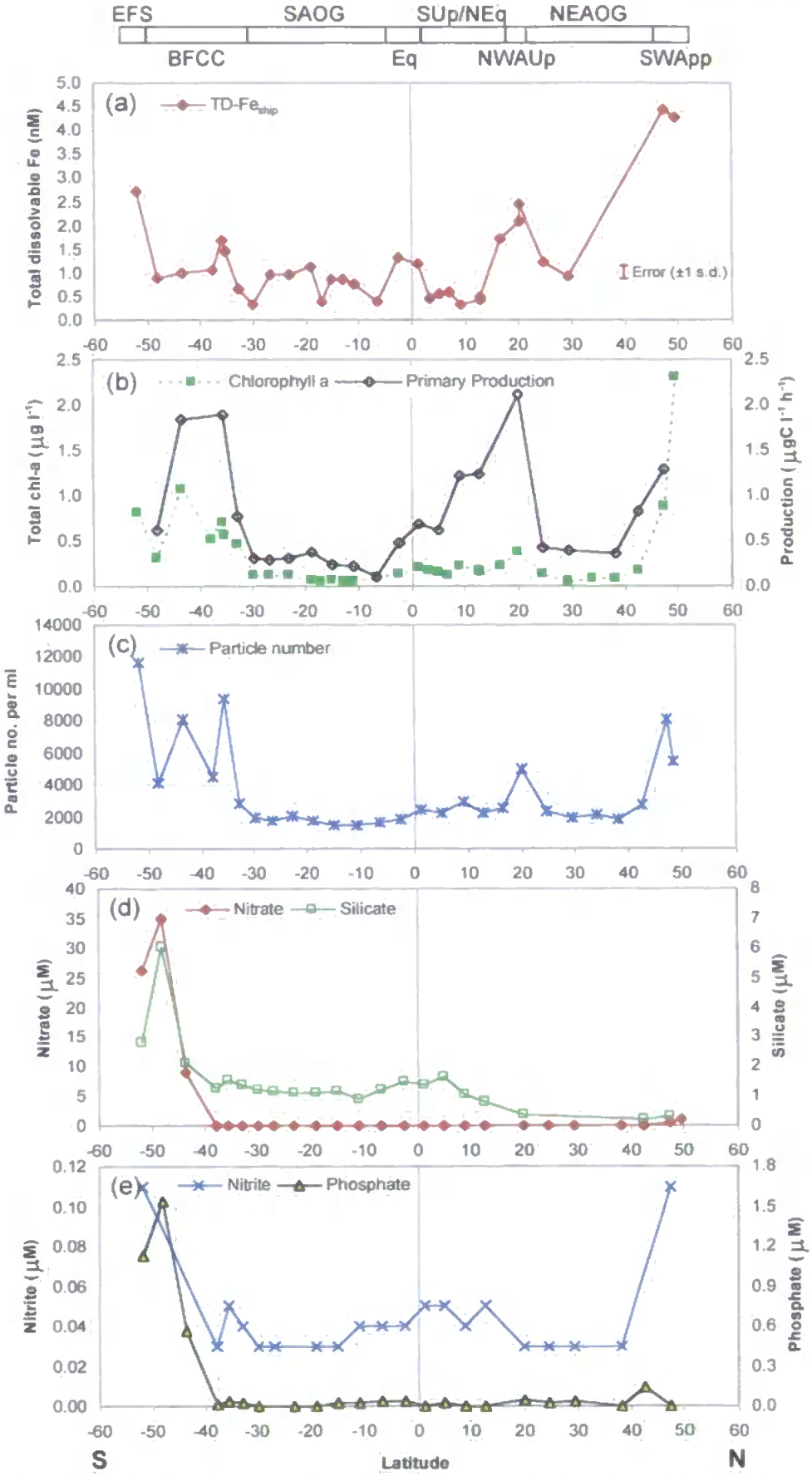

Figure V.18. Surface water distributions of (a) TD-Fe$_{ship}$, (b) chlorophyll *a* and primary productivity, (c) Coulter particle number, (d) nitrate and silicate and (e) nitrite and phosphate along AMT-3 from Portsmouth (UK) to Stanley (FI) during September / October 1996

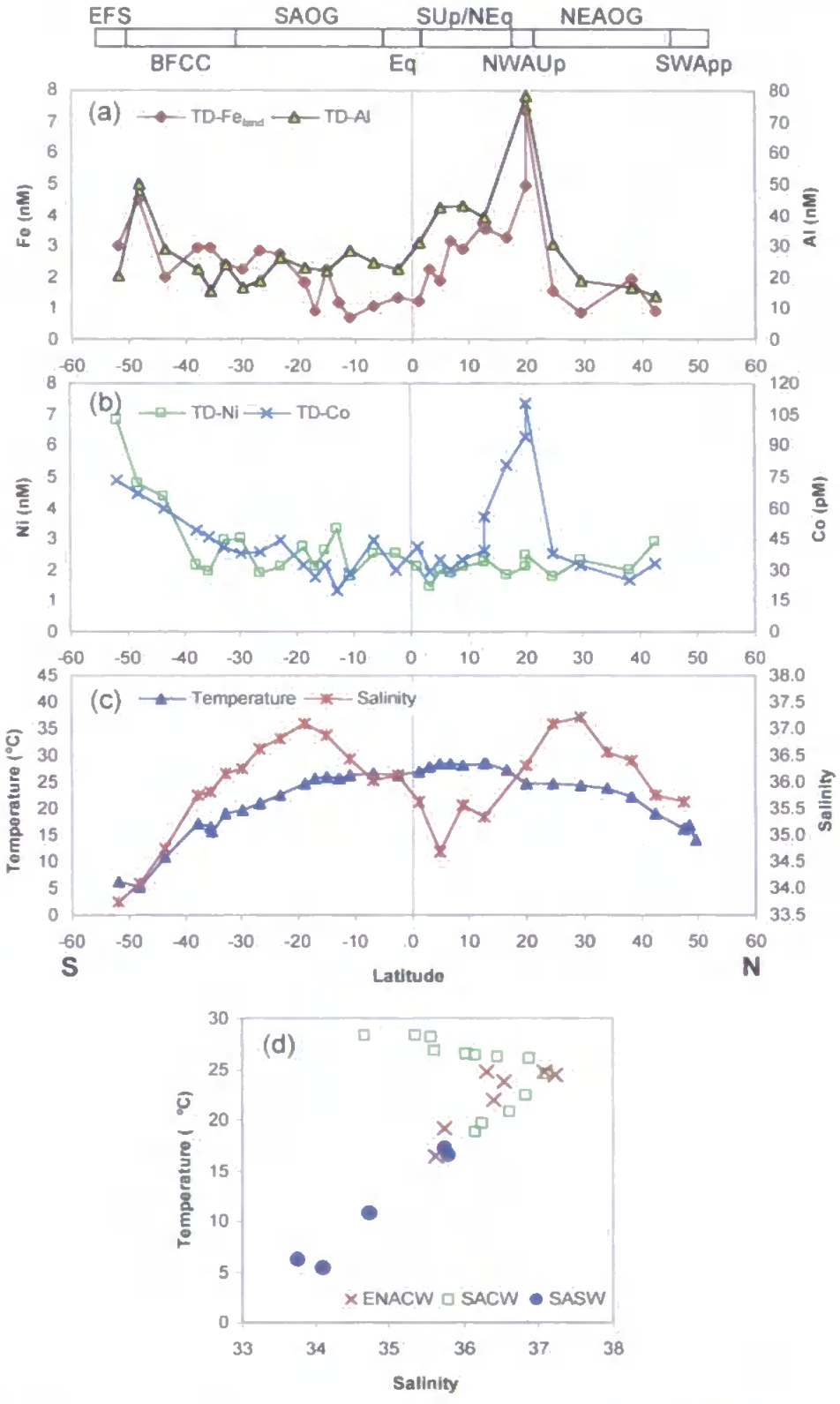

Figure V.19. Surface water distributions of (a) TD-Fe$_{land}$ and TD-Al (b) TD-Co and TD-Ni, (c) temperature and salinity and (d) T-S plot along AMT-3 from Portsmouth (UK) to Stanley (FI) during September / October 1996

SOUTH-WEST APPROACHES (SWApp)

The influence of the European shelf was identified by enhanced chlorophyll *a* concentrations, primary productivity and SPM, which correlated well with TD-Fe_{ship} concentrations, which were the highest of the whole transect. This was consistent with inputs of continental atmospheric dusts in addition to benthic shelf sedimentary regeneration, aided by strong bottom water currents at the European continental margin (Tappin *et al.*, 1993). Along the whole transect, surface NO_3^- was only detectable (>0.05 μM) through the temperate waters of the SWApp. Unfortunately, no land-based trace metal (Al, Co, Ni) data is available for this province.

NORTH-EAST ATLANTIC OLIGOTROPHIC GYRE (NEAOG)

The North Atlantic gyre was identified by high salinities resulting from evaporation. The weak input from upwelling or aerosol fluxes and absence of bottom shelf inputs (water column >4 km) resulted in low TD-Fe and other total dissolvable trace metals (Al, Co, Ni), coupled with low nutrients, chlorophyll *a*, primary production and SPM. Values obtained during the AMT-3 survey (TD-Fe_{ship}=1.0 nM, TD-Fe_{land}=1.5 nM, TD-Al=22.9 nM, TD-Ni=2.2 nM) were consistent with previously reported data for this region (Powell *et al.*, 1995: TD-Fe_{avg}=2 nM, TD-Al=16 nM; Hydes *et al.*, 1986: diss Ni=2.4 nM, diss ('reactive') Al=10.3 nM). However, differences were noted between AMT-3 TD-Fe values and surface diss-Fe data reported by Martin *et al.* (1993; 0.07-0.26 nM) in the JGOFS North-east Atlantic Bloom Experiment. The higher TD-Fe concentrations observed in our study indicates a significant contribution in AMT-3 samples from Fe colloids or suspended particles which would not pass through a 0.4 μm filter. In addition, a permanent frontal system near to 45°N would result in poor lateral mixing due to slow advection of water masses of widely different densities and thus unlikely to result in metal enrichment to the north. This may have explained the differing Fe signatures for southerly stations versus the 47°N site of Martin *et al.* (1993). Previously high surface TD-Fe_{ship} concentrations observed over the continental shelf (SWApp) decayed rapidly with distance away from the coast, because of a high removal rate in the mixed layer caused by biological uptake and particle scavenging (Johnson *et al.*, 1997).

Province; Acronym	*Latitude*	*SDY*	*Stations*	*Go-Flo casts*	*TD-Fe$_{shlp}$ (nM)*	*Salinity*	*Temp. (°C)*	*Nitrate (μM)*	*Nitrite (μM)*	*Phosphate (μM)*	*Silicate (μM)*	*Chl. a (μg l^{-1})*	*Particle no. per ml[a]*
European Shelf													
SWApp	50°N to 47°N	266-268	A301-A303	A3-01 to A3-03	4.36±0.13	35.8±0.1	13.6±1.4	3.2±2.6	0.10±0.08	n.o.	1.28±1.03	0.96±0.72	6793±1906
North Atlantic Gyre													
NEAOG	30°N to 24°N	269-273	A304-A308	A3-04 to A3-08	1.03±0.36	36.3±0.5	17.6±3.8	2.4±3.6	0.01±0.03	0.25±0.28	1.07±0.76	0.24±0.15	2218±351
Open-ocean Upwelling													
NWAUp	20°N	274	A309	A3-09	1.42±1.20	36.5±0.2	19.6±2.8	0.2±0.2	0.06±0.06	0.06±0.02	1.59±2.06	0.48±0.35	4967±0
North Equatiorial Region													
SUp/NEq	13°N to 5°N	276-278	A310-A312	A3-10 to A3-12	0.58±0.37	35.5±0.3	18.0±5.5	7.5±7.6	0.13±0.18	0.61±0.63	4.02±2.73	0.45±0.24	2496±303
Equatirial Upwelling													
Eq	2°N to -3°S	279-280	A313-A314	A3-13 to A3-14	0.64±0.47	35.7±0.3	19.7±6.0	4.8±7.1	0.08±0.06	0.41±0.54	3.18±2.62	0.33±0.23	2185±413
South Atlantic Gyre													
SAOG	-6°S to -30°S	281-287	A315-A323	A3-15 to A3-21	0.60±0.30	36.4±0.5	21.1±3.5	1.8±4.0	0.07±0.05	0.16±0.29	1.58±1.23	0.21±0.15	1736±208
South-west Atlantic Confluence													
BFCC	-32°S to -48°S	288-298	A324-A329	A3-22 to A3-26	1.52±0.74	35.2±0.8	12.2±5.4	11.2±14.1	0.13±0.13	0.57±0.66	3.62±3.37	0.43±0.26	5795±2800
Coastal shelf													
EFS	-52°S	299	A330	A3-27	4.40±1.85	33.8±0.0	6.1±0.1	27.5±0.8	0.11±0.00	1.14±0.02	3.03±0.22	0.59±0.19	11673±0

[a]Surface(-7 m) data only; n.o.: no observations

Table V.10. Characterisation of biogeochemical provinces; values represent shipboard averages through upper water column (<200 m)

Province; acronym	*Latitude*	*SDY*	*Stations*	*Go-Flo casts*	*Land-based sub-sample analysis*[a]			
					TD-Fe_{land} (nM)	*TD-Al (nM)*	*TD-Co (pM)*	*TD-Ni (nM)*
SWApp	50°N to 47°N	266-268	A301-A303	A3-01 to A3-03	n.o.	n.o.	n.o.	n.o.
NEAOG	30°N to 24°N	269-273	A304-A308	A3-04 to A3-08	1.49	22.88	35.77	2.22
NWAUp	20°N	274	A309	A3-09	3.21	32.89	72.18	2.76
SUp/NEq	13°N to 5°N	276-278	A310-A312	A3-10 to A3-12	2.83	41.40	36.23	2.13
Eq	2°N to -3°S	279-280	A313-A314	A3-13 to A3-14	1.30	26.68	35.47	2.32
SAOG	-6°S to -30°S	281-287	A315-A323	A3-15 to A3-21	1.49	20.98	38.15	2.46
BFCC	-32°S to -48°S	288-298	A324-A329	A3-22 to A3-26	3.54	28.15	50.47	3.06
EFS	-52°S	299	A330	A3-27	3.00	20.63	73.20	6.80

[a]After ca. 16 months storage and acidification n.o.: no observations

Table V.11. Land-based sub-sample trace metal concentration averages through different biogeochemical provinces

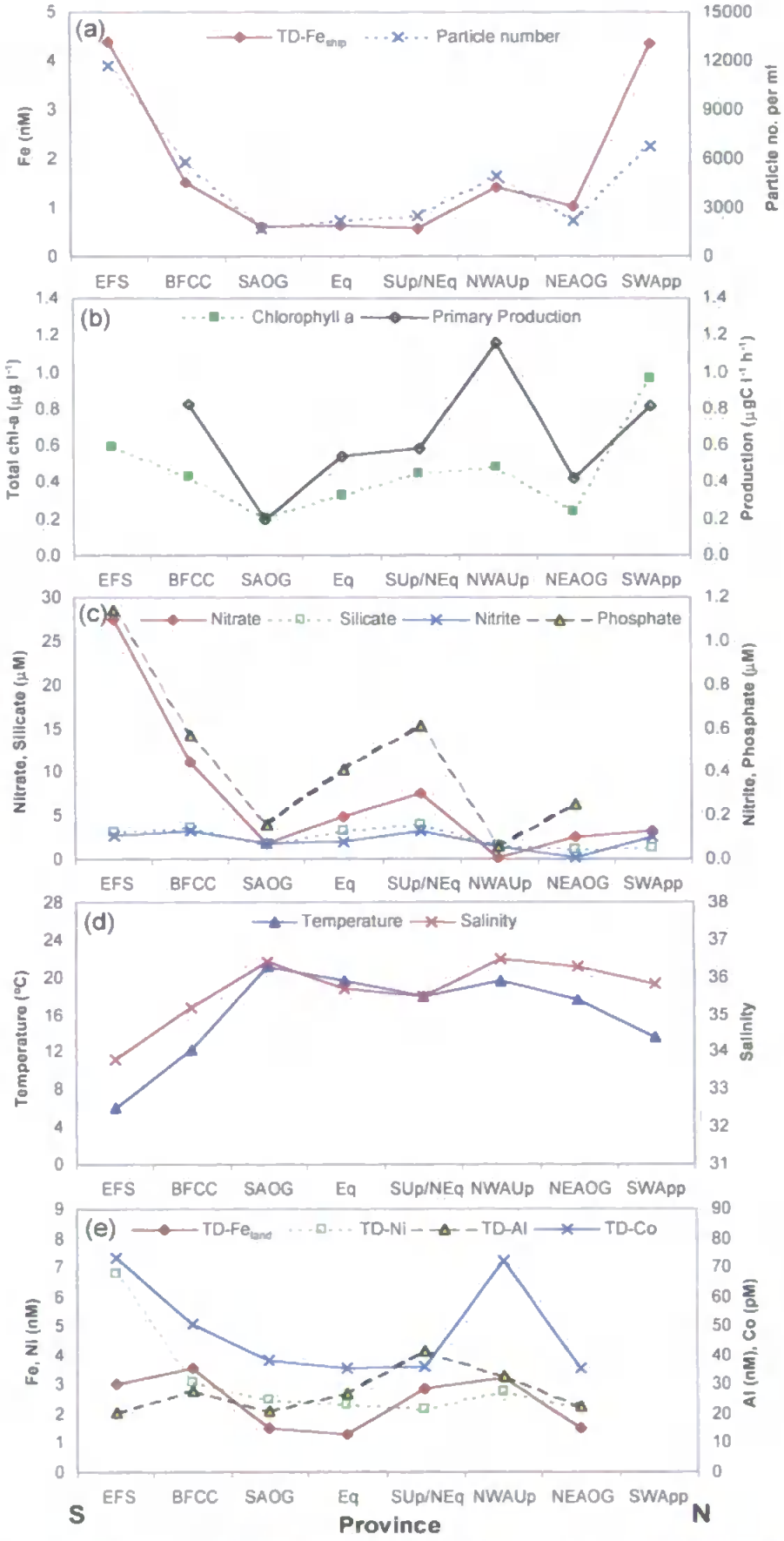

Figure V.20. Variations in mean AMT-3 upper water column (<200 m) shipboard and land-based data through different biogeochemical provinces. (a) TD-Fe$_{ship}$ and particle number, (b) chlorophyll *a* and primary production, (c) nutrients (NO_3^-, NO_2^-, $Si(OH)_4$, PO_4^{3-}), (d) hydrographic data (temperature, salinity), and (e) TD-Fe$_{land}$, TD-Al, TD-Co and TD-Ni

NORTH-WEST AFRICAN UPWELLING SYSTEM (NWAUp)

This region was characterised by both inputs through upwelling (which was patchy as revealed by SeaWiFS satellite imaging; see previous Figure V.4) and by enhanced trace metal release and/or scavenging due to dry deposition of atmospheric particles to the sea surface. The highest open-ocean concentrations of TD-Fe_{ship} (2.5 nM), TD-Fe_{land} (7.4 nM), TD-Al (78.5 nM) and TD-Co (110 pM) were located during AMT-3 survey at ca. 20°N. The difference between TD-Fe_{land} concentrations in surface samples collected at two locations within this province at a distance of less than 0.1 of a degree of latitude apart (Figure V.19(a)) confirms the high variability in leaching of metal from seawater receiving high atmospheric dust loading. The concentration of TD-Ni (2.5 nM) remained at its baseline level and demonstrated a contrasting behaviour. This was probably due to the nature of the particulate material, coupled with a different seawater solubility and removal rate for aerosol delivered Ni from a lithogenic source. This was consistent with the findings of Yeats *et al.* (1995), who noted no significant difference in Ni measured in both filtered and unfiltered samples in the Eastern central and South Atlantic. Enhanced chlorophyll *a*, primary production and number of suspended particles were also observed at the same sampling station. Major plant nutrient levels, however, showed no increase in surface waters, indicating either near complete utilisation or the absence of any upwelling of these nutrients. Furthermore, the concentration of deep water diss-Fe is assumed to show no inter-ocean fractionation and to average 0.7 nM (Johnson *et al.*, 1997). Since upwelled water at this station would not have recently passed over shelf sediment (water column >3600 m), the enhanced surface concentration of TD-Fe measured during AMT-3 was unlikely to have originated from internal advective processes.

The station at 20°N was situated in the zone of maximum dry input of dust, approximately 650 km from the west coast of Mauritania. This region underlies the path of north-east trade winds associated with the strong African Easterly Jet, where some of the highest oceanic particulate loadings occur, the Sahara desert acting as the largest individual source. Indeed, a layer of red "sand" indicative of intensified deposition of mineral aerosol coated the ship on day 274, just prior to the sampling station, and the horizon to the east was thick with atmospheric particles.

This high particulate flux was consistent with the observations of Helmers (1996) and Powell *et al.* (1995) during the 1990 IOC Trace Metals Baseline Expedition. Powell *et al.* reported high TD-Fe levels (4 yr acidification) at 20°N of 5.5 nM and a corresponding SPM concentration of 420 $\mu g\ l^{-1}$, consistent with the findings of AMT-3. However, Helmers argued that the input of Fe and Al in the North Atlantic between 0° and 20°N should be dominated by wet deposition through the ITCZ further south. However, the observations of Helmers and Powell were made during a different season (May) when the ITCZ was expected to shift more towards the Equator (Peterson and Stramma, 1991). Observations from AMT-3 showed distinct Fe, Al, and Co maxima associated with aerosol dry inputs in the northern tropics, but also a broad increase in background signal between the Equator and 20°N, encompassing the ITCZ. During AMT-3, no sampling was performed during a heavy rain event associated with the ITCZ.

Dust storms leaving the west coast of Africa are sporadic, with considerable seasonal, and even daily, variations in mineral aerosol concentrations, maximum aerosol transportation to the north of the region occurring during the summer months (Kremling and Streu, 1993; Husar *et al.*, 1997, Figure V.21). A localised input of aeolian dusts, as observed at 20°N on AMT-3, could account for a sharp peak superimposed on a broad region of elevated trace metals due to continuous aerosol inputs. Quétel *et al.* (1993) have reported that on short time-scales, concentrations and fluxes in the upper water column can increase significantly following dust transport and deposition events, with a response time of the order of one week. Such observations imply that a non steady-state behaviour must be taken into account when assessing the impact of pulsed atmospheric inputs on particle trace element concentrations and fluxes in the water column. The significant difference in Fe concentrations at this location from measurements made on-board ($[TD\text{-}Fe]_{ship}$=2.5 nM) to those made in the laboratory ($[TD\text{-}Fe]_{land}$=7.4 nM) after an acidification and 16 month storage period indicated a clear increase in the quantity of metal leached from suspended particles into solution over time. This observation confirms that total dissolvable (TD) measurements are operationally defined in areas of high particle flux.

Sediment trap deployment near to Cap Blanc (21°N, 20°W) revealed high lithogenic and organic particulate matter fluxes in this region during the northern summer (Wefer and Fischer, 1993) resulting from a combination of aerosol inputs and upwelling activity, and suggesting a common mechanism for the sinking processes of particulate aluminosilicates and organic matter. The observations of Kremling and Streu (1993) from sediment trap deployment outside the upwelling region showed a close correlation between particulate trace metal flux and Al, but not PO_4^{3-}, indicating that trace element levels were controlled by strong aerosol deposition and not the flux of organic material. However, contrasting signals may be observed, due to particle scavenging by enhanced productivity and lithogenic fluxes. For example, Al is known to be associated with relatively large crustal-derived aerosol particles that have high dry deposition velocities (Duce *et al.*, 1991). Upwelling events may bring waters of lower Al concentrations to the surface, although vertical exchange by eddy diffusion through the thermocline is slow. The major removal process of a particle-reactive element such as Al is scavenging. Rutgers van der Loeff *et al.* (1997) observed a film of red dust during a 1990 Atlantic transect, but Al levels (unfiltered) remained low (<18 nM). The authors reasoned that this was possible due to active uptake by diatoms or passive scavenging through a strong upwelling region which out compensated the additional atmospheric supply. The upwelling activity during AMT-3 may have been less pronounced, and consequentially particle scavenging reduced. In addition, the exact dry deposition flux at 20°N may well have been different between AMT-3 and the cruise of Rutgers van der Loeff. Unfortunately, no quantitative data on aerosol dust fluxes during AMT-3 is available.

Figures V.21 and V.22 (taken from Husar *et al.*, 1997 and Duce and Tindale, 1991, respectively) illustrate that atmospheric dry deposition from the African continent occurs in a wide area of the Atlantic Ocean. Saharan dust fluxes may be as high as 1000 mg m^{-2} yr^{-1} in this region and the influence of such intense dry and wet deposition is unclear. The solubility of atmospherically delivered particle-bound metals, their mobility in surface layers, their bioavailability (especially Fe) and their subsequent effects on Atlantic primary productivity are all unknown factors requiring further systematic study.

SOUTH OF UPWELLING / NORTH OF EQUATOR (SUp/NEq)

The area south of the Mauritanian upwelling system, but north of the Equator was characterised by wet deposition through the ITCZ. The ITCZ is dominated by trade winds carrying terrigenic dusts from the African continent westwards. These air masses converge in the ITCZ, inducing heavy rain shower activity. Mineral material dissolved in rain will contribute to dissolved elemental ambient levels in surface waters. Rain events through the ITCZ are often short-lived and limited to an area covering only a few square miles. However, showers are very heavy and the annual rainfall intensity can be up to 2000 mm (Tchernia, 1980; Helmers and Schrems, 1995).

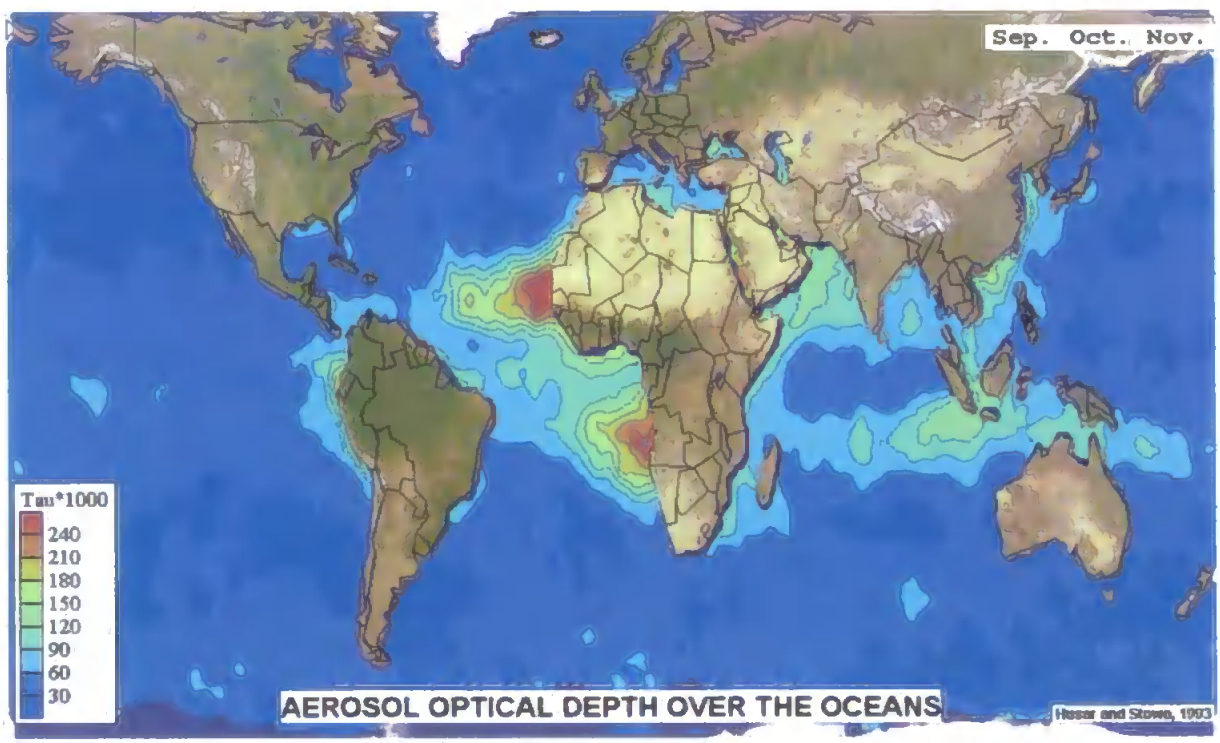

Figure V.21. Radiatively equivalent aerosol optical thickness (EAOT x 1000) over the oceans derived from NOAA AVHRR satellites for the autumn season (data for the period July 1989 to June 1991 (reproduced from Husar *et al.*, 1997)

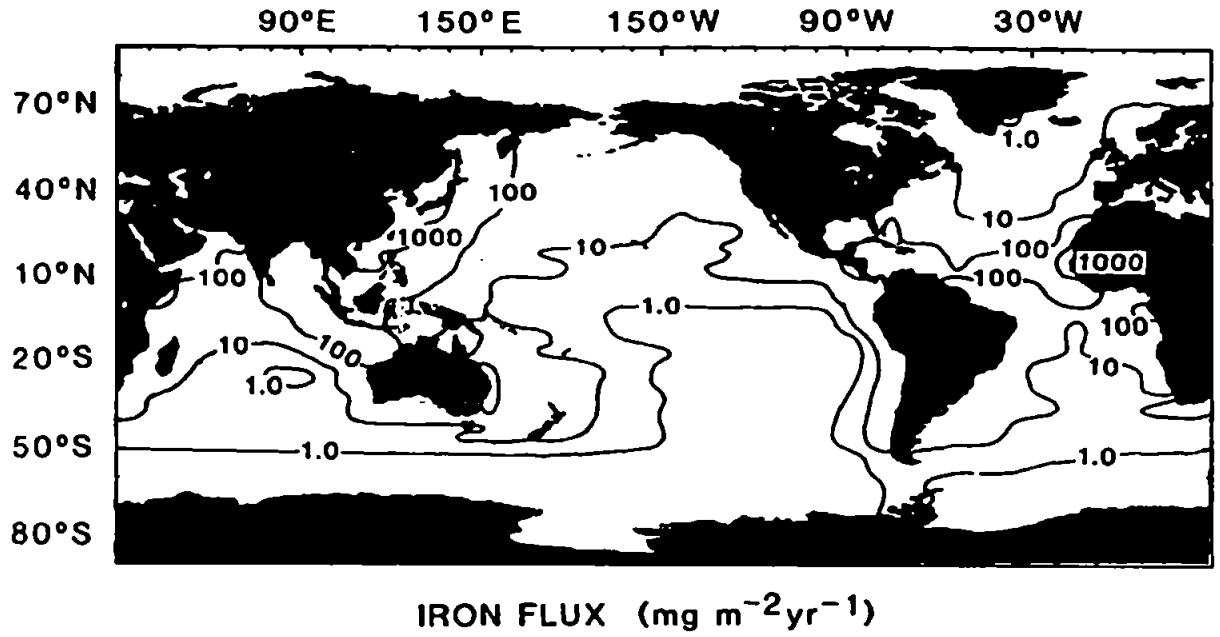

Figure V.22. Calculated flux of total (dissolved plus particulate) Fe from the atmosphere to the ocean (reproduced from Duce and Tindale, 1991)

The AMT-3 cruise experienced heavy rain showers during humid evenings on days 277 and 278, latitudes 7° - 3°N, corresponding with the extent of the ITCZ predicted by the tropical salinity minimum shown in Figure V.19(c) and discussed in detail by Peterson and Stramma (1991). Interestingly, no increase in TD-Fe_{ship} was observed through the region encompassing the ITCZ, perhaps because of the slow dissolution and release of matrix bound Fe from particles, which will be deposited mainly in the form of aluminosilicate dusts. However, no sampling for trace metals in surface seawater was performed during an actual rain event. The region between the 20°N and the Equator does however show generally high land based trace metals (Fe, Al, Co), through wet deposition of particulate material, which may have been solubilised during atmospheric cloud transport or in surface seawater (Zhuang *et al.*, 1990). Elevated Al (42 nM) was observed through the salinity minimum, as previously reported by Measures (1995), although the peak was dwarfed by the intense maximum recorded in the previous province. The absence of a significant increase in nutrients ($Si(OH)_4$, PO_4^{3-}) was consistent with an atmospheric origin of freshwater. Interestingly, though, the primary productivity in the surface layer remained high. This could be the result of filaments of enriched upwelled waters penetrating into the mixed layer in an eastern boundary current.

EQUATORIAL REGION (Eq)

Observations across the Equator during October 1996 showed small increases in TD-Fe_{ship} and chlorophyll *a*, but only slightly elevated $Si(OH)_4$, and no clear NO_3^- or PO_4^{3-} signals. No significant increase between TD-Fe_{land} and TD-Fe_{ship} values was observed. Equatorial upwelling is strongest in boreal spring, lasting only one month and coinciding with the onset of strong easterly wind stress (between July to September; Weingartner and Weisberg, 1991) and this may explain the amplitude of the chemical and biological signals observed on cruise AMT-3.

SOUTH ATLANTIC OLIGOTROPHIC GYRE (SAOG)

The region between the South Equatorial Current and extending towards 30°S in the western South Atlantic contained waters of the Brazilian Basin. This province was the most remote from continental land masses that was experienced during AMT-3, and was characterised by low concentrations of trace metals (e.g. $[TD\text{-}Fe]_{ship} < 1.1$ nM), plant nutrients (NO_3^- and PO_4^{3-}) and suspended particles. Biomass abundance ([chl-*a*] < 0.1 μg l^{-1}) and primary productivity were very low, similar to the northern oligotrophic gyre. Cyanobacteria and small flagellates dominated phytoplankton biomass in this low productivity area (Marañón and Holligan, 1999). Salinity values rose to a maximum of 37.1, which is the result of a combination of high evaporation and low precipitation.

BRAZIL AND FALKLAND CURRENTS CONFLUENCE (BFCC)

The province bounded by the South Atlantic oligotrophic gyre to the north and the Falkland Islands' coast to the south displayed many interesting features. This region encompassed the confluence between the southern extremity of the warm, saline Brazilian Current and the northern limit of the cold, fresh sub-Antarctic water of the Falkland Current. The Brazilian Current, associated with the subtropical gyre in the South Atlantic Ocean, flows south along the continental margin to a point off South America where it separates from the coast in the region of 36°S. The Falkland Current originates as a branch of the Sub-Antarctic Front, the northernmost front associated with the Antarctic Circumpolar Current (ACC) in Drake's Passage, its mean separation from the South American shelf break occurring at 39°S. A

transitional mixing zone consisting of intermediate temperature surface waters therefore exists in this region. The confluence is up to 300 km wide and is characterised by intense eddying and is seasonally variable. The separation of the two fronts, and hence the confluence, are at their northern extreme during the winter months. The sea surface temperature (SST) images (Figure V.23) illustrate large persistent patches of water which travel long distances into the opposing water mass before dispersing (Olson *et al.*, 1988).

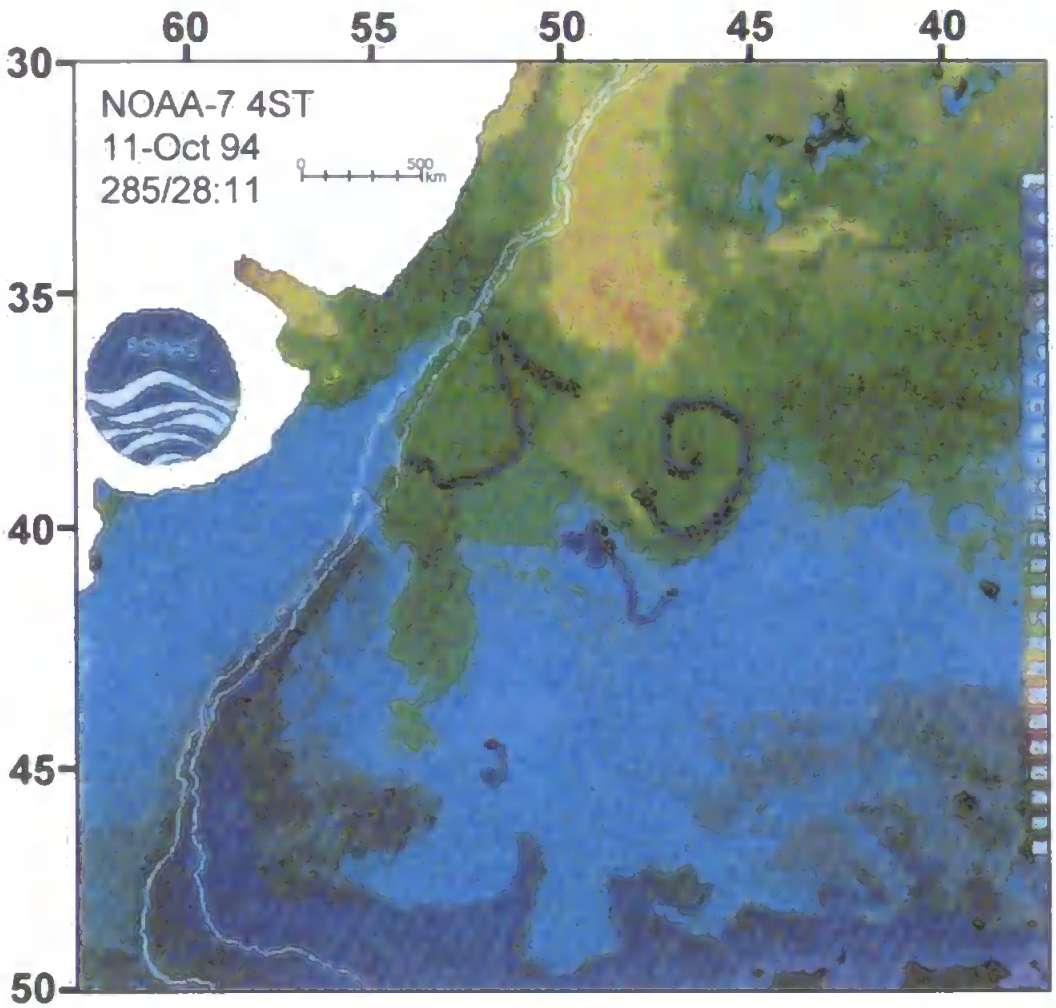

Figure V.23. Atmospherically corrected NOAA AVHRR images of the Brazil-Falkland Currents confluence region in October 1984, when the Brazil Current separation was at its northern extreme. A temperature scale is provided along the side of the image, coded such that warm waters are yellow to green while cold waters are light blue. Drifter trajectories centred about ±20 days are shown in blue. The white contours are the 200 and 1000 m isobaths (reproduced from Olson *et al.*, 1988)

Within this province, AMT-3 chemical and biological measurements showed high spatial variability, a characteristic feature of the nature of the water mixing. Classical nutrients rose to their uppermost values towards the southern limit of the region ($[NO_3^-]_{max}$=35 μM,

$[PO_4^{3-}]_{max}$=1.5 μM, $[Si(OH)_4]_{max}$=6 μM), chlorophyll *a* concentrations fluctuated, but fell no lower than 0.5 μg l^{-1} and carbon fixation rates (> 1.5 μgC l^{-1} h^{-1}) were the highest recorded away from the strong northwest African upwelling. Such responses were indicative of a South Atlantic austral spring bloom, and indeed, the diatom contribution to phytoplankton biomass increased through these temperate waters (Marañón and Holligan, 1999). The region also contained high and variable levels of SPM (Figure V.18(c)). Such observations were in-line with a November 1990 expedition south of the Subtropical Front at 35°S, reported by Rutgers van der Loeff *et al.* (1997). A small pulsed increase in TD-Fe_{ship} was noted at 35°S, correlating with a sharp rise in suspended particles, small increases in nutrients (NO_3^-, NO_2^-, PO_4^{3-}) and chlorophyll *a*, and a slight decrease in temperature and salinity. One can reason that the enrichment in TD-Fe_{ship} was due to convergence circulation resulting in the concentration of material along the front. However, one cannot rule out lithogenic origins or the release of cellular Fe from phytoplankton, and a slight fluctuation in surface salinity and temperature (Figure V.19(c)) suggested a freshwater signal from the plume of the Rio de la Plata. This sampling area, however, surprisingly showed no clear enhanced land-based trace metal concentrations (Al, Co, Ni).

Further to the south, a distinct increase in all land-based trace metal data was observed. The plot in Figure V.24 illustrates the good correlation in this region between trace metals (Co, Ni) and salinity. The excellent coefficients (Co: r^2=0.99, Ni: r^2=0.84, n=6) imply a conservative mixing between two water masses of salinities 33.7 and 36.1; namely, the trace metal enriched, fresh waters of the Falkland Current and the low metal, saline waters of the Brazilian Current. A similar feature has been reported in the North Atlantic by Saager *et al.* (1997), who observed conservative behaviour of Ni in the mixing of two contrasting water masses. In addition, on AMT-3, a good correlation between nutrient enrichment and decreasing salinity was observed in the BFCC (NO_3^- r^2=0.85, $Si(OH)_4$ r^2=0.51, PO_4^{3-} r^2=0.87, n=6). This supports the general contention that increased mixing towards the south with waters originating in the ACC supplied enriched nutrients to this province. The conservative mixing and enrichment of trace metals in the Falkland Current observed during AMT-3 is supported by the data presented by Westerlund

and Öhman (1991), which showed elevated dissolved Ni (6-7 nM) and surface dissolved Co (30-40 pM) concentrations in the Weddell Sea.

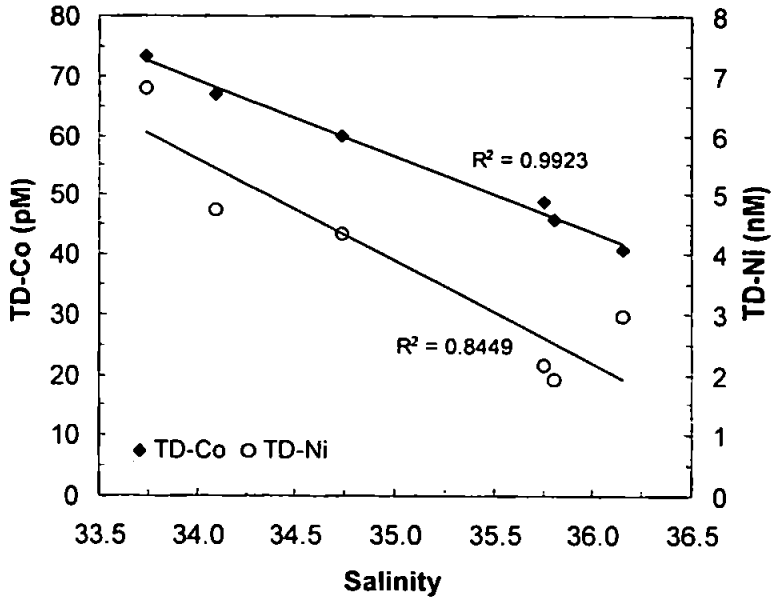

Figure V.24. Trace metals (Co, Ni) versus salinity in the Brazil and Falkland Currents Confluence

However, TD-Fe_{ship} concentrations through the Falkland Current remained low (ca. 1.0 nM). This may be as a result of active uptake by phytoplankton in an area of stimulated production. The relationships for TD-Fe_{ship}, TD-Fe_{land}, TD-Al, and chlorophyll *a* with salinity show poor correlation (r^2=0.26, 0.19, 0.24, 0.04, respectively, n=6). This may be the result of the chemical reactivity of Fe and Al and the non-conservative mixing of the Brazilian Current waters with the low-Fe, low-Al waters of the Southern Ocean ACC (Löscher *et al.*, 1997). Fe and Al distributions in this region are more likely to be dominated by dusts off the Patagonian desert. In summary, the high and variable concentrations of nutrients and trace metals in the south west Atlantic Ocean point to an intense mixing zone under the influence of strong coastal and internal advective sources.

EAST FALKLAND SHELF (EFS)

The location for the most southerly sampling station during AMT-3 was on the shelf off East Falkland Island. The coastline was clearly visible from the ship and the water column was only 76 m deep. Increased [TD-$Fe]_{ship}$ (2.7 nM) was concurrent with an influence from the nearby

land mass and continental shelf. Bacterial remineralisation of organic detritus at the sediment-water interface will reduce the redox potential and result in a diffusion of redox sensitive trace elements (Fe, Mn, Cr) from porewaters into a shallow water column (Chester, 1990). Nutrient enrichment together with chlorophyll *a* and particle number increases were also observed in surface layers. TD-Co and TD-Ni concentrations rose to 73 pM and 6.8 nM, respectively, although TD-Al (20.6 nM) showed no increase compared with open-ocean values. The flux of dissolved Al into bottom waters across the sediment-water interface has been reported to be insignificant (Measures and Edmond, 1990), supporting the hypothesis that the elevated Fe, Co and Ni at this station originated *via* regeneration processes occurring at the underlying coastal shelf.

V.3.4.4 Iron – Aluminium Relationships

One may assume that particulate Fe may be divided into two fractions; one linked with particulate Al (oxy-hydroxides and refractory Fe) and the other with particulate organic carbon (biogenic Fe). In order to investigate the association between particulate Fe in both aluminosilicate and biogenic phases in land-based samples, the total dissolvable Fe to total dissolvable Al $(Fe/Al)_{land}$ ratio was determined. This ratio in surface samples along the transport was not constant and varied from 0.02 in the SAOG to 0.19 in the BFCC, with a mean of 0.09 ± 0.04. This ratio is normally calculated on digested particulate (>0.4 μm) fractions, but in this study included the dissolved form plus any metal leached from particulate material. All values were lower than the crustal Fe/Al ratio of 0.33, defined by Taylor (1964). The upper limit, however, was close to the Fe/Al ratio of 0.13 (Kuss and Kremling, 1999) reported on near-surface particulates in the North Atlantic and also in good agreement with the granite rock values (0.17) documented by Turekian and Wedepohl (1961), implying the dust origin of Fe. The generally low ratios observed during AMT-3 may, at first glance, imply that a significant portion of Fe_{land} in surface seawater was not of lithogenic origin. However, the most likely explanation was that the dissolved Al contribution to TD values was very significant in the calculations. Helmers (1996) found that particulate Al represented less than 14% of total Al along a similar transect, and calculations performed here will therefore be biased towards lower

values, providing an underestimate of the Fe/Al ratio. For this reason, coupled with a general poor understanding of the solubilisation of atmospherically deposited aerosols in seawater, ratio data must be treated with caution.

TD-Fe measurements were very strongly biased by particles, as illustrated by the excellent correlation between province data for TD-Fe_{ship} and particle numbers in Figure V.20(a). One can assume that the TD-Fe_{ship} measurement included the dissolved fraction (including colloidal and organically complexed forms), plus easily available metal leached from reactive particulate material (e.g. of biogenic origin). In addition, the TD-Fe_{land} concentration included the above fractions, plus a further contribution leached from more refractory particulate material after 16 months of storage at pH 2 (e.g. of lithogenic origin). The resulting difference (TD-Fe_{land}-TD-Fe_{ship}) value may represent the Fe released from refractory lithogenic material. The relationship between (TD-Fe_{land}-TD-Fe_{ship}) and TD-Al (r^2=0.52, n=21, Figure V.25(a)) supports this assumption and implies that over an extended acidification period, Fe values are more indicative of their lithogenic origin. Indeed, a correlation of similar magnitude is observed between TD-Fe_{ship} and chlorophyll *a* (r^2=0.57, n=30, Figure V.25(b)), supporting the above assumption that shipboard measurements were strongly biased by the exchangeable particulate Fe of biogenic origin in addition to dissolved Fe. One data point does strongly bias the relationship in Figure V.25(b), though.

Further evidence of variation in inputs of lithogenic Fe with geographical location is provided in Table V.12, which lists (TD-Fe_{land}-TD-Fe_{ship}) enrichments for surface water (-7 m) samples taken in each province along the transect. It is clear that the strongest input of Fe of crustal origin occurred in the vicinity of the west coast of Africa (provinces NWAUp and SUp/NEq), and towards the South American continent in the BFCC. In contrast, the NEAOG and the region crossing the Equator received the lowest amount of lithogenic Fe, and it is interesting to note that these provinces were the furthest geographically from any continental land mass along AMT-3. The data for the EFS appears anomalous, but it was based upon only one data point.

Province	*NEAOG*	*NWAUp*	*SUp/NEq*	*Eq*	*SAOG*	*BFCC*	*EFS*
No. of observations	2	2	7	2	9	6	1
TD-Fe_{ship}	1.07	2.28	0.66	1.26	0.74	1.12	2.71
TD-Fe_{land}	1.33	6.17	2.96	1.30	1.75	2.74	3.00
TD-Fe_{land}-TD-Fe_{ship}	0.15	3.89	2.30	0.04	1.01	1.62	0.29

All data in nM

Table V.12. Enrichment in TD-Fe between land-based and shipboard analyses of identical surface water (-7 m) sub-samples

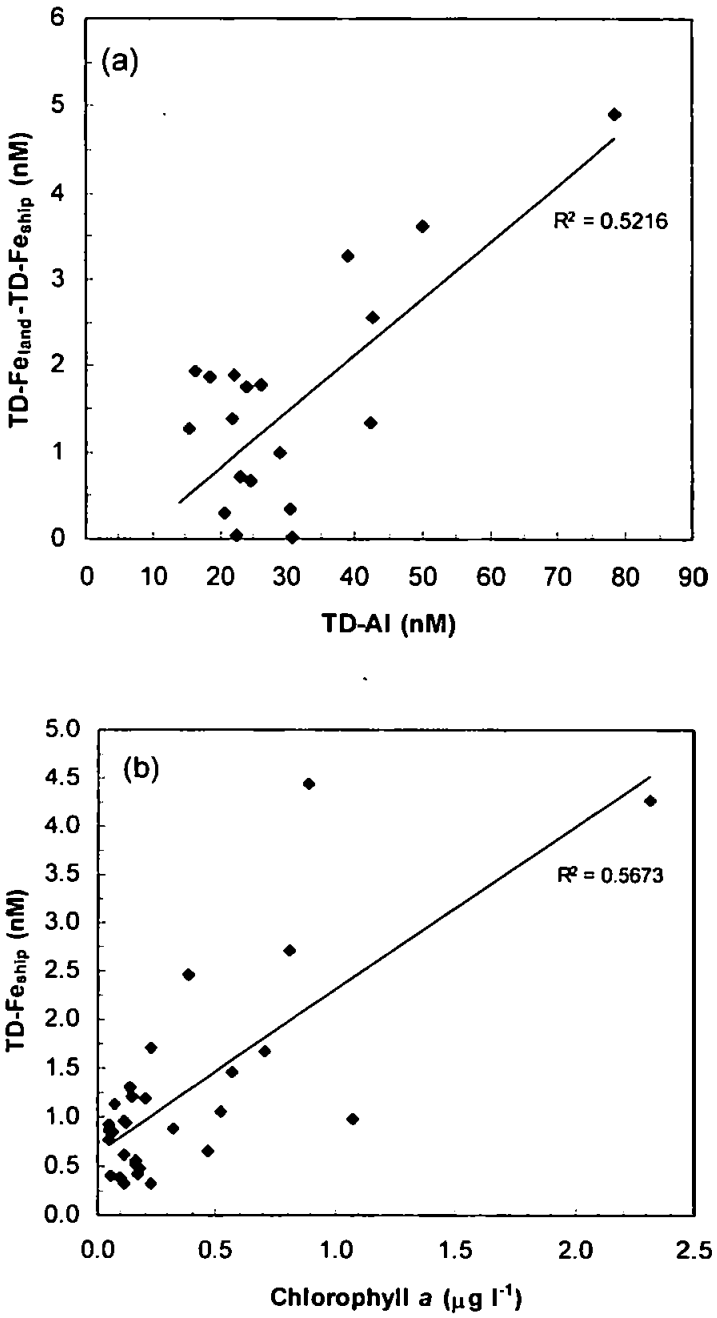

Figure V.25. (a) TD-Fe_{land}-TD-Fe_{ship} versus TD-Al in the surface Atlantic Ocean; (b) TD-Fe_{ship} versus chlorophyll *a* in the surface Atlantic Ocean

V.3.4.5 Aluminium – Silicate Relationships

Al is a major component of crustal materials (ca. 8.2% by weight) and the strong deposition of aeolian material into the ocean results in partial dissolution (ca. 5-10%; Maring and Duce, 1987) of this element. The residence time of dissolved Al in surface waters has been estimated to be of the order of 3-4 yr in oligotrophic waters of the central North Pacific gyre (Orians and Bruland, 1986). The major supply route of Al to the surface ocean (e.g. aluminosilicate dust particles) will also be a source of dissolved Si since dissolution rates are comparable (5% Si soluble in seawater, Duce *et al.*, 1991). However, the crustal molar Al/Si ratio is 3.3 (Vinogradov, 1962) and therefore the atmospheric supply of dissolved Si will be negligible if one assumes a conservative dissolution between the two elements. Al and Si are also supplied by rivers, but the Al/Si ratio is far lower than that associated with atmospheric inputs since a significant part of Al released from riverine particles will be removed in estuaries (Regnier and Wollast, 1993). In areas of high production and export, Al will be scavenged by the flux of organic matter far more effectively than Si. Particle scavenging results in poor recycling of Al in upwelling areas.

The distribution of Si is controlled by gradual opal dissolution and conservative mixing and consequentially its residence time in deep waters is of the order of 20,000 yr compared to the 100-200 yr for Al (Orians and Bruland, 1986). Si is recycled at a greater depth than N and P and is thus less influenced by upwelling across the thermocline. The primary source of Si to surface waters is riverine inputs, which may extend far off shore. Si may also become depleted due to active uptake by diatoms during the early summer months.

Since Al is a scavenged element and its low solubility and short residence time ensures a low background signal in the surface ocean, its measurement allows the observation of what are essentially local processes in the surface waters. Al is expected to show some recycled behaviour in deeper waters (like other scavanged elements Pb and Mn), although this will be much less than nutrient-type metals. In addition, the distributions of Al and Si are controlled by external continental sources, the Al/Si ratio being dependent on the origin (atmospheric, fluvial, coastal

shelf), as discussed above. Hence it is possible to use the different signatures for Al and Si in freshwater sources to help fingerprint input mechanisms for trace elements.

Aluminium reached maximum concentrations (78.5 nM) in the vicinity of 20°N off the west coast of Africa. Silicate values were relatively low at these latitudes, despite the presence of upwelling activity. At 48°S, towards the South American continent, Al showed another maximum (50 nM), this time accompanied by a distinct Si maximum (6 μM). In general, the influence of the Falkland Current in waters of the south-west Atlantic below 35°S resulted in high Si concentrations which were observed at all stations, albeit with strong variations.

Figure V.26 contains a plot of Al versus Si for all surface samples along AMT-3. Two distinct correlations exist. The high-Al, low-Si end-member (A) approaching the crustal ratio is indicative of a source of dry deposition, confirmed by the maintenance of relatively high salinity at this location. Points along line AB signify a dry or wet atmospheric dust source, consistent with the points within the province SUp/NEq which encompassed the ITCZ. The high-Si, low-Al end-member (D) points towards a riverine or shelf source of freshwater. Points along line CD are locations in the south-west Atlantic, which were most likely influenced by the plume of the Rio de la Plata (confirmed by the drop in salinity and temperature at this latitude), a mixing with Si enriched waters of the ACC or a shelf influence near the Falkland Islands. The majority of the Al/Si points (shaded area) lie on the intersect of the lines AB and CD and indicate the typical, non-enhanced, non-depleted Al and Si concentrations along the transect. The point lying in the NEAOG is Al- and Si- depleted.

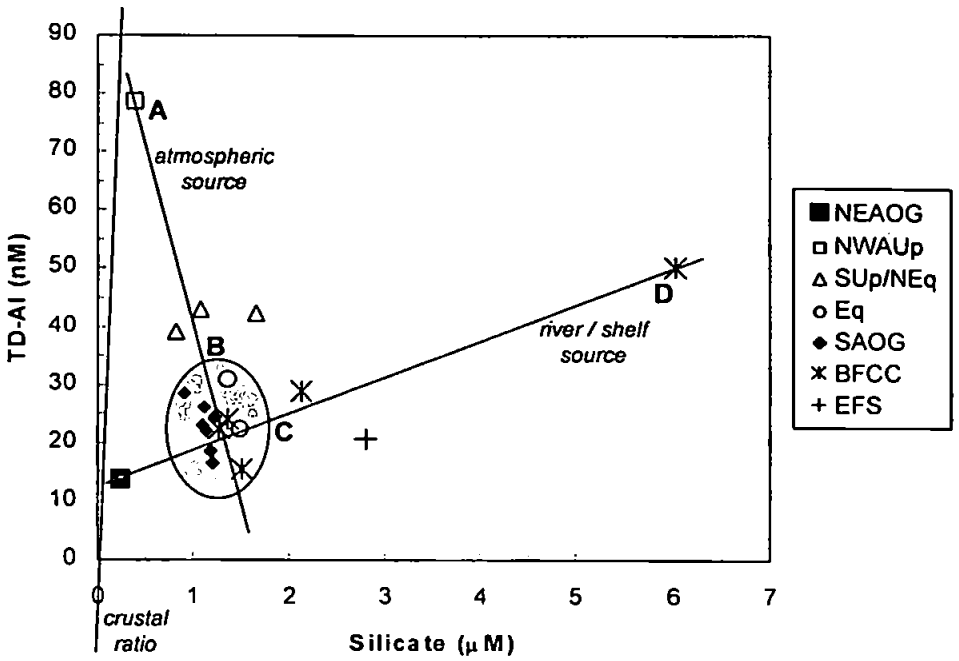

Figure V.26. Aluminium versus silicate for surface waters data along AMT-3

V.3.4.6 Residence Times

The effect of atmospheric deposition on surface water concentrations in a region of high aerosol flux (such as that off the west coast of Africa) is critically linked to residence times. A relatively short residence time (a few years) would allow seasonality in trace metal concentrations to be detected. Longer residence times (>10 yr) would prevent small changes associated with atmospheric inputs being observed, as any increase would be buffered against the background concentration.

If one assumes an upper solubility estimate of 2.1% for total aerosol "dust" Fe entering the ocean (Jickells and Spokes, 1999), and applies this to an estimated aeolian flux of 100 mg m^{-2} yr^{-1} in the tropical north Atlantic (35° – 5°N, Duce and Tindale, 1991), then this is equivalent to a 0.5 nM increase in TD-Fe concentration per year in an isolated mixed water layer depth of approximately 80 m (estimated from AMT-3 vertical σ_t distributions). The mean surface water concentration of $TD\text{-}Fe_{ship}$ in that region has been found in this study to be 1.08 nM. If TD-Fe was removed entirely by re-incorporation into particles, the necessary residence time would be 2.2 yr. This residence time is lower, but not wholly different, than that predicted by Sarthou *et al.* (1997) for the upper 100 m in the Indian sector of the Southern Ocean (3.7 yr). However,

differences are to be expected as residence times depend heavily on biological uptake and scavenging processes, which will vary in different oceanic provinces. Indeed, the large flux of aerosol material into this region of the Atlantic will increase suspended solid concentrations, and accordingly increase scavenging rates for dissolved metal species. It should be noted that the same calculation using the lower limit of Fe solubility in seawater (0.8%; Jickells and Spokes, 1999) and the upper limit of aerosol flux in the tropical north Atlantic (1000 mg m^{-2} yr^{-1}; Duce and Tindale, 1991) results in a residence time prediction of 0.6 yr. There are clearly caveats associated with these calculations which have been addressed by Jickells and Spokes (1999).

A similar calculation can be performed for Al in this region. Given a flux of 80 μg Al cm^{-2} yr^{-1} (Chester, 1982), a solubility in seawater of 8% (Maring and Duce, 1987) and a wind mixed layer depth of 80 m, an increase of 29.6 nM Al per year can be estimated for an isolated water layer between 35° and 5°N. The mean surface water concentration of TD-Al in this region has been measured during AMT-3 as 42.0 nM, resulting in a residence time of 1.4 yr. This value is low in comparison with literature data. Jickells *et al.* (1994) reported a residence time of 6.6 yr for Al in the upper 100 m waters of the Sargasso Sea, where productivity and suspended particle concentrations are relatively low, and scavenging rates for dissolved trace metals are accordingly low. Helmers and Rutgers van der Loeff (1993) calculated a similar value of 2-4 yr in the North Atlantic, although Kremling (1985) reported a residence time of 6.9 yr between latitudes of 10° and 30°N. The residence time calculated on AMT-3 for a particle reactive element such as Al will be strongly influenced by the high scavenging rates due to dry deposition and upwelling activity occurring in these latitudes.

Residence times calculated above for Fe and Al (2.2 and 1.4 yr, respectively) would result in a geographical distribution in surface waters that is controlled primarily by the distribution of the inputs from the atmosphere. However, values are long enough to allow for some dispersion and for a memory effect after a change in the input pattern. This is well illustrated through the ITCZ, where during seasonal migration trace metal maxima are expected to lag behind the inputs by several weeks (Rutgers van der Loeff *et al.*, 1997).

V.3.5 Vertical Distributions Through the Upper water Column

V.3.5.1 Overview

Figures V.27 to V.36 show upper water column (<200 m) vertical distributions of TD-Fe_{ship}, and other chemical, biological and physical parameters, at ten selected stations along AMT-3. These profiles are representative of the vertical distributions for Fe in six of the biogeochemical provinces crossed during AMT-3. Ancillary data presented for each profile include macro-nutrients (NO_3^-, NO_2^-, PO_4^{3-}, $Si(OH)_4$), total chlorophyll *a*, primary productivity, temperature and salinity. In addition, land-based sub-sample analyses for TD-Fe_{land}, TD-Al, TD-Co and TD-Ni are included for stations A308, A309, A315, A319 and A325. Table V.13 summarises the data available for each selected station. Typical precision (Section V.3.1.5) for the analysis of TD-Fe_{ship} in sub-aliquots taken from the same Go-Flo sampler bottle and for TD-Fe_{land} in sub-aliquots taken from the same HDPE collection bottle are shown on the profiles for station A308. In addition, the structure of the water column at each vertical profile station is described by a temperature – salinity (T-S) plot.

Station	A308	A309	A311	A313	A315	A316	A319	A321	A325	A328
TD-Fe_{ship}	•	•	•	•	•	•	•	•	•	•
TD-Fe_{land}	•	•			•	•	•		•	
TD-Al	•	•			•					
TD-Ni	•	•			•	•	•		•	
TD-Co	•	•			•	•	•		•	
Temperature	•	•	•	•	•	•	•	•	•	•
Salinity	•	•	•	•	•	•	•	•	•	•
NO_3^-	•	•	•	•	•	•	•	•	•	•
NO_2^-	•	•	•	•	•	•	•	•	•	
PO_4^{3-}	•	•	•	•	•	•	•		•	•
$Si(OH)_4$		•	•	•	•	•	•	•	•	•
Chl. *a*	•	•	•	•	•	•	•	•	•	•
Production	•	•	•	•	•	•	•	•	•	•

Table V.13. Summary of AMT vertical profile data available for each selected station

V.3.5.2 Results

Table V.14 contains a summary of trace metal concentrations in the upper water column of the Atlantic Ocean (50°N to 50°S) for the complete AMT-3 transect. A total of 152 shipboard analyses were performed during the 27 day cruise period. The wide range of elemental

concentrations for all metals, especially Fe, serves to illustrate the diverse input and removal mechanisms encountered in the coastal, shelf and open-ocean waters along AMT-3.

The vertical distributions for TD-Fe_{ship} showed many similar characteristics for different stations along AMT-3. Generally speaking, the vertical profiles consisted of a steady background concentration of TD-Fe_{ship} through the upper 200 m, with fluctuations caused by biological activity, water column stratification or atmospheric inputs in the surface layers. The ambient Fe level was governed by the geographical location of the station and consequentially the internal and external inputs, which were dominated by aerosol flux. An individual examination of each of the ten selected vertical profiles, investigating relationships between TD-Fe and input mechanisms, hydrography and biological processes is contained in V.3.5.4.

Element	*Number of observations, n*	*Maximum*[a]	*Minimum*[a]	*Mean*[a]	*Standard deviation*	*RSD (%)*
TD-Fe_{ship}	152	6.07	0.04	**1.08**	0.98	90.7
TD-Fe_{land}	62	8.28	0.71	**2.28**	1.51	66.2
TD-Al	41	78.5	10.8	**25.6**	11.85	46.3
TD-Co	66	110	20.3	**45.0**	19.17	42.6
TD-Ni	66	8.15	1.43	**2.57**	1.13	44.0

[a] All data in nM, except TD-Co (pM)

Table V.14. Mean upper water column (<200 m) total dissolvable trace metal data for the waters of the Atlantic Ocean experienced during AMT-3

V.3.5.3 Sectioned [TD-Fe]$_{ship}$ Vertical Distributions through Biogeochemical Provinces

Table V.15 presents averaged results of all vertical profiling data for TD-Fe_{ship} through each biogeochemical province. The data are presented for the complete profile through the upper water column (<200 m) and has been sectioned into three categories: (i) samples above, (ii) samples through, and (iii) samples below the chlorophyll maximum. Examining the data in this way gives an indication of the ambient Fe levels away from areas of high biogenic or lithogenic particulate matter in the surface layers.

Data for samples collected in the *SW App* are sparse; however, the enhanced concentration of TD-Fe_{ship} in this province reflected a strong continental influence to surface waters, as discussed

in V.3.4.3. The TD-Fe_{ship} average concentration through the *NEAOG* was 1.03±0.36 nM. The vertical structure of Fe in this oligotrophic gyre was characterised by a TD-Fe minimum that coincided with the chlorophyll maximum. This may have been a result of active uptake of bioavailable Fe by phytoplankton at these depths and/or increased scavenging of dissolved Fe due to the higher concentration of biotic particulate material. Indeed, Symes and Kester (1985) found that at open-ocean stations in the north-west Atlantic, Fe in samples taken in the vicinity of the chlorophyll maximum was almost totally in the particulate form, which may have resulted in a reduction in the fraction of Fe_{ship} amenable to the analytical method. The *NWAUp* province was characterised by enhanced TD-Fe_{ship} in surface layers, depletion at the chlorophyll maximum and an ambient level below the thermocline of 1.01±0.37 nM.

Average TD-Fe_{ship} data for all samples taken from three provinces in the central and south Atlantic Ocean showed strikingly good consistency (*SUp/NEq*=0.58±0.37 nM, *Eq*=0.64±0.47 nM, *SAOG*=0.60±0.30 nM). There appeared to be no inter-province fractionation, despite major changes in trace element input mechanisms over the ~8000 km of ocean traversed through the three provinces. Such observations are consistent with deep water data presented by Johnson *et al.* (1997), who proposed that Fe profiles are maintained by a mechanism which reduced the scavenging rate of dissolved Fe at concentrations less than 0.6 nM, possibly due to complexation by strong binding ligands. However, they also reported dissolved Fe concentrations of <0.2 nM at the surface, at least a factor of 3 less than the AMT-3 dataset for the open-ocean. However, the dissolved Fe concentrations in the Pacific Ocean that the Moss Landing Marine Laboratories report cannot be directly compared with the Atlantic Ocean TD-Fe data presented here for the upper water column for the following reasons. Firstly, there are methodological differences with the filtration, pretreatment and analysis steps; and secondly, the two regions are environmentally different, with the tropical and central Atlantic Ocean receiving a high and seasonal atmospheric dust flux. Sectioned TD-Fe_{ship} averages for these provinces showed only minor Fe depletion through the chlorophyll maximum, possibly due to the low biomass and production rates in such waters, due to N or P limitation.

Conversely, waters of the *BFCC* were enriched in TD-Fe, with a mean concentration in the upper water column of 1.52±0.74 nM. The vertical structure showed a differing pattern to that of the under productive waters of the other provinces. A Fe maximum in the vertical structure was observed which corresponded with a shallow chlorophyll maximum in the spring bloom conditions. Several possible explanations exist for such an observation at these depths:

(i) Recycled Fe - release of nutrient Fe due to breakdown of decaying biota,

(ii) Organically complexed Fe - excretion of ligands (e.g. siderophores, porphyrins) by biota and subsequent organic complexation maintaining high dissolved levels,

(iii) Regenerated Fe – degradation of organic matter (e.g. heterotrophic bacteria) or ingestion of particles (e.g. zooplankton grazers) and subsequent dissolution and release of bioavailable Fe to seawater (Barbeau and Moffett, 1998),

(iv) Cellular Fe - release of intra- (or extra-) cellular-bound Fe on sample acidification / reduction, or

(v) Ambient Fe - higher ambient levels maintaining increased phytoplankton growth.

Neither one of these hypotheses can be proven or rejected, although each one is investigated in more detail for individual station profiles in Section V.3.5.4. Finally, waters in the *EFS* province showed enhanced surface and deep concentrations (ca. 6.0 nM) with depletion (2.8 nM) at the chlorophyll maximum.

Province acronym	*Latitude*	*SDY*	*Stations*	*Go-Flo casts*	*Representative station(s)*	*Shipboard analyses TD-Fe_{ship} (nM)*			
						Whole profile	*Above chl. max*	*Chl. max.*	*Below chl. max.*
SWApp	50°N to 47°N	266-268	A301-A303	A3-01 to A3-03	n/a	4.36±0.13 (n=2)	n.o.	n.o.	n.o.
NEAOG	30°N to 24°N	269-273	A304-A308	A3-04 to A3-08	A308	1.03±0.36 (n=16)	1.15±0.21	0.42±0.04	1.19±0.28
NWAUp	20°N	274	A309	A3-09	A309	1.42±1.20 (n=7)	2.23±1.49	0.21±0.00	1.01±0.37
SUp/NEq	13°N to 5°N	276-278	A310-A312	A3-10 to A3-12	A311	0.58±0.37 (n=21)	0.78±0.55	0.47±0.21	0.50±0.14
Eq	2°N to -3°S	279-280	A313-A314	A3-13 to A3-14	A313	0.64±0.47 (n=15)	1.04±0.45	0.33±0.30	0.43±0.17
SAOG	-6°S to -30°S	281-287	A315-A323	A3-15 to A3-21	A316, A319, A321	0.60±0.30 (n=40)	0.61±0.27	0.64±0.39	0.52±0.25
BFCC	-32°S to -48°S	288-298	A324-A329	A3-22 to A3-26	A325, A328	1.52±0.74 (n=36)	1.11±0.30	1.89±1.03	1.52±0.57
EFS	-52°S	299	A330	A3-27	n/a	4.40±1.85 (n=4)	5.92±0.00	2.80±0.13	6.07±0.00

n.o.: no observations

Table V.15. Mean TD-Fe_{ship} concentrations (all data) vertically sectioned through the upper water column (<200 m) of each oceanographic province

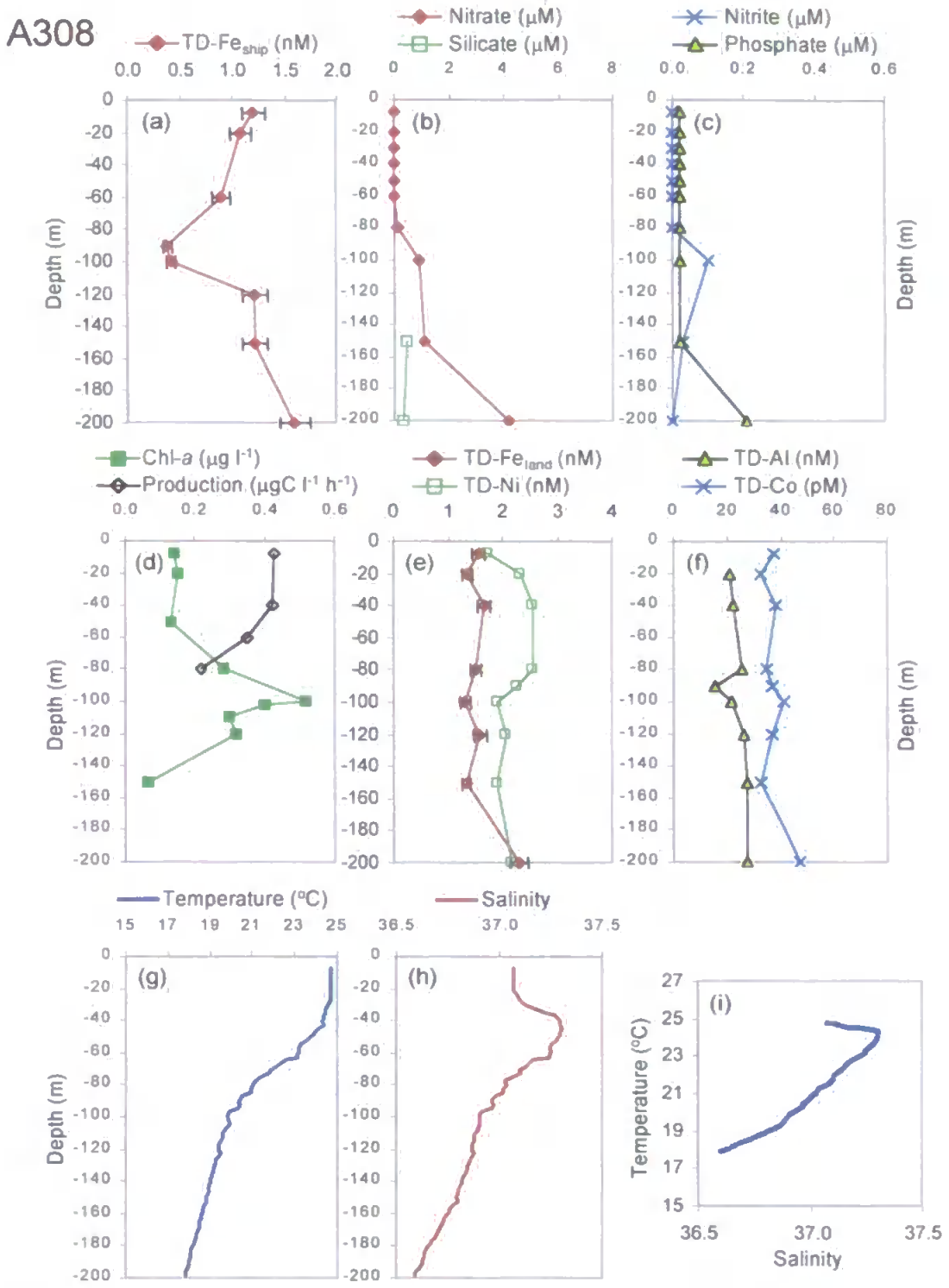

Figure V.27. Station A308, Go-Flo A3-08, SDY 273 (24°40.6'N, 21°24.1'W): Trace metal, nutrient, chlorophyll, production and hydrographic profiles through the upper water column. (a) TD-Fe$_{ship}$, (b) NO_3^- & $Si(OH)_4$, (c) NO_2^- & PO_4^{3-}, (d) chlorophyll *a* & production, (e) TD-Fe$_{land}$ & TD-Ni, (f) TD-Al and TD-Co, (g) temperature, (h) salinity, and (i) T-S plot

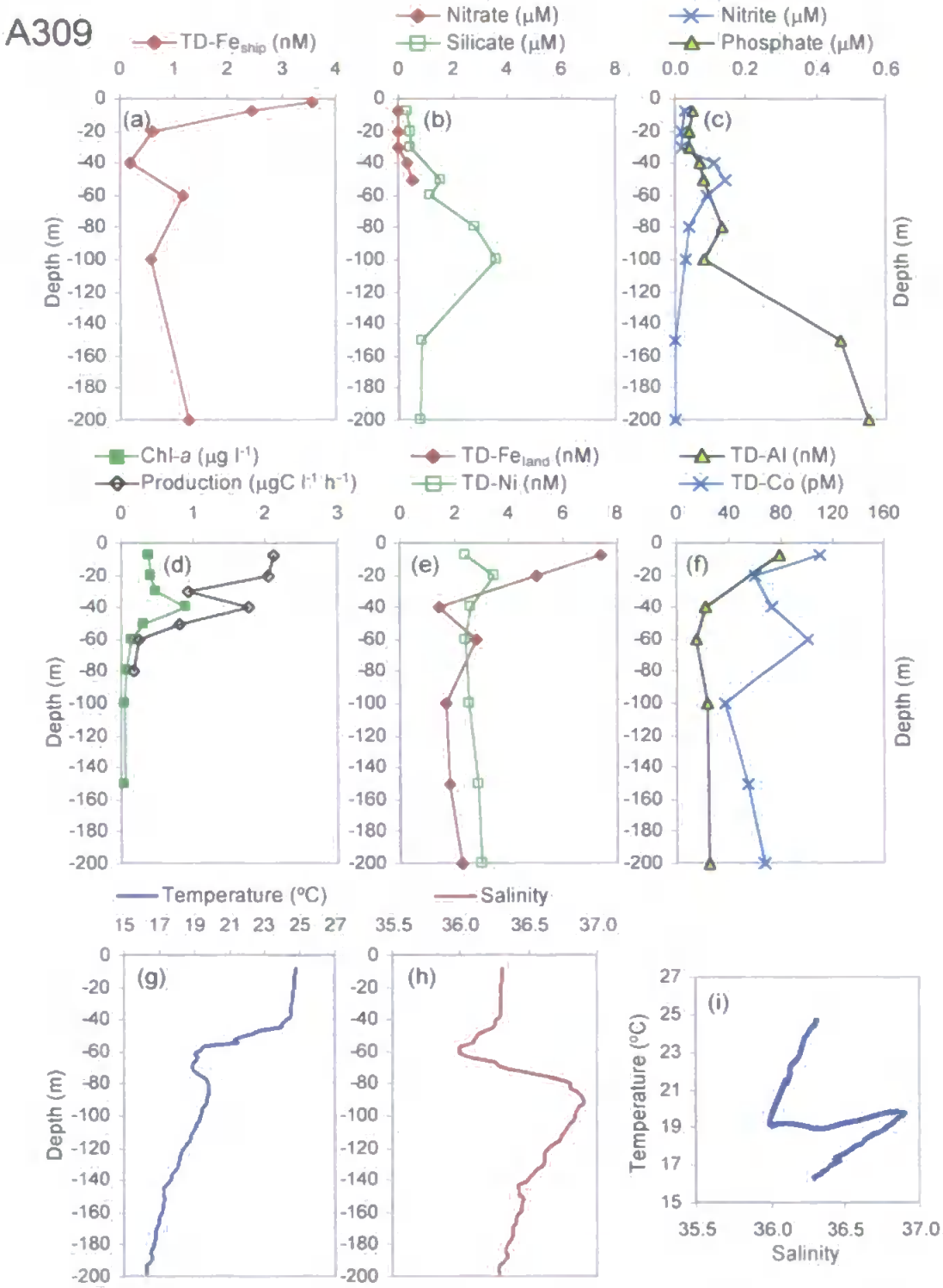

Figure V.28. Station A309, Go-Flo A3-09, SDY 274 (20°05.1'N, 20°37.7'W): Trace metal, nutrient, chlorophyll, production and hydrographic profiles through the upper water column. (a) TD-Fe$_{ship}$, (b) NO_3^- & $Si(OH)_4$, (c) NO_2^- & PO_4^{3-}, (d) chlorophyll *a* & production, (e) TD-Fe$_{land}$ & TD-Ni, (f) TD-Al and TD-Co, (g) temperature, (h) salinity, and (i) T-S plot

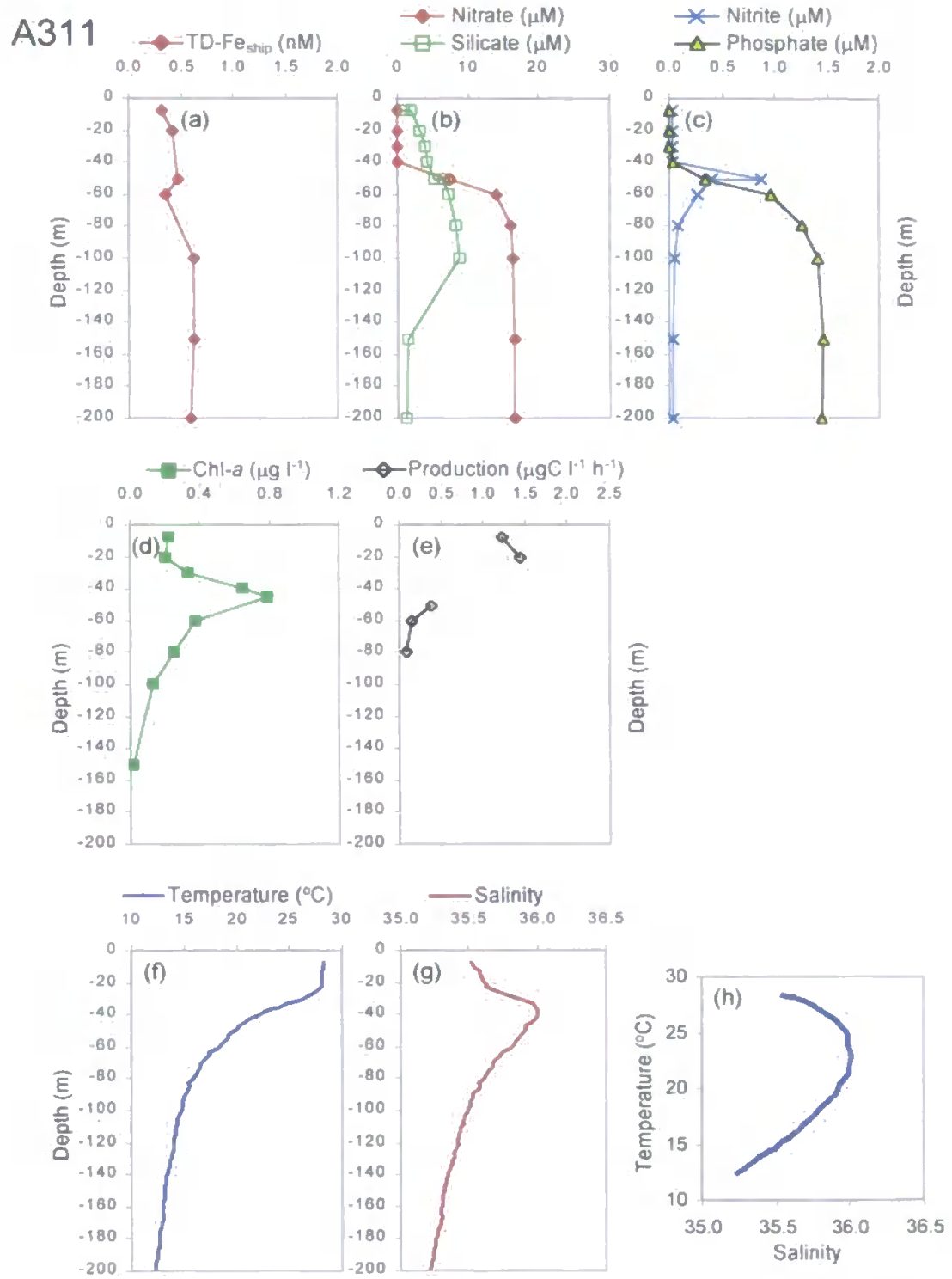

Figure V.29. Station A311, Go-Flo A3-11, SDY 277 (09°03.1'N, 22°16.6'W): Trace metal, nutrient, chlorophyll, production and hydrographic profiles through the upper water column. (a) TD-Fe$_{ship}$, (b) NO_3^- & $Si(OH)_4$, (c) NO_2^- & PO_4^{3-}, (d) chlorophyll *a*, (e) primary production, (f) temperature, (g) salinity, (h) T-S plot

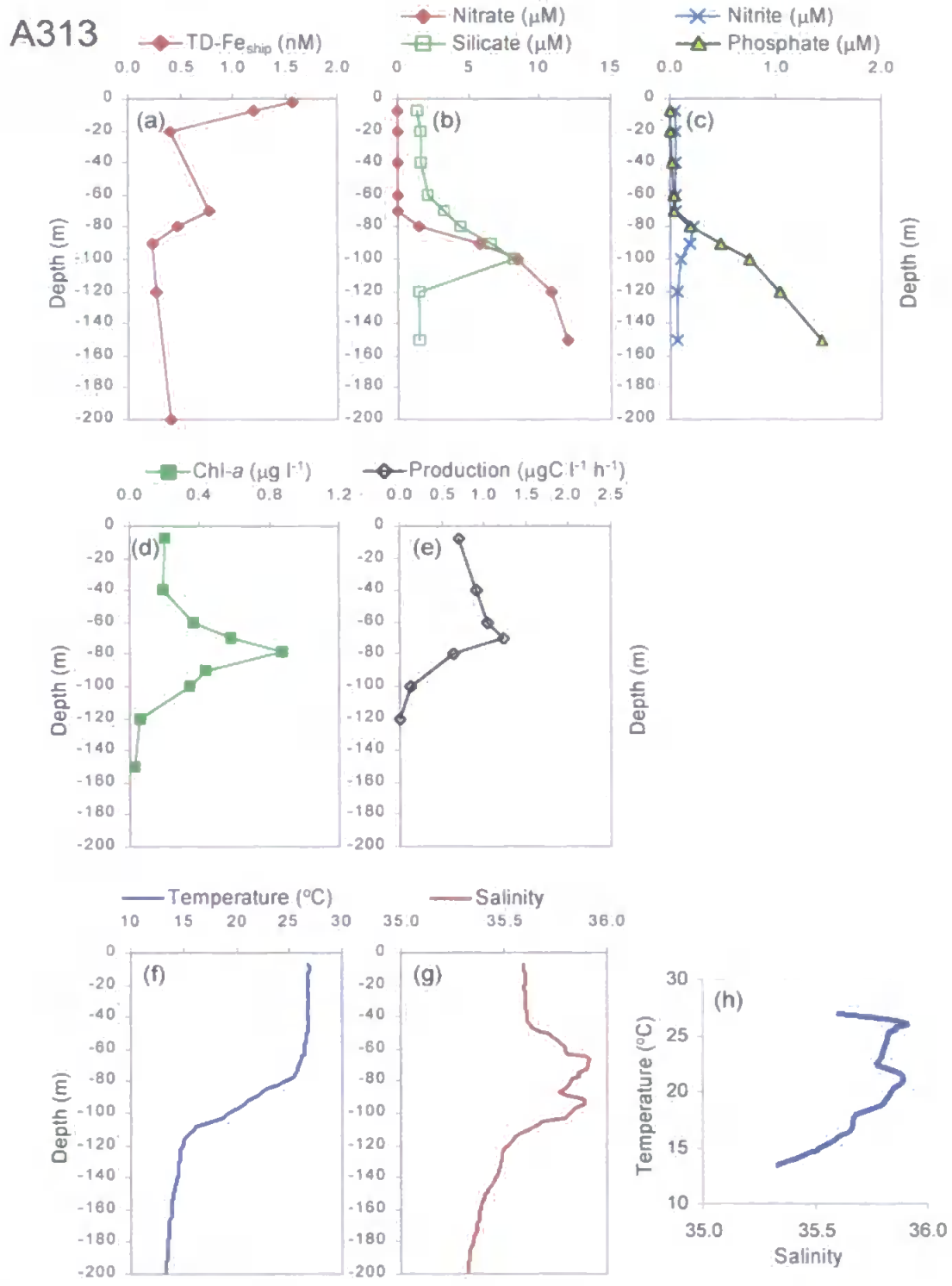

Figure V.30. Station A313, Go-Flo A3-13, SDY 279 (01°17.4'N, 25°46.9'W): Trace metal, nutrient, chlorophyll, production and hydrographic profiles through the upper water column. (a) TD-Fe$_{ship}$, (b) NO_3^- & $Si(OH)_4$, (c) NO_2^- & PO_4^{3-}, (d) chlorophyll *a*, (e) primary production, (f) temperature, (g) salinity, (h) T-S plot

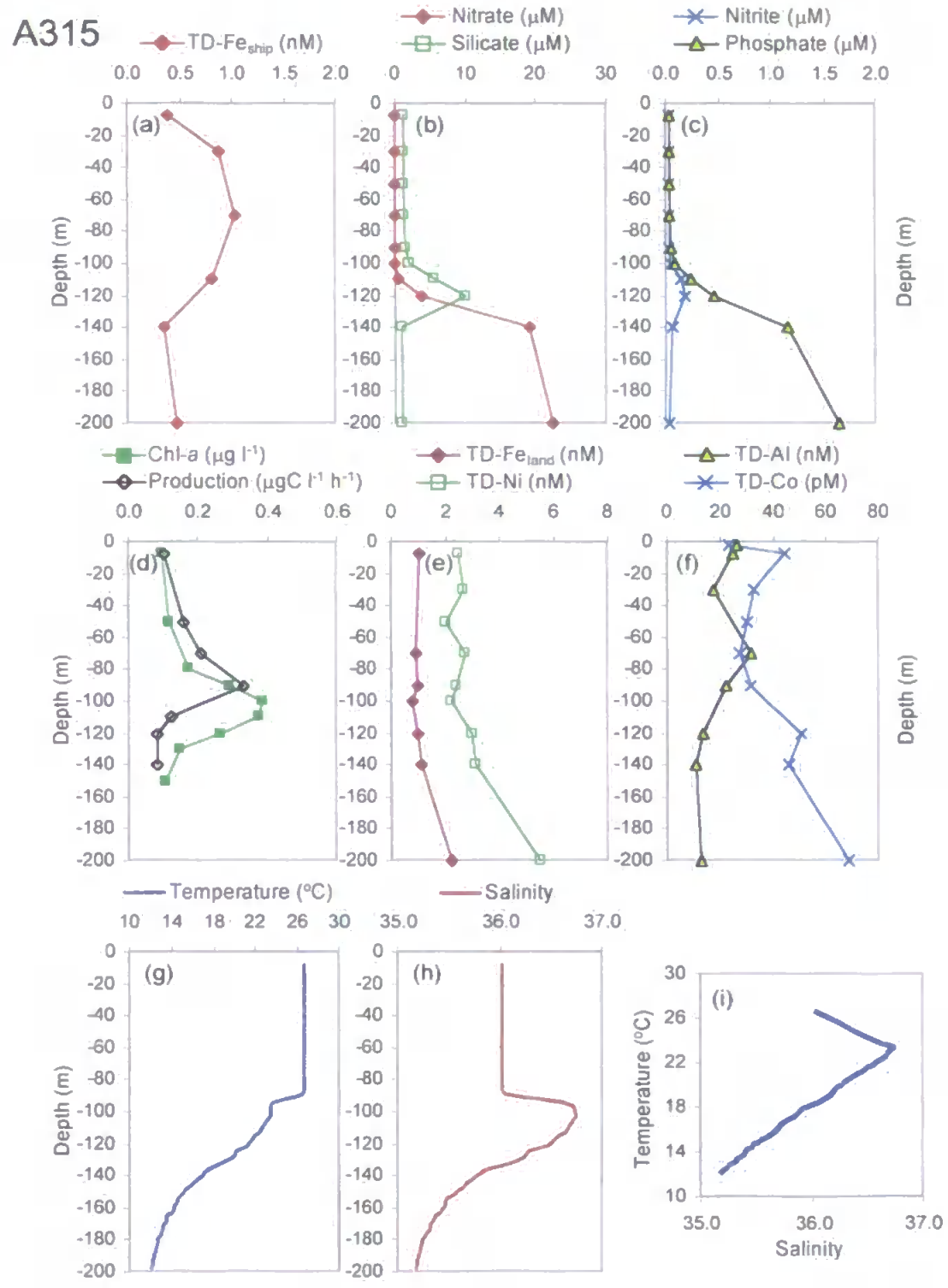

Figure V.31. Station A315, Go-Flo A3-15, SDY 281 (06°29.0'S, 29°16.2'W): Trace metal, nutrient, chlorophyll, production and hydrographic profiles through the upper water column. (a) TD-Fe$_{ship}$, (b) NO_3^- & $Si(OH)_4$, (c) NO_2^- & PO_4^{3-}, (d) chlorophyll *a* & production, (e) TD-Fe$_{land}$ & TD-Ni, (f) TD-Al and TD-Co, (g) temperature, (h) salinity, and (i) T-S plot

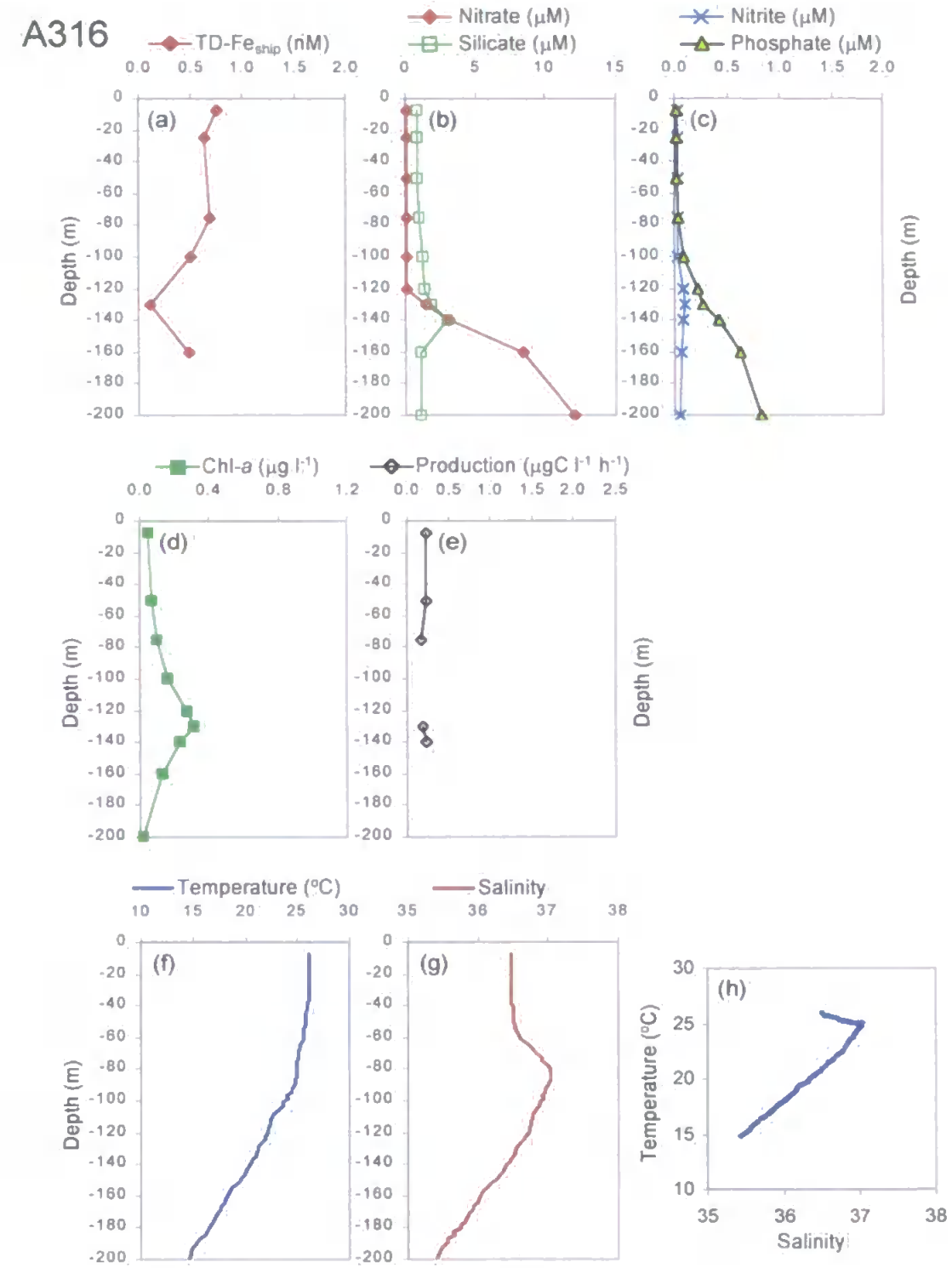

Figure V.32. Station A316, Go-Flo A3-16, SDY 282 (10°46.8'S, 31°14.5'W): Trace metal, nutrient, chlorophyll, production and hydrographic profiles through the upper water column. (a) TD-Fe$_{ship}$, (b) NO_3^- & $Si(OH)_4$, (c) NO_2^- & PO_4^{3-}, (d) chlorophyll *a*, (e) primary production, (f) temperature, (g) salinity, (h) T-S plot

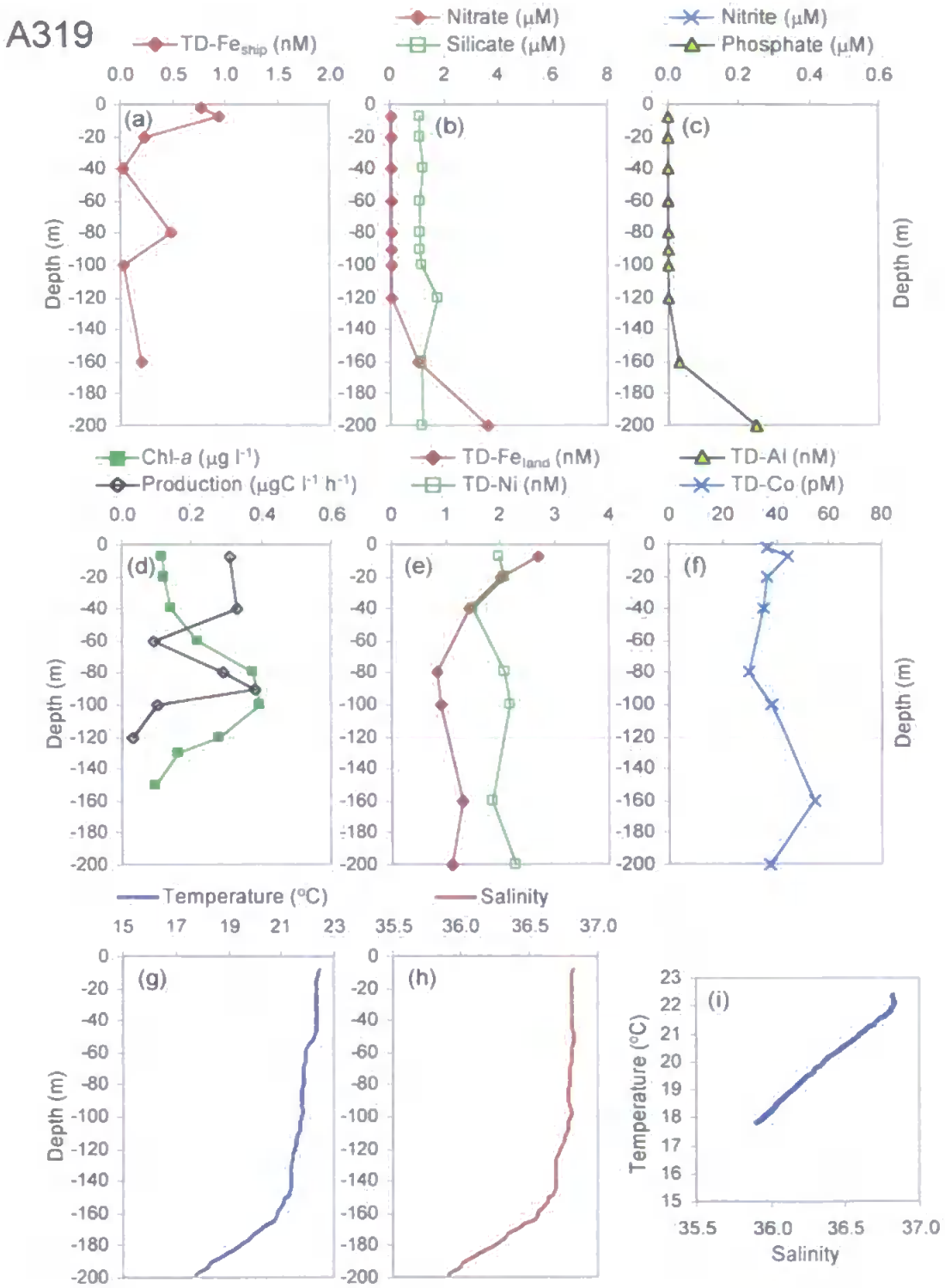

Figure V.33. Station A319, Go-Flo A3-19, SDY 285 (22°55.9'S, 36°57.3'W): Trace metal, nutrient, chlorophyll, production and hydrographic profiles through the upper water column. (a) TD-Fe$_{ship}$, (b) NO_3^- & $Si(OH)_4$, (c) NO_2^- & PO_4^{3-}, (d) chlorophyll *a* & production, (e) TD-Fe$_{land}$ & TD-Ni, (f) TD-Al and TD-Co, (g) temperature, (h) salinity, and (i) T-S plot

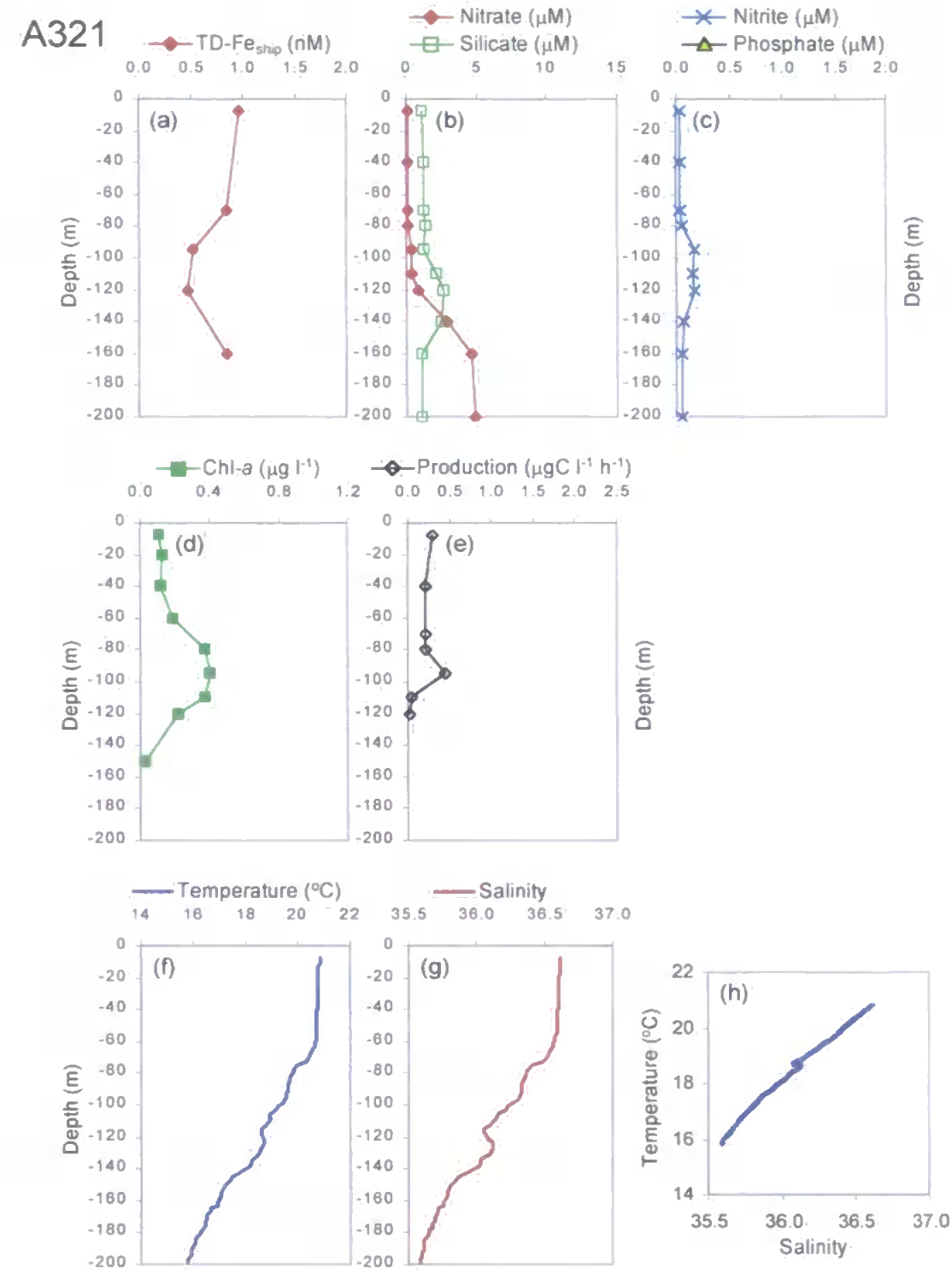

Figure V.34. Station A321, Go-Flo A3-20, SDY 286 (26°36.9'S, 39°36.0'W): Trace metal, nutrient, chlorophyll, production and hydrographic profiles through the upper water column. (a) TD-Fe$_{ship}$, (b) NO_3^- & $Si(OH)_4$, (c) NO_2^- & PO_4^{3-}, (d) chlorophyll *a*, (e) primary production, (f) temperature, (g) salinity, (h) T-S plot

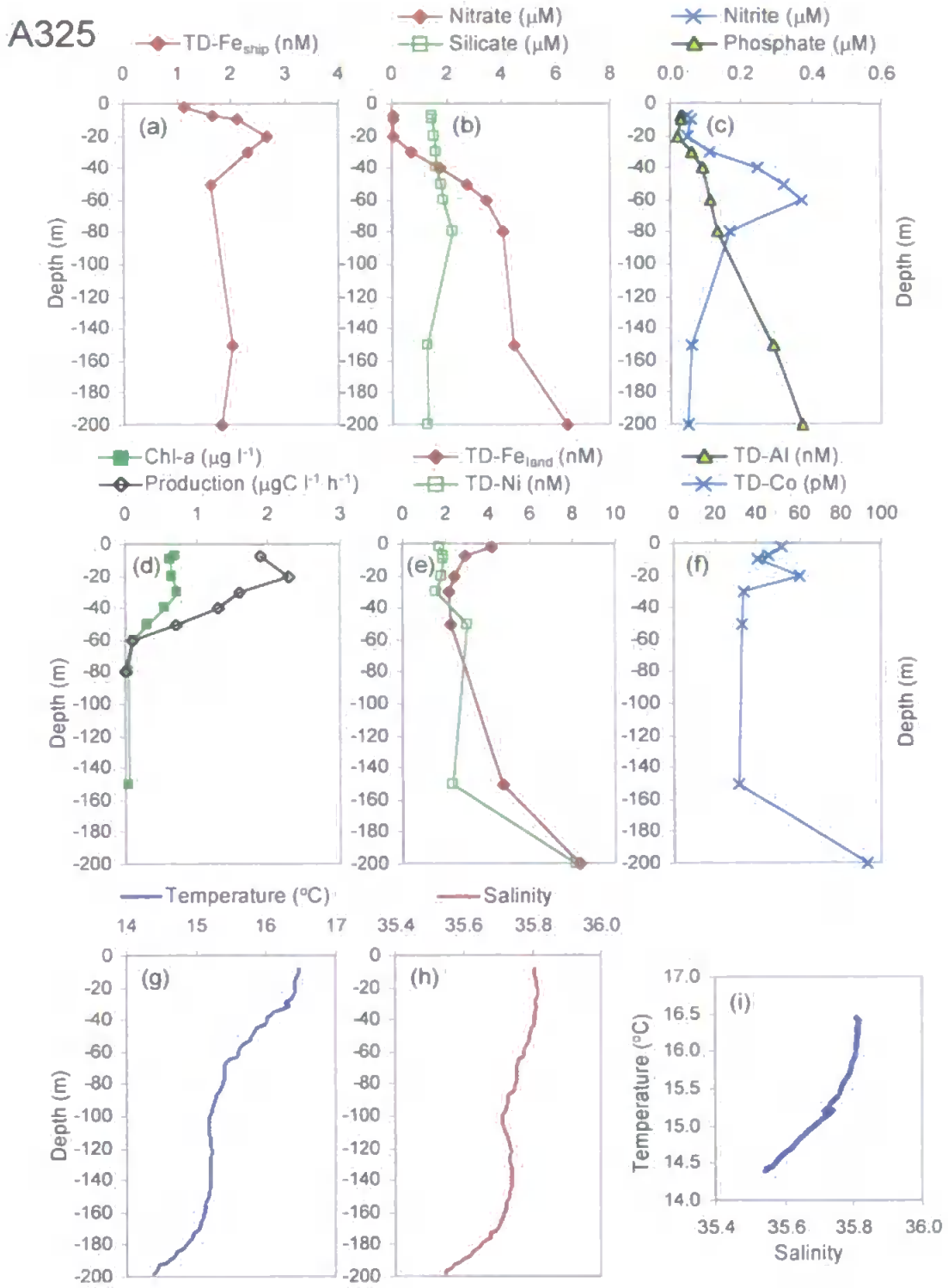

Figure V.35. Station A325, Go-Flo A3-23, SDY 289 (35°42.7'S, 49°34.0'W): Trace metal, nutrient, chlorophyll, production and hydrographic profiles through the upper water column.
(a) TD-Fe$_{ship}$, (b) NO_3^- & $Si(OH)_4$, (c) NO_2^- & PO_4^{3-}, (d) chlorophyll *a* & production, (e) TD-Fe$_{land}$ & TD-Ni, (f) TD-Al and TD-Co, (g) temperature, (h) salinity, and (i) T-S plot

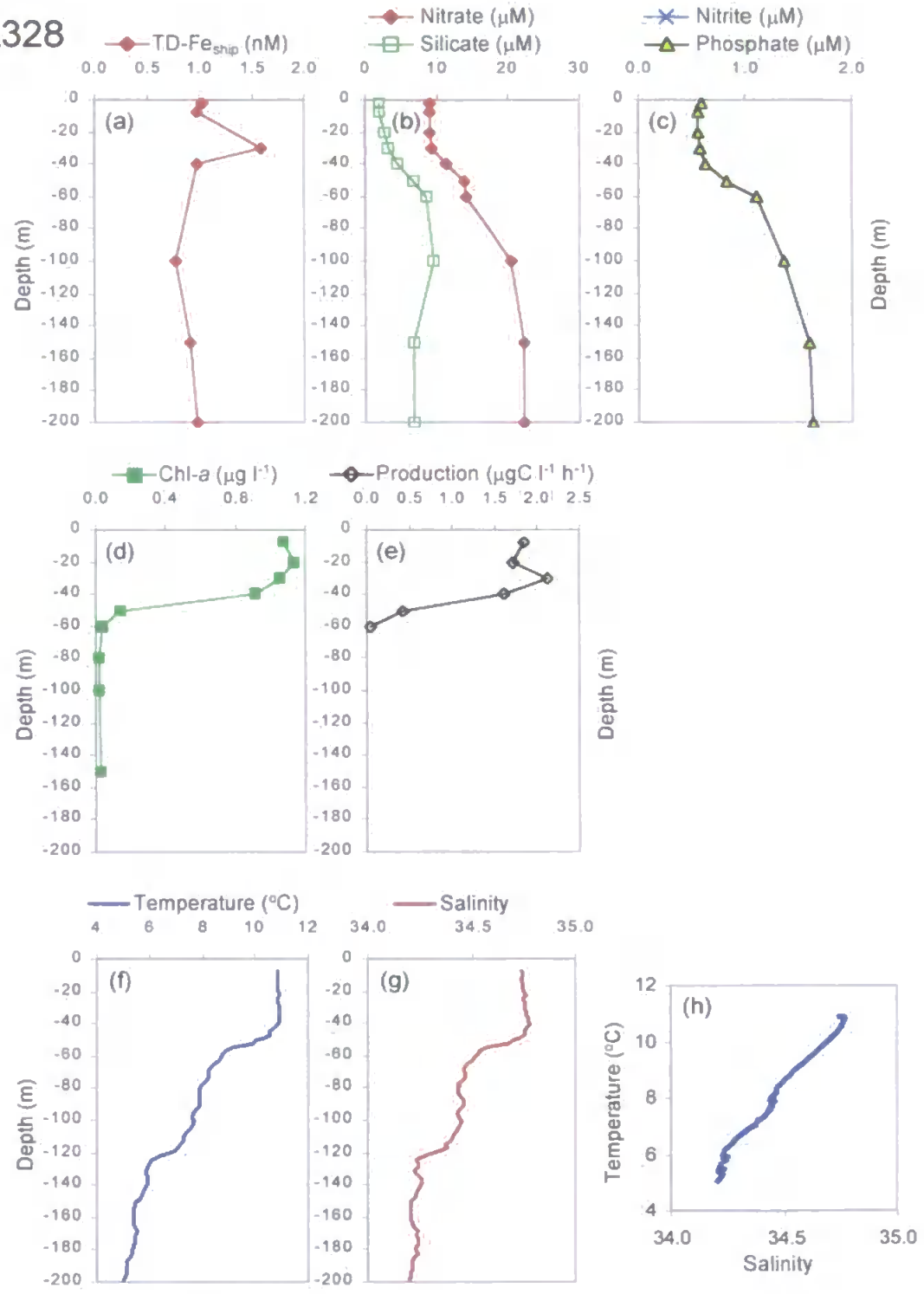

Figure V.36. Station A328, Go-Flo A3-25, SDY 297 (43°34.7'S, 55°01.4'W): Trace metal, nutrient, chlorophyll, production and hydrographic profiles through the upper water column.
(a) TD-Fe$_{ship}$, (b) NO_3^- & $Si(OH)_4$, (c) NO_2^- & PO_4^{3-}, (d) chlorophyll *a*, (e) primary production, (f) temperature, (g) salinity, (h) T-S plot

V.3.5.4 Examination of Individual Stations

STATION A308, PROVINCE NEAOG (Figure V.27)

The surface layers for this station were characterised by high salinities and temperature, typical of an oligotrophic gyre. Surface waters (<80 m) were depleted in nutrients ([NO_3^-]<=0.07 μM, [PO_4^{3-}]<=0.37 μM, [$Si(OH)_4$]<=0.05 μM). There appears to have been a mixing between two water masses, as shown by the T-S plot and indicated by a reduction in salinity (37.1) in the upper 30 m. This may be the result of atmospheric freshwater input and/or the build up of summer stratified layers. Increased TD-Fe_{ship} concentrations at the surface (1.2 nM), possibly due to wet deposition, decreased with depth through the euphotic zone and reached a sharp minimum (0.4 nM) coinciding with the chlorophyll maximum at –90 to –100 m depth. This Fe minimum was probably the result of active uptake of the bioavailable fraction by photosynthesising organisms. The NO_2^- maximum (0.1 μM) at this depth is a common phenomenon for marine phytoplankton growing in the presence of excess NO_3^- and at low light intensities. This production (and release) of extracellular NO_2^- by phytoplankton is thought to be the result of the failure to complete photosynthetic nitrogen assimilation (Riley and Chester, 1971). TD-Fe_{ship} concentrations showed an increase below -100 m depth, which may have been caused by release of Fe upon breakdown of Fe-containing detritus. A comparison between TD-Fe_{land} and TD-Fe_{ship} shows that the Fe incorporated into phytoplankton at the –90 to –100 m depth is released into solution during storage at pH 2.

STATION A309, PROVINCE NWAUp (Figure V.28)

Located off the west coast of Africa, this station received diverse trace metal inputs in the form of episodic atmospheric deposition and seasonal upwelling of enriched sub-surface water. The physical structure of the upper water column was complicated, and appeared to be highly stratified with a mixing of different water types. A sharp salinity discontinuity, also indicated by a smaller fluctuation in the temperature profile, occurred between -61 and -91 m (salinity 36.0 to 36.9), which resulted in a low rate of advective mixing across the thermocline. The chlorophyll *a* maximum (0.9 μg l^{-1}) coincided with a peak in primary production (1.8 μgC l^{-1} h^{-1}) and a minimum (0.2 nM) in TD-Fe_{ship}, the elevated biomass contrasting with the oligotrophic gyre to

the north. Nutrient levels increased immediately below the chlorophyll maximum, consistent with their upwelling source from below.

Elevated concentrations of TD-Fe_{ship}, TD-Fe_{land}, TD-Al and TD-Co were observed throughout the upper 60 m. The very high levels observed were most likely the result of a strong flux of atmospheric dusts (indicated by the good correlation of surface (-7 m) Fe, Al and Co and discussed in detail in V.3.4.3) coupled with stratification which served to retain leachable particulate material in the upper 60 m. Fe, Al and Co profiles showed similar structures, consisting of a maximum at the surface ($[TD\text{-}Fe]_{ship}$=3.6 nM, $[TD\text{-}Fe]_{land}$=7.4 nM, [TD-Al]=79 nM, [TD-Co]=110 pM) decreasing sharply with depth to background concentrations ($[TD\text{-}Fe]_{ship}$=0.9±0.5 nM, $[TD\text{-}Fe]_{land}$=1.9±0.3 nM, [TD-Al]=24±1, [TD-Co]=54±15) observed in the deeper layers. The somewhat erratic profiles for Fe and Co in the upper 100 m were linked to a combination of aerosol fluxes, lateral advection from the boundary of the upwelling, biological scavenging or uptake and a pronounced mixed later effect, where the distributions and discontinuities between –60 and -80 m correspond exactly with the linear sections of the salinity structure. This correlation implies that the mixing lines defined by both σ_t and the Fe and Co concentrations may be used as indicators of a series of shallow mixed layers and their subsequent stratification. Hence, the 100 m data represented the mixing of a water mass end-member of $[TD\text{-}Fe]_{ship}$=0.6 nM, $[TD\text{-}Fe]_{land}$=1.7 nM, [TD-Co]=38 pM and S=36.9 with a previous mixed layer of $[TD\text{-}Fe]_{ship}$=1.2 nM, $[TD\text{-}Fe]_{land}$=2.9 nM, [TD-Co]=101 pM and S=36.0 observed at -60 m. This is demonstrated by the good correlation (r^2=0.88, n=6) shown in Figure V.37, which plots TD-Co versus salinity for the upper water column and is consistent with the Co enrichment observed in the less saline surface waters of the BFCC mixing zone (Section V.3.4.3, Figure V.24). In contrast, the profile for Ni showed no evidence of stratification and little variation on a background concentration (2.8±0.4 nM), with minor depletion at the surface and increased values at depth.

Furthermore, an Fe minimum at –40 m (0.21 nM) corresponded with the chlorophyll maximum (0.91 $\mu g\ l^{-1}$) through the vertical profile. Variations in elemental (e.g. Fe) and plant nutrient

concentrations between the layers through the chlorophyll maximum and mean ambient levels represents biological uptake of the element. This difference is a poorly constrained estimate as the source of Fe is uncertain (atmospheric c.f. upwelling) and bioavailability of TD-Fe fractions need further clarification. However, these concentration variations were calculated for Fe, NO_3^- and PO_4^{3-}, using the following equations:

$$\Delta Fe = [Fe]_{avg} - [Fe]_{chl}$$
$$\Delta NO_3^- = [NO_3^-]_{avg} - [NO_3^-]_{chl}$$
$$\Delta PO_4^{3-} = [PO_4^{3-}]_{avg} - [PO_4^{3-}]_{chl}$$

where $[Fe]_{chl}$, $[NO_3^-]_{chl}$ and $[PO_4^{3-}]_{chl}$ are nutrient concentrations at the chlorophyll maximum (0.21 nM, 0.35 µM and 0.07 µM, respectively). $[Fe]_{avg}$ is the averaged AMT-3 upper water column TD-Fe_{ship} concentration for this station (1.42 nM) (note: source of Fe unknown). $[NO_3^-]_{avg}$ and $[PO_4^{3-}]_{avg}$ are averaged concentrations through the nutricline (assuming aerosol delivered nutrients to be negligible), previously reported for the region during the GEOSECS[1] expeditions (Station 114, 21.18°N, 21.78°W, $[NO_3^-]$=31 µM, $[PO_4^{3-}]$=2.0 µM, depth=-1000 m). Hence, ΔFe=1.21 nM, ΔNO_3^-=30.65 µM, and ΔPO_4^{3-}=1.93 µM. Applying the Redfield ratio (103 C:16 N:1 P; Redfield, 1934; Redfield *et al.*, 1963) to $\Delta Fe/\Delta NO_3^-$ and $\Delta Fe/\Delta PO_4^{3-}$ values, one can estimate the ΔFe/ΔC ratio corresponding to the removal of Fe and C from the water by phytoplankton growth. Thus, $\Delta Fe/\Delta NO_3^-$ and $\Delta Fe/\Delta PO_4^{3-}$ ratios are 41 and 627 µmol mol^{-1} respectively, corresponding with a ΔFe/ΔC of 6.1 µmol mol^{-1}. This ratio is higher than the minimum reported metabolic requirement for oceanic species to maintain adequate growth at Fe-limited rates (e.g. 2 µmol Fe (mol C)$^{-1}$ for a specific growth rate of 0.5 d^{-1}; Sunda *et al.*, 1991), implying that phytoplankton were not stressed by Fe availability in the *NWAUp*. Note the "Redfield" ratio for Fe:C incorporated in Fe-replete phytoplankton is 3 µmol Fe (mol C)$^{-1}$ (de Baar and Boyd, 1999).

In addition, the upper flux limit of Fe into the upper water column from atmospheric sources at this location has been estimated to be 1000 mg m^{-2} yr^{-1} (Duce and Tindale, 1991). One may assume that Fe from above is the dominant source in this region and atmospheric dusts were

[1] Geochemical Ocean Sections Study; http://ingrid.ldgo.columbia.edu/SOURCES/.GEOSECS

distributed in the upper mixed layer (above -60 m depth), as confirmed by the vertical structure of TD-Fe and the temperature minimum which showed a strong stratification in the waters below. Taking the upper limit of solubility of Fe contained in aerosol dust entering the ocean (2.1%; Jickells and Spokes, 1999), this results in a dry deposition of 4.3×10^{-8} mol Fe m^{-2} h^{-1}. Dividing this flux by the Fe/C uptake ratio calculated above (6.1 µmol mol^{-1}), one calculates that the upper 60 m could support primary production rates of 1.4 µgC l^{-1} h^{-1}. This is slightly lower than shipboard carbon fixation measurements in the upper 60 m, which vary between maximum values of 1.8 and 2.1 µgC l^{-1} h^{-1}. Therefore, the results presented here suggest that the Fe dust flux alone may not support the observed primary production rates and if the atmosphere is the only source, Fe may be a limiting nutrient for phytoplankton growth in these waters. There are caveats in such calculations however. Firstly, the ^{14}C primary productivity measurements are an instantaneous measure of photosynthetic activity over 1 day, and not integrated over the season; secondly, one has little knowledge of the bioavailabiltiy of the atmospheric Fe that is solubilised in surface seawater; and thirdly, the atmospheric dust flux in the weeks and months preceeding the sampling observations at this station are unknown.

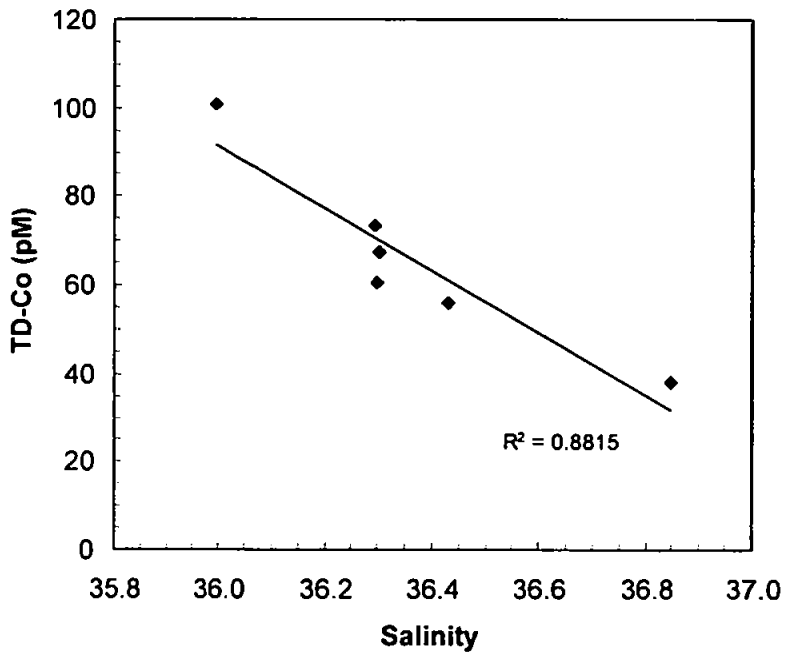

Figure V.37. TD-Co versus salinity for station A3-09, demonstrating the stratified mixed layer effect. Note: data point at –7 m depth (circled, [TD-Co]=110 pM, S=36.3) has been removed from the correlation, as the Co increase in this sample has been attributed to strong atmospheric deposition (see text)

STATIONA311, PROVINCE SUp/NEq (Figure V.29)

Hydrographic data for this station was indicative of a recent rain input to surface waters, typical of the ITCZ located in this region and characterised by the low salinity (35.5) in the upper 20 m. Nutrients were depleted in the upper 50 m, consistent with a chlorophyll maximum occurring at –45 m depth. The excretion of extracellular NO_2^- by phytoplankton or bacteria during de-nitrification resulted in a maximum (0.88 μM) occurring at –50 m, just below the chlorophyll maximum, where light levels became deficient. The TD-Fe_{ship} vertical distribution showed a nutrient-like profile with depletion in the surface layers (0.3 nM at –7 m), gradually increasing with depth (0.6 nM at –200 m).

STATION A313, PROVINCE Eq (Figure V.30)

Located in the Equatorial region, the structure of the water column at this station was complex, as shown by fluctuations in salinity data between –45 and –100 m and a strong stratification indicated by the sharp temperature gradient at –80 m. Once again, the possibility of recent rain event(s) cannot be ruled out, as indicated by the lower salinities in the upper 45 m. The supply of trace metals through wet deposition would explain the enhanced TD-Fe_{ship} concentrations (0-20 m), which decreased with distance away from the surface. A fluctuation in the Fe profile occurred at –70 m, which coincided with a salinity discontinuity and a maximum in primary production (1.2 μgC l^{-1} h^{-1}). A mixed layer effect, as discussed in previously for station A3-09, was once again observed for this profile, although not so apparent, and Co data were not available to substantiate this theory. TD-Fe levels converged to a deep-water (-200 m) mean of 0.4 nM. The chlorophyll maximum (0.9 μg l^{-1}) lay at the top of a sharp thermocline (–78 m) and the slightly increased biomass (compared with surrounding waters), coupled with elevated deep water nutrient levels ($[NO_3^-]_{max}$=12 μM, $[Si(OH)_4]_{max}$=8 μM, $[PO_4^{3-}]_{max}$=1.4 μM) were observed.

STATION A315, PROVINCE SAOG (Figure V.31)

Station A315, in the heart of the Atlantic Ocean's southern gyre, was one of the most remote sampling locations away from continental land masses experienced along AMT-3. A sharp discontinuity in the vertical salinity profile was observed at –100 m, indicating a stratification

between the homogeneous saline, warm waters in the upper layers (e.g. at –90 m, S=36.0, T=26.5°C) and the cooler, less saline waters below the thermocline (e.g. at –200 m, S=35.2, T=12.1°C). A deep chlorophyll maximum (DCM) and deep production maximum were observed at –100 and –90 m respectively, features which did not exist in the corresponding waters of the North Atlantic oligotrophic gyre. A DCM was possible, due to increased irradiance levels penetrating to depth through clear, pristine waters. Trace elemental levels were generally below AMT-3 averages ($[TD\text{-}Fe]_{ship}$=0.7±0.3 nM, $[TD\text{-}Fe]_{land}$=1.2±0.5 nM, [TD-Al]=19.9±7.5 nM, [TD-Co]=39.5±14.2 pM, [TD-Ni]=2.9±1.0 nM, c.f. Table V.14). Vertical distributions showed little structure, except a broad maximum in $TD\text{-}Fe_{ship}$ (1.0 nM) which occurred in the upper mixed layer and converged to 0.4 nM below the thermocline. Interestingly, there was no indication of removal of $TD\text{-}Fe_{ship}$ through the region of the chlorophyll maximum. There was, however, evidence of increased Fe_{land}, Co and Ni at depth, which could be explained by the release of micro-nutrients on the decay of sinking biogenic material. The absence of elevated Al at depth supported such a hypothesis.

STATION A316, PROVINCE SAOG (Figure V.32)

This station was characterised by a weak stratification which existed at -60 m, and very low plant nutrients levels which only became detectable at the base of the upper water column (>120 m). Biomass was low and centred at a DCM of 0.3 $\mu g\ l^{-1}$ at –130 m. $TD\text{-}Fe_{ship}$ was strongly coupled to biological activity, with a constant concentration through the upper 200 m (0.6±0.1 nM, excluding waters in the vicinity of the chlorophyll maximum), and depletion through the chlorophyll maximum (0.1 nM). The strong relationship between TD-Fe depletion and total chlorophyll *a* abundance is illustrated by the negative gradient and excellent correlation coefficient (r^2=0.96, n=5) between the two variables (Figure V.38). Active uptake of bioavailable Fe or scavenging of dissolved species by biogenic particles are two possible explanations for the vertical structure of Fe. Such observations suggest the possible existence of a Fe-limited, light-deficient ecosystem existing in the vicinity of the DCM at the bottom of the euphotic zone in oligotrophic gyres, as postulated by Sunda and Huntsman (1997), de Baar and

Boyd (1999) and Johnson *et al.* (1997). In such stratified waters where light intensities are lower, the Fe requirements for photosynthetic activities are higher (Sunda and Huntsman, 1997).

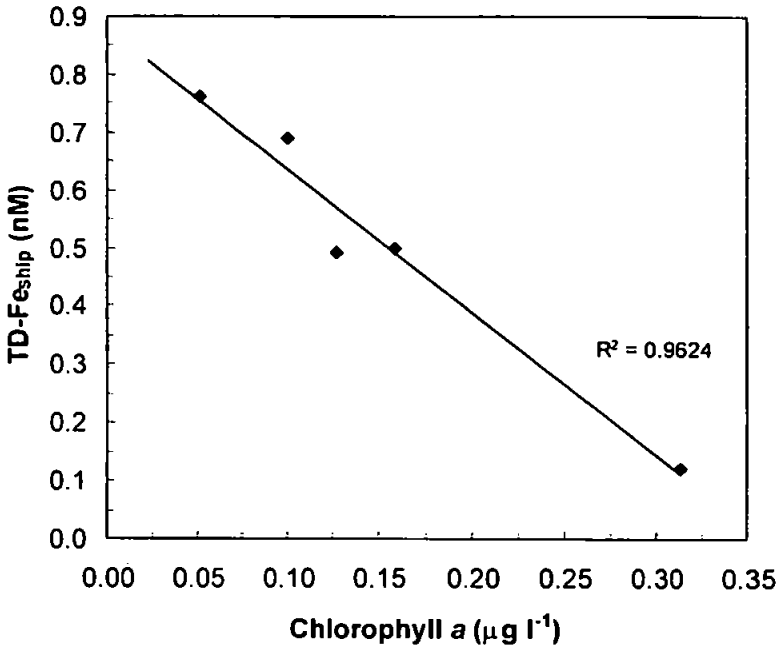

Figure V.38. Relationship between TD-Fe$_{ship}$ and chlorophyll *a* through the upper water column of station A316 located in the South Atlantic oligotrophic gyre

To test this hypothesis, the following calculations were performed. As a result of uptake and regeneration of Fe and classical nutrients, the concentrations of Fe, NO_3^- and PO_4^{3-} with depth are linearly correlated, and the slopes equal the ratios of nutrients found in phytoplankton (Redfield *et al.*, 1963, adapted for trace metals by Sunda and Huntsman, 1995b). Hence, one can estimate the ratio of $\Delta Fe/\Delta N$ and $\Delta Fe/\Delta P$ for incorporation of Fe, N and P into phytoplankton species and by inference, the $\Delta Fe/\Delta C$ ratio. The waters in the vicinity of the chlorophyll minimum contained [TD-Fe]=0.12 nM, [NO_3^-]=1.47 μM and [PO_4^{3-}]=0.27 μM. Mean ambient TD-Fe through the upper water column from AMT-3 measurements was 0.62 nM (this estimate allows for Fe supply from above or below). The maximum concentrations for NO_3^- and PO_4^{3-} through a well-constrained nutricline for a similar location on the GEOSECS expedition (Station 53, 11.98°S, 27.98°W, depth=-900 m) were 34 and 2.3 μM respectively. Based on GEOSECS Redfield ratios (Takahashi *et al.* 1985) of C/N=6.4 and C/P=106, $\Delta Fe/\Delta C$ varies between 2.3 and 2.4 μmol mol^{-1}, values close to the reported minimum ratio for limitation (Sunda *et al.*, 1991). Such observations imply that algae may have

been stressed by Fe availability in the SAOG (possibly in combination with other factors such as light), and production rates will have been below optimum values.

STATION A319, PROVINCE SAOG (Figure V.33)

The water column of this South Atlantic station was homogeneous to –160 m and salinity levels remained high due to low precipitation and increased evaporation. The chlorophyll maximum was broad and weak (0.4 $\mu g\ l^{-1}$) and located between -80 and –100 m. Primary productivity levels were also low (0.4 $\mu gC\ l^{-1}\ h^{-1}$), with a maximum at –90 m. Nutrient levels were typical of the SAOG, low concentrations which increased at the base of the euphotic zone. The vertical distribution for TD-Fe_{ship} appeared complicated. Elevated levels existed in the upper 7 m, possibly the result of a recent input of dry or wet deposition. This was supported by the TD-Fe_{land} structure which showed a smooth profile, with increased surface water concentrations (2.7 nM at –7 m) decreasing with distance away from the surface to a converging limit of 1.1 nM at –200 m. TD-Fe_{ship} concentrations fluctuated between –40 and –100 m with no clear minimum or maximum which could be related to the chlorophyll *a* levels. Such variation may have been an analytical artefact or the result of contamination in the Go-Flo samplers or collection bottles, as there was no hydrographic variation to explain the TD-Fe_{ship} fluctuations. An examination of the TD-$Fe_{land\text{-}ship}$ vertical structure (Figure V.39) provides some interesting information. The differences between the two determinations were high in the upper layers (maximum 1.8 nM at –20 m, indicating an atmospheric source of labile particulate Fe), and decreased smoothly with depth. The minimum in the profile occurred at –80 m, suggesting that labile particulate Fe at this depth was of biogenic origin, consistent with chlorophyll *a* data. Below the chlorophyll maximum the difference between TD-Fe_{land} and TD-Fe_{ship} values was constant (ca. 1.0 nM). TD-Co and TD-Ni profiles showed a homogeneous structure, with mean values of 39±7 pM and 2.0±0.3 nM respectively.

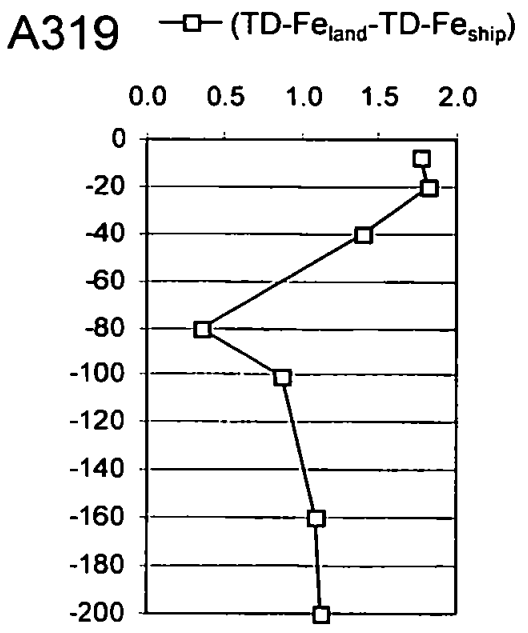

Figure V.39. Vertical distribution of TD-Fe$_{land}$-TD-Fe$_{ship}$ in the upper water column at station A319

STATION A321, PROVINCE SAOG (Figure V.34)

Upper water column profiles for this station were very similar to A3-16. Biomass and productivity were low (<0.41 μg l^{-1}, <0.45 μgC l^{-1} h^{-1}, respectively), and plant nutrients depleted in the upper –100 m where waters were well-mixed. TD-Fe$_{ship}$ structure suggested Fe depletion (0.5 nM) coinciding with a DCM, although the average concentration for layers of the profile away from biological activity (0.9±0.1 nM) was slightly higher than the province mean (c.f. Table V.15). Once again, one may estimate the depletion of Fe and N through the chlorophyll maximum and hence the incorporation of these elements into phytoplankton. The depleted NO_3^- concentration through the chlorophyll maximum (depth -95 m) was 0.43 μM and the maximum value in the nutricline (Station 58, 27.00°S, 37.02°W, depth -1090 m) from GEOSECS was 33 μM. This corresponds to a ΔFe/ΔN ratio of 11.7 μmol mol^{-1}, and hence using the Redfield ratio, a ΔFe/ΔC value of 1.8 μmol mol^{-1}. Since this is below the value known to be the minimum Fe requirement for optimum growth (2 μmol mol^{-1}, Sunda *et al.*, 1991), one can postulate that the algae were Fe-stressed at this station. Such reasoning suggests that the bioavailable fraction must be a quantity less than TD-Fe measurements, since recent findings (Coale *et al.*, 1998) showed that phytoplankton populations were limited by Fe concentrations below 0.5 nM, and community growth rates saturated between 0.5 and 0.75 nM.

STATION A325, PROVINCE BFCC (Figure V.35)

The station on SDY 289 was located in the vicinity of the Brazil and Falkland Currents Confluence, discussed in detail in Section V.3.4.3. The region was characterised by its stimulated production and increased, variable chlorophyll *a* concentrations (as illustrated by SeaWiFS satellite images, see Figure V.4), and increased SPM, nutrient and trace metal concentrations which existed in an intense mixing zone several degrees of latitude wide. The hydrographic data at this station displayed a temperate, non-stratified upper water column, with the high salinities suggesting that the Brazilian current was the primary source. Chlorophyll *a* and productivity maxima were strong (0.7 $\mu g\ l^{-1}$, 2.3 $\mu gC\ l^{-1}\ h^{-1}$, respectively) and located in the upper 30 m, with an strong elevation of classical nutrients existing below 20 m.

TD-Fe_{ship} showed a distinct vertical profile, which was dominated by biological organisms in the surface layers, and converged to 1.8±0.2 nM below the phytoplankton biomass maximum. A TD-Fe maximum (2.7 nM) existed at the same depth as the production maximum (–20 m) in a layer of high chlorophyll *a* concentration. High production values indicated phytoplankton were in a stage of growth and did not suggest the TD-Fe_{max} was the result of regenerated Fe entering the system through decay of biota. However, the feature may be explained by a biosynthesis of organic ligands (e.g. siderophores) which will be excreted in response to Fe requirements. Such exudates will subsequently complex Fe species, elevating labile concentrations at these depths and providing an Fe source that would be generally accessible to the phytoplankton community *via* cell-surface reduction processes and/or photochemical cycling. It is not known which Fe species will be complexed (e.g. dissolved, colloidal, particulate) and such hypotheses need to be substantiated by labile Fe and ligand concentration data obtainable using electro-analytical techniques (e.g. cathodic stripping voltammetry; Gledhill and van den Berg, 1994; Rue and Bruland, 1995; Wu and Luther, 1995; Witter and Luther, 1998). In contrast, land-based total dissolvable trace metal profiles (Fe, Co, Ni) showed a homogeneous structure to -150 m (3.1±1.1 nM, 42±11 pM, 2.1±0.5 nM, respectively) with a sharp increase in concentrations at -200 m (8.3 nM, 93 pM, 8.2 nM, respectively). This may have been the result of a release and recycling of bio-incorporated elements from the breakdown of sinking detrital material. It is

interesting to note the small Co maximum coinciding with the production maximum; this could also be the result of ligand complexation and solubilisation

STATION A328, PROVINCE BFCC (Figure V.36)

This was the first station after a Montevideo port-call and the physical parameters for this station indicated a complicated water column structure with fluctuating salinity and temperature profiles. The water masses will have predominately originated in the Falkland Current, as indicated by cold, less saline characteristics. High biomass ([chl-*a*]=1.1 μg l^{-1}) and carbon fixation rates (2.1 μgC l^{-1} h^{-1}) were observed in the upper 40 m at the top of a weak thermocline, which were typical of the province. Nutrient levels were high and showed smooth profiles without depletion throughout the entire upper water column. The vertical distribution of TD-Fe_{ship} was similar to the other reported station in the same province (station A325). A sharp Fe peak (1.6 nM at –30 m) coincided with the primary productivity maximum, and was superimposed on top of a steady background concentration (1.0±0.1 nM). Once again, it was not clear which biological mechanisms served to retain high TD-Fe at the depth of maximum phytoplankton growth, as neither Fe, plant nutrients or light appear to be depleted.

V.3.5.5 Summary

Table V.15 contains a summary of the trace element concentrations for each of the ten profiles discussed above. In short, stations A308 and A309 were characterised by elevated trace metal values under the influence of an atmospheric dust plume originating in the Saharan desert. Stations A311, A313, A315, A319 and A321 were open-ocean stations showing lower mean concentrations in the upper water column due to the remoteness of their location. Stations A325 and A328 displayed increased trace metal values due to the influence of the South American continent and mixing of Brazilian and Falkland waters in a strong frontal system.

Station	TD-Fe_{ship} (nM)	TD-Fe_{land} (nM)	TD-Al (nM)	TD-Co (pM)	TD-Ni (nM)
A308	1.01±0.42	1.58±0.32	23.3±4.2	37.7±4.7	2.16±0.26
A309	1.42±1.20	3.21±2.20	32.9±25.8	72.2±25.3	2.76±0.37
A311	0.49±0.13	n.o.	n.o.	n.o.	n.o.
A313	0.67±0.49	n.o.	n.o.	n.o.	n.o.
A315	0.66±0.29	1.15±0.49	19.9±7.5	39.5±14.2	2.92±1.02
A316	0.54±0.23	n.o.	n.o.	n.o.	n.o.
A319	0.39±0.36	1.48±0.68	n.o.	39.3±7.2	1.97±0.26
A321	0.73±0.22	n.o.	n.o.	n.o.	n.o.
A325	1.93±0.47	3.87±2.19	n.o.	48.7±20.6	2.82±2.20
A328	1.04±0.26	n.o.	n.o.	n.o.	n.o.

n.o.: no observations

Table V.15. Mean trace metal concentrations for the upper water column (<200 m) of each of ten selected stations

V.3.6 Latitudinal Distribution through the Upper Water Column

Figure V.40 shows a latitudinal contour plot of TD-Fe_{ship} through the upper water column (<200 m) along cruise AMT-3. Daily sampling protocols with high vertical spatial resolution enabled the generation of a contour plot over large latitudinal scales (30°N to 50°S). The figure illustrates many of the biogeochemical processes discussed above. Aerosol Fe enriched surface waters were observed off the west coast of Africa in the vicinity of 20°N, a region which also shows signs of elevated Fe at the base of the upper water column, possibly due to upwelling. TD-Fe concentrations showed good consistency over several degrees of latitude between 15°N and 30°S, averaging 0.4-0.6 nM. A sharp horizontal gradient through the upper water column was observed towards 35°S (in line with temperature and salinity gradients, see previous Figure V.16), possibly due to a concentration of trace metals in the frontal system between the Brazil and Falkland Currents. Lower levels (ca. 1.0 nM) were observed further south, before a continental shelf influence resulted in a sharp increase in TD-Fe (to a maximum of 6.0 nM) near the Falkland Islands. This observation is consistent with a coastal Fe gradient reported by Johnson *et al.* (1997), who estimated that concentrations typical of the open-ocean would be observed at a distance of only 64 km away from the continent, with a natural logarithmic decay of Fe with respect to distance away from the shore.

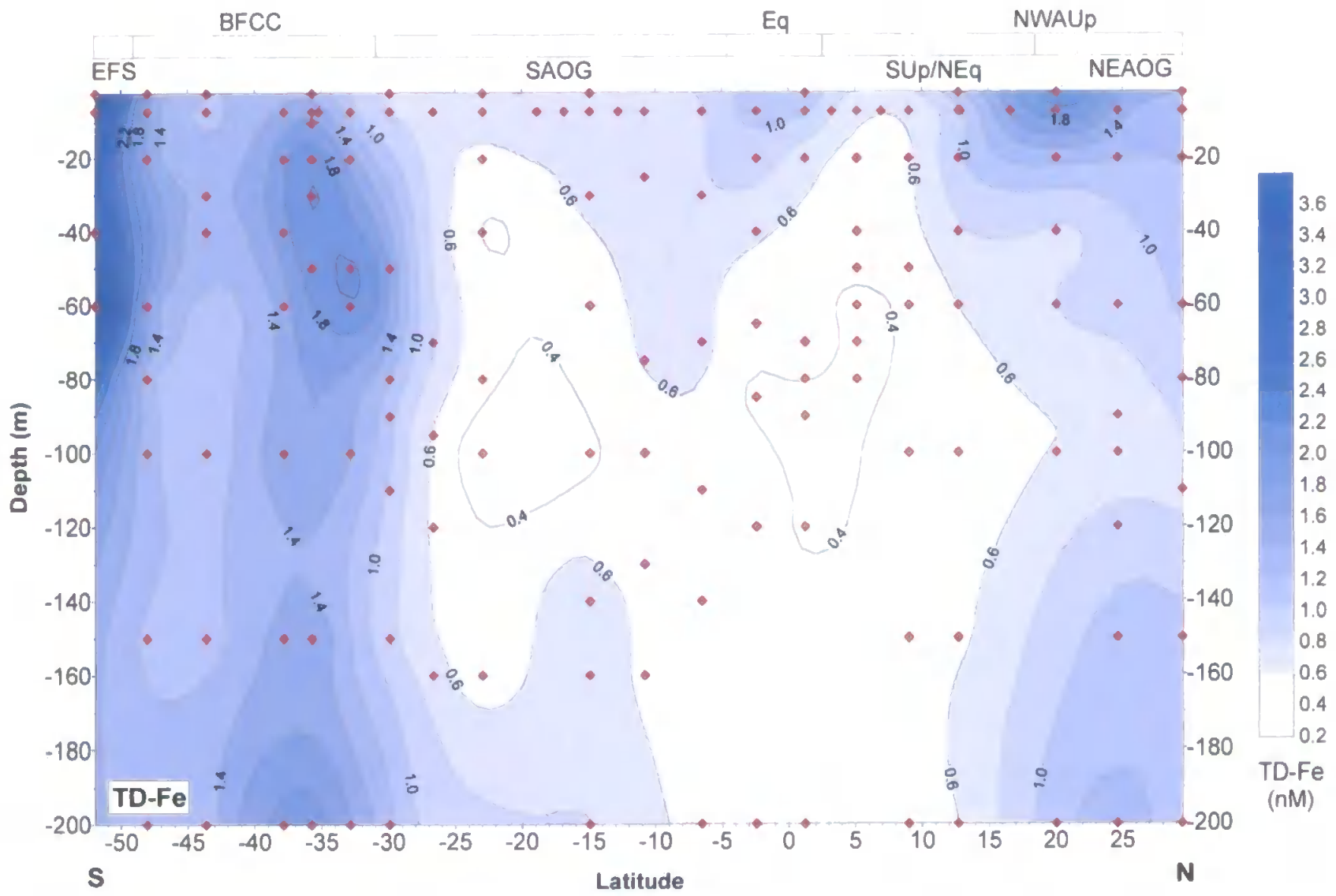

Figure V.40. Latitudinal distribution of TD-Fe_{ship} in the upper water column of the Atlantic Ocean during September / October 1996 (AMT-3)

V.3.7 Deep Water Vertical Distributions in the North-east Atlantic

Figure V.41 shows a deep-water cast (-7 to –1500 m) at station A6-50, performed in the NEAOG (44°40.8'N, 14°00.6'W) during cruise AMT-6, June 12th 1998. This deep-water profile serves to illustrate the vertical structure of Fe, Co and Ni in waters below the mixed layer, away from strong influences due to atmospheric dusts or biological activity. The hydrography of the north-east Atlantic Ocean has previously been described by McCartney (1992) and Tsuchiya *et al.* (1992), and only the major features will be described here, as illustrated on the T-S plot (Figure V.41(g)). A close examination of the hydrographic structure in the upper water column reveals a wind mixed layer (MLW) depth of ca. 40 m, and a fluctuating salinity in the upper 50 m. Between 50 m and 700 m depth, Sub-Polar mode water (SPMW) of western Atlantic origin was present with a salinity maximum at –75 m. The SPMW was underlain by Mediterranean Outflow Water (MOW) which was characterised by a salinity maximum at -1000 m. Below MOW and to the base of profile A6-50, North Atlantic Deep Water (NADW) was present. No nutrient or primary productivity data are currently available for this station. TD-Fe_{ship}, TD-Co and TD-Ni profiles (Figure V.41(a), (b) & (c), respectively) showed distributions which were strongly correlated with chlorophyll *a* concentrations in the euphotic zone above and hydrographic structure in deeper waters. In the upper 50 m, Fe, Co and Ni concentrations fluctuated in a similar manner which was weakly correlated with salinity, and strongly influenced by biological activity through the chlorophyll maximum at —35 m (Figure V.41(d)). In deeper waters (-50 to –1500 m), trace metal distributions showed less variations. TD-Fe_{ship} concentrations averaged 0.78±0.11 nM, with a small increase to 0.94 nM at –1250 m. TD-Co displayed a more varied pattern, with an average of 51±16 pM and a clear maximum of 81 pM at –1000 m, coinciding with a salinity maximum at this depth. This was due to the entrainment of saline MOW, which has its outflow at the Straits of Gibraltar and can easily be traced through the eastern North Atlantic, having its northern extremity at these latitudes (Pickard and Emery, 1990). Below the thermocline, TD-Ni concentrations increased gradually with depth, displaying a typical nutrient-like profile (e.g. 1.7 nM at –50 m, 3.1 nM at -1500 m).

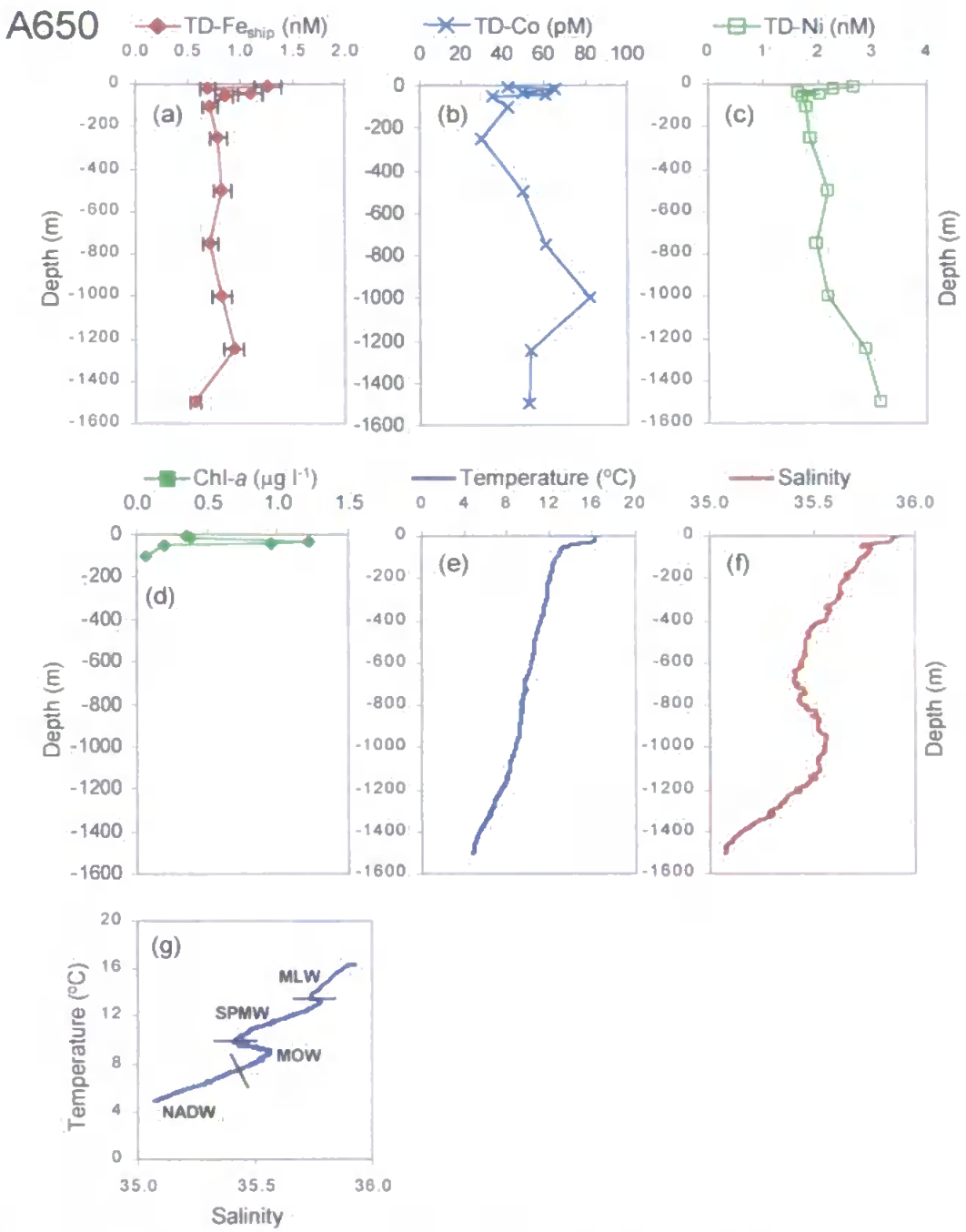

Figure V.41. Station A650, Cruise AMT-6, SDY 163, June 12th 1998, (44°40.8'N, 14°00.6'W): Trace metal (Fe, Co, Ni) and hydrographic profiles for a deep water cast (-7 to –1500 m) in the NEAOG. (a) TD-Fe$_{ship}$, (b) TD-Co, (c) TD-Ni, (d) chlorophyll *a*, (e) temperature, (f) salinity, and (g) T-S plot

The trace metal data presented here corresponds well with literature values. Most previously reported deep water Fe data has been from the North Pacific (e.g. Gordon *et al.*, 1982; Rue and Bruland, 1995, Obata *et al.*, 1993), profiles for which showed similarity to that presented here. In addition, Johnson *et al.* (1997) have discussed at length the theory of a common deep water Fe concentration, which displays no inter-ocean fractionation. The dissolved Fe value of 0.76±0.25 nM (n=117) reported in the MLML dataset as the mean concentration below 500 m

shows excellent consistency with the TD-Fe data (0.78±0.11 nM, n=8) obtained from cast A6-50. Typical precision for Fe data obtained from replicate analyses on sub-aliquots taken from the identical Go-Flo bottles were within 12% (V.3.1.5). Furthermore, such observations imply that there is no statistical difference between dissolved and total dissolvable measurements made in the deep ocean, although a clear discrepancy exists in surface waters, which has been discussed previously in this text (Section V.3.5.4). In addition, a comparison between the smooth profile obtained in the eastern North Atlantic by Flegal (UCSC, unfiltered, reported in Landing *et al.*, 1995) during the IOC comparison exercise and the distribution obtained by Martin *et al.* (1993) during the North Atlantic Bloom Experiment (47°N, 20°W) display excellent similarities with deep water AMT-6 data presented here.

Literature data for Co in deep waters of the eastern North Atlantic is sparse. AMT data does agree with the IOC baseline range (20–40 pM) reported by Landing *et al.* (1995), allowing for the enrichment between –800 and –1200 m by MOW, the Co content of which has been measured to be as high as 75 pM (Morley *et al.*, 1997). This observation of Co enrichment with elevated salinity is the opposite of that observed in the surface waters of the BFCC (Figure V.24) and the stratified mixed layer effect at station A309 (Figure V.37), and is a result of the Mediterranean Co source. Ni data also shows good consistency with Saager *et al.* (1997) who reported concentrations in NADW of 3.5-4.0 nM, and with Martin *et al.* (1993), Yeats *et al.* (1995) and Danielsson *et al.* (1985) who reported 3.7, 3.3 and 3.4 nM, respectively, at ca. –1500 m at similar locations.

In summary, Fe displayed a homogeneous profile and Ni and Co nutrient-like profiles, except through the mixed layer euphotic zone, which contains the majority of phytoplankton species. In waters at these depths, increased and fluctuating trace metal concentrations were observed, dependent on several factors such as hydrography, atmospheric dusts inputs and biological activity. In addition, the lack of a "ferricline" or similar for Co and Ni (a substantial concentration gradient across the thermocline, similar to a classical "nutricline") in TD-measurements implies that vertical mixing had only a minor effect in controlling the Fe, Co and

Ni surface layer values. Any minor concentration difference can be attributed to a small biogenic flux out of the euphotic zone or the recycling of trace elements through biological cycling. Such a ferricline may be more apparent in dissolved Fe measurements.

V.4 CONCLUSIONS

The FI-CL technique was thoroughly validated and extensively deployed in oceanic and coastal environments, showing excellent reliability and good analytical figures of merit for sub-nanomolar determinations of Fe. Data was presented for a North to South latitudinal transect of the Atlantic Ocean. TD-Fe concentrations showed significant spatial differences and ranged between 0.04 (limit of detection) and 6.1 nM. Input sources for Fe were fingerprinted *via* correlation with trace metals (Al, Co, Ni), nutrients (N, P, Si) and hydrography (temperature, salinity). The highest Fe values were found in the *SWApp* and *EFS* provinces, both regions influenced strongly by the continents, whereas the lowest concentrations were observed in Equatorial and South Atlantic waters. Unfortunately, the daily sampling intervals employed along AMT-3 led to poor topographical resolution at the surface, which did not allow for the detailed investigation of small-scale (<500 km), localised events.

As well as ensuring that all possible precautions have been taken to minimise contamination risks and assure analytical accuracy, a trace metal dataset must also show oceanographic consistency (Boyle *et al.*, 1977). This, I believe, was achieved during the 1996 AMT-3 expedition. Subtle changes in trace element concentrations result from biological activity and input mechanisms, and it is important to be able to ascribe such responses to biogeochemical behaviour as opposed to sampling and analytical artefacts. Some vertical profiles for TD-Fe did show signs of scatter (e.g. station A319), albeit very minimal. Although this may at first glance be explained by contamination problems, in reality it was probably due to a larger extent by the fact that unfiltered, acidified samples were measured, and an inhomogeneous distribution of particle-bound Fe has shown up in the results. Unfortunately, no SPM data is available to substantiate this theory.

Several stratified mixed layers have been shown to persist in the sub-tropical waters of the oligotrophic gyres. Such physical phenomena further complicate trace metal distributions. However, it has been demonstrated that Co and Fe can be used as indicators or tracers of water mass stratification, (e.g. stations A309 and A313), where a conservative mixing was noted between two contrasting end-members. If a series of unmixed layers develop in a region of significant aeolian input, the upper water trace element concentrations may record the recent mixing, stratification and deposition history.

The dataset clearly illustrates that Fe was associated to a significant extent with particulate matter in open-ocean waters, but not in a uniform manner through the water column. A fraction of such particles will have been exchanged into solution during the acidification and reduction steps of the analytical method. This was apparent from the significant difference between TD-Fe_{land} and TD-Fe_{ship} measurements performed on unfiltered samples collected in surface layers. TD-Fe_{ship} correlated well with chlorophyll *a*, as measured on-board during AMT-3, indicating the rapid release of exchangeable Fe from biogenic particles. The strong relationship between TD-Fe_{land} and TD-Al in surface waters suggested a slower release, during the extended storage period, of leachable metal into solution from lithogenic particulate material. This particle reactive nature of Fe was further complicated by the variable and sporadic nature of atmospheric inputs of mineral material, together with a dynamic coupling between Fe and biogenic SPM or phytoplankton particles.

It is apparent, therefore, that there is a need for filtering of samples taken from the Atlantic Ocean where aerosol deposition is a significant input mechanism, and especially through the upper mixed layer where the majority of cellular incorporated Fe and particles of lithogenic or biogenic origin are located. Indeed, Saharan dust fluxes have been shown in this study (station A309) to maintain high concentrations of Fe (and other metals) in the surface waters to the west of the African continent. Deeper in the water column, however, more resistant matrix-bound and crystalline particulate forms are present, which will not release metals as readily, resulting in little difference between dissolved and dissolvable analyses. This is confirmed by the

consistency between AMT total dissolvable deep water trace metal levels and literature data for dissolved Fe, Co and Ni (Johnson *et al.*, 1997; Landing *et al.*, 1995; Saager *et al.*, 1997; respectively).

The mean open-ocean concentration of TD-Fe in the upper water column of the Equatorial and South Atlantic was 0.6 nM. Such a value is at least a factor of three greater than the concentrations reported for dissolved Fe in the surface waters (<200 m) of the MLML World Ocean dataset (Johnson *et al.* (1997). However, the striking similarity to the deep water (>500 m) dissolved Fe content reported by Johnson *et al.* (0.76 nM) suggests that the difference between TD-Fe and diss-Fe values, certainly in the surface Atlantic Ocean, is due to the presence of SPM which serves to actively uptake / scavenge dissolved species or contributes a leachable particulate fraction.

The presence of plankton has a substantial effect on the variability of trace metal concentrations, as shown through the chlorophyll maximum on several vertical profiles. Observations of Fe maxima and minima are critically linked to the photosynthetic state of the micro-organisms, together with the taxonomic structure of the water column. In addition, the abundance of Fe in samples collected from within the chlorophyll maximum will only provide a snapshot concentration through very complex photochemical and microbial cycling loops. Such interactions will not be fully understood until a thorough investigation into the size-fractionation and (in)organic complexation of trace elements is achieved alongside a trophic classification and micro-organism photosynthetic state measurements. These observations need to be performed with high temporal (diurnal / seasonal) resolution either *in situ* or in laboratory cultures. Stations characterised by high production to biomass ratios (indicative of a growth stage) tended to show elevated Fe concentrations through the chlorophyll maximum (e.g. A325, A328). Conversely, stations characterised by low production to biomass ratios (indicative of a stage of senescent growth) displayed a minimum in the Fe profile through the chlorophyll maximum (e.g. A316, A321). The location of the chlorophyll maximum in the water column will have a critical effect on the Fe vertical structure. Fe requirements will be greater in a DCM where light intensities are

lower; conversely, photosynthetic activity nearer to the surface will require less Fe (Sunda and Huntsman 1997).

The vertical Fe profiles were never completely depleted at the sea surface, suggesting that this element does not limit primary productivity in the majority of the Atlantic Ocean, an observation substantiated by the diurnal fluorescence patterns observed along AMT-1 by Behrenfeld and Kolber (1999). However, AMT measurements show biomass, new production, and consequentially carbon export in the *SAOG* province to be localised as a recycled ecosystem at a DCM existing at the base of the euphotic zone near the nutricline. Despite the presence of elevated nitrate at such depths, TD-Fe concentrations were at a minimum (due to biological uptake and scavenging), and may have been low enough to limit primary production.

In conclusion, the thorough examination of each vertical profile revealed TD-Fe distributions to exhibit strong relationships with hydrography and biological processes. Furthermore, Equatorial and tropical North Atlantic waters showed evidence of the recent input of atmospheric dusts elevating surface water Fe levels. There is clearly a need for accurate remote sensing of aerosol events (e.g. from the Sahara desert) using satellite technology (SeaWIFS, AVHRR, MEDUSE, TRMM; Longhurst *et al.*, 1995) in order to investigate the direct effect of atmospheric deposition on phytoplankton species growth.

Chapter VI

CONCLUSIONS AND FUTURE WORK

VI.1 General Conclusions

In addition to the detailed summaries at the end of each chapter, the following general conclusions can be drawn from the work presented in this thesis:

The attraction of the flow injection (FI) approach with luminol chemiluminescence (CL) detection for monitoring of iron (Fe) in marine systems is the simplicity, robustness and portability of instrumentation coupled with the excellent detection limits (sub-nanomolar) and rapid response (minutes) that makes it ideally suited to shipboard operation. This methodology generates validated trace metal data at sea with high topographical and temporal resolution, eliminates the need for expensive sampling procedures and minimises the risk of sample contamination and change of sample integrity.

Total dissolvable iron (TD-Fe) concentrations in the surface North and South Atlantic were observed to be high compared with other oceanic regimes (range: <0.1 – 6.1 nM) and showed spatial variability and inter-province fractionation. Elevated TD-Fe concentrations (> 2 nM) existed in Equatorial and tropical North Atlantic regions which experienced high atmospheric loadings from the Saharan desert. Away from strong input mechanisms, TD-Fe concentrations averaged 0.6 nM. Fe inputs mechanisms were fingerprinted through correlation with other trace metals, nutrients and hydrographic data. High suspended particulate material content, nutrients and chlorophyll *a* concentrations were indicative of coastal influences or upwelling waters, whilst elevated TD-Al pointed at a input of continental particles delivered through atmospheric deposition. TD-Fe vertical distributions through the upper mixed layer displayed strong relationships with biological activity (indicated by chlorophyll *a* concentrations and primary production) and evidence of water column stratification (consistent with salinity structure). Measurements in the deep chlorophyll maximum of the South Atlantic oligotrophic gyre showed that Fe concentrations were at a minimum and may have been low enough to limit primary production at such depths were light levels were extremely low.

VI.2 SUGGESTIONS FOR FURTHER WORK

Future work arising from the research reported in this thesis can be divided into two separate areas: (i) the continued development of shipboard analytical monitors for trace elements, and (ii) research focussed on unravelling the complex Fe marine biogeochemical cycle.

VI.2.1 Analytical Developments

VI.2.1.1 Iron Redox Speciation

The luminol CL reaction reported in this thesis is selective towards Fe(II) species. Dissolved or total dissolvable Fe(II+III) measurements are performed after a Fe(III) reduction using sodium sulphite. The redox cycling of Fe in marine systems is critically linked to its solubility and bioavailability and therefore there is an urgent need to develop reliable analytical methods which are selective towards the ferrous form. The next stage in the development of the current FI-CL technique is the validation of a Fe(II) method which employs the same instrumentation and chemical reaction, but without any pre-treatment steps (acidification, reduction) which may alter species composition. The method will need to be rapid, to prevent loss of analyte through oxidation, be based upon a reliable calibration which may be very difficult to perform at ambient seawater pH, and will require a thorough testing of interfering species. After simultaneous determination of Fe(II+III) on an identical samples, the analyst would, through subtraction, be able to generate a Fe(II) and Fe(III) data set which would be invaluable in exploring the dynamic redox speciation of Fe.

VI.2.1.2 Organic Complexation and In-line Ultraviolet Digestion

The incorporation of an in-line U.V. photo-oxidation unit for breakdown of organically bound Fe complexes would enable a series of studies to be performed aimed at resolving the organic complexation of Fe in seawater. In addition, experiments could be designed to investigate the effect of a suite of pre-bound model organic compound on the recovery of Fe using the 8-hydroxyquinoline chelating resin.

VI.2.1.3 In-line Standard Addition(s)

The application of the FI-CL technique reported in this thesis relies on an internal standard addition method for quantification of Fe in the sample. The reason for adopting such a procedure was to eliminate any possible change in calibration sensitivity that may have resulted from a change in sample matrix. This was particularly important in an estuarine environment where the full salinity range was experienced. However, this may have equally posed a problem in the open-ocean where a change in quantity of suspended particulate material (e.g. through the chlorophyll maximum, dust particles at the surface) may have altered the preconcentration extraction efficiency and / or sensitivity of the Fe-catalysed CL reaction. One possible improvement to this method would be to incorporate an extra flow line and mixing loop, which would enable an automated in-line standard addition to be performed, reducing operator time and risk of sample contamination.

VI.2.1.4 Multi-element FI-CL Technique

Advantages of field monitors using FI coupled with CL detection include rapid analysis, high sensitivity, robustness, minimal sampling handling, compatibility to automated data acquisition facilities and low maintenance and running costs. As discussed in Section I.4, the potential of CL-based analytical techniques for trace metals has been documented in numerous papers over the past decade. Such methods lend themselves to marine applications, although relatively few have actually been exploited for practical shipboard use. The next generation of FI-CL monitors will be based upon novel CL chemistries for the determination of a variety of trace metal species (e.g. Mn, Co, Cu, Cr) in seawater. Since the instrumentation is generic, in the future it may be possible to adapt the current FI-CL monitor for the simultaneous, selective determination of two or more analytes based on different reaction chemistries. The success of such a multi-element monitor, however, will depend on an ingenious design of flow configuration to eliminate any interfering effect of one reaction on another.

VI.2.1.5 Upgrade of Instrumentation

Since the onset of this research, there have been a number of commercial developments concerning the instrumentation used in the FI-CL monitor. The current detection system is based upon a high voltage (typically 1000 V) photomultiplier unit, which possesses excellent sensitivity and has proved successful during the field work reported in this thesis, but remains relatively large and somewhat fragile. The next generation of CL detectors are based on a miniature, low voltage (typically 5 V) and more robust design. The incorporation of such a detection system into the current instrumentation will reduce the size of the current monitor and additionally, due to the nature of the output signals from such detectors, aid in the PC acquisition of CL spectra. Such portable analytical monitors may then be controlled using user-friendly graphical programming operating and acquisition systems (e.g. LabVIEW®, National Instruments) run using notebook computers.

VI.2.1.6 Submersible FI-CL Units

A much longer term goal for FI-CL trace metal monitoring would be the development of truly *in situ* (i.e. submersible) units. Such systems have already been designed and successfully deployed at sea for macro-nutrients based on spectrophotometry (David *et al.*, 1998), although it would be a considerable challenge to modify the instrumentation for submersible CL detection. However, such a monitor would posses numerous advantages, eliminating the need for remote sample collection, minimising contamination problems and increasing the temporal and spatial resolution of a real-time data set. Deployments could be buoy or CTD mounted and accommodate several chemistries in tandem with sophisticated automation and communication technologies. One interesting application of such a unit would be the *in situ* deployment at km depths for mapping and tracing of species in hydrothermal vent plumes (e.g. Fe, Mn).

VI.2.2 Marine Iron Biogeochemistry

Reliable analytical methods for trace metals were first reported less than two decades ago and the advent of shipboard techniques occurred only at the start of the 1990s. Therefore, there clearly exists huge areas of marine chemistry and vast regions of the World's oceans and coastal

seas which remain unexplored in terms of trace metal biogeochemistry. Specific areas of interest include:

VI.2.2.1 Iron Limitation in the Southern Ocean

The Southern Ocean is the largest high nutrient, low chlorophyll (HNLC) region of the World's oceans, with cold nitrate-rich waters potentially acting as a sink for atmospheric carbon dioxide (CO_2). The extremely low Fe levels found in surface waters (Martin *et al.*, 1990a) indicate the Southern Ocean to be severely Fe limited. Such theories have been confirmed in bottle incubations (de Baar *et al.*, 1990) and more recently during an international *in situ* enrichment experiment (SOIREE, Boyd *et al.*, 1999a,b), where Fe was found to stimulate plankton blooms and alter plant physiology, resulting in significant drawdown of CO_2 from the atmosphere as well as dramatic releases of dimethyl sulphide (DMS). During glacial periods, it has been suggested that low atmospheric CO_2 was intrinsically linked to natural Fe fertilisation of the Southern Ocean caused by elevated atmospheric dust loading. Moreover, any present-day stimulated increases in phytoplankton productivity would clearly result in changes in global carbon and sulphur cycles. However, the Southern Ocean Fe database is sparse and complicated by the existence of numerous water masses and fronts, and considerable variations in reported ambient concentrations currently exist in the literature. Thus, there is an urgent need to systematically map the distribution and reactivity of Fe in these waters in order to investigate the effect of Fe additions (natural and artificial) on algal size structure, biomass, species composition and ultimately on atmosphere – ocean biogas exchange and carbon export.

VI.2.2.2 Atlantic Meridional Transect Database

The Atlantic Meridional Transect programme provides a unique opportunity to investigate long-term (decades) changes in trace element levels through several contrasting biogeochemical provinces of the Atlantic Ocean. Other detailed AMT measurements such as nutrients, primary productivity and chlorophyll biomass have aided in the interpretation of the Fe data set reported here. In addition, the project voyages pass close to the West African continent and hence present an ideal opportunity to investigate the effect of the Saharan dust plume on trace Fe

concentrations. It is important to continue to deploy shipboard analytical monitors for trace elements on such cruises of opportunity in order to improve the temporal resolution of database, observe seasonal and annual changes and aid in modelling predictions.

VI.2.2.3 Effect of Atmospheric Deposition

The remote open-ocean receives the largest input of trace elements through atmospheric deposition. However, the effect of such inputs on ocean productivity is poorly understood and several laboratory and shipboard studies are required to investigate the solubility, mobility and reactivity of Fe received through dust inputs. Laboratory studies could be conveniently performed using a sequential leaching protocol based on a variety of dusts of anthropogenic and lithogenic origin. Shipboard studies would be more difficult but would aim acquire a suite of chemical, biological and physical measurements in the path of a large dust plume (e.g. off the West African continent).

VI.2.2.4 Iron Distributions in Coastal Regions

Coastal regions are the most productive areas of the ocean, and certain regimes have recently been shown to be Fe (co-)limited (Hutchins *et al.*, 1998). However, there have been relatively few studies on the input (e.g. reducing shelf sediments, riverine inputs) and uptake mechanisms of trace elements along shelf-slope margins and in upwelling systems. Shipboard research could be conveniently performed in these relatively accessible areas and, through a long-term series of short expeditions, would allow for the observation of seasonal changes.

VI.2.2.5 Clean Filtration Methods

A dynamic Fe cycling mechanism between the dissolved and particulate phase exists in areas of the ocean which are heavily influenced by particle fluxes from the atmosphere or sediments. It is imperative in such regions to be able to simultaneously conduct dissolved, total dissolvable and particulate determinations. All these analyses can be performed at the sub-nanomolar level using the FI-CL technique reported in this thesis; however, clean trace metal sampling techniques are necessary to generate a reliable data set. Surface sampling systems are based on a

continuous on-line pumped supply from a towed torpedo fish and vertical profiling is performed using specially designed Go-Flo bottles deployed on Kevlar rope. Such methods remain expensive, but should be utilised in future oceanographic trace metal studies.

In summary, recent research suggests that biological productivity in 40% of the open-ocean is Fe limited and that Fe may act as a co-limitant in significant regions of the remaining 60% of surface waters. It is imperative, therefore, that this element is routinely measured as part of any oceanographic expedition using a shipboard analytical technique such as that detailed in this thesis.

Achterberg E.P. and van den Berg C.M.G., 1994. In-line ultraviolet digestion of natural water samples for trace metal determination using an automated voltammetric system. *Analytica Chimica Acta*, **291**, 213-232.

Achterberg E.P. and van den Berg C.M.G., 1996. Automated monitoring of Ni, Cu and Zn in the Irish sea. *Marine Pollution Bulletin*, **32**, 471-479.

Achterberg E.P. and van den Berg C.M.G., 1997. Chemical speciation of chromium and nickel in the western Mediterranean. *Deep-Sea Research Part II-Topical Studies in Oceanography*, **44**, 693-720.

Aiken J., 1981. A chlorophyll sensor for automatic, remote, operation in the marine environment. *Marine Ecology-Progress Series*, **4**, 235-239.

Albrecht H.O., 1928. Uber die Chemiluminescenz des Aminophthasaurehydrazids. *Zeitschrift fur physikalischen Chemie*, **136**, 321-330.

Alwarthan A.A. and Townshend A., 1987. Chemiluminescence determination of iron(II) and titanium(III) by flow injection analysis based on reactions with and without luminol. *Analytica Chimica Acta*, **196**, 135-140.

Alwarthan A.A., Habib K.A.J. and Townshend A., 1990. Flow injection ion-exchange preconcentration for the determination of iron(II) with chemiluminescence detection. *Fresenius Journal of Analytical Chemistry*, **337**, 848-851.

Alwarthan A.A., Almuaibed A. and Townshend A., 1991. Chemiluminescence determination of titanium(IV) by flow injection analysis using a Jones reductor column on-line. *Analytical Sciences*, **7**, 623-625.

Anderson M.A. and Morel F.M.M., 1982. The influence of aqueous iron chemistry on the uptake of iron by the coastal diatom *Thalassiosira weissflogii*. *Limnology and Oceanography*, **27**, 789-813.

Atkins P.W., 1990. *"Physical Chemistry"*, 4th edition, Oxford University Press: Oxford.

Baes C.F. and Mesmer R.E., 1976. *"The Hydrolysis of Cations"*, Wiley-Interscience: New York.

Banse K., 1990. Does iron really limit phytoplankton production in the offshore sub-Arctic Pacific? *Limnology and Oceanography*, **35**, 772-775.

Barbeau K.A. and Moffett J.W., 1998. Dissolution of iron oxides by phagotrophic protists: using a novel method to quantify reaction rates. *Environmental Science and Technology*, **32**, 2969-2975.

Bause D.E. and Patterson H.H., 1979. Enhancement of luminol chemiluminescence with halide ions. *Analytical Chemistry*, **51**, 2288-2289.

Beere H.G. and Jones P., 1994. Investigation of chromium(III) and chromium(VI) speciation in water by ion chromatography with chemiluminescence detection. *Analytica Chimica Acta*, **293**, 237-243.

Behrenfeld M.J., Bale A.J., Kolber Z.S., Aiken J. and Falkowski P.G., 1996. Confirmation of iron limitation of phytoplankton photosynthesis in the equatorial Pacific Ocean. *Nature*, **383**, 508-511.

Behrenfeld M.J. and Kolber Z.S., 1999. Widespread iron limitation of phytoplankton in the South Pacific Ocean. *Science*, **283**, 840-843.

Berner R.A., 1980. *"Early Diagenesis: a Theoretical Approach"*, Princeton University Press: Princeton, NJ.

Blain S. and Tréguer P., 1995. Iron(II) and iron(III) determination in seawater at the nanomolar level with selective on-line preconcentration and spectrophotometric determination. *Analytica Chimica Acta*, **308**, 425-432.

Blain S., Bucciarelli E. and Tréguer P., 1998. Iron and manganese distributions in the wake of the Kerguelen Islands and comments on the iron hypothesis in the Southern Ocean. Proccedings of SCOR Working Group 109: *"Biogeochemistry of Iron in Seawater"*, Amsterdam, 1-5 November, 1998, p. 52.

Blasco F., Medina-Hernandez M.J. and Sagrado S., 1997. Use of pH gradients in continuous-flow systems and multivariate regression techniques applied to the determination of methionine and cysteine in pharmaceuticals. *Analytica Chimica Acta*, **348**, 151-159.

Bowie A.R., Fielden P.R., Lowe R.D. and Snook R.D., 1995. Sensitive determination of manganese using flow injection and chemiluminescent detection. *Analyst*, **120**, 2119-2127.

Bowie A.R., Sanders M.G. and Worsfold P.J., 1996. Analytical applications of liquid-phase chemiluminescence reactions - a review. *Journal of Bioluminescence and Chemiluminescence*, **11**, 61-90.

Bowie A.R., Achterberg E.P., Mantoura R.F.C. and Worsfold P.J., 1998. Determination of sub-nanomolar levels of iron in seawater using flow injection with chemiluminescence detection. *Analytica Chimica Acta*, **361**, 189-200.

Boyd P.W., Wong C.S., Merrill J., Whitney F., Snow J., Harrison P.J. and Gower J., 1998. Atmospheric iron supply and enhanced vertical carbon flux in the NE subarctic Pacific: Is there a connection? *Global Biogeochemical Cycles*, **12**, 429-441.

Boyd P.W. and Harrison P.J., 1999. Phytoplankton dynamics in the NE subarctic Pacific. *Deep-Sea Research Part II-Topical Studies in Oceanography*, **46**, 2405-2432.

Boyd P.W. and Newton P.P., 1999. Does planktonic community structure determine downward particulate organic carbon flux in different oceanic provinces? *Deep-Sea Research Part I-Oceanographic Research Papers*, **46**, 63-91.

Boyd P.W., Watson A.J. and Law C.S., 1999a. Spotlight is on iron at international SOIREE in Southern Ocean. *US JGOFS news*, February 1999, 10-11.

Boyd P.W., Watson A.J., Law C.S., Abraham E., Trull T., Murdoch R., Bakker D.C.E., Bowie A.R., Charette M., Croot P.L., Downing K., Frew R., Gall M., Hadfield M., Hall J., Marvey M., Jameson G., La Roche J., Liddicoat M.I., Ling R., Maldonado M.T., McKay R.M.L., Nodder S., Pickmere S., Pridmore R., Rintoul S., Safi K., Sutton P., Strzepek R., Tannenberger K., Turner S.M., Waite A. and Zeldis J., 1999b. Diatoms bloom upon mesoscale iron fertilisation in polar Southern Ocean waters. *Nature*, submitted.

Boyle E.A., Sclater F.R. and Edmond J.M., 1977. The distribution of dissolved copper in the Pacific. *Earth and Planetary Science Letters*, **37**, 38-54.

Boyle E.A., Handy B. and van Geen A., 1987. Cobalt determination in natural waters using cation-exchange liquid chromatography with luminol chemiluminescence detection. *Analytical Chemistry*, **59**, 1499-1503.

Broecker W.S. and Peng T.H., 1982. *"Tracers in the Sea"*, Eldigio Press, Columbia University: New York.

Brown C.M. and Trick C.G., 1992. Response of the cyanobacterium, *oscillatoria-tenuis*, to low iron environments - the effect on growth-rate and evidence for siderophore production. *Archives of Microbiology*, **157**, 349-354.

Bruland K.W., Franks R.P., Knauer G.A. and Martin J.H., 1979. Sampling and analytical methods for the determination of copper, cadmium, zinc and nickel at the nanogram per litre level in seawater. *Analytica Chimica Acta*, **105**, 233-245.

Bruland K.W. and Franks R.P., 1983. Mn, Ni, Cu, Zn and Cd in the western North Atlantic. In: Wong C. S., Boyle E. A., Bruland K. W. and Goldberg E. D. (Eds.), *"Trace Metals in Seawater"*, Plenum Press: New York, pp. 395-414.

Bruland K.W., Donat J.R. and Hutchins D.A., 1991. Interactive influences of bioactive trace metals on biological production in oceanic waters. *Limnology and Oceanography*, **36**, 1555-1577.

Bruland K.W., Orians K.J. and Cowen J.P., 1994. Reactive trace metals in the stratified central North Pacific. *Geochimica et Cosmochimica Acta*, **58**, 3171-3182.

Buat-Ménard P. and Chesselet R., 1979. Variable influence of the atmospheric flux on the trace metal chemistry of oceanic suspended matter. *Earth and Planetary Science Letters*, **42**, 399-411.

Burguera J.L. and Townshend A., 1980. Flow injection analysis for monitoring chemiluminescent reactions. *Analytica Chimica Acta*, **114**, 209-214.

Byrne R.H. and Kester D.R., 1976. Solubility of hydrous ferric oxide and iron speciation in seawater. *Marine Chemistry*, **4**, 255-274.

Byrne R.H., Kump L.R. and Cantrell K.J., 1988. The influence of temperature and pH on trace metal speciation in seawater. *Marine Chemistry*, **25**, 163-181.

Campbell A.K., 1988. *"Chemiluminescence"*, Ellis Horwood: Chichester.

Carey J.M., Vela N.P. and Caruso J.A., 1994. Chromium determination by supercritical-fluid chromatography with inductively-coupled plasma-mass spectrometric and flame ionization detection. *Journal of Chromatography A*, **662**, 329-340.

Carmona M., Silva M. and Pérez-Bendito D., 1992. Automatic kinetic determination of oxazepam by the continuous addition of reagent technique. *Talanta*, **39**, 1175-1180.

Cepas J., Silva M. and Pérez-Bendito D., 1993. Automated kinetic spectrofluorometric method for the determination of morphine in urine. *Analyst*, **118**, 923-927.

Cepas J., Silva M. and Pérez-Bendito D., 1994. Improved peroxyoxalate chemiluminescence-based determinations by use of continuous reagent addition to remove background emission. *Analytical Chemistry*, **66**, 4079-4084.

Chalk S.J. and Tyson J.F., 1994. Comparison of the maximum sensitivity of different flow injection manifold configurations - alternating variable search optimization of the iron(II)/1,10-phenanthroline system. *Analytical Chemistry*, **66**, 660-666.

Chang C.A. and Patterson H.H., 1980. Halide ion enhancement of chromium(III), iron(II) and cobalt(II) catalysis of luminol chemiluminescence. *Analytical Chemistry*, **52**, 653-656.

Chang C.A., Patterson H.H., Mayer L.M. and Bause D.E., 1980. Determination of trivalent chromium in seawater by chemiluminescence. *Analytical Chemistry*, **52**, 1264-1267.

Chapin T.P., Johnson K.S. and Coale K.H., 1991. Rapid determination of manganese in seawater by flow injection analysis with chemiluminescence detection. *Analytica Chimica Acta*, **249**, 469-478.

Charlson R.J., Lovelock J.E., Andreae M.O. and Warren S.G., 1987. Oceanic phytoplankton, atmospheric sulfur, cloud albedo and climate. *Nature*, **326**, 655-661.

Chen G.N., Duan J.P. and Hu Q.F., 1994. Flow injection chemiluminescent detection of trace Co(II) with dibromoalizarin violet-H_2O_2-CTMAB system. *Mikrochimica Acta*, **116**, 227-238.

Chester R., 1982. Particulate aluminum fluxes in the eastern Atlantic. *Marine Chemistry*, **11**, 1-16.

Chester R., 1990. *"Marine Geochemistry"*, Unwin Hyman: London.

Chin C.S., Coale K.H., Elrod V.A., Johnson K.S., Massoth G.J. and Baker E.T., 1994. *In situ* observations of dissolved iron and manganese in hydrothermal vent plumes, Juan de Fuca ridge. *Journal of Geophysical Research-Solid Earth*, **99**, 4969-4984.

Chisholm S.W. and Morel F.M.M., 1991. What controls phytoplankton production in nutrient-rich areas of the open sea - ASLO symposium - 22-24 February 1991 San Marcos, California - preface. *Limnology and Oceanography*, **36**, U1507-U1511.

Coale K.H., 1991. Effects of iron, manganese, copper, and zinc enrichments on productivity and biomass in the sub-Arctic Pacific. *Limnology and Oceanography*, **36**, 1851-1864.

Coale K.H., Johnson K.S., Stout P.M. and Sakamoto C.M., 1992. Determination of copper in seawater using a flow injection method with chemiluminescence detection. *Analytica Chimica Acta*, **266**, 345-351.

Coale K.H., Fitzwater S.E., Gordon R.M., Johnson K.S. and Barber R.T., 1996a. Control of community growth and export production by upwelled iron in the equatorial Pacific Ocean. *Nature*, **379**, 621-624.

Coale K.H., Johnson K.S., Fitzwater S.E., Gordon R.M., Tanner S., Chavez F.P., Ferioli L., Sakamoto C.M., Rogers P., Millero F., Steinberg P., Nightingale P., Cooper D., Cochlan W.P., Landry M.R., Constantinou J., Rollwagen G., Trasvina A. and Kudela R., 1996b. A massive phytoplankton bloom induced by an ecosystem-scale iron fertilization experiment in the equatorial Pacific Ocean. *Nature*, **383**, 495-501.

Coale K.H., Fitzwater S.E., Gordon R.M., Tanner S. and Johnson K.S., 1998. Iron limitation of phytoplankton growth affects nutrient drawdown ratios in the Southern Ocean: Results from recent Southern Ocean US JGOFS cruises. Proccedings of SCOR Working Group 109: *"Biogeochemistry of Iron in Seawater"*, Amsterdam, 1-5 November, 1998, p. 23.

Cobo M., Silva M. and Pérez-Bendito D., 1997. Chemiluminescence measurement of tertiary amines using the continuous addition of reagent technique. Determination of trimethylamine in fish samples. *Analytica Chimica Acta*, **356**, 51-59.

Cooper D.J., Watson A.J. and Nightingale P.D., 1996. Large decrease in ocean-surface CO_2 fugacity in response to *in situ* iron fertilization. *Nature*, **383**, 511-513.

Cooper L.H.N., 1935. Iron in the sea and in marine plankton. *Proceedings of the Royal Society of London*, **B 118**, 419-438.

Cooper L.H.N., 1937. Some conditions governing the solubility of iron. *Proceedings of the Royal Society of London*, **B 124**, 299-307.

Cooper L.H.N., 1948a. Some chemical considerations on the distribution of iron in the sea. *Journal of the Marine Biological Association of the United Kingdom*, **27**, 314-321.

Cooper L.H.N., 1948b. The distribution of iron in the waters of the western English Channel. *Journal of the Marine Biological Association of the United Kingdom*, **27**, 279-313.

Danielsson L.-G., Magnusson B. and Westerlund S., 1985. Cadmium, copper, iron, nickel, and zinc in the northeast Atlantic Ocean. *Marine Chemistry*, **17**, 23-41.

David A.R.J., McCormack T., Morris A.W. and Worsfold P.J., 1998. A submersible flow injection-based sensor for the determination of total oxidised nitrogen in coastal waters. *Analytica Chimica Acta*, **361**, 63-72.

de Baar H.J.W., Buma A.G.J., Nolting R.F., Cadee G.C., Jacques G. and Treguer P.J., 1990. On iron limitation of the Southern Ocean - experimental observations in the Weddell and Scotia Seas. *Marine Ecology-Progress Series*, **65**, 105-122.

de Baar H.J.W., de Jong J.T.M., Bakker D.C.E., Löscher B.M., Veth C., Bathmann U. and Smetacek V., 1995. Importance of iron for plankton blooms and carbon dioxide drawdown in the Southern Ocean. *Nature*, **373**, 412-415.

de Baar H.J.W. and Boyd P.W., 1999. The Role of Iron in Plankton Ecology and Carbon Dioxide Transfer of the Global Oceans. In: Ducklow H. W., Field J. G. and Hanson R. B. (Eds.), *"The Dynamic Ocean Carbon Cycle: A midterm synthesis of the Joint Global Ocean Flux Study"*, Cambridge University Press:

de Jong J.T.M., den Das J., Bathmann U., Stoll M.H.C., Kattner G., Nolting R.F. and de Baar H.J.W., 1998. Dissolved iron at sub-nanomolar levels in the Southern Ocean as determined by shipboard analysis. *Analytica Chimica Acta*, **377**, 113-124.

Duce R.A. and Tindale N.W., 1991. Atmospheric transport of iron and its deposition in the ocean. *Limnology and Oceanography*, **36**, 1715-1726.

Duce R.A., Liss P.S., Merrill J.T., Atlas E.L., Buat-Menard P., Hicks B.B., Miller J.M., Prospero J.M., Arimoto R., Church T.M., Ellis W., Galloway J.N., Hansen L., Jickells T.D., Knap A.H., Reinhardt K.H., Schneider B., Soudine A., Tokos J.J., Tsunogai S., Wollast R. and Zhou M., 1991. The atmospheric input of trace species to the world ocean. *Global Biogeochemical Cycles*, **5**, 193-259.

Dugdale R.C. and Wilkerson F.P., 1990. Iron addition experiments in the Antarctic: a re-analysis. *Global Biogeochemical Cycles*, **4**, 13-19.

Earle C.W., Baker M.E., Denton M.B. and Pomeroy R.S., 1993. Imaging applications for chemical analysis utilizing charge-coupled device array detectors. *TRAC - Trends in Analytical Chemistry*, **12**, 395-403.

Elderfield H., 1976. Hydrogeneous Material in Marine Sediments: excluding Manganese Nodules. In: Riley J. P. and Chester R. (Eds.), *"Chemical Oceanography"*, Academic Press: London, pp. 137-215.

Elrod V.A., Johnson K.S. and Coale K.H., 1991. Determination of sub-nanomolar levels of iron(II) and total dissolved iron in seawater by flow injection analysis with chemiluminescence detection. *Analytical Chemistry*, **63**, 893-898.

Emery W.J. and Meincke J., 1986. Global water masses - summary and review. *Oceanologica Acta*, **9**, 383-391.

Emmenegger L., King D.W., Sigg L. and Sulzberger B., 1998. Oxidation kinetics of Fe(II) in a eutrophic Swiss lake. *Environmental Science and Technology*, **32**, 2990-2996.

Escobar R., Lin Q.X., Guiraum A. and Delarosa F.F., 1993. Flow injection chemiluminescence method for the selective determination of chromium(III). *Analyst*, **118**, 643-647.

Escobar R., Lin Q., Guiraum A. and Delarosa F.F., 1995. Determination of trivalent and hexavalent chromium in waste water by flow injection chemiluminescence analysis. *International Journal of Environmental Analytical Chemistry*, **61**, 169-175.

Escobar R., Garcia-Dominguez M.S., Guiraum A. and Delarosa F.F., 1998. Determination of Cr(III) in urine, blood serum and hair using flow injection chemiluminescence analysis. *Fresenius Journal of Analytical Chemistry*, **361**, 509-511.

Feely R.A., Geiselman T.L., Baker E.T., Massoth G.J. and Hammond S.R., 1990. Distribution and composition of hydrothermal plume particles from the ashes vent field at axial volcano, Juan de Fuca ridge. *Journal of Geophysical Research-Solid Earth*, **95**, 12855-12873.

Filik H., Ozturk B.D., Dogutan M., Gumus G. and Apak R., 1997. Separation and preconcentration of iron(II) and iron(III) from natural water on a melamine-formaldehyde resin. *Talanta*, **44**, 877-884.

Frost B.W., 1991. The role of grazing in nutrient-rich areas of the open sea. *Limnology and Oceanography*, **36**, 1616-1630.

Gaikwad A., Silva M. and Pérez-Bendito D., 1994. Sensitive determination of periodate and tartaric acid by stopped-flow chemiluminescence spectrometry. *Analyst*, **119**, 1819-1824.

Gaikwad A., Silva M. and Pérez-Bendito D., 1995. Selective stopped-flow determination of manganese with luminol in the absence of hydrogen peroxide. *Analytica Chimica Acta*, **302**, 275-282.

Gammelgaard B., Jons O. and Nielsen B., 1992. Simultaneous determination of chromium(III) and chromium(VI) in aqueous-solutions by ion chromatography and chemiluminescence detection. *Analyst*, **117**, 637-640.

Geider R.J. and La Roche J., 1994. The role of iron in phytoplankton photosynthesis, and the potential for iron-limitation of primary productivity in the sea. *Photosynthesis Research*, **39**, 275-301.

Geider R.J., 1999. Complex lessons of iron uptake. *Nature*, **400**, 815-816.

Gledhill M. and van den Berg C.M.G., 1994. Determination of complexation of iron(III) with natural organic complexing ligands in seawater using cathodic stripping voltammetry. *Marine Chemistry*, **47**, 41-54.

Gledhill M. and van den Berg C.M.G., 1995. Measurement of the redox speciation of iron in seawater by catalytic cathodic stripping voltammetry. *Marine Chemistry*, **50**, 51-61.

Gonzalez-Robledo D., Silva M. and Pérez-Bendito D., 1989. Performance of the stopped-flow technique in chemiluminescence spectrometry based on direct rate measurements. *Analytica Chimica Acta*, **217**, 239-247.

Gordon R.M., Martin J.H. and Knauer G.A., 1982. Iron in northeast Pacific waters. *Nature*, **299**, 611-612.

Gordon R.M., Coale K.H. and Johnson K.S., 1997. Iron distributions in the equatorial Pacific: implications for new production. *Limnology and Oceanography*, **42**, 419-431.

Gordon R.M., Johnson K.S. and Coale K.H., 1998. The behaviour of iron and other trace elements during the IronEx-I and PlumEx experiments in the equatorial Pacific. *Deep-Sea Research Part II-Topical Studies In Oceanography*, **45**, 995-1041.

Gran H.H., 1931. On the conditions for the production of plankton in the sea. *Rapports et Proces-Verbaux des Reunions Conseil International pour l'Exploration de la Mer*, **75**, 37-46.

Grashoff K., Erhardt M. and Kremling K., 1983. *"Methods in Seawater Analyses"*, Verlag Chemie: Weinheim, Germany.

Greene R.M., Kolber Z.S., Swift D.G., Tindale N.W. and Falkowski P.G., 1994. Physiological limitation of phytoplankton photosynthesis in the eastern equatorial Pacific determined from variability in the quantum yield of fluorescence. *Limnology and Oceanography*, **39**, 1061-1074.

Gross M.G., 1996. *"Oceanography - A View of the Earth"*, 7th edition, Prentice Hall, Inc.: New Jersey.

Gu X.X. and Zhou T.Z., 1996. Determination of iron(II) in water by a spectrophotometric method after preconcentration on an organic solvent-soluble membrane-filter. *Analytical Letters*, **29**, 463-476.

Haber F. and Weiss J., 1934. The catalytic decomposition of hydrogen peroxide by iron salts. *Proceedings of the Royal Society of London*, **Series A**, 332-351.

Hart T.J., 1934. On the phytoplankton of the southwest Atlantic and the Bellingshausen Sea. *Discovery Reports*, **VIII**, 1-268.

Hart T.J., 1942. Phytoplankton periodicity in Antarctic surface waters. *Discovery Reports*, **XXI**, 261-356.

Helmers E. and Rutgers van der Loeff M.M., 1993. Lead and aluminum in Atlantic surface waters (50°N to 50°S), reflecting anthropogenic and natural sources in the eolian transport. *Journal of Geophysical Research-Oceans*, **98**, 20261-20273.

Helmers E. and Schrems O., 1995. Wet deposition of metals to the tropical north and the south Atlantic Ocean. *Atmospheric Environment*, **29**, 2475-2484.

Helmers E., 1996. Trace metals in suspended particulate matter of Atlantic Ocean surface water (40°N to 20°S). *Marine Chemistry*, **53**, 51-67.

Hervas C., Ventura S., Silva M. and Pérez-Bendito D., 1998. Computational neural networks for resolving non-linear multicomponent systems based on chemiluminescence methods. *Journal of Chemical Information and Computer Sciences*, **38**, 1119-1124.

Hirata S., Hashimoto Y., Aihara M. and Mallika G.V., 1996. On-line column preconcentration for the determination of cobalt in sea water by flow injection chemiluminescence detection. *Fresenius Journal of Analytical Chemistry*, **355**, 676-679.

Howard A.G. and Statham P.J., 1993. *"Inorganic Trace Analysis: Philosophy and Practice"*, John Wiley and Sons: Chichester.

Hunter C.N., Gordon R.M., Fitzwater S.E. and Coale K.H., 1996. A rosette system for the collection of trace metal clean seawater. *Limnology and Oceanography*, **41**, 1367-1372.

Hunter K.A. and Leonard M.W., 1988. Colloid stability and aggregation in estuaries .1. aggregation kinetics of riverine dissolved iron after mixing with seawater. *Geochimica et Cosmochimica Acta*, **52**, 1123-1130.

Husar R.B., Prospero J.M. and Stowe L.L., 1997. Characterization of tropospheric aerosols over the oceans with the NOAA advanced very high resolution radiometer optical thickness operational product. *Journal of Geophysical Research-Atmospheres*, **102**, 16889-16909.

Hutchins D.A., Ditullio G.R. and Bruland K.W., 1993. Iron and regenerated production - evidence for biological iron recycling in two marine environments. *Limnology and Oceanography*, **38**, 1242-1255.

Hutchins D.A., 1995. Iron and the marine phytoplankton community. In: Round F. E. and Chapman D. J. (Eds.), *"Progress in Phycological Research"*, Biopress Ltd.: New York, pp. 1-48.

Hutchins D.A. and Bruland K.W., 1995. Fe, Zn, Mn and N transfer between size classes in a coastal phytoplankton community – trace metal and major nutrient recycling compared. *Journal of Marine Research*, **53**, 297-313.

Hutchins D.A. and Bruland K.W., 1998. Iron-limited diatom growth and Si:N uptake ratios in a coastal upwelling regime. *Nature*, **393**, 561-564.

Hutchins D.A., Ditullio G.R., Zhang Y. and Bruland K.W., 1998. An iron limitation mosaic in the California upwelling regime. *Limnology and Oceanography*, **43**, 1037-1054.

Hutchins D.A., Witter A.E., Butler A. and Luther G.W., 1999. Competition among marine phytoplankton for different chelated iron species. *Nature*, **400**, 858-861.

Hydes D.J. and Liss P.S., 1976. Fluorimetric method for the determination of low concentrations of dissolved aluminium in natural waters. *Analyst*, **101**, 922-931.

Hydes D.J., Statham P.J. and Burton J.D., 1986. A vertical profile of dissolved trace-metals (Al, Cd, Cu, Mn, Ni) over the median valley of the mid-Atlantic ridge, 43°N - implications for hydrothermal activity. *Science of the Total Environment*, **49**, 133-145.

Imdadullah, Fujiwara T. and Kumamaru T., 1991. Chemiluminescence from the reaction of chloroauric acid with luminol in reverse micelles. *Analytical Chemistry*, **63**, 2348-2352.

Imdadullah, Fujiwara T. and Kumamaru T., 1993. Solvent-extraction and chemiluminescence determination of gold in silver alloy with luminol in reverse micelles. *Analytical Chemistry*, **65**, 421-424.

Imdadullah, 1994. Development of new hybrid analytical methods based on the combination of solvent-extraction with reversed micellar-mediated chemiluminescence detection and their application to the trace determination of precious metals. *Bunseki Kagaku (Japan Analyst)*, **43**, 363-364.

Imdadullah, Fujiwara T. and Kumamaru T., 1994. Catalytic effect of rhodium(III) on the chemiluminescence of luminol in reverse micelles and its analytical application. *Analytica Chimica Acta*, **292**, 151-157.

Ishii M., Anazawa Y. and Akai T., 1992. Development of flow injection and continuous-flow system using 1,10-phenanthroline chemiluminescent detection for determination of small amounts of rare-earth metal ions. *Nippon Kagaku Kaishi*, 1332-1338.

Jickells T.D., Church T., Veron A. and Arimoto R., 1994. Atmospheric inputs of manganese and aluminum to the Sargasso Sea and their relation to surface water concentrations. *Marine Chemistry*, **46**, 283-292.

Jickells T.D. and Spokes L.J., 1999. Atmospheric Iron Input to the Oceans. In: Turner D. R. and Hunter K. A. (Eds.), *"The Biogeochemistry of Iron in Seawater"*, SCOR-IUPAC: Baltimore, in press.

Jimenez-Prieto R. and Silva M., 1998. Improved simultaneous reaction-rate determination of phosphate and silicate by use of the continuous addition of reagent technique. *Analyst*, **123**, 2389-2394.

Jimenez-Prieto R. and Silva M., 1999. The continuous addition of reagent technique as an effective tool for enhancing kinetic-based multicomponent determinations using computational neural networks. *Analytica Chimica Acta*, **389**, 131-139.

Johnson K.S., Coale K.H., Elrod V.A. and Tindale N.W., 1994. Iron photochemistry in seawater from the equatorial Pacific. *Marine Chemistry*, **46**, 319-334.

Johnson K.S., Gordon R.M. and Coale K.H., 1997. What controls dissolved iron concentrations in the World ocean? *Marine Chemistry*, **57**, 137-161.

Jones P. and Beere H.G., 1995. Ion chromatography determination of trace silver ions using hydrophilic resins with chemiluminescence detection. *Analytical Proceedings*, **32**, 169-171.

Karlberg B. and Pacey G., 1989. *"Flow Injection Analysis - a practical guide"*, Elsevier: Amsterdam.

Kebarle P. and Tang L., 1993. From ions in solution to ions in the gas-phase - the mechanism of electrospray mass-spectrometry. *Analytical Chemistry*, **65**, A972-A986.

Kester D.R., Duedall I.W., Connors D.N. and Pytkowicz R.M., 1967. Preparation of artificial seawater. *Limnology and Oceanography*, **12**, 176-179.

King D.W., Lin J. and Kester D.R., 1991. Spectrophotometric determination of iron(II) in seawater at nanomolar concentrations. *Analytica Chimica Acta*, **247**, 125-132.

King D.W., Lounsbury H.A. and Millero F.J., 1995. Rates and mechanism of Fe(II) oxidation at nanomolar total iron concentrations. *Environmental Science and Technology*, **29**, 818-824.

King D.W., 1998. Role of carbonate speciation on the oxidation rate of Fe(II) in aquatic systems. *Environmental Science and Technology*, **32**, 2997-3003.

Klinkhammer G.P., Heggie D.T. and Graham D.W., 1982. Metal diagenesis in oxic marine sediments. *Earth and Planetary Science Letters*, **61**, 211-219.

Klopf L.L. and Nieman T.A., 1983. Effect of iron(II), cobalt(II), copper(II), and manganese(II) on the chemiluminescence of luminol in the absence of hydrogen peroxide. *Analytical Chemistry*, **55**, 1080-1083.

Knauer G.A., Martin J.H. and Gordon R.M., 1982. Cobalt in northeast Pacific waters. *Nature*, **297**, 49-51.

Kolber Z.S., Barber R.T., Coale K.H., Fitzwater S.E., Greene R.M., Johnson K.S., Lindley S. and Falkowski P.G., 1994. Iron limitation of phytoplankton photosynthesis in the equatorial Pacific Ocean. *Nature*, **371**, 145-149.

Kolotyrkina I.Y., Shpigun L.K., Zolotov Y.A. and Malahoff A., 1995. Application of flow injection spectrophotometry to the determination of dissolved iron in seawater. *Analyst*, **120**, 201-206.

Krekler S., Frenzel W. and Schulze G., 1994. Simultaneous determination of iron(II)/iron(III) by sorbent extraction with flow injection atomic-absorption detection. *Analytica Chimica Acta*, **296**, 115-117.

Kremling K., 1985. The distribution of cadmium, copper, nickel, manganese, and aluminum in surface waters of the open Atlantic and European shelf area. *Deep-Sea Research Part I-Oceanographic Research Papers*, **32**, 531-555.

Kremling K. and Hydes D., 1988. Summer distribution of dissolved Al, Cd, Co, Cu, Mn and Ni in surface waters around the British Isles. *Continental Shelf Research*, **8**, 89-105.

Kremling K. and Pohl C., 1989. Studies on the spatial and seasonal variability of dissolved cadmium, copper and nickel in northeast Atlantic surface waters. *Marine Chemistry*, **27**, 43-60.

Kremling K. and Streu P., 1993. Saharan dust influenced trace element fluxes in deep North Atlantic subtropical waters. *Deep-Sea Research Part I-Oceanographic Research Papers*, **40**, 1155-1168.

Kricka L.J. and Thorpe G.H.G., 1983. Chemiluminescent and bioluminescent methods in Analytical Chemistry - a review. *Analyst*, **108**, 1274-1296.

Kuma K., Nakabayashi S., Suzuki Y., Kudo I. and Matsunaga K., 1992. Photo-reduction of Fe (III) by dissolved organic-substances and existence of Fe(II) in seawater during spring blooms. *Marine Chemistry*, **37**, 15-27.

Kuma K. and Matsunaga K., 1995. Availability of colloidal ferric oxides to coastal marine phytoplankton. *Marine Biology*, **122**, 1-11.

Kuma K., Nishioka J. and Matsunaga K., 1996. Controls on iron(III) hydroxide solubility in seawater - the influence of pH and natural organic chelators. *Limnology and Oceanography*, **41**, 396-407.

Kuma K., Katsumoto A., Nishioka J. and Matsunaga K., 1998. Size-fractionated iron concentrations and Fe(III) hydroxide solubilities in various coastal waters. *Estuarine Coastal and Shelf Science*, **47**, 275-283.

Kumar N., Anderson R.F., Mortlock R.A., Froelich P.N., Kubik P., Dittrichhannen B. and Suter M., 1995. Increased biological productivity and export production in the glacial Southern Ocean. *Nature*, **378**, 675-680.

Kuss J. and Kremling K., 1999. Particulate trace element fluxes in the deep northeast Atlantic Ocean. *Deep-Sea Research Part I-Oceanographic Research Papers*, **46**, 149-169.

Kyaw T., Fujiwara T., Inoue H., Okamoto Y. and Kumamaru T., 1998. Reversed micellar mediated luminol chemiluminescence detection of iron(II, III) combined with on-line solvent extraction using 8-quinolinol. *Analytical Sciences*, **14**, 203-207.

Landing W.M., Haraldsson C. and Paxeus N., 1986. Vinyl polymer agglomerate based transition metal cation chelating ion-exchange resin containing the 8-hydroxyquinoline functional group. *Analytical Chemistry*, **58**, 3031-3035.

Landing W.M. and Bruland K.W., 1987. The contrasting biogeochemistry of iron and manganese in the Pacific Ocean. *Geochimica et Cosmochimica Acta*, **51**, 29-43.

Landing W.M., Cutter G.A., Dalziel J.A., Flegal A.R., Powell R.T., Schmidt D., Shiller A., Statham P.J., Westerlund S. and Resing J., 1995. Analytical intercomparison results from the 1990 Intergovernmental Oceanographic Commission open-ocean baseline survey for trace metals – Atlantic Ocean. *Marine Chemistry*, **49**, 253-265.

Landing W.M. and Powell R.T., 1998. Iron biogeochemistry in the Atlantic Ocean: results from IOC expeditions. Proccedings of SCOR Working Group 109: *"Biogeochemistry of Iron in Seawater"*, Amsterdam, 1-5 November, 1998, p. 29.

La Roche J., Boyd P.W., McKay R.M.L. and Geider R.J., 1996. Flavodoxin as an *in situ* marker for iron stress in phytoplankton. *Nature*, **382**, 802-805.

Lewis S.W., Price D. and Worsfold P.J., 1993. Flow injection assays with chemiluminescence and bioluminescence detection - a review. *Journal of Bioluminescence and Chemiluminescence*, **8**, 183-199.

L'Herroux L., Le Roux S.M. and Appriou P., 1998. Behaviour and speciation of metallic species Cu, Cd, Mn and Fe during estuarine mixing. *Marine Pollution Bulletin*, **36**, 56-64.

Lin J.M. and Hobo T., 1995. Chemiluminescence investigation of NH_2OH-fluorescein-Cu^{2+} system and its application to copper analysis in serum. *Talanta*, **42**, 1619-1623.

Lin Q.X., Guiraum A., Escobar R. and Delarosa F.F., 1993. Flow injection chemiluminescence determination of cobalt(II) and manganese(II). *Analytica Chimica Acta*, **283**, 379-385.

Longhurst A., Sathyendranath S., Platt T. and Caverhill C., 1995. An estimate of global primary production in the ocean from satellite radiometer data. *Journal of Plankton Research*, **17**, 1245-1271.

Löscher B.M., de Baar H.J.W., de Jong J.T.M., Veth C. and Dehairs F., 1997. The distribution of Fe in the Antarctic circumpolar current. *Deep-Sea Research Part II-Topical Studies in Oceanography*, **44**, 143-187.

Lu J.Z. and Zhang Z.J., 1995. A sensor-based on chemiluminescence for the determination of Mn^{2+}. *Chemical Journal of Chinese Universities*, **16**, 1034-1036.

Mackey D.J. and O'Sullivan J.E., 1990. Metal-organic interactions in seawater: An ecosystem experiment. *Analytica Chimica Acta*, **232**, 161-170.

Makita Y., Umebayashi H., Suzuki T., Masuda A., Yamada M. and Hobo T., 1993. New analytical chemiluminescence system using peroxymonosulfate as oxidant. *Chemistry Letters*, 1575-1578.

Makita Y., Suzuki T., Yamada M. and Hobo T., 1994. Flow injection determinations of cobalt(II) and iron(II) based on chemiluminescence induced by the catalytic decomposition of peroxomonosulfate. *Nippon Kagaku Kaishi*, 701-706.

Maldonado M.T. and Price N.M., 1996. Influence of N substrate on Fe requirements of marine centric diatoms. *Marine Ecology-Progress Series*, **141**, 161-172.

Maldonado M.T. and Price N.M., 1999. Utilization of iron bound to strong organic ligands by plankton communities in the subarctic Pacific Ocean. *Deep-Sea Research Part II-Topical Studies in Oceanography*, **46**, 2447-2473.

Marañón E. and Holligan P.M., 1999. Photosynthetic parameters of phytoplankton from 50°N to 50°S in the Atlantic Ocean. *Marine Ecology-Progress Series*, **176**, 191-203.

Maring H.B. and Duce R.A., 1987. The impact of atmospheric aerosols on trace metal chemistry in open ocean surface seawater. 1. Aluminum. *Earth and Planetary Science Letters*, **84**, 381-392.

Marquez M., Silva M. and Pérez-Bendito D., 1988. Direct rate measurements on millisecond reactions by continuous addition of reagent for routine analysis. *Analyst*, **113**, 1733-1736.

Marquez M., Silva M. and Pérez-Bendito D., 1990a. Continuous addition of reagent technique - a new approach to differential reaction-rate methods. *Analytica Chimica Acta*, **239**, 221-227.

Marquez M., Silva M. and Pérez-Bendito D., 1990b. Kinetic determination of vitamin-B_{12} in pharmaceuticals by the continuous addition of reagent technique. *Journal of Pharmaceutical and Biomedical Analysis*, **8**, 563-567.

Marshall M.A. and Mottola H.A., 1983. Synthesis of silica-immobilized 8-quinolinol with (aminophenyl)trimethoxysilane. *Analytical Chemistry*, **55**, 2089-2093.

Martin J.H. and Fitzwater S.E., 1988. Iron-deficiency limits phytoplankton growth in the northeast Pacific sub-Arctic. *Nature*, **331**, 341-343.

Martin J.H. and Gordon R.M., 1988. Northeast Pacific iron distributions in relation to phytoplankton productivity. *Deep-Sea Research Part I-Oceanographic Research Papers*, **35**, 177-196.

Martin J.H., Gordon R.M., Fitzwater S. and Broenkow W.W., 1989. VERTEX - phytoplankton iron studies in the Gulf of Alaska. *Deep-Sea Research Part I-Oceanographic Research Papers*, **36**, 649-680.

Martin J.H., 1990. Glacial-interglacial CO_2 change: The iron hypothesis. *Paleoceanography*, **5**, 1-13.

Martin J.H., Gordon R.M. and Fitzwater S.E., 1990a. Iron in Antarctic waters. *Nature*, **345**, 156-158.

Martin J.H., Fitzwater S.E. and Gordon R.M., 1990b. Iron deficiency limits phytoplankton growth in Antarctic waters. *Global Biogeochemical Cycles*, **4**, 5-12.

Martin J.H., Gordon R.M. and Fitzwater S.E., 1991. The case for iron. *Limnology and Oceanography*, **36**, 1793-1802.

Martin J.H., Fitzwater S.E., Gordon R.M., Hunter C.N. and Tanner S.J., 1993. Iron, primary production and carbon nitrogen flux studies during the JGOFS North Atlantic bloom experiment. *Deep-Sea Research Part II-Topical Studies in Oceanography*, **40**, 115-134.

Martin J.H., Coale K.H., Johnson K.S., Fitzwater S.E., Gordon R.M., Tanner S.J., Hunter C.N., Elrod V.A., Nowicki J.L., Coley T.L., Barber R.T., Lindley S., Watson A.J., Van Scoy K.A., Law C.S., Liddicoat M.I., Ling R., Stanton T., Stockel J., Collins C., Anderson A., Bidigare R., Ondrusek M., Latasa M., Millero F.J., Lee K., Yao W., Zhang J.Z., Friederich G., Sakamoto C.M., Chavez F., Buck K., Kolber Z., Greene R., Falkowski P., Chisholm S.W., Hoge F., Swift R., Yungel J., Turner S., Nightingale P., Hatton A., Liss P. and Tindale N.W., 1994. Testing the iron hypothesis in ecosystems of the equatorial Pacific Ocean. *Nature*, **371**, 123-129.

Martin J.-M. and Whitfield M., 1983. Trace Metals in Seawater. In: Wong C. S., Boyle E. A., Bruland K. W., Burton J. D. and Goldberg E. D. (Eds.), *"Trace Metals in Seawater"*, Plenum Press: New York, pp. 256-298.

Massoth G.J., Baker E.T., Lupton J.E., Feely R.A., Butterfield D.A., Vondamm K.L., Roe K.K. and Lebon G.T., 1994. Temporal and spatial variability of hydrothermal manganese and iron at cleft segment, Juan de Fuca ridge. *Journal of Geophysical Research-Solid Earth*, **99**, 4905-4923.

McCartney M.S., 1992. Recirculating components to the deep boundary current of the northern North Atlantic. *Progress in Oceanography*, **29**, 283-383.

McKnight D.M., Kimball B.A. and Bencala K.E., 1988. Iron photoreduction and oxidation in an acidic mountain stream. *Science*, **240**, 637-640.

Measures C.I. and Edmond J.M., 1990. Aluminum in the South Atlantic - steady-state distribution of a short residence time element. *Journal of Geophysical Research-Oceans*, **95**, 5331-5340.

Measures C.I., 1995. The distribution of Al in the IOC stations of the eastern Atlantic between 30°S and 34°N. *Marine Chemistry*, **49**, 267-281.

Measures C.I., Yuan J. and Resing J.A., 1995. Determination of iron in seawater by flow injection analysis using in-line preconcentration and spectrophotometric detection. *Marine Chemistry*, **50**, 3-12.

Merenyi G., Lind J. and Eriksen T.E., 1990. Luminol chemiluminescence - chemistry, excitation, emitter. *Journal of Bioluminescence and Chemiluminescence*, **5**, 53-56.

Miller J.C. and Miller J.N., 1993. *"Statistics for Analytical Chemistry"*, 3rd edition, Ellis Horwood: Chichester.

Millero F.J., Sotolongo S. and Izaguirre M., 1987. The oxidation-kinetics of Fe(II) in seawater. *Geochimica et Cosmochimica Acta*, **51**, 793-801.

Millero F.J. and Sotolongo S., 1989. The oxidation of Fe(II) With H_2O_2 in seawater. *Geochimica et Cosmochimica Acta*, **53** , 1867-1873.

Millero F.J., 1990. Marine solution chemistry and ionic interactions. *Marine Chemistry*, **30**, 205-229.

Millero F.J., Yao W.S. and Aicher J., 1995a. The speciation of Fe(II) and Fe(III) in natural waters. *Marine Chemistry*, **50**, 21-39.

Millero F.J., Gonzalez-Davila M. and Santana-Casiano J.M., 1995b. Reduction of Fe(III) with sulfite in natural waters. *Journal of Geophysical Research-Atmospheres*, **100**, 7235-7244.

Millero F.J., 1998. Solubility of Fe(III) in seawater. *Earth and Planetary Science Letters*, **154**, 323-329.

Millward G.E., 1995. Processes affecting trace element speciation in estuaries. *Analyst*, **120**, 609-614.

Minas H.J., Minas M. and Packard T.T., 1986. Productivity in upwelling areas deduced from hydrographic and chemical fields. *Limnology and Oceanography*, **31**, 1182-1206.

Morel F.M.M., Hudson R.J.M. and Price N.M., 1991. Limitation of productivity by trace metals in the sea. *Limnology and Oceanography*, **36**, 1742-1755.

Morley N.H., Statham P.J. and Burton J.D., 1993. Dissolved trace metals in the southwestern Indian Ocean. *Deep-Sea Research Part I-Oceanographic Research Papers*, **40**, 1043-1062.

Morley N.H., Burton J.D., Tankere S.P.C. and Martin J.-M., 1997. Distribution and behaviour of some dissolved trace metals in the western Mediterranean Sea. *Deep-Sea Research Part II-Topical Studies in Oceanography*, **44**, 675-691.

Morris A.W., Howland R.J.M. and Bale A.J., 1978. A filtration unit for use with continuous autoanalytical systems applied to highly turbid waters. *Estuarine Coastal and Marine Science*, **6**, 105-109.

Morris A.W., Bale A.J., Howland R.J.M., Millward G.E., Ackroyd D.R., Loring D.H. and Rantala R.T.T., 1986. Sediment mobility and its contribution to trace metal cycling and retention in a macrotidal estuary. *Water Science And Technology*, **18**, 111-119.

Nakano S., Fukuda M., Kageyama S., Itabashi H. and Kawashima T., 1993. Flow injection determination of chromium(III) by pyrogallol chemiluminescence. *Talanta*, **40**, 75-80.

Nakashima K., Yamasaki H., Shimoda R., Kuroda N., Akiyama S. and Baeyens, 1997. Flow-injection analysis of cobalt(II) utilizing enhanced lophine chemiluminescence with hydroxylammonium chloride. *Biomedical Chromatography*, **11**, 63-64.

Nickson R.A., Hill S.J. and Worsfold P.J., 1995. Solid phase techniques for the preconcentration of trace metals from natural waters. *Analytical Proceedings*, **32**, 387-395.

Nishikawa Y., Hiraki K., Morishige K. and Shigematsu T., 1967. Fluoriemtric determination of aluminium and gallium with lumogallion. *Bunseki Kagaku (Japan Analyst)*, **16**, 692-697.

Nolting R.F. and de Jong J.T.M., 1994. Sampling and analytical methods for the determination of trace metals in surface seawater. *International Journal of Environmental Analytical Chemistry*, **57**, 189-196.

Obata H., Karatani H. and Nakayama E., 1993. Automated determination of iron in seawater by chelating resin concentration and chemiluminescence detection. *Analytical Chemistry*, **65**, 1524-1528.

Obata H., Karatani H., Matsui M. and Nakayama E., 1997. Fundamental studies for chemical speciation of iron in seawater with an improved analytical method. *Marine Chemistry*, **56**, 97-106.

Ohshima H., Yamada M. and Suzuki S., 1990. Flavin mononucleotide chemiluminescence in cationic micellar media for determination of chromium(III, IV) by flow injection. *Analytica Chimica Acta*, **232**, 385-388.

Okamura K., Gamo T., Obata H., Nakayama E., Karatani H. and Nozaki Y., 1998. Selective and sensitive determination of trace manganese in sea water by flow through technique using luminol hydrogen peroxide chemiluminescence detection. *Analytica Chimica Acta*, **377**, 125-131.

Okumura M., Seike Y., Fujinaga K. and Hirao K., 1997. *In situ* preconcentration method for iron(II) in environmental water samples using solid phase extraction followed by spectrophotometric determination. *Analytical Sciences*, **13**, 231-235.

Olson D.B., Podesta G.P., Evans R.H. and Brown O.B., 1988. Temporal variations in the separation of Brazil and Malvinas Currents. *Deep-Sea Research Part I-Oceanographic Research Papers*, **35**, 1971-1990.

Orians K.J. and Bruland K.W., 1986. The biogeochemistry of aluminum in the Pacific Ocean. *Earth and Planetary Science Letters*, **78**, 397-410.

O'Sullivan D.W., Hanson A.K., Miller W.L. and Kester D.R., 1991. Measurement of Fe(II) in surface water of the equatorial Pacific. *Limnology and Oceanography*, **36**, 1727-1741.

O'Sullivan D.W., Hanson A.K. and Kester D.R., 1995. Stopped flow luminol chemiluminescence determination of Fe(II) and reducible iron in seawater at sub-nanomolar levels. *Marine Chemistry*, **49**, 65-77.

O'Sullivan D.W., Hanson A.K. and Kester D.R., 1997. The distribution and redox chemistry of iron in the Pettaquamscutt Estuary. *Estuarine Coastal and Shelf Science*, **45**, 769-788.

Pérez-Bendito D., Gomez-Hens A. and Silva M., 1996. Advances in drug analysis by kinetic methods. *Journal of Pharmaceutical and Biomedical Analysis*, **14**, 917-930.

Peterson R.G. and Stramma L., 1991. Upper-level circulation in the South Atlantic ocean. *Progress in Oceanography*, **26**, 1-73.

Peterson W., Wallman K., Li P., Schroder F. and Knauth H.O., 1995. Exchange of trace elements at the sediment water interface during early diagenetic processes. *Marine and Freshwater Research*, **46**, 19-26.

Pickard G.L. and Emery W.J., 1990. *"Descriptive Physical Oceanography: An Introduction"*, 5th edition, Pergamon Press: Oxford.

Powell R.T., King D.W. and Landing W.M., 1995. Iron distributions in surface waters of the South Atlantic. *Marine Chemistry*, **50**, 13-20.

Powell R.T., Landing W.M. and Mann S.E., 1997. Distributions of colloidal Fe in the surface waters of the South and equatorial Atlantic. *Abstracts of Papers of the American Chemical Society*, **213**, 117-GEOC.

Price D., Worsfold P.J. and Mantoura R.F.C., 1994. Determination of hydrogen peroxide in seawater by flow-injection analysis with chemiluminescence detection. *Analytica Chimica Acta*, **298**, 121-128.

Price D., 1995. *"The Determination of Hydrogen Peroxide in Seawater using Flow Injection with Chemiluminescence Detection"*. Ph.D. thesis, University of Plymouth (UK).

Price N.M., Ahner B.A. and Morel F.M.M., 1994. The equatorial Pacific Ocean – grazer controlled phytoplankton populations in an iron-limited ecosystem. *Limnology and Oceanography*, **39**, 520-534.

Prospero J.M., 1999. Long-term measurements of the transport of African mineral dust to the southeastern United States: Implications for regional air quality. *Journal of Geophysical Research-Atmospheres*, **104**, 15917-15928.

Qin W., Zhang Z.J. and Zhang C.J., 1997. Chemiluminescence flow system for vanadium(V) with immobilized reagents. *Analyst*, **122**, 685-688.

Qin W., Zhang Z.J. and Zhang C.J., 1998. Chemiluminescence flow sensor with immobilized reagents for the determination of iron(III). *Mikrochimica Acta*, **129**, 97-101.

Qiu Y., Zhang F., Zhao F. and Song X., 1995. Multichannel chemiluminescence detector based on the charge-coupled device and optical fibre technology. *Instrumentation Science and Technology*, **23**, 49-55.

Quass U. and Klockow D., 1995. Determination of Fe(II) and H_2O_2 in atmospheric liquid water by peroxyoxalate chemiluminescence. *International Journal of Environmental Analytical Chemistry*, **60**, 361-375.

Quétel C.R., Remoudaki E., Davies J.E., Miquel J.C., Fowler S.W., Lambert C.E., Bergametti G. and Buatmenard P., 1993. Impact of atmospheric deposition on particulate iron flux and distribution in northwestern Mediterranean waters. *Deep-Sea Research Part I-Oceanographic Research Papers*, **40**, 989-1002.

Quintero M.C., Silva M. and Pérez-Bendito D., 1991. Kinetic determination of zineb in agricultural samples by continuous addition of reagent. *Talanta*, **38**, 359-363.

Raven J.A., 1988. The iron and molybedum use efficiencies of plant growth with different energy, carbon and nitrogen sources. *New Phytologist*, **109**, 279-287.

Raven J.A., 1990. Predictions of Mn and Fe use efficiencies of phototrophic growth as a function of light availability for growth and of C assimilation pathway. *New Phytologist*, **116**, 1-18.

Redfield A.C., 1934. On the proportions of organic derivatives in seawater and their relation to the composition of phytoplankton. In: Daniel R. J. (Eds.), *"James Johnson Memorial Volume"*, Liverpool University Press: Liverpool, pp. 177-192.

Redfield A.C., Ketchum B.H. and Richards F.A., 1963. The influence of organisms on the composition of seawater. In: Hill M. N. (Eds.), *"The Sea, volume 2"*, Wiley-Interscience: New York, pp. 26-77.

Regnier P. and Wollast R., 1993. Distribution of trace metals in suspended matter in the Scheldt Estuary. *Marine Chemistry*, **43**, 3-19.

Rich H.W. and Morel F.M.M., 1990. Availability of well-defined iron colloids to the marine diatom *Thalassiosira weissflogii*. *Limnology and Oceanography*, **35**, 652-662.

Riley J.P. and Taylor D., 1968. Chelating resins for the concentration of trace elements from seawater and their analytical use in conjunction with atomic absorption spectrometry. *Analytica Chimica Acta*, **40**, 479-485.

Riley J.P. and Chester R., 1971. *"Introduction to Marine Chemistry"*, Academic Press Inc.: London.

Robards K. and Worsfold P.J., 1992. Analytical applications of liquid-phase chemiluminescence. *Analytica Chimica Acta*, **266**, 147-173.

Robins D.B. and Aiken J., 1996. The Atlantic Meridional Transect - an oceanographic research program to investigate physical, chemical, biological and optical variables of the Atlantic Ocean. *Underwater Technology*, **21**, 8-14.

Rubi E., Forteza R. and Cerda V., 1996. Preconcentration and colorimetric determination of Fe(III) by sequential-injection analysis. *Laboratory Robotics and Automation*, **8**, 149-156.

Rue E.L. and Bruland K.W., 1995. Complexation of iron(III) by natural organic ligands in the central North Pacific as determined by a new competitive ligand equilibration adsorptive cathodic stripping voltammetric method. *Marine Chemistry*, **50**, 117-138.

Rue E.L. and Bruland K.W., 1997. The role of organic complexation on ambient iron chemistry in the equatorial Pacific Ocean and the response of a mesoscale iron addition experiment. *Limnology and Oceanography*, **42**, 901-910.

Rueter J.G. and Ades D.R., 1987. The role of iron nutrition in photosynthesis and nitrogen assimilation in *scenedesmus-quadricauda (Chlorophyceae)*. *Journal of Phycology*, **23**, 452-457.

Rueter J.G., Ohki K. and Fujita Y., 1990. The effect of iron nutrition on photosynthesis and nitrogen-fixation in cultures of *trichodesmium (Cyanophyceae)*. *Journal of Phycology*, **26**, 30-35.

Rueter J.G. and Unsworth N.L., 1991. Response of marine synechococcus (*Cyanophyceae*) cultures to iron nutrition. *Journal of Phycology*, **27**, 173-178.

Rutgers van der Loeff M.M., Helmers E. and Kattner G., 1997. Continuous transects of cadmium, copper, and aluminium in surface waters of the Atlantic Ocean, 50°N to 50°S: Correspondence and contrast with nutrient-like behaviour. *Geochimica et Cosmochimica Acta*, **61**, 47-61.

Ruzicka J. and Hansen E.H., 1988. *"Flow Injection Analysis"*, Wiley-Interscience: New York.

Saager P.M., de Baar H.J.W. and Burkill P.H., 1989. Manganese and iron in Indian Ocean waters. *Geochimica et Cosmochimica Acta*, **53**, 2259-2267.

Saager P.M., de Baar H.J.W. and Howland R.J., 1992. Cd, Zn, Ni and Cu in the Indian Ocean. *Deep-Sea Research Part I-Oceanographic Research Papers*, **39**, 9-35.

Saager P.M., de Baar H.J.W., de Jong J.T.M., Nolting R.F. and Schijf J., 1997. Hydrography and local sources of dissolved trace metals Mn, Ni, Cu, and Cd in the northeast Atlantic Ocean. *Marine Chemistry*, **57**, 195-216.

Saitoh K., Hasebe T., Teshima N., Kurihara M. and Kawashima T., 1998. Simultaneous flow injection determination of iron(II) and total iron by micelle enhanced luminol chemiluminescence. *Analytica Chimica Acta*, **376**, 247-254.

Sakamoto-Arnold C.M. and Johnson K.S., 1987. Determination of picomolar levels of cobalt in seawater by flow-injection analysis with chemiluminescence detection. *Analytical Chemistry*, **59**, 1789-1794.

Sarantonis E.G. and Townshend A., 1986. Flow injection determination of iron(II), iron(III) and total iron with chemiluminescence detection. *Analytica Chimica Acta*, **184**, 311-315.

Sarthou G., Jeandel C., Brisset L., Amouroux D., Besson T. and Donard O.F.X., 1997. Fe and H_2O_2 distributions in the upper water column in the Indian sector of the Southern Ocean. *Earth and Planetary Science Letters*, **147**, 83-92.

Sato K. and Tanaka S., 1996. Determination of metal ions by flow injection analysis with peroxyoxalate chemiluminescence detection. *Microchemical Journal*, **53** , 93-98.

Sedwick P.N. and Ditullio G.R., 1997. Regulation of algal blooms in Antarctic shelf waters by the release of iron from melting sea ice. *Geophysical Research Letters*, **24**, 2515-2518.

Sedwick P.N., Edwards P.R., Mackey D.J., Griffiths F.B. and Parslow J.S., 1997. Iron and manganese in surface waters of the Australian sub-Antarctic region. *Deep-Sea Research Part I-Oceanographic Research Papers*, **44**, 1239-1253.

Segawa T., Ishikawa H., Kamidate T. and Watanabe H., 1994. Micelle-enhanced fluorescein chemiluminescence catalyzed by horseradish-peroxidase for the determination of hydrogen peroxide. *Analytical Sciences*, **10**, 589-593.

Segura-Carretero A., Rodriguez-Fernandez J., Bowie A.R. and Worsfold P.J., 1999. Acquisition of chemiluminescence spectral profiles using a continuous flow manifold with two-dimensional charge coupled device detection. *Analytical Communications*, in preparation.

Seitz W.R. and Hercules D.M., 1972. Determination of trace amounts of iron(II) using chemiluminescence analysis. *Analytical Chemistry*, **44**, 2143-2149.

Seitz W.R., Suydam W.W. and Hercules D.M., 1972. Determination of trace amounts of chromium(III) using chemiluminescence analysis. *Analytical Chemistry*, 44, 957-963.

Seitz W.R. and Hercules D.M., 1973. Chemiluminescence analysis for trace elements. In: Cormier M. J., Hercules D. M. and Lee J. (Eds.), *"Chemiluminescence and Bioluminescence"*, Plenum Press: New York, pp. 427-449.

Sholkovitz E.R., 1978. The flocculation of dissolved Fe, Mn, Al, Cu, Ni, Co and Cd during estuarine mixing. *Earth and Planetary Science Letters*, **41**, 77-86.

Sillén L.G., 1964. *"Stability Constants of Metal-Ion Complexes, Special Publications no. 17"*, volume 2, The Chemical Society: London, p.598.

Sohrin Y., Iwamoto S., Akiyama S., Fujita T., Kugii T., Obata H., Nakayama E., Goda S., Fujishima Y., Hasegawa H., Ueda K. and Matsui M., 1998. Determination of trace elements in seawater by fluorinated metal alkoxide glass-immobilized 8-hydroxyquinoline concentration and high- resolution inductively coupled plasma mass spectrometry detection. *Analytica Chimica Acta*, **363**, 11-19.

Soper S.A., Warner I.M. and McGown L.B., 1998. Molecular fluorescence, phosphorescence, and chemiluminescence spectrometry. *Analytical Chemistry*, **70**, R477-R494.

Stanley P.E., 1997. Commercially available luminometers and imaging devices for low-light level measurements and kits and reagents utilizing bioluminescence or chemiluminescence: Survey update 5. *Journal of Bioluminescence and Chemiluminescence*, **12**, 61-78.

Stumm W. and Morgan J.J., 1996. *"Aquatic Chemistry: Chemical Equilibria and Rates in Natural Waters"*, 3rd edition. Wiley-Interscience: New York.

Sunda W.G., 1989. Trace metal interactions with marine phytoplankton. *Biological Oceanography*, **6**, 411-442.

Sunda W.G. and Huntsman S.A., 1991. The use of chemiluminescence and ligand competition with EDTA to measure copper concentration and speciation in seawater. *Marine Chemistry*, **36**, 137-163.

Sunda W.G., Swift D.G. and Huntsman S.A., 1991. Low iron requirement for growth in oceanic phytoplankton. *Nature*, **351**, 55-57.

Sunda W.G. and Huntsman S.A., 1995a. Iron uptake and growth limitation in oceanic and coastal phytoplankton. *Marine Chemistry*, **50**, 189-206.

Sunda W.G. and Huntsman S.A., 1995b. Regulation of copper concentration in the oceanic nutricline by phytoplankton uptake and regeneration cycles. *Limnology and Oceanography*, **40**, 132-137.

Sunda W.G. and Huntsman S.A., 1997. Interrelated influence of iron, light and cell size on marine phytoplankton growth. *Nature*, **390**, 389-392.

Sverdrup H.U., Johnson M.W. and Fleming R.H., 1942. *"The Oceans: their Physics, Chemistry and General Biology"*, Prentice-Hall Inc.: New York.

Symes J.L. and Kester D.R., 1985. The distribution of iron in the northwest Atlantic. *Marine Chemistry*, **17**, 57-74.

Taguchi S., Xia M., Shibata M., Hata N., Kasahara I. and Goto K., 1994. Solvent soluble membrane-filter for a simple and rapid preconcentration and spectrophotometric determination of traces of iron(II) in natural-water. *Bunseki Kagaku (Japan Analyst)*, **43**, 97-103.

Takahashi T., Broecker W.S. and Langer S., 1985. Redfield ratio based on chemical-data from isopycnal surfaces. *Journal of Geophysical Research-Oceans*, **90**, 6907-6924.

Takeda S., Kamatani A. and Kawanobe K., 1995. Effects of nitrogen and iron enrichments on phytoplankton communities in the northwestern Indian Ocean. *Marine Chemistry*, **50**, 229-241.

Tappin A.D., Hydes D.J., Burton J.D. and Statham P.J., 1993. Concentrations, distributions and seasonal variability of dissolved Cd, Co, Cu, Mn, Ni, Pb and Zn in the English Channel. *Continental Shelf Research*, **13**, 941-969.

Taylor S.R., 1964. Abundance of chemical elements in the continental crust: a new table. *Geochimica et Cosmochimica Acta*, **28**, 1273-1285.

Tchernia P., 1980. *"Descriptive Regional Oceanography"*, Pergamon: New York.

Timmermans K.R., Stolte W. and de Baar H.J.W., 1994. Iron-mediated effects on nitrate reductase in marine phytoplankton. *Marine Biology*, **121**, 389-396.

Tortell P.D., Maldonado M.T., Granger J. and Price N.M., 1999. Marine bacteria and biogeochemical cycling of iron in the oceans. *Fems Microbiology Ecology*, **29**, 1-11.

Trick C.G., Andersen R.J., Gillam A. and Harrison P.J., 1983. Prorocentrin - an extracellular siderophore produced by the marine dinoflagellate *prorocentrum-minimum*. *Science*, **219**, 306-308.

Tsuchiya M., Talley L.D. and McCartney M.S., 1992. An eastern Atlantic section from Iceland southward across the equator. *Deep-Sea Research Part I-Oceanographic Research Papers*, **39**, 1885-1917.

Turekian K.K. and Wedepohl K.H., 1961. Distribution of the elements in some major units of the Earth's crust. *Geological Society of America Bulletin*, **72**, 175-192.

Turner S.M., Nightingale P.D., Spokes L.J., Liddicoat M.I. and Liss P.S., 1996. Increased dimethyl sulphide concentrations in seawater from *in situ* iron enrichment. *Nature*, **383**, 513-517.

Valcarcel M. and Luque de Castro M.D., 1987. *"Flow Injection Analysis: principles and applications"*, Ellis Horwood: Chichester.

van Leeuwe M.A., 1997. *"A Barren Ocean: Iron and Light Interactions with Phytoplankton in the Southern Ocean"*. Ph.D. thesis, University of Groningen (The Netherlands).

Vega M. and van den Berg C.M.G., 1997. Determination of cobalt in seawater by catalytic adsorptive cathodic stripping voltammetry. *Analytical Chemistry*, **69**, 874-881.

Velasco A., Silva M. and Pérez-Bendito D., 1992. Processing analytical data obtained from 2nd order reactions by using continuous reagent addition. *Analytical Chemistry*, **64**, 2359-2365.

Ventura S., Silva M., Pérez-Bendito D. and Hervas C., 1997. Computational neural networks in conjunction with principal component analysis for resolving highly non-linear kinetics. *Journal of Chemical Information and Computer Sciences*, **37**, 287-291.

Vinogradov A.P., 1962. Average contents of chemical elements in the principle types of igneous rocks of the Earth's crust. *Geokhimiya*, **7**, 63-69.

von Langen P.J., Johnson K.S., Coale K.H. and Elrod V.A., 1997. Oxidation kinetics of manganese (II) in seawater at nanomolar concentrations. *Geochimica et Cosmochimica Acta*, **61**, 4945-4954.

Waite T.D. and Morel M.M., 1984a. Coulometric study of the redox dynamics of iron in seawater. *Analytical Chemistry*, **56**, 787-792.

Waite T.D. and Morel F.M.M., 1984b. Photoreductive dissolution of colloidal iron oxides in natural waters. *Environmental Science and Technology*, **18**, 860-868.

Waite T.D., Szymczak R., Espey Q.I. and Furnas M.J., 1995. Diel variations in iron speciation in northern Australian shelf waters. *Marine Chemistry*, **50**, 79-91.

Watanabe K.W., Yamasaki T. and Itagaki M., 1996. Chemiluminescence determination of iron(III) with 1,10- phenanthroline. *Bunseki Kagaku (Japan Analyst)*, **45**, 407-413.

Watanabe K.W., Miyamoto H. and Itagaki M., 1999. Determination of zinc(II) using the micellar enhanced chemiluminescence of 1,10-phenanthroline. *Bunseki Kagaku (Japan Analyst)*, **48**, 705-710.

Watson A.J., Law C.S., van Scoy K.A., Millero F.J., Yao W., Friederich G.E., Liddicoat M.I., Wanninkhof R.H., Barber R.T. and Coale K.H., 1994. Minimal effect of iron fertilization on sea-surface carbon dioxide concentrations. *Nature*, **371**, 143-145.

Watson A.J., Jickells T.D. and Maher B.A., 1999. Glaical to interglacial atmospheric carbon dioxide and the role of iron. Conference abstract, Second International Symposium on CO_2, Tsukaba, Japan.

Wayne R.P., 1994. *"Chemical Instrumentation"*, Oxford University Press: Oxford.

Wefer G. and Fischer G., 1993. Seasonal patterns of vertical particle-flux in equatorial and coastal upwelling areas of the eastern Atlantic. *Deep-Sea Research Part I-Oceanographic Research Papers*, **40**, 1613-1645.

Weingartner T.J. and Weisberg R.H., 1991. On the annual cycle of equatorial upwelling in the central Atlantic Ocean. *Journal of Physical Oceanography*, **21**, 68-82.

Wells M.L. and Mayer L.M., 1991a. The photoconversion of colloidal iron oxyhydroxides in seawater. *Deep-Sea Research Part I-Oceanographic Research Papers*, **38**, 1379-1395.

Wells M.L. and Mayer L.M., 1991b. Variations in the chemical lability of iron in estuarine, coastal and shelf waters and its implications for phytoplankton. *Marine Chemistry*, **32**, 195-210.

Wells M.L. and Goldberg E.D., 1992. Marine sub-micron particles. *Marine Chemistry*, **40**, 5-18.

Wells M.L. and Goldberg E.D., 1994. The distribution of colloids in the North Atlantic and Southern Oceans. *Limnology and Oceanography*, **39**, 286-302.

Wells M.L., Price N.M. and Bruland K.W., 1995. Iron chemistry in seawater and its relationship to phytoplankton: A workshop report. *Marine Chemistry*, **48**, 157-182.

Welschmeyer N.A., 1994. Fluorometric analysis of chlorophyll *a* in the presence of chlorophyll *b* and pheopigments. *Limnology and Oceanography*, **39**, 1985-1992.

Westall J.C., Zachary J.L. and Morel F.M.M., 1976. MINEQL: A computer program for the calculation of chemical equilibrium composition of aqueous solutions. MIT Technical Note 18.

Westerlund S. and Öhman P., 1991. Cadmium, copper, cobalt, nickel, lead, and zinc in the water column of the Weddell Sea, Antarctica. *Geochimica et Cosmochimica Acta*, **55**, 2127-2146.

Whitworth D.J., Achterberg E.P., Nimmo M. and Worsfold P.J., 1998. Validation and *in situ* application of an automated dissolved nickel monitor for estuarine studies. *Analytica Chimica Acta*, **371**, 235-246.

Whitworth D.J., 1999. *"Chemical Speciation and Abundance of Trace Metals in Estuarine and Marine Waters"*. Ph.D. thesis, University of Plymouth (UK).

Wilhelm S.W. and Trick C.G., 1994. Iron-limited growth of cyanobacteria - multiple siderophore production is a common response. *Limnology and Oceanography*, **39**, 1979-1984.

Wilhelm S.W., Maxwell D.P. and Trick C.G., 1996. Growth, iron requirements, and siderophore production in iron-limited *Synechococcus PCC 7002*. *Limnology and Oceanography*, **41**, 89-97.

Witter A.E. and Luther G.W., 1998. Variation in Fe-organic complexation with depth in the northwestern Atlantic Ocean as determined using a kinetic approach. *Marine Chemistry*, **62**, 241-258.

Woodward E.M.S., Rees A.P. and Stephens J.A., 1999. The influence of the southwest monsoon upon the nutrient biogeochemistry of the Arabian Sea. *Deep-Sea Research Part II-Topical Studies in Oceanography*, **46**, 571-591.

Worsfold P.J., Achterberg E.P., Bowie A.R. and Sandford R.G., 1999. Flow injection with chemiluminescence detection for the shipboard monitoring of trace metals. In: Varney M. (ed.), *"Chemical Sensors in Oceanography"*, Gordon and Breach: London, in press.

Wu J.F. and Luther G.W., 1994. Size-fractionated iron concentrations in the water column of the western North Atlantic ocean. *Limnology and Oceanography*, **39**, 1119-1129.

Wu J.F. and Luther G.W., 1995. Complexation of Fe(III) by natural organic ligands in the northwest Atlantic Ocean by a competitive ligand equilibration method and a kinetic approach. *Marine Chemistry*, **50**, 159-177.

Wu J.F. and Luther G.W., 1996. Spatial and temporal distribution of iron in the surface water of the northwestern Atlantic Ocean. *Geochimica et Cosmochimica Acta*, **60**, 2729-2741.

Wu J.F. and Boyle E.A., 1998. Determination of iron in seawater by high-resolution isotope dilution inductively coupled plasma mass spectrometry after $Mg(OH)_2$ co-precipitation. *Analytica Chimica Acta*, **367**, 183-191.

Yamada M. and Suzuki S., 1984. Micellar enhanced chemiluminescence of 1,10-phenanthroline for the determination of ultratraces of copper(II) by flow injection method. *Analytical Letters Part A-Chemical Analysis*, **17**, 251-263.

Yamada M., Kanai H. and Suzuki S., 1985a. Flavin mononucleotide chemiluminescence for determination of traces of copper(II) by continuous-flow and flow injection methods. *Bulletin of the Chemical Society of Japan*, **58**, 1137-1142.

Yamada M., Kamiyama S. and Suzuki S., 1985b. Eosin Y-sensitized chemiluminescence of 7,7,8,8-tetracyanoquinodimethane in surfactant vesicles for determination of manganese(II) at sub-nanogram levels by a flow injection method. *Chemistry Letters*, 1597-1600.

Yamada M., Sudo A. and Suzuki S., 1985c. Chemiluminescence method for selective determination of iron(II) and chromium(III) with single reaction system. *Chemistry Letters*, 801-804.

Yan G.F., Shi G.R. and Liu Y.M., 1992. Fluorometric determination of iron with 5-(4-methylphenylazo)-8-aminoquinoline in the presence of surfactants. *Analytica Chimica Acta*, **264** , 121-124.

Yeats P.A., Westerlund S. and Flegal A.R., 1995. Cadmium, copper and nickel distributions at 4 stations in the eastern central and South Atlantic. *Marine Chemistry*, **49**, 283-293.

Zamzow H., Coale K.H., Johnson K.S. and Sakamoto C.M., 1998. Determination of copper complexation in seawater using flow injection analysis with chemiluminescence detection. *Analytica Chimica Acta*, **377**, 133-144.

Zhang L.P. and Terada K., 1994. Spectrophotometric determination of iron(II) in seawater after preconcentration by sorption of its 3-(2-pyridyl)-5,6-bis(4-phenylsulphonic acid)-1,2,4-triazine complex with poly(chlorotrifluoroethylene) resin. *Analytica Chimica Acta*, **293**, 311-318.

Zhou Y.X. and Zhu G.Y., 1997. Rapid automated *in situ* monitoring of total dissolved iron and total dissolved manganese in underground water by reverse-flow injection with chemiluminescence detection during the process of water treatment. *Talanta*, **44**, 2041-2049.

Zhu X.R., Prospero J.M., Millero F.J., Savoie D.L. and Brass G.W., 1992. The solubility of ferric ion in marine mineral aerosol solutions at ambient relative humidities. *Marine Chemistry*, **38**, 91-107.

Zhu X.R., Prospero J.M., Savoie D.L., Millero F.J., Zika R.G. and Saltzman E.S., 1993. Photoreduction of iron(III) in marine mineral aerosol solutions. *Journal of Geophysical Research-Atmospheres*, **98**, 9039-9046.

Zhuang G.S., Duce R.A. and Kester D.R., 1990. The dissolution of atmospheric iron in surface seawater of the open ocean. *Journal of Geophysical Research-Oceans.*, **95**, 16207-16216.

Zhuang G.S., Yi Z., Duce R.A. and Brown P.R., 1992. Link between iron and sulfur cycles suggested by detection of Fe(II) in remote marine aerosols. *Nature*, **355**, 537-539.

Zhuang G.S., Yi Z. and Wallace G.T., 1995. Iron(II) in rainwater, snow, and surface seawater from a coastal environment. *Marine Chemistry*, **50**, 41-50.

Zuehlke R.W. and Kester D.R., 1985. Development of shipboard copper analyses by atomic-absorption spectroscopy. In: Alberto Z. (ed.), *"Mapping Strategies in Chemical Oceanography"*, American Chemical Society: Washington D.C., pp.117-137.

FI-CL SYSTEM QUICKBASIC® SOFTWARE PROGRAMMING CODE

Filename: "Analy1.bas" - Full cycle to analyse seawater sample

```
'*********************************************************
'*    Define variables, syntax, parameters, sub-routines    *
'*********************************************************

DEFINT A-Z                      'All variables now of type INTEGER
DECLARE SUB Pause ()            'Wait For Any Key Press
DECLARE SUB Comline (HexAddr, irqline, DmaLine, Count, Freq, Across, Down, Chans())     'Any
Command Line Parameter is AD1200 Hex I/O Address
DECLARE SUB SetGraph (Gmode, xi(), yi(), xx(), yx(), B(), d(), F(), t(), l, w, A, d)
DECLARE FUNCTION ShowPacer$ ()
REM $INCLUDE: 'AD1200.INC'
CONST FALSE = 0, TRUE = NOT FALSE
DIM PF%(0 TO 15)                'Pass Fail Data space for Diag
DIM ADSpace%(0 TO 4096)         'Put A/D Conversion Data Here
DIM chanlist%(0 TO 100)         'Put Channel List Here
DIM x1(0 TO 15), y1(0 TO 15), x2(0 TO 15), y2(0 TO 15)    'Arrays for screen coords
DIM bo(0 TO 15), bg(0 TO 15), fg(0 TO 15), tr(0 TO 15)    'border, background, fground and
trace colours
DIM lx(0 TO 15), ly(0 TO 15)    'x,y coords for screen labels
DIM Ch(0 TO 15)
'Print address as hex byte and with the level then revision number
CLS
A = &H218:       ' SET DEFAULT
IRQ = 7          ' SET DEFAULT
DMA = 1          ' Set Default
MaxCnt = 256     ' Set Default Count of Readings to get
pacer = Hz50     ' Set Default
Ax = 4           ' Set DEFAULT
Dn = 4           ' Set DEFAULT
FOR i = 0 TO 0  'by default use channels in order 0 to 15
  Ch(i) = i
NEXT

CALL Comline(A, IRQ, DMA, MaxCnt, pacer, Ax, Dn, Ch())   'Process Any Command line Argument
MaxChan = (Ax * Dn) - 1                 ' 0 TO MAXCHAN Channels to do
FOR i = 0 TO MaxChan
  chanlist%(i) = Ch(i)          'Each Channel In Order
  R = GainSet(i, 0)         'Gain Of 1
NEXT
chanlist%(MaxChan + 1) = 255   'End Marker When using ADListIn
' Subroutine to interpret command line parameter as a hex address.
'               HexAddr  : Set To &H218 BEFORE Calling Comline
' Parameters:   HexAddr  : Integer Variable To Place Valid Hex Address
'                        : If NO command line arqument HexAddr Unchanged.
'                        : If BAD command line argument then EXIT program
'                          with Error message.
CLS
PRINT "AD1200 Driver QuickBASIC Graph The A/D Input Program"
PRINT "First: Ensure We Have AD1200 Card Present."
PRINT "Second: List Command Line Options."
PRINT
BaseSet (A)          'Set base address to default or User Input
PRINT "Base I/O Address Read Back           := "; HEX$(BaseGet)
V% = Version%:       'Get Version Number
'print address as hex byte and with the level then revision number
PRINT "Driver Major.Minor Version           := "; HEX$(V% \ 256); "."; HEX$(V% MOD 256)
'*************************************************************************
'* IMPORTANT ! Call The Diag Routine BEFORE performing Any A/D I/O Etc *
'*           Diag  Tests Out The Cards A/D Conversion Hardware          *
'*                 If all those tests are successful THEN tests the     *
'*                 Pacer Clock                                          *
'*                 Finally Updates The Cards Functional Table by        *
'*                 calling WhichCard                                    *
'* if test Fail   Returns ADERR = -1                                    *
'* if test Pass   Returns the card type eg 1211, 1221 1210 1200 etc     *
'*     WhichCard  Determines whether Card has the following capability  *
'*                Programmable Gain                                     *
'*                DMA                                                   *
'*                Xtended Mode                                          *
'*    WhichCard   Returns the card type eg 1211, 1221 1210 1200 etc     *
'*************************************************************************
d = Diag(PF%(0))        'Perform Diagnostic Tests
IF d = ADERR THEN
PRINT
```

```
PRINT "Card Failed Diagnostic Test"
PRINT "Error: Card Failed At Least One Diagnostic Test":
PRINT "Error: AD1200 Card Failed Test Or Not Found At I/O Address :="; HEX$(BaseGet); " hex"
PRINT "Exitting Program"
END
ELSE
PRINT "Card Passed Diagnostic Tests, Card Is := AD"; RIGHT$(STR$(d), 4)
END IF
'Card Passed Diag Test So Continue'
Init                    'Initialise AD1200 registers
ID = WhichCard          'Identify Card
PRINT "AD"; RIGHT$(STR$(ID), 4); " Card Initialised OK"
'Print Out Command lIne parameters
R = IntrSet(IRQ)        'Set Irq Line to default or User Input
PRINT "Interrupt Line Set To                    := "; HEX$(IntrGet)
'Set DMA Channel If The Card Can Do It
IF (ID = 1200) OR (ID = 1201) THEN
R = DmaSet(DMA)         'Set Dma Channel to default or User Input
PRINT "DMA Channel Set To                       :="; STR$(DmaGet)
ELSE
PRINT "DMA Not Available On This Card           :"
END IF
PRINT "No Of Samples Per Channel                :="; MaxCnt
R = PacerSet(pacer):     'Set To Default Or User Specified Frequency
R = ModeSet(1)
PRINT "Pacer Clock Set To      :="; STR$(pacer); " Equal To :="; ShowPacer$
PRINT "Display Format Is                        :="; Ax; " Channels Across"
PRINT "Display Format Is                        :="; Dn; " Channels Down"
FOR B = 0 TO Dn - 1
  PRINT SPACE$(40);
    FOR A = 0 TO Ax - 1
      PRINT " Ch"; RIGHT$(STR$(chanlist%(B * Ax + A)), 2); "  ";
    NEXT A
  PRINT
NEXT B

'************************************************************
'      Initialise data aquisition routine - not used        *
'************************************************************
PRINT
PRINT "Demonstrate: ADManyIn (chan, array , count)   Plot Data On A Graph"
PRINT
Pause
CALL SetGraph(Gmode, x1(), y1(), x2(), y2(), bg(), bo(), fg(), tr(), l, w, Ax, Dn)
xmax = w
ymax = 1
xmin = 1
ymin = 1
xdiff = xmax - xmin
ydiff = ymax - ymin
FOR A = 0 TO Ax - 1
  FOR B = 0 TO Dn - 1
    lx(B * Ax + A) = INT(xmin + (A MOD Ax) * (xdiff / Ax))
    ly(B * Ax + A) = CINT((1 / 2) + ymin + (B MOD Dn) * (ydiff / Dn))
NEXT B, A
```

```
'************************************************************
'    Start automation routine with no data acquisition     *
'************************************************************
'             Sample with no standard addition             *
'************************************************************
'Sample with no standard addition
t2& = TIMER
SCREEN Mode
CLS
rowpos% = 6
colpos% = 70
PRINT "FI-CL System Automation Routine"
PRINT "==============================="
PRINT
PRINT "SAMPLE ONLY: NO STANDARD ADDITION"
PRINT

t1& = TIMER + 1
PRINT "Switch injection valve           1  s "
LOCATE rowpos%, colpos% - 15
PRINT "Time remaining:    s"
WHILE TIMER < t1&
```

```
  t5% = t1& - TIMER
  LOCATE rowpos%, colpos%
  PRINT t5%
  DigOut (3)                    'Switch injection valve 1s
WEND

rowpos% = rowpos% + 1
t1& = TIMER + 60
PRINT "Sample exchange                    60 s"
LOCATE rowpos%, colpos% - 15
PRINT "Time remaining:    s"
WHILE TIMER < t1&
  t5% = t1& - TIMER
  LOCATE rowpos%, colpos%
  PRINT t5%
  DigOut (145)                  'Flush sample lines 60s
WEND

rowpos% = rowpos% + 1
t1& = TIMER + 10
PRINT "UHP water flush                    10 s"
LOCATE rowpos%, colpos% - 15
PRINT "Time remaining:    s"
WHILE TIMER < t1&
  t5% = t1& - TIMER
  LOCATE rowpos%, colpos%
  PRINT t5%
  DigOut (9)                    'UHP water flush 10s
WEND

rowpos% = rowpos% + 1
t1& = TIMER + 1
PRINT "Switch injection valve             1  s"
LOCATE rowpos%, colpos% - 15
PRINT "Time remaining:    s"
WHILE TIMER < t1&
  t5% = t1& - TIMER
  LOCATE rowpos%, colpos%
  PRINT t5%
  DigOut (3)                    'Switch injection valve 1s
WEND

rowpos% = rowpos% + 1
t1& = TIMER + 10
PRINT "UHP water wash                     10 s"
LOCATE rowpos%, colpos% - 15
PRINT "Time remaining:    s"
WHILE TIMER < t1&
  t5% = t1& - TIMER
  LOCATE rowpos%, colpos%
  PRINT t5%
  DigOut (9)                    'UHP water column wash 10s
WEND

rowpos% = rowpos% + 1
t1& = TIMER + 60
PRINT "Sample preconcentration peak 1   60 s"
LOCATE rowpos%, colpos% - 15
PRINT "Time remaining:    s"
WHILE TIMER < t1&
  t5% = t1& - TIMER
  LOCATE rowpos%, colpos%
  PRINT t5%
  DigOut (144)                  'Sample preconcentration 60s
WEND

rowpos% = rowpos% + 1
t1& = TIMER + 20
PRINT "UHP water wash                     20 s"
LOCATE rowpos%, colpos% - 15
PRINT "Time remaining:    s"
WHILE TIMER < t1&
  t5% = t1& - TIMER
  LOCATE rowpos%, colpos%
  PRINT t5%
  DigOut (8)                    'UHP water column rinse 20s
WEND

rowpos% = rowpos% + 1
```

```
t1& = TIMER + 1
PRINT "Switch injection valve          1  s"
LOCATE rowpos%, colpos% - 15
PRINT "Time remaining:    s"
WHILE TIMER < t1&
  t5% = t1& - TIMER
  LOCATE rowpos%, colpos%
  PRINT t5%
  DigOut (2)                   'Switch injection valve 1s
WEND

rowpos% = rowpos% + 1
t1& = TIMER + 60
PRINT "Column elution peak 1           60 s"
LOCATE rowpos%, colpos% - 15
PRINT "Time remaining:    s"
WHILE TIMER < t1&
  t5% = t1& - TIMER
  LOCATE rowpos%, colpos%
  PRINT t5%
  DigOut (0)                   'Elution and detection 60s
WEND

rowpos% = rowpos% + 1
t1& = TIMER + 1
PRINT "Switch injection valve          1  s"
LOCATE rowpos%, colpos% - 15
PRINT "Time remaining:    s"
WHILE TIMER < t1&
  t5% = t1& - TIMER
  LOCATE rowpos%, colpos%
  PRINT t5%
  DigOut (2)                   'Switch injection valve 1s
WEND

rowpos% = rowpos% + 1
t1& = TIMER + 10
PRINT "UHP water wash                  10 s"
LOCATE rowpos%, colpos% - 15
PRINT "Time remaining:    s"
WHILE TIMER < t1&
  t5% = t1& - TIMER
  LOCATE rowpos%, colpos%
  PRINT t5%
  DigOut (8)                   'UHP water column wash 10s
WEND

'************************************************************
'*            Sample plus one standard addition             *
'************************************************************
NextSam1:
'Sample plus one standard addition
t2& = TIMER
rowpos% = 6
colpos% = 70
CLS
LOCATE 1, 1
PRINT "FI-CL System Automation Routine"
PRINT "==============================="
PRINT
PRINT "SAMPLE PLUS ONE STANDARD ADDITION"
PRINT

t1& = TIMER + 10
PRINT "Pause between flask change      10 s "
LOCATE rowpos%, colpos% - 15
PRINT "Time remaining:    s"
WHILE TIMER < t1&
  t5% = t1& - TIMER
  LOCATE rowpos%, colpos%
  PRINT t5%
  DigOut (1)                   'System pause 10s
WEND

rowpos% = rowpos% + 1
t1& = TIMER + 1
PRINT "Switch injection valve          1  s "
LOCATE rowpos%, colpos% - 15
PRINT "Time remaining:    s"
```

```
WHILE TIMER < t1&
  t5% = t1& - TIMER
  LOCATE rowpos%, colpos%
  PRINT t5%
  DigOut (3)                    'Switch injection valve 1s
WEND

rowpos% = rowpos% + 1
t1& = TIMER + 60
PRINT "Sample exchange                  60 s"
LOCATE rowpos%, colpos% - 15
PRINT "Time remaining:    s"
WHILE TIMER < t1&
  t5% = t1& - TIMER
  LOCATE rowpos%, colpos%
  PRINT t5%
  DigOut (209)                  'Flush sample lines 60s
WEND

rowpos% = rowpos% + 1
t1& = TIMER + 10
PRINT "UHP water flush                  10 s"
LOCATE rowpos%, colpos% - 15
PRINT "Time remaining:    s"
WHILE TIMER < t1&
  t5% = t1& - TIMER
  LOCATE rowpos%, colpos%
  PRINT t5%
  DigOut (9)                    'UHP water flush 10s
WEND

rowpos% = rowpos% + 1
t1& = TIMER + 1
PRINT "Switch injection valve           1  s"
LOCATE rowpos%, colpos% - 15
PRINT "Time remaining:    s"
WHILE TIMER < t1&
  t5% = t1& - TIMER
  LOCATE rowpos%, colpos%
  PRINT t5%
  DigOut (3)                    'Switch injection valve 1s
WEND

rowpos% = rowpos% + 1
t1& = TIMER + 10
PRINT "UHP water wash                   10 s"
LOCATE rowpos%, colpos% - 15
PRINT "Time remaining:    s"
WHILE TIMER < t1&
  t5% = t1& - TIMER
  LOCATE rowpos%, colpos%
  PRINT t5%
  DigOut (9)                    'UHP water column wash 10s
WEND

rowpos% = rowpos% + 1
t1& = TIMER + 60
PRINT "Sample preconcentration peak 1   60 s"
LOCATE rowpos%, colpos% - 15
PRINT "Time remaining:    s"
WHILE TIMER < t1&
  t5% = t1& - TIMER
  LOCATE rowpos%, colpos%
  PRINT t5%
  DigOut (208)                  'Sample preconcentration 60s
WEND

rowpos% = rowpos% + 1
t1& = TIMER + 20
PRINT "UHP water wash                   20 s"
LOCATE rowpos%, colpos% - 15
PRINT "Time remaining:    s"
WHILE TIMER < t1&
  t5% = t1& - TIMER
  LOCATE rowpos%, colpos%
  PRINT t5%
  DigOut (8)                    'UHP water column rinse 20s
WEND
```

```
rowpos% = rowpos% + 1
t1& = TIMER + 1
PRINT "Switch injection valve          1  s"
LOCATE rowpos%, colpos% - 15
PRINT "Time remaining:    s"
WHILE TIMER < t1&
  t5% = t1& - TIMER
  LOCATE rowpos%, colpos%
  PRINT t5%
  DigOut (2)                    'Switch injection valve 1s
WEND

rowpos% = rowpos% + 1
t1& = TIMER + 60
PRINT "Column elution peak 1           60 s"
LOCATE rowpos%, colpos% - 15
PRINT "Time remaining:    s"
WHILE TIMER < t1&
  t5% = t1& - TIMER
  LOCATE rowpos%, colpos%
  PRINT t5%
  DigOut (0)                    'Elution and detection 60s
WEND

rowpos% = rowpos% + 1
t1& = TIMER + 1
PRINT "Switch injection valve          1  s"
LOCATE rowpos%, colpos% - 15
PRINT "Time remaining:    s"
WHILE TIMER < t1&
  t5% = t1& - TIMER
  LOCATE rowpos%, colpos%
  PRINT t5%
  DigOut (2)                    'Switch injection valve 1s
WEND

rowpos% = rowpos% + 1
t1& = TIMER + 10
PRINT "UHP water wash                  10 s"
LOCATE rowpos%, colpos% - 15
PRINT "Time remaining:    s"
WHILE TIMER < t1&
  t5% = t1& - TIMER
  LOCATE rowpos%, colpos%
  PRINT t5%
  DigOut (8)                    'UHP water column wash 10s
WEND

'************************************************************
'*            Sample plus two standard additions            *
'************************************************************
NextSam2:
'Sample plus two standard additions
t2& = TIMER
SCREEN Mode
rowpos% = 6
colpos% = 70
CLS
LOCATE 1, 1
PRINT "FI-CL System Automation Routine"
PRINT "================================"
PRINT
PRINT "SAMPLE PLUS TWO STANDARD ADDITIONS"
PRINT

t1& = TIMER + 10
PRINT "Pause between flask change      10 s "
LOCATE rowpos%, colpos% - 15
PRINT "Time remaining:    s"
WHILE TIMER < t1&
  t5% = t1& - TIMER
  LOCATE rowpos%, colpos%
  PRINT t5%
  DigOut (1)                    'System pause 10s
WEND

rowpos% = rowpos% + 1
t1& = TIMER + 1
PRINT "Switch injection valve          1  s "
```

```
LOCATE rowpos%, colpos% - 15
PRINT "Time remaining:    s"
WHILE TIMER < t1&
  t5% = t1& - TIMER
  LOCATE rowpos%, colpos%
  PRINT t5%
  DigOut (3)                    'Switch injection valve 1s
WEND

rowpos% = rowpos% + 1
t1& = TIMER + 60
PRINT "Sample exchange                    60 s"
LOCATE rowpos%, colpos% - 15
PRINT "Time remaining:    s"
WHILE TIMER < t1&
  t5% = t1& - TIMER
  LOCATE rowpos%, colpos%
  PRINT t5%
  DigOut (241)                  'Flush sample lines 60s
WEND

rowpos% = rowpos% + 1
t1& = TIMER + 10
PRINT "UHP water flush                    10 s"
LOCATE rowpos%, colpos% - 15
PRINT "Time remaining:    s"
WHILE TIMER < t1&
  t5% = t1& - TIMER
  LOCATE rowpos%, colpos%
  PRINT t5%
  DigOut (9)                    'UHP water flush 10s
WEND

rowpos% = rowpos% + 1
t1& = TIMER + 1
PRINT "Switch injection valve             1  s"
LOCATE rowpos%, colpos% - 15
PRINT "Time remaining:    s"
WHILE TIMER < t1&
  t5% = t1& - TIMER
  LOCATE rowpos%, colpos%
  PRINT t5%
  DigOut (3)                    'Switch injection valve 1s
WEND

rowpos% = rowpos% + 1
t1& = TIMER + 10
PRINT "UHP water wash                     10 s"
LOCATE rowpos%, colpos% - 15
PRINT "Time remaining:    s"
WHILE TIMER < t1&
  t5% = t1& - TIMER
  LOCATE rowpos%, colpos%
  PRINT t5%
  DigOut (9)                    'UHP water column wash 10s
WEND

rowpos% = rowpos% + 1
t1& = TIMER + 60
PRINT "Sample preconcentration peak 1   60 s"
LOCATE rowpos%, colpos% - 15
PRINT "Time remaining:    s"
WHILE TIMER < t1&
  t5% = t1& - TIMER
  LOCATE rowpos%, colpos%
  PRINT t5%
  DigOut (240)                  'Sample preconcentration 60s
WEND

rowpos% = rowpos% + 1
t1& = TIMER + 20
PRINT "UHP water wash                     20 s"
LOCATE rowpos%, colpos% - 15
PRINT "Time remaining:    s"
WHILE TIMER < t1&
  t5% = t1& - TIMER
  LOCATE rowpos%, colpos%
  PRINT t5%
  DigOut (8)                    'UHP water column rinse 20s
```

```
WEND

rowpos% = rowpos% + 1
t1& = TIMER + 1
PRINT "Switch injection valve          1  s"
LOCATE rowpos%, colpos% - 15
PRINT "Time remaining:    s"
WHILE TIMER < t1&
  t5% = t1& - TIMER
  LOCATE rowpos%, colpos%
  PRINT t5%
  DigOut (2)                    'Switch injection valve 1s
WEND

rowpos% = rowpos% + 1
t1& = TIMER + 60
PRINT "Column elution peak 1           60 s"
LOCATE rowpos%, colpos% - 15
PRINT "Time remaining:    s"
WHILE TIMER < t1&
  t5% = t1& - TIMER
  LOCATE rowpos%, colpos%
  PRINT t5%
  DigOut (0)                    'Elution and detection 60s
WEND

rowpos% = rowpos% + 1
t1& = TIMER + 1
PRINT "Switch injection valve          1  s"
LOCATE rowpos%, colpos% - 15
PRINT "Time remaining:    s"
WHILE TIMER < t1&
  t5% = t1& - TIMER
  LOCATE rowpos%, colpos%
  PRINT t5%
  DigOut (2)                    'Switch injection valve 1s
WEND

rowpos% = rowpos% + 1
t1& = TIMER + 10
PRINT "UHP water wash                  10 s"
LOCATE rowpos%, colpos% - 15
PRINT "Time remaining:    s"
WHILE TIMER < t1&
  t5% = t1& - TIMER
  LOCATE rowpos%, colpos%
  PRINT t5%
  DigOut (8)                    'UHP water column wash 10s
WEND

DigOut (1)
    END

Message:
  NoGraphics = TRUE
  RESUME NEXT
```

```
'*************************************************************
'*                        Subroutines                        *
'*************************************************************
DEFLNG X
SUB Comline (HexAddr, irqline, DmaLine, Count, Freq, Across, Down, Chans()) STATIC
'Treat Command Line parameters as
'HexAddr   : Base I/O Address Of Card
'Irqline   : Interrupt Line Set On Jumpers
'DMAline   : DMA Channel Set On Jumpers
'Freq      : Frequency To set Pacer Clock
'Chans()   : Channels to use when performing A/D Input
CONST TRUE = -1, FALSE = 0
DIM Args$(1 TO 25)
   NumArgs = 0: In = FALSE
   MaxArgs = 25
  'Get the command line using the COMMAND$ function.
   cl$ = COMMAND$
   l = LEN(cl$)
  'Go through the command line a character at a time.
   FOR i = 1 TO l
      c$ = MID$(cl$, i, 1)
```

```
      'Test for character being a blank or a tab.
       IF (c$ <> " " AND c$ <> CHR$(9)) THEN
      'Neither blank nor tab.
      'Test to see if you're already
      'inside an argument.
      IF NOT In THEN
      'You've found the start of a new argument.
      'Test for too many arguments.
      IF NumArgs = MaxArgs THEN EXIT FOR
      NumArgs = NumArgs + 1
      In = TRUE
      END IF
      'Add the character to the current argument.
      Args$(NumArgs) = Args$(NumArgs) + c$
      ELSE
      'Found a blank or a tab.
      'Set "Not in an argument" flag to FALSE.
      In = FALSE
      END IF
   NEXT i
IF NumArgs = 0 THEN EXIT SUB: ' USE THE DEFAULT
' PROCESS COMMAND LINE ADDRESS
' VALIDATE A HEX ADDRESS
l = LEN(Args$(1))
IF l > 4 THEN c$ = "ADDRESS PARAMETER TOO LONG": GOTO 14800
x = 0
FOR d = 1 TO l: ' FEED WAY THROUGH THE TEXT
  AV$ = MID$(Args$(1), d, 1): AV = ASC(AV$)
  IF AV < 48 THEN 14700: ' CHR$(0)-CHR$(47) BAD
  IF AV < 58 THEN AV = AV - 48: GOTO 14300: '"0-9" CHR$(48-57) OK
  IF AV < 65 THEN 14700: ' CHR$(58-64) BAD
  IF AV > 70 THEN 14700: ' CHR$9 71-255 BAD
  AV = AV - 55
  14300   x = x * 16 + AV
NEXT
HexAddr = (x AND &HFFF):          ' Pass input back to calling routine
IF NumArgs = 1 THEN EXIT SUB: ' USE THE DEFAULT
'Validate An Irqline setting range =2-7
x = VAL(Args$(2))
IF x < 2 OR x > 7 THEN c$ = "INVALID IRQLINE SETTING": GOTO BadIrq
irqline = x                       'Pass input back To main Program
IF NumArgs = 2 THEN EXIT SUB: ' USE THE DEFAULT
'Validate An DmaLine setting range =1-3
x = VAL(Args$(3))
IF x < 1 OR x > 3 THEN c$ = "INVALID DMA CHANNEL SETTING": GOTO BadDma
DmaLine = x                       'Pass input back To main Program
IF NumArgs = 3 THEN EXIT SUB: ' USE THE DEFAULT
'Validate An Sample Count range =1 4096
x = VAL(Args$(4))
IF x < 1 OR x > 4096 THEN c$ = "INVALID SAMPLE COUNT": GOTO BadCount
Count = x                        'Pass input back To main Program
IF NumArgs = 4 THEN EXIT SUB: ' USE THE DEFAULT
'Validate An Pacer Divisor setting range =0 -63
x = VAL(Args$(5))
IF x < 0 OR x > 63 THEN c$ = "INVALID PACER DIVISOR": GOTO BadPacer
Freq = x                         'Pass input back To main Program
IF NumArgs = 5 THEN EXIT SUB: ' USE THE DEFAULT
'Validate An Across range =1 -16
x = VAL(Args$(6))
IF x < 1 OR x > 16 THEN c$ = "INVALID ACROSS SETTING": GOTO BadAcross
Across = x                        'Pass input back To main Program
IF NumArgs = 6 AND (Across * Down) > 16 THEN c$ = "INVALID Across X Down PRODUCT": GOTO

BadAcross
IF NumArgs = 6 THEN EXIT SUB: ' USE THE DEFAULT
'Validate An Down range =1 -16
x = VAL(Args$(7))
IF x < 1 OR x > 16 THEN c$ = "INVALID DOWN SETTING": GOTO BadAcross
Down = x                         'Pass input back To main Program
IF (Across * Down) > 16 THEN c$ = "INVALID Across X Down PRODUCT": GOTO BadAcross
IF NumArgs = 7 THEN EXIT SUB: ' USE THE DEFAULT
'Validate An Channels setting range =0 -63
i = 0
WHILE ((8 + i < NumArgs + 1) AND (i < 16))
  x = VAL(Args$(8 + i))
  IF x < 0 OR x > 15 THEN c$ = "INVALID CHANNEL SETTING": GOTO BadChan
  Chans(i) = x                        'Pass input back To main Program
  i = i + 1
WEND
```

```
EXIT SUB

14700 c$ = "INVALID CHARACTER IN ADDRESS"
14800 ' ERROR IN COMMAND LINE
PRINT "USER COMMAND LINE INPUT := "; cl$
PRINT "COMMAND LINE ERROR! "; c$
PRINT "COMMAND FORMAT IS:-"
PRINT "<Prog Name> <IoAddr> <IrqLine> <DmaChan> <Count> <Pacer> <Across> <Down> <Chan0
Chan2.. Chan15>"
PRINT "<Prog Name> 02D8    TO SET AD1200  ADDRESS TO 02D8"
PRINT "                    WHERE ADDRESS IS A 4 DIGIT HEX ADDRESS"
END

BadIrq:
'ERROR IN COMMAND LINE
PRINT "USER COMMAND LINE INPUT := "; cl$
PRINT "COMMAND LINE ERROR! "; c$
PRINT "COMMAND FORMAT IS:-"
PRINT "<Prog Name> <IoAddr> <IrqLine> <DmaChan> <Count> <Pacer> <Across> <Down> <Chan0
Chan2.. Chan15>"
PRINT "<Prog Name> 0218  5  TO SET IRQLINE TO 5"
PRINT "                     WHERE IRQLINE = 2,3,4,5,6 or 7"
END

BadDma:
' ERROR IN COMMAND LINE
PRINT "USER COMMAND LINE INPUT := "; cl$
PRINT "COMMAND LINE ERROR! "; c$
PRINT "COMMAND FORMAT IS:-"
PRINT "<Prog Name> <IoAddr> <IrqLine> <DmaChan> <Count> <Pacer> <Across> <Down> <Chan0
Chan2.. Chan15>"
PRINT "<Prog Name> 0218  7  2  TO SET DMACHANNEL TO 2"
PRINT "                        WHERE DMACHANNEL = 1,2, or 3"
END

BadCount:
' ERROR IN COMMAND LINE
PRINT "USER COMMAND LINE INPUT := "; cl$
PRINT "COMMAND LINE ERROR! "; c$
PRINT "COMMAND FORMAT IS:-"
PRINT "<Prog Name> <IoAddr> <IrqLine> <DmaChan> <Count> <Pacer> <Across> <Down> <Chan0
Chan2.. Chan15>"
PRINT "<Prog Name> 0218  7  2  128 TO SET COUNT NO READINGS TO 1024"
PRINT "                           WHERE COUNT = 1 to 4096"
END

BadPacer:
' ERROR IN COMMAND LINE
PRINT "USER COMMAND LINE INPUT := "; cl$
PRINT "COMMAND LINE ERROR! "; c$
PRINT "COMMAND FORMAT IS:-"
PRINT "<Prog Name> <IoAddr> <IrqLine> <DmaChan> <Count> <Pacer> <Across> <Down> <Chan0
Chan2.. Chan15>"
PRINT "<Prog Name> 0218  7  2 128 10 TO SET PACER DIVISOR TO 10"
PRINT "                           WHERE PACER = 0 to 63"
END

BadAcross:
' ERROR IN COMMAND LINE
PRINT "USER COMMAND LINE INPUT := "; cl$
PRINT "COMMAND LINE ERROR! "; c$
PRINT "COMMAND FORMAT IS:-"
PRINT "<Prog Name> <IoAddr> <IrqLine> <DmaChan> <Count> <Pacer> <Across> <Down> <Chan0
Chan2.. Chan15>"
PRINT "<Prog Name> 0218  7  2 128 10 3 4 TO SET 3 Graphs Across by 4 Graphs Down"
PRINT "                           WHERE Across = 1 to 16"
PRINT "                           WHERE Down   = 1 to 16"
PRINT "            WHERE Product of Across x Down = 1 to 16"
END

BadChan:
' ERROR IN COMMAND LINE
PRINT "USER COMMAND LINE INPUT := "; cl$
PRINT "COMMAND LINE ERROR! "; c$
PRINT "COMMAND FORMAT IS:-"
PRINT "<Prog Name> <IoAddr> <IrqLine> <DmaChan> <Count> <Pacer> <Across> <Down> <Chan0
Chan2.. Chan15>"
PRINT "<Prog Name> 0218  7  2 128 10 3 3 4 3 2 TO USE CHANNEL 4 3 & 2 FOR INPUT"
PRINT "                                      WHERE CHANNEL = 0 to 15"
```

```
END

END SUB

DEFSNG A-Z
SUB Pause       'Wait For Any Key Press
YT = CSRLIN: XT = POS(0)        'save current pos
LOCATE 25, 27: PRINT "Press Any Key To Continue";
1 A$ = INKEY$: IF A$ = "" THEN 1
LOCATE 25, 1: PRINT SPACE$(70);
LOCATE YT, XT   'restore old position

END SUB

DEFINT A-Z
SUB SetGraph (Gmode, xi(), yi(), xx(), yx(), bk(), bd(), fr(), tr(), nol, wid, Across, Down)
CONST FALSE = 0, TRUE = NOT FALSE
SHARED NoGraphics
'Set Up For 16 Colour Graphics
FOR i = 0 TO 15         'Set Up The Background colours
  bk(i) = i
NEXT

FOR i = 0 TO 15         'Set Up The Border colours
  bd(i) = i
NEXT

FOR i = 0 TO 15         'Set Up The Forground colours
  fr(i) = 12
NEXT

fr(4) = 9
fr(5) = 9
fr(6) = 9
fr(7) = 9
fr(12) = 9
fr(13) = 9
fr(14) = 9
fr(15) = 9

FOR i = 0 TO 15         'Set Up The Sample Trace colours
  tr(i) = 15
NEXT

FOR Mode = 12 TO 0 STEP -1
  'Ignore Mode 13 low resolution lots of colours
  'Ignore Mode 8
  'Modes 5,6 do not exist!
  ON ERROR GOTO Message   'Turn On error Trap
  NoGraphics = FALSE      'Assume we have some graphics hardware
  SCREEN Mode
  IF NoGraphics = FALSE THEN      'If Still FALSE Then can support this mode
  SELECT CASE Mode
  CASE 0  'Text Mode Only
  Gmode = 0
  PRINT "Cannot Draw Graphs Using This Hardware"
  PRINT "IF You Are Using A Hercules Compatible Mono Adapter"
  PRINT "   THEN Run The MSHERC Program BEFORE Using This Program"
  PRINT "Exitting Program"
END

CASE 1  'Graphics mode screen 1, 200 x 320
Gmode = 1
xmin = 0: ymin = 0
xmax = 319: ymax = 199
csize = 8
nol = 25: wid = 40
FOR i = 0 TO 15
  bd(i) = 0       'black
NEXT

FOR i = 0 TO 15
  bk(i) = i AND 3:
  fr(i) = (i + 1) AND 3 'black
  tr(i) = (i + 2) AND 3 'black
NEXT
EXIT FOR

CASE 2 'Use 2 640 x 200 Monochrome
```

```
Gmode = 2
xmin = 0: ymin = 0
xmax = 639: ymax = 199
csize = 8
nol = 25: wid = 80
FOR i = 0 TO 15
  bd(i) = i AND 1
  bk(i) = i AND 1
  fr(i) = (i + 1) AND 1
  tr(i) = (i + 1) AND 1
NEXT
EXIT FOR

CASE 3 'Hercules Mono 720 x 348
Gmode = 3
xmin = 0: ymin = 0
xmax = 719: ymax = 347
csize = 14
nol = 25: wid = 80
FOR i = 0 TO 15
  bd(i) = i AND 1
  bk(i) = i AND 1
  fr(i) = (i + 1) AND 1
  tr(i) = (i + 1) AND 1
NEXT
EXIT FOR

CASE 7 'Use 7 320 x 200
Gmode = 7
xmin = 0: ymin = 0
xmax = 319: ymax = 199
csize = 8
nol = 25: wid = 40
EXIT FOR

CASE 9 'EGA Colour 640 x 350
Gmode = 9
xmin = 0: ymin = 0
xmax = 639: ymax = 349
csize = 14
nol = 25: wid = 80
EXIT FOR

CASE 10 'EGA/VGA Monochrome 640 x 350
Gmode = 10
xmin = 0: ymin = 0
xmax = 639: ymax = 349
csize = 14
nol = 25: wid = 80

FOR i = 0 TO 15
  bd(i) = 1       'black
NEXT

FOR i = 0 TO 12 STEP 3
  bk(i) = 0       'black
  bk(i + 1) = 1   'grey
  bk(i + 2) = 3   'white
NEXT
bk(15) = 0

FOR i = 0 TO 12 STEP 6
  fr(i) = 1
  fr(i + 1) = 3
  fr(i + 2) = 0
  fr(i + 3) = 3
  fr(i + 4) = 0
  fr(i + 5) = 1
  tr(i) = 3
  tr(i + 1) = 0
  tr(i + 2) = 1
  tr(i + 3) = 1
  tr(i + 4) = 3
  tr(i + 5) = 0
NEXT
EXIT FOR

CASE 11 'MCGA 640 x 480
Gmode = 11
```

```
xmin = 0: ymin = 0
xmax = 639: ymax = 479
csize = 16
nol = 30: wid = 80

FOR i = 0 TO 15
  bk(i) = i AND 1
  fr(i) = (i + 1) AND 1
  tr(i) = (i + 1) AND 1
NEXT
EXIT FOR

CASE 12 'VGA Use 12, 640 x 480
Gmode = 12
xmin = 0: ymin = 0
xmax = 639: ymax = 479
csize = 16
nol = 30: wid = 80
EXIT FOR
END SELECT
END IF
NEXT

'Adjust screen For Borders
'Divide the screen up into 4 quadrants
'Set the Whole Up screen jic
xi(0) = xmin: yi(0) = ymin
xx(0) = xmax / 2: yx(0) = ymax / 2
xdiff = xmax - xmin
ydiff = ymax - ymin
FOR A = 0 TO Across - 1
  FOR B = 0 TO Down - 1
    xi(B * Across + A) = INT(xmin + (A MOD Across) * (xdiff / Across) + (A AND 1))
    xx(B * Across + A) = INT(xmin + ((A MOD Across) + 1) * (xdiff / Across))
    yi(B * Across + A) = INT(ymin + (B MOD Down) * (ydiff / Down) + (B AND 1))
    yx(B * Across + A) = INT(ymin + ((B MOD Down) + 1) * (ydiff / Down))
NEXT B, A
ON ERROR GOTO 0          'Turn Off Error Trap
END SUB

DEFSNG A-Z
FUNCTION ShowPacer$
 DIM Freq$(64)
 Freq$(&H0) = "600k    "
 Freq$(&H1) = " 60k    "
 Freq$(&H2) = "  6k    "
 Freq$(&H3) = " 600    "
 Freq$(&H4) = "  60    "
 Freq$(&H5) = "   6    "
 Freq$(&H6) = "   0.6  "
 Freq$(&H7) = "   0.06 "
 Freq$(&H8) = " 60k    "
 Freq$(&H9) = "  6k    "
 Freq$(&HA) = " 600    "
 Freq$(&HB) = "  60    "
 Freq$(&HC) = "   6    "
 Freq$(&HD) = "   0.6  "
 Freq$(&HE) = "   0.06 "
 Freq$(&HF) = "   0.006"
 Freq$(&H10) = "300k    "
 Freq$(&H11) = " 30k    "
 Freq$(&H12) = "  3k    "
 Freq$(&H13) = " 300    "
 Freq$(&H14) = "  30    "
 Freq$(&H15) = "   3    "
 Freq$(&H16) = "   0.3  "
 Freq$(&H17) = "   0.03 "
 Freq$(&H18) = "200k    "
 Freq$(&H19) = " 20k    "
 Freq$(&H1A) = "  2k    "
 Freq$(&H1B) = " 200    "
 Freq$(&H1C) = "  20    "
 Freq$(&H1D) = "   2    "
 Freq$(&H1E) = "   0.2  "
 Freq$(&H1F) = "   0.02 "
 Freq$(&H20) = "150k    "
 Freq$(&H21) = " 15k    "
 Freq$(&H22) = "1500    "
 Freq$(&H23) = " 150    "
 Freq$(&H24) = "  15    "
 Freq$(&H25) = "   1.5  "
 Freq$(&H26) = "   0.15 "
 Freq$(&H27) = "   0.015"
 Freq$(&H28) = "120k    "
 Freq$(&H29) = " 12k    "
 Freq$(&H2A) = "1200    "
 Freq$(&H2B) = " 120    "
 Freq$(&H2C) = "  12    "
 Freq$(&H2D) = "   1.2  "
 Freq$(&H2E) = "   0.12 "
 Freq$(&H2F) = "   0.012"
 Freq$(&H30) = "100k    "
 Freq$(&H31) = " 10k    "
 Freq$(&H32) = "  1k    "
 Freq$(&H33) = " 100    "
 Freq$(&H34) = "  10    "
 Freq$(&H35) = "   1    "
 Freq$(&H36) = "   0.1  "
 Freq$(&H37) = "   0.01 "
 Freq$(&H38) = " 50k    "
 Freq$(&H39) = "  5k    "
 Freq$(&H3A) = " 500    "
 Freq$(&H3B) = "  50    "
 Freq$(&H3C) = "   5    "
 Freq$(&H3D) = "   0.5  "
 Freq$(&H3E) = "   0.05 "
 Freq$(&H3F) = "   0.005"

 Ret = PacerGet
 IF Ret < 0 OR Ret > 63 THEN
 ShowPacer$ = "Unknown Value!"
 ELSE
 ShowPacer$ = Freq$(Ret) + "Hz "
 END IF

END FUNCTION
```

SODIUM SULPHITE REDUCTION CALCULATIONS

Appendix B: Sodium Sulphite Reduction Calculations

Fe(III) reducing reagent: Na_2SO_3, S(IV)

Based on constants in Millero *et al., 1995. Reduction of Fe(III) with sulfite in natural waters* (Journal of Geophysical Research-Atmospheres, 100, 7235-7244)

Calculations

$Fe(III) + S(IV) = ^{k}$= products

$d[Fe(III)]/dt = -k[Fe(III)]^a[S(IV)]^b$

$d[Fe(III)]/dt = -k'[Fe(III)]$

where $k' = k[S(IV)]^b$

Integrates to:

$dy/dt = -k'.y = f(y)$

$1/y.\ dy/dt = -k'$

$\ln y - \ln y_0 = -k't - k't_0$

$\ln [Fe(III)]_{t/2} - \ln [Fe(III)]_0 = -k'.t_{1/2} - k'.t_0$

$t_{1/2} = \ln 2 / k'$

$\ln k' = \ln k + b.\ln[S(IV)]$

b is the order of the reaction (first order)

$\ln k' = \ln k + \ln[(S(IV)]$

Results

ln k = 7.34 +/- 0.04 S=35, pH=3.5, T=25°C (Millero, 1995)

ln k = 4.30 S=35, pH=2.0, T=20°C (Bowie, 1997)

Data Variable temperature

Conditions:

pH = 3.5

$Fe[(III)]_0$ = 100 nM

$[S(IV)]_0$ = 100 µM

S = 35

ln k wrt temperature estimated from Millero graph

Temp (°C)	Temp (K)	1/T (x 10^{-4})	ln k (M^{-1} min^{-1})	ln [(S(IV)]	ln k'	k'	$t_{1/2\ (min)}$	$t_{1/2\ (h)}$	>98% reduction (h)
5	278.15	3.60	3.2	-9.21	-6.01	0.00	282.54	4.71	28.25
10	283.15	3.53	4.3	-9.21	-4.91	0.01	94.05	1.57	9.41
15	288.15	3.47	5.4	-9.21	-3.81	0.02	31.31	0.52	3.13
20	293.15	3.41	6	-9.21	-3.21	0.04	17.18	0.29	1.72
25	298.15	3.35	7.1	-9.21	-2.11	0.12	5.72	0.10	0.57

Data Variable pH

Conditions:

Temp = 25°C

$Fe(III)_0$ = 100 nM

$[S(IV)]_0$ = 100 µM

S = 35

Line of best fit:

$y = -0.5911x2 + 5.2542x - 4.0134$

pH	ln k (M^{-1} min^{-1})	ln [(S(IV)]	ln k'	k'	$t_{1/2\ (min)}$	$t_{1/2\ (h)}$	>98% reduction (h)	>96% reduction (h)	>93% reduction (h)
1.996	4.08	-9.21	-5.13	0.01	117.19	1.953	11.72	9.77	7.81
2.49	5.38	-9.21	-3.83	0.02	31.94	0.532	3.19	2.66	2.13
2.968	6.48	-9.21	-2.73	0.07	10.63	0.177	1.06	0.89	0.71
3.5	7.32	-9.21	-1.89	0.15	4.59	0.076	0.46	0.38	0.31
3.75	7.44	-9.21	-1.77	0.17	4.07	0.068	0.41	0.34	0.27
3.817	7.4	-9.21	-1.81	0.16	4.24	0.071	0.42	0.35	0.28
4.267	7.41	-9.21	-1.80	0.17	4.19	0.070	0.42	0.35	0.28
4.399	7.51	-9.21	-1.70	0.18	3.80	0.063	0.38	0.32	0.25
4.856	7.42	-9.21	-1.79	0.17	4.15	0.069	0.42	0.35	0.28
5.389	7.2	-9.21	-2.01	0.13	5.17	0.086	0.52	0.43	0.34
6.088	6.75	-9.21	-2.46	0.09	8.12	0.135	0.81	0.68	0.54
6.357	5.15	-9.21	-4.06	0.02	40.20	0.670	4.02	3.35	2.68
6.74	4.42	-9.21	-4.79	0.01	83.41	1.390	8.34	6.95	5.56
2.2	4.684916	-9.21	-4.53	0.01	64.00	1.067	6.40	5.33	4.27
2.4	5.191944	-9.21	-4.02	0.02	38.55	0.642	3.85	3.21	2.57
3.3	6.886381	-9.21	-2.32	0.10	7.07	0.118	0.71	0.59	0.47

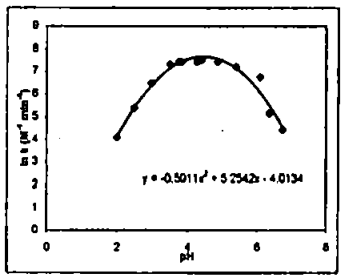

Data Variable [S(IV)]
Conditions:
$Fe[(III)]_0$ = 100 nM
Temp = 25°C
S = 35

[S(IV)] (μM)	[S(IV)] (M)	pH	ln k (M^{-1} min^{-1})	ln [(S(IV)]	ln k'	k'	$t_{1/2\,(min)}$	$t_{1/2\,(h)}$	>98% reduction (h)	>96% reduction (h)	>93% reduction (h)
50	5.00E-05	1.996	4.119031342	-9.90	-5.78	0.00	225.42	3.757	22.54	18.78	15.03
100	1.00E-04	1.996	4.119031342	-9.21	-5.09	0.01	112.71	1.878	11.27	9.39	7.51
200	2.00E-04	1.996	4.119031342	-8.52	-4.40	0.01	56.35	0.939	5.64	4.70	3.76
400	4.00E-04	1.996	4.119031342	-7.82	-3.71	0.02	28.18	0.470	2.82	2.35	1.88

[S(IV)] (μM)	[S(IV)] (M)	pH	ln k (M^{-1} min^{-1})	ln [(S(IV)]	ln k'	k'	$t_{1/2\,(min)}$	$t_{1/2\,(h)}$	>98% reduction (h)	>96% reduction (h)	>93% reduction (h)
50	5.00E-05	2.4	5.191944	-9.90	-4.71	0.01	77.09	1.285	7.71	6.42	5.14
100	1.00E-04	2.4	5.191944	-9.21	-4.02	0.02	38.55	0.642	3.85	3.21	2.57
200	2.00E-04	2.4	5.191944	-8.52	-3.33	0.04	19.27	0.321	1.93	1.61	1.28
400	4.00E-04	2.4	5.191944	-7.82	-2.63	0.07	9.64	0.161	0.96	0.80	0.64

[S(IV)] (μM)	[S(IV)] (M)	pH	ln k (M^{-1} min^{-1})	ln [(S(IV)]	ln k'	k'	$t_{1/2\,(min)}$	$t_{1/2\,(h)}$	>98% reduction (h)	>96% reduction (h)	>93% reduction (h)
50	5.00E-05	3.5	7.135325	-9.90	-2.77	0.06	11.04	0.184	1.10	0.92	0.74
100	1.00E-04	3.5	7.135325	-9.21	-2.08	0.13	5.52	0.092	0.55	0.46	0.37
200	2.00E-04	3.5	7.135325	-8.52	-1.38	0.25	2.76	0.046	0.28	0.23	0.18
400	4.00E-04	3.5	7.135325	-7.82	-0.69	0.50	1.38	0.023	0.14	0.12	0.09

[S(IV)] (μM)	[S(IV)] (M)	pH	ln k (M^{-1} min^{-1})	ln [(S(IV)]	ln k'	k'	$t_{1/2\,(min)}$	$t_{1/2\,(h)}$	>98% reduction (h)	>96% reduction (h)	>93% reduction (h)
1000	1.00E-03	2	4.1306	-6.91	-2.78	0.06	11.14	0.186	1.11	0.93	0.74

Data Variable ionic strength
Conditions:
$Fe[(III)]_0$ = 100 nM
Temp = 25°C
pH = 3.5

log k = 4.2 at zero ionic strength (estimated from Millero graph)
Thus ln k = 9.6708574

[S(IV)] (μM)	[S(IV)] (M)	ln k (M^{-1} min^{-1})	ln [(S(IV)]	ln k'	k'	$t_{1/2\,(s)}$	$t_{1/2\,(min)}$	$t_{1/2\,(h)}$	>98% reduction (h)	>96% reduction (h)	>93% reduction (h)
100	1.00E-04	9.670857391	-9.21	0.46	1.5849	26.2408	0.44	0.0073	0.0437	0.0364	0.0292
400	4.00E-04	9.670857391	-7.82	1.85	6.3396	6.5602	0.11	0.0018	0.0109	0.0091	0.0073
1000	1.00E-03	9.670857391	-6.91	2.76	15.8489	2.6241	0.04	0.0007	0.0044	0.0036	0.0029

Note: Impossible to obtain a value for ln k in zero ionic strength media (MQ water) at pH=2.4 without further experiments

---

Data Chosen FI conditions
Conditions:
Temp = 20°C $[S(IV)]_0$ = 100 μM
$Fe(III)]_0$ = 100 nM S = 35
pH = 2.2

ln k (M^{-1} min^{-1}	ln [(S(IV)]	ln k'	k'	$t_{1/2\,(min)}$	$t_{1/2\,(h)}$	>98% reduction (h)	>96% reduction (h)	>93% reduction (h)
4.3028	-9.21	-4.91	0.01	93.79	1.563	9.38	7.82	6.25

Interpolated from ln k' vs ln [S(IV)]

Data Chosen CAR conditions
Conditions:
Temp = 25°C $[S(IV)]_0$ = 400 μM
$Fe(III)]_0$ = 100 nM S = 0 (MQ water matrix)
pH = 2.4

ln k (M^{-1} min^{-1}	ln [(S(IV)]	ln k'	k'	$t_{1/2\,(min)}$	$t_{1/2\,(h)}$	>98% reduction (h)	>96% reduction (h)	>93% reduction
Unknown	-9.21	#VALUE!	#VALUE!	#VALUE!	#VALUE!	#VALUE!	#VALUE!	#VALUE!

Dependance of ln k on Temp and pH under given conditions is unknown

---

AMT Dataset

Appendix C: AMT Data

Cruise AMT-3

Part (i): Surface data (-7 m)

Station details			Date/Time			Position			Hydrographic Data (N.Rees)			Coulter (A.Bale)	Trace Metals (A.Bowie / D.Whitworth)					Nutrients (M.Woodward)				Chlorophyll (R.Barlow)	Photosynthesis (E.Maranon)
Station	*Go-Flo*	*CTD*	*Date*	*SDY*	*GMT*	*Latitude* (°)	*Lonitude* (°)	*Depth* (m)	*Sill depth* (m)	*Temperature* (°C)	*Salinity*	*Particle number* (per ml)	*TD-Fe $_{shp}$* (nM)	*TD-Fe $_{sms}$* (nM)	*TD-Al* (nM)	*TD-Co* (pM)	*TD-Ni* (nM)	*Nitrate* (µM)	*Nitrite* (µM)	*Phosphate* (µM)	*Silicate* (µM)	*Total chl a* (µg l^{-1})	*Primary production* (mgC m^{-3} h^{-1})
A301	A3-01		22-Sep-96	266	08:00	49.67 N	-5.69 W	-8	122	13.96			4.27					1.16				2.317	
A302	A3-02		23-Sep-96	267	09:30	48.41	-12.50	-7		16.80		5445											
A303	A3-03	1	24-Sep-96	268	10:30	47.35	-18.21	-7	4518	16.39	35.63	8141	4.45					0.51	0.11	0.00	0.31	0.887	1.29
A304	A3-04	2	25-Sep-96	269	10:30	42.90	-19.99	-7	2966	19.21	35.75	2764	[]	0.92	14.05	32.94	2.92	0.00		0.14	0.22	0.164	0.83
A305	A3-05	3	26-Sep-96	270	11:25	38.17	-20.01	-7	4070	22.13	36.40	1893	[]	1.95	16.82	24.74	1.97	0.00	0.00	0.00		0.088	0.38
A306	A3-06	4	27-Sep-96	271	11:25	34.03	-21.28	-7	5110	23.83	36.55	2177										0.085	
A307	A3-07	5	28-Sep-96	272	11:25	29.48	-21.81	-7	4766	24.42	37.23	1941	0.93	0.68	18.07	32.26	2.32	0.00	0.00	0.03		0.052	0.39
A308	A3-08	6	29-Sep-96	273	11:25	24.67	-21.40	-7	4387	24.78	37.08	2317	1.21	1.56	30.60	37.56	1.75	0.00	0.00	0.02		0.145	0.43
A309	A3-09	7	30-Sep-96	274	10:55	20.08	-20.63	-7	3823	24.62	36.31	4967	2.46	7.38	76.50	109.97	2.45	0.00	0.03	0.05	0.35	0.382	2.12
Underway	uw1		30-Sep-96	274	12:00	20.06	-20.58	-7	3629	24.66			2.09	4.95		94.40	2.12						
Underway	uw2		01-Oct-96	275	11:39	16.66	-20.41	-7	3448	27.19			1.71	3.25		80.25	1.82						
Underway			01-Oct-96	275	13:06	16.42	-20.42	-7				2578										0.222	
Underway	uw3		02-Oct-96	276	09:47	12.91	-20.49	-7	4571	28.54			0.51	3.58		55.40	2.35					0.158	
A310	A3-10	8	02-Oct-96	276	10:55	12.75	-20.55	-7	4600	28.42	35.35	2246	0.42	3.70	39.02	39.48	2.28	0.00	0.05	0.00	0.81	0.171	1.24
A311	A3-11	9	03-Oct-96	277	10:55	9.05	-22.28	-7	4130	28.27	35.55	2890	0.32	2.89	42.86	34.47	2.12	0.00	0.04	0.00	1.08	0.221	1.22
Underway	uw5		04-Oct-96	278	00:23	6.99	-23.14	-7	4987	28.50			0.61	3.16		29.71	1.69					0.115	
A312	A3-12	10	04-Oct-96	278	10:55	5.17	-24.02	-7	4232	28.45	34.68	2271	0.55	1.89	42.31	34.76	2.01	0.00	0.05	0.02	1.68	0.158	0.82
Underway	uw6		04-Oct-96	278	23:28	3.27	-24.91	-7	3770	27.82			0.48	2.27		29.15	1.43					0.178	
A313	A3-13	11	05-Oct-96	279	10:55	1.28	-25.78	-7	3646	28.68	35.61	2477	1.20	1.23	30.90	40.97	2.08	0.00	0.05	0.00	1.36	0.199	0.69
A314	A3-14	12	06-Oct-96	280	10:55	-2.38 S	-27.46	-7	4992	26.34	36.13	1893	1.31	1.36	22.45	29.97	2.55	0.00	0.04	0.04	1.49	0.137	0.48
A315	A3-15	13	07-Oct-96	281	10:55	-6.48	-29.27	-7	5329	28.63	36.03	1663	0.39	1.07	24.58	44.41	2.50	0.00	0.04	0.04	1.23	0.098	0.10
A316	A3-16	14	08-Oct-96	282	11:55	-10.77	-31.24	-7	5058	28.17	36.45	1492	0.78	0.71	28.50	28.04	1.76	0.07	0.04	0.02	0.91	0.050	0.23
Underway	uw8		08-Oct-96	282	23:58	-12.75	-32.14	-7	4529	25.74			0.87	1.20		20.29	3.33					0.045	
A317	A3-17	15	09-Oct-96	283	12:15	-14.68	-33.12	-7	4441	28.08	36.88	1505	0.65	2.23	22.08	32.39	2.61	0.07	0.03	0.02	1.15	0.061	0.24
Underway	uw9		10-Oct-96	284	00:45	-16.80	-34.01	-7	4342	25.56			0.40	0.93		26.75	2.11					0.057	
A318	A3-18	16	10-Oct-96	284	11:55	-18.85	-35.05	-7	4039	24.63	37.10	1780	1.13	1.85	23.16	32.50	2.71	0.00	0.03	0.00	1.11	0.069	0.38
A319	A3-19	17	11-Oct-96	285	11:55	-22.92	-38.96	-7	3873	22.39	36.83	2067	0.95	2.72	26.14	44.57	2.11	0.08		0.00	1.13	0.119	0.31
A321	A3-20	18	12-Oct-96	286	11:55	-26.60	-39.60	-7	4218	20.85	36.62	1733	0.96	2.82	18.69	38.36	1.90	0.08	0.03		1.18	0.115	0.30
A323	A3-21	19	13-Oct-96	287	12:00	-29.85	-42.91	-7	3917	19.78	36.24	1911	0.33	2.26	16.42	38.23	3.01	0.07	0.03	0.00	1.22	0.115	0.31
A324	A3-22	20	14-Oct-96	288	12:00	-32.80	-46.12	-7	3900	18.91	36.15	2883	0.65	2.40	24.00	40.80	2.95	0.08	0.04	0.02	1.36	0.463	0.77
Underway	uw10		15-Oct-96	289	08:08	-35.18	-48.76	-7	4377	15.61			1.46	1.64								0.571	
A325	A3-23	21	15-Oct-96	289	12:30	-35.70	-49.57	-7	4292	16.49	35.80	9371	1.68	2.95	15.45	45.78	1.92	0.09	0.05	0.03	1.52	0.703	1.80
A327	A3-24	22	16-Oct-96	290	11:50	-37.80	-52.19	-7	4034	17.18	35.75	4517	1.05	2.94	22.38	46.78	2.14	0.07	0.03	0.01	1.27	0.519	
A328	A3-25	23	23-Oct-96	297	12:55	-43.57	-55.02	-7	5244	10.85	34.74	8131	0.99	1.99	28.90	59.69	4.35	9.13		0.58	2.10	1.076	1.84
A329	A3-26	24	24-Oct-96	298	12:55	-48.00	-55.88	-7	4850	5.48	34.10	4096	0.88	4.50	50.00	68.85	4.75	35.02		1.54	6.03	0.317	0.62
A330	A3-27	25	25-Oct-96	299	11:00	-51.90	-57.89	-7	76	8.22	33.74	11873	2.71	3.00	20.63	73.20	6.80	28.30	0.11	1.13	2.81	0.810	

Appendix C: AMT Data

Cruise AMT-3

Part (ii): Vertical profiling data, upper water column (0-200 m)

Station details			Date/Time			Position								
Station	*Go-Flo*	*CTD*	*Date*	*SDY*	*GMT*	*Latitude (°)*	*Lonitude (°)*	*Sill depth (m)*						
A308	A3-08	6	29-Sep-96	273	11:25	24.67 N	-21.40 W	4387						
Hydrographic Data (N.Rees)				**Trace Metals (A.Bowie / D.Whitworth)**					**Nutrients (M.Woodward)**				**Chlorophyll (R.Barlow)**	**Photosynthesis (E.Maranon)**
Depth	*Temperature*	*Salinity*	*Sigma T*	*TD-Fe ship*	*TD-Fe land*	*TD-Al*	*TD-Co*	*TD-Ni*	*Nitrate*	*Nitrite*	*Phosphate*	*Silicate*	*Total chl a*	*Primary production*
(m)	(°C)			(nM)	(nM)	(nM)	(pM)	(nM)	(µM)	(µM)	(µM)	(µM)	(µg l^{-1})	(µgC m^{-3} h^{-1})
-7	24.7716	37.0706	24.9787	1.21	1.56		37.56	1.75	0.00	0.00	0.02		0.14	0.43
-20	24.7718	37.0758	24.9826	1.09	1.35	21.00	33.13	2.33	0.00	0.00	0.02		0.15	
-30	24.6941	37 1165	25.0371						0.00	0.00	0.02			
-40	24.4111	37.2880	25.2528		1.67	21.97	38.17	2.57	0.00	0.00	0.02			0.42
-50	23.9365	37.2988	25.4034						0.00	0.00	0.02		0.13	
-60	23.2214	37.2546	25.5817	0.90					0.00	0.00	0.02			0.35
-80	21.1052	37.0291	26.0120		1.51	25.24	35.27	2.55	0.13	0.00	0.02		0.29	0.22
-90	20.4643	36.9725	26.1439	0.38		15.46	37.07	2.26						
-100	19.9104	36.9084	26.2434	0.42	1.32	21.31	41.34	1.91	0.94	0.10	0.02		0.52	
-102	19.8756	36.9105	26.2542										0.40	
-110	19.7015	36.9031	26.2947										0.30	
-120	19.4788	36.8749	26.3317	1.22	1.58	26.41	36.84	2.05					0.32	
-150	18.8786	36.7967	26.4276	1.22	1.33	27.58	32.81	1.89	1.12	0.03	0.02	0.47	0.07	
-200	17.8171	36.5927	26.5390	1.60	2.30	27.74	47.08	2.16	4.18	0.00	0.21	0.35		

Station details			Date/Time			Position								
Station	*Go-Flo*	*CTD*	*Date*	*SDY*	*GMT*	*Latitude (°)*	*Lonitude (°)*	*Sill depth (m)*						
A309	A3-09	7	30-Sep-96	274	10:55	20.08 N	-20.62 W	3823						
Hydrographic Data (N.Rees)				**Trace Metals (A.Bowie / D.Whitworth)**					**Nutrients (M.Woodward)**				**Chlorophyll (R.Barlow)**	**Photosynthesis (E.Maranon)**
Depth	*Temperature*	*Salinity*	*Sigma T*	*TD-Fe ship*	*TD-Fe land*	*TD-Al*	*TD-Co*	*TD-Ni*	*Nitrate*	*Nitrite*	*Phosphate*	*Silicate*	*Total chl a*	*Primary production*
(m)	(°C)			(nM)	(nM)	(nM)	(pM)	(nM)	(µM)	(µM)	(µM)	(µM)	(µg l^{-1})	(µgC m^{-3} h^{-1})
-2	24.7507	36.3070		3.59										
-7	24.7543	36.3069	24.4060	2.46	7.38	78.50	109.97	2.45	0.00	0.03	0.05	0.35	0.38	2.12
-20	24.6786	36.3000	24.4238	0.63	5.02		60.37	3.45	0.00	0.02	0.04	0.43	0.41	2.04
-30	24.5390	36.2958	24.4628						0.00	0.02	0.04	0.43	0.50	0.93
-40	24.4691	36.2945	24.4829	0.21	1.44	22.19	73.49	2.60	0.35	0.11	0.07	1.58	0.91	1.77
-50	22.2227	36.1212	25.0086						0.50	0.14	0.08	1.19	0.31	0.82
-60	19.4362	35.9950	25.6704	1.17	2.85	15.51	100.60	2.44		0.09			0.15	0.25
-80	19.7677	36.7825	26.1851							0.04	0.13	2.65	0.06	0.17
-100	19.3990	36.8497	26.3333	0.58	1.70	23.36	37.83	2.53		0.03	0.08	3.62	0.05	
-150	17.2451	36.4326	26.5562		1.82		55.79	2.86		0.00	0.47	0.82	0.04	
-200	16.2815	36.3020	26.6852	1.27	2.28	24.91	67.19	3.01		0.00	0.55	0.80		

Station details			Date/Time			Position								
Station	*Go-Flo*	*CTD*	*Date*	*SDY*	*GMT*	*Latitude (°)*	*Lonitude (°)*	*Sill depth (m)*						
A311	A3-11	9	03-Oct-96	277	10:55	9.05 S	-22.28 W	4130						
Hydrographic Data (N.Rees)				**Trace Metals (A.Bowie / D.Whitworth)**					**Nutrients (M.Woodward)**				**Chlorophyll (R.Barlow)**	**Photosynthesis (E.Maranon)**
Depth	*Temperature*	*Salinity*	*Sigma T*	*TD-Fe ship*	*TD-Fe land*	*TD-Al*	*TD-Co*	*TD-Ni*	*Nitrate*	*Nitrite*	*Phosphate*	*Silicate*	*Total chl a*	*Primary production*
(m)	(°C)			(nM)	(nM)	(nM)	(pM)	(nM)	(µM)	(µM)	(µM)	(µM)	(µg l^{-1})	(µgC m^{-3} h^{-1})
-7	28.2397	35.5275	22.7149	0.32					0.00	0.04	0.00	1.91	0.22	1.22
-20	28.1975	35.6148	22.7944	0.43					0.00	0.04	0.00	3.34	0.20	1.45
-30	26.7117	35.8277	23.4355						0.00	0.04	0.00	3.95	0.34	
-40	22.6828	36.0094	24.7924						0.01	0.04	0.04	4.19	0.65	
-45	20.7284	35.9626	25.3023										0.79	
-50	20.0189	35.9282	25.4660	0.47					7.32	0.88	0.34	5.30		0.39
-60	18.6358	35.8286	25.7487	0.35					14.20	0.27	0.96	7.24	0.38	0.15
-80	16.0415	35.6209	26.2167						16.21	0.08	1.25	8.28	0.26	0.09
-100	14.7984	35.5004	26.4030	0.63					16.40	0.05	1.41	8.80	0.14	
-150	13.2276	35.3248	26.5992	0.62					16.75	0.04	1.45	1.48	0.02	
-200	12.3550	35.2270	26.6974	0.59					16.75	0.04	1.44	1.21		

Station details			Date/Time			Position								
Station	*Go-Flo*	*CTD*	*Date*	*SDY*	*GMT*	*Latitude (°)*	*Lonitude (°)*	*Sill depth (m)*						
A313	A3-13	11	05-Oct-96	279	10:55	1.28 N	-25.78 W	3646						
Hydrographic Data (N.Rees)				**Trace Metals (A.Bowie / D.Whitworth)**					**Nutrients (M.Woodward)**				**Chlorophyll (R.Barlow)**	**Photosynthesis (E.Maranon)**
Depth	*Temperature*	*Salinity*	*Sigma T*	*TD-Fe ship*	*TD-Fe land*	*TD-Al*	*TD-Co*	*TD-Ni*	*Nitrate*	*Nitrite*	*Phosphate*	*Silicate*	*Total chl a*	*Primary production*
(m)	(°C)			(nM)	(nM)	(nM)	(pM)	(nM)	(µM)	(µM)	(µM)	(µM)	(µg l^{-1})	(µgC m^{-3} h^{-1})
-2				1.58										
-7	26.8706	35.6035	23.2159	1.20					0.00	0.05	0.00	1.36	0.20	0.69
-20	26.8659	35.6047	23.2182	0.40					0.00	0.05	0.00	1.60		
-40	26.8844	35.6161	23.2273						0.00	0.05	0.02	1.65	0.19	0.91
-60	26.4171	35.7971	23.5058						0.00	0.05	0.03	2.16	0.36	1.04
-70	25.9805	35.9168	23.7333	0.78					0.00	0.05	0.03	3.30	0.58	1.22
-78	25.4714	35.8698	23.8558										0.88	
-80	25.1973	35.8349	23.9139	0.47					1.56	0.22	0.19	4.47		0.63
-90	22.1381	35.8066	24.7934	0.23					5.83	0.18	0.47	6.61	0.44	
-100	19.5757	35.8307	25.5084						8.45	0.11	0.74	8.16	0.35	0.13
-120	15.0081	35.5283	26.3789	0.27					10.88	0.07	1.04	1.49	0.06	0.01
-150	14.0382	35.4265	26.5095						11.92	0.06	1.43	1.49	0.03	
-200	13.3871	35.3288	26.5695	0.40										

Station details			Date/Time			Position								
Station	*Go-Flo*	*CTD*	*Date*	*SDY*	*GMT*	*Latitude (°)*		*Lonitude (°)*		*Sill depth (m)*				
A315	A3-15	13	07-Oct-96	281	10:55	-6.48 S		-29.27 W		5329				
Hydrographic Data (N.Rees)				**Trace Metals (A.Bowie / D.Whitworth)**						**Nutrients (M.Woodward)**			**Chlorophyll (R.Barlow)**	**Photosynthesis (E.Maranon)**
Depth	*Temperature*	*Salinity*	*Sigma T*	*TD-Fe $_{ship}$*	*TD-Fe $_{land}$*	*TD-Al*	*TD-Co*	*TD-Ni*	*Nitrate*	*Nitrite*	*Phosphate*	*Silicate*	*Total chl a*	*Primary production*
(m)	(°C)			(nM)	(nM)	(nM)	(pM)	(nM)	(µM)	(µM)	(µM)	(µM)	(µg l^{-1})	(µgC m^{-3} h^{-1})
-2						26.25	23.69							
-7	26.6241	36.0283	23.6146	0.39	1.07	24.56	44.41	2.50	0.00	0.04	0.04	1.23	0.10	0.10
-30	26.5943	36.0282	23.6240	0.88		17.65	33.19	2.68	0.00	0.04	0.04	1.22		
-50	26.5996	36.0283	23.6224				30.43	2.05	0.00	0.04	0.04	1.23	0.11	0.16
-70	26.6023	36.0286	23.6217	1.03	0.89	31.57	27.41	2.76	0.00	0.04	0.03	1.21		0.21
-80	26.5988	36.0294	23.6235										0.18	
-90	26.4525	36.0622	23.6946		0.97	22.34	31.86	2.41	0.00	0.04	0.05	1.46	0.29	0.33
-100	23.4769	36.7327	25.1105		0.81			2.23	0.08	0.05	0.09	2.13	0.39	
-110	22.7047	36.6787	25.2944	0.81					0.59	0.16	0.24	5.58	0.38	0.12
-120	21.4945	36.5087	25.5079		0.96	13.14	50.73	3.02	3.74	0.19	0.45	10.04	0.26	0.08
-130	19.7724	36.2276	25.7600										0.15	
-140	17.1068	35.8256	26.1236	0.35	1.13	10.76	45.43	3.17	19.17	0.07	1.16	0.91	0.11	0.08
-200	12.0522	35.1767	26.7170	0.48	2.23	12.52	68.72	5.48	22.40	0.03	1.64	0.92		

Station details			Date/Time			Position								
Station	*Go-Flo*	*CTD*	*Date*	*SDY*	*GMT*	*Latitude (°)*		*Lonitude (°)*		*Sill depth (m)*				
A316	A3-16	14	08-Oct-96	282	11:55	-10.77 S		-31.24 W		5058				
Hydrographic Data (N.Rees)				**Trace Metals (A.Bowie / D.Whitworth)**						**Nutrients (M.Woodward)**			**Chlorophyll (R.Barlow)**	**Photosynthesis (E.Maranon)**
Depth	*Temperature*	*Salinity*	*Sigma T*	*TD-Fe $_{ship}$*	*TD-Fe $_{land}$*	*TD-Al*	*TD-Co*	*TD-Ni*	*Nitrate*	*Nitrite*	*Phosphate*	*Silicate*	*Total chl a*	*Primary production*
(m)	(°C)			(nM)	(nM)	(nM)	(pM)	(nM)	(µM)	(µM)	(µM)	(µM)	(µg l^{-1})	(µgC m^{-3} h^{-1})
-7	26.1604	36.4884	24.1083	0.76					0.07	0.04	0.02	0.91	0.05	0.23
-25	26.1544	36.4881	24.1100	0.65					0.07	0.04	0.02	0.91		
-50	25.7333	36.5208	24.2666						0.07	0.04	0.02	0.91	0.07	0.23
-75	24.9895	36.9251	24.8020	0.69					0.07	0.04	0.04	0.97	0.10	0.17
-100	24.0993	36.9370	25.0807	0.50					0.07	0.04	0.08	1.21	0.16	
-120	22.3025	36.7347	25.4523						0.16	0.09	0.22	1.33	0.27	
-130	21.3095	36.5601	25.5983	0.12					1.47	0.10	0.27	1.93	0.31	0.19
-140	20.6646	36.4827	25.7008						3.14	0.09	0.43	3.04	0.23	0.24
-160	18.4273	36.0690	25.9854	0.49					8.50	0.07	0.63	1.15	0.13	
-200	14.6552	35.4221	26.3737						12.12	0.05	0.83	1.15	0.02	

Station details			Date/Time			Position								
Station	*Go-Flo*	*CTD*	*Date*	*SDY*	*GMT*	*Latitude (°)*		*Lonitude (°)*		*Sill depth (m)*				
A319	A3-19	17	11-Oct-96	285	11:55	-22.92 S		-36.96		3873				
Hydrographic Data (N.Rees)				**Trace Metals (A.Bowie / D.Whitworth)**						**Nutrients (M.Woodward)**			**Chlorophyll (R.Barlow)**	**Photosynthesis (E.Maranon)**
Depth	*Temperature*	*Salinity*	*Sigma T*	*TD-Fe $_{ship}$*	*TD-Fe $_{land}$*	*TD-Al*	*TD-Co*	*TD-Ni*	*Nitrate*	*Nitrite*	*Phosphate*	*Silicate*	*Total chl a*	*Primary production*
(m)	(°C)			(nM)	(nM)	(nM)	(pM)	(nM)	(µM)	(µM)	(µM)	(µM)	(µg l^{-1})	(µgC m^{-3} h^{-1})
-2	22.4562	36.8257		0.78			36.68	2.01						
-7	22.4589	36.8254	25.4766	0.95	2.72		44.57	2.11	0.08		0.00	1.13	0.12	0.31
-20	22.3178	36.8216	25.5140	0.23	2.04		37.00	1.50	0.08		0.00	1.13	0.12	
-40	22.3087	36.8216	25.5165	0.04	1.44		35.44	2.08	0.08		0.00	1.23	0.14	0.33
-60	21.9323	36.8143	25.6178						0.08		0.00	1.11	0.22	0.09
-80	21.8419	36.8015	25.6335	0.49	0.84		30.04	2.19	0.08		0.00	1.11	0.38	0.29
-90	21.8025	36.7921	25.6374						0.08		0.00	1.11		0.38
-100	21.8086	36.8135	25.6520	0.04	0.91		38.49	1.85	0.08		0.00	1.15	0.39	0.10
-120	21.5235	36.7360	25.6728						0.08		0.00	1.75	0.28	0.03
-130	21.4060	36.7007	25.6786										0.16	
-150	21.3003	36.6801	25.6922										0.10	
-160	20.8706	36.5748	25.7302	0.21	1.31		54.16	2.29	1.02		0.03	1.16		
-200	17.7847	35.8984	26.0147		1.12		37.58	1.71	3.59		0.25	1.17		

Station details			Date/Time			Position								
Station	*Go-Flo*	*CTD*	*Date*	*SDY*	*GMT*	*Latitude (°)*		*Lonitude (°)*		*Sill depth (m)*				
A321	A3-20	18	12-Oct-96	286	11:55	-26.60 S		-39.60 W		4218				
Hydrographic Data (N.Rees)				**Trace Metals (A.Bowie / D.Whitworth)**						**Nutrients (M.Woodward)**			**Chlorophyll (R.Barlow)**	**Photosynthesis (E.Maranon)**
Depth	*Temperature*	*Salinity*	*Sigma T*	*TD-Fe $_{ship}$*	*TD-Fe $_{land}$*	*TD-Al*	*TD-Co*	*TD-Ni*	*Nitrate*	*Nitrite*	*Phosphate*	*Silicate*	*Total chl a*	*Primary production*
(m)	(°C)			(nM)	(nM)	(nM)	(pM)	(nM)	(µM)	(µM)	(µM)	(µM)	(µg l^{-1})	(µgC m^{-3} h^{-1})
-7	20.8424	36.6176	25.7705	0.96					0.08	0.03		1.18	0.11	0.30
-20	20.8046	36.6144	25.7784										0.13	
-40	20.7623	36.6049	25.7827						0.08	0.03		1.20	0.12	0.21
-60	20.7019	36.5862	25.7848										0.19	
-70	20.4692	36.5273	25.8029	0.84					0.09	0.03		1.24		0.22
-80	19.8152	36.3793	25.8645						0.10	0.05		1.45	0.38	0.21
-95	19.5608	36.3231	25.8885	0.52					0.43	0.17		1.25	0.41	0.45
-110	18.9417	36.1469	25.9142						0.40	0.16		2.09	0.38	0.05
-120	18.6625	36.0733	25.9292	0.48					0.84	0.17		2.59	0.22	0.03
-140	18.1955	36.0243	26.0093						2.96	0.07		2.56		
-150	17.2870	35.8250	26.0797										0.03	
-160	17.0333	35.7790	26.1054	0.85					4.65	0.05		1.20		
-200	15.7995	35.5850	26.2445						4.92	0.05		1.20		

Station details			Date/Time			Position								
Station	*Go-Flo*	*CTD*	*Date*	*SDY*	*GMT*	*Latitude (°)*	*Lonitude (°)*	*Sill depth (m)*						
A325	A3-23	21	15-Oct-96	289	12:30	-35.70 S	-49.57 W	4292						
Hydrographic Data (N.Rees)				Trace Metals (A.Bowie / D.Whitworth)						Nutrients (M.Woodward)				Chlorophyll (R.Barlow)	Photosynthesis (E.Maranon)
Depth	*Temperature*	*Salinity*	*Sigma T*	*TD-Fe $_{ship}$*	*TD-Fe $_{land}$*	*TD-Al*	*TD-Co*	*TD-Ni*	*Nitrate*	*Nitrite*	*Phosphate*	*Silicate*	*Total chl a*	*Primary production*
(m)	(°C)			(nM)	(nM)	(nM)	(pM)	(nM)	(µM)	(µM)	(µM)	(µM)	(µg l^{-1})	(µgC m^{-3} h^{-1})
-2				1.14	4.23		51.98	1.77						
-7	16.4712	35.8051	26.2586	1.68	2.95		45.76	1.92	0.09	0.05	0.03	1.52	0.70	1.90
-10	16.4671	35.8052	26.2596	2.12			40.65	1.94	0.09	0.06	0.03	1.51	0.64	
-20	16.4245	35.8140	26.2764	2.68	2.42		60.06	1.87	0.09	0.05	0.02	1.55	0.68	2.29
-30	16.2724	35.8086	26.3077	2.33	2.20		33.51	1.56	0.70	0.11	0.06	1.62	0.73	1.60
-40	16.0245	35.8068	26.3637						1.74	0.25	0.09	1.63	0.56	1.31
-50	15.8065	35.7930	26.4031	1.64	2.26		32.90	3.03	2.77	0.32		1.84	0.33	0.72
-60	15.6222	35.7772	26.4329						3.45	0.37	0.11	1.89	0.13	0.11
-80	15.3921	35.7532	26.4663						4.07	0.17	0.13	2.25	0.04	0.01
-150	15.1871	35.7353	26.4983	2.03	4.73		31.26	2.33	4.49	0.06	0.29	1.33	0.04	
-200	14.3729	35.5512	26.5345	1.84	8.28		93.11	8.15	6.45	0.05	0.37	1.31		

Station details			Date/Time			Position								
Station	*Go-Flo*	*CTD*	*Date*	*SDY*	*GMT*	*Latitude (°)*	*Lonitude (°)*	*Sill depth (m)*						
A328	A3-25	23	23-Oct-96	297	12:55	-43.57 S	-55.02 W	5244						
Hydrographic Data (N.Rees)				Trace Metals (A.Bowie / D.Whitworth)						Nutrients (M.Woodward)				Chlorophyll (R.Barlow)	Photosynthesis (E.Maranon)
Depth	*Temperature*	*Salinity*	*Sigma T*	*TD-Fe $_{ship}$*	*TD-Fe $_{land}$*	*TD-Al*	*TD-Co*	*TD-Ni*	*Nitrate*	*Nitrite*	*Phosphate*	*Silicate*	*Total chl a*	*Primary production*
(m)	(°C)			(nM)	(nM)	(nM)	(pM)	(nM)	(µM)	(µM)	(µM)	(µM)	(µg l^{-1})	(µgC m^{-3} h^{-1})
-2	10.8762	34.7390		1.04					9.08		0.59	2.09		
-7	10.8695	34.7377	26.5952	0.99					9.13		0.58	2.10	1.08	1.84
-20	10.8809	34.7499	26.6027						9.11		0.56	2.69	1.14	1.71
-30	10.8912	34.7556	26.6053	1.60					9.25		0.57	3.38	1.06	2.11
-40	10.9166	34.7764	26.6170	0.99					11.23		0.62	4.44	0.92	1.61
-50	10.3373	34.7341	26.6865						13.88		0.83	6.91	0.15	0.43
-60	8.7998	34.5264	26.7794						14.00		1.10	8.57	0.04	0.05
-80	7.9962	34.4403	26.8351										0.02	
-100	7.6591	34.4472	26.8902	0.78					20.30		1.35	9.64	0.02	
-150	5.5879	34.2189	26.9875	0.92					22.07		1.59	6.84	0.03	
-200	4.9872	34.1996	27.0423	0.99					22.25		1.62	6.82		

Appendix C: AMT Data

Cruise AMT-6

Part (iii): Vertical profiling data, deep water cast (0-1500 m)

Station details			**Date/Time**			**Position**		
Station	*Go-Flo*	*CTD*	*Date*	*SDY*	*GMT*	*Latitude (°)*	*Lonitude (°)*	*Sill depth (m)*
A660	A6-50	50	12-Jun-98	163	08:28-09:5(	44.68 N	-14.01 W	4240
Hydrographic Data (N.Rees)			**Trace Metals** (A.Bowie / D.Whitworth)			**Chlorophyll** (R.Barlow)		
Depth	*Temperature*	*Salinity*	*TD-Fe $_{ship}$*	*TD-Co*	*TD-Ni*	*Total chl a*		
(m)	(°C)		(nM)	(pM)	(nM)	(µg l^{-1})		
-7	16.2768	35.8927	1.27	42.37	2.67	0.36		
-20	16.2743	35.8926	0.70	65.77	2.26	0.39		
-35	15.9427	35.8692		50.26	1.66	1.22		
-40	14.5379	35.7832	1.10	60.52	2.04	0.96		
-50	13.4362	35.7344	0.85	35.07	1.74	0.19		
-100	12.8008	35.7522	0.71	42.42	1.80	0.06		
-250	11.8841	35.6327	0.79	29.83	1.86			
-500	10.6867	35.4718	0.83	50.45	2.17			
-750	9.6521	35.4447	0.72	60.47	1.98			
-1000	8.8008	35.5539	0.82	81.40	2.17			
-1250	6.9475	35.3629	0.94	53.68	2.85			
-1500	4.8573	35.0780	0.57	53.08	3.14			

Appendix C: AMT Data

Cruise AMT-3

Part (iv): Full shipboard TD-Fe data set

Andrew R. Bowie (UoP and CCMS-PML)

Processed data tabulated from shipboard analyses

Station details			Date/Time			Position			Iron dataset
Station	*Go-Flo*	*CTD*	*Date*	*SDY*	*GMT*	*Latitude* (°)	*Lonitude* (°)	*Depth* (m)	*[TD-Fe]$_{ship}$* (nM)
A301	A3-01		22-Sep-96	266	8:00	49.67	-5.68	-6	4.27
A303	A3-03	1	24-Sep-96	268	10:30	47.35	-18.20	-7	4.45
A304	A3-04	2	25-Sep-99	269	10:30	42.72	-19.99	-7	[]
A305	A3-05	3	26-Sep-99	270	11:25	38.17	-20.01	-7	[]
A307	A3-07	5	28-Sep-96	272	11:25	29.48	-21.80	-2	1.54
						29.48	-21.80	-7	0.93
						29.48	-21.80	-20	1.31
						29.48	-21.80	-60	1.08
						29.48	-21.80	-80	1.15
						29.48	-21.80	-110	0.46
						29.48	-21.80	-150	1.08
						29.48	-21.80	-200	0.84
A308	A3-08	6	29-Sep-96	273	11:25	24.67	-21.40	-7	1.21
						24.67	-21.40	-20	1.09
						24.67	-21.40	-60	0.90
						24.67	-21.40	-90	0.38
						24.67	-21.40	-100	0.42
						24.67	-21.40	-120	1.22
						24.67	-21.40	-150	1.22
						24.67	-21.40	-200	1.60
A309	A3-09	7	30-Sep-96	274	10:55	20.08	-20.62	-2	3.59
						20.08	-20.62	-7	2.46
						20.08	-20.62	-20	0.63
						20.08	-20.62	-40	0.21
						20.08	-20.62	-60	1.17
						20.08	-20.62	-100	0.58
						20.08	-20.62	-200	1.27
Underway	uw1		30-Sep-99	274	12:00	20.06	-20.58	-7	2.09
Underway	uw2		01-Oct-99	275	11:39	16.66	-20.41	-7	1.71
Underway	uw3		02-Oct-99	276	9:47	12.91	-20.49	-7	0.51
10	10	8	02-Oct-96	276	10:55	12.75	-20.53	-2	1.75
						12.75	-20.53	-7	0.42
						12.75	-20.53	-20	1.38
						12.75	-20.53	-40	0.91
						12.75	-20.53	-60	0.65
						12.75	-20.53	-100	0.29
						12.75	-20.53	-150	0.47
						12.75	-20.53	-200	0.37
A311	A3-11	9	03-Oct-96	277	10:55	9.05	-22.80	-2	[]
						9.05	-22.80	-7	0.32
						9.05	-22.80	-20	0.43
						9.05	-22.80	-50	0.47
						9.05	-22.80	-60	0.35
						9.05	-22.80	-100	0.63
						9.05	-22.80	-150	0.62
						9.05	-22.80	-200	0.59
Underway	uw5		04-Oct-99	278	0:23	6.99	-23.14	-7	0.61

A312	A3-12	10	04-Oct-96	278	10:55	5.17	-24.01	-2	[]
						5.17	-24.01	-7	0.55
						5.17	-24.01	-20	0.48
						5.17	-24.01	-40	0.52
						5.17	-24.01	-50	0.42
						5.17	-24.01	-60	0.28
						5.17	-24.01	-70	0.33
						5.17	-24.01	-80	0.35
Underway	uw6		04-Oct-99	278	23:28	3.27	-24.91	-7	0.48
A313	A3-13	11	05-Oct-96	279	10:55	1.28	-25.47	-2	1.58
						1.28	-25.47	-7	1.20
						1.28	-25.47	-20	0.40
						1.28	-25.47	-70	0.78
						1.28	-25.47	-80	0.47
						1.28	-25.47	-90	0.23
						1.28	-25.47	-120	0.27
						1.28	-25.47	-200	0.40
A314	A3-14	12	06-Oct-96	280	10:55	-2.38	-27.45	-7	1.31
						-2.38	-27.45	-20	1.16
						-2.38	-27.45	-40	0.59
						-2.38	-27.45	-65	0.04
						-2.38	-27.45	-85	0.13
						-2.38	-27.45	-120	0.67
						-2.38	-27.45	-200	0.37
A315	A3-15	13	07-Oct-96	281	10:55	-6.48	-29.27	-2	[]
						-6.48	-29.27	-7	0.39
						-6.48	-29.27	-30	0.88
						-6.48	-29.27	-70	1.03
						-6.48	-29.27	-110	0.81
						-6.48	-29.27	-140	0.35
						-6.48	-29.27	-200	0.48
A316	A3-16	14	08-Oct-96	282	11:55	-10.77	-31.23	-2	[]
						-10.77	-31.23	-7	0.76
						-10.77	-31.23	-25	0.65
						-10.77	-31.23	-75	0.69
						-10.77	-31.23	-100	0.50
						-10.77	-31.23	-130	0.12
						-10.77	-31.23	-160	0.49
						-10.77	-31.23	-200	[]
Underway	uw8		08-Oct-99	282	23:56	-12.75	-32.14	-7	0.87
A317	A3-17	15	09-Oct-96	283	12:15	-14.88	-33.12	-2	0.53
						-14.88	-33.12	-7	0.85
						-14.88	-33.12	-30	0.76
						-14.88	-33.12	-60	0.50
						-14.88	-33.12	-100	0.25
						-14.88	-33.12	-140	1.29
						-14.88	-33.12	-160	0.78
						-14.88	-33.12	-200	0.93
Underway	uw9		10-Oct-99	284	0:45	-16.80	-34.01	-7	0.40
A318	A3-18	16	10-Oct-96	284	11:55	-18.85	-35.03	-7	1.13
A319	A3-19	17	11-Oct-96	285	11:55	-22.92	-36.95	-2	0.78
						-22.92	-36.95	-7	0.95
						-22.92	-36.95	-20	0.23
						-22.92	-36.95	-40	0.04
						-22.92	-36.95	-80	0.49
						-22.92	-36.95	-100	0.04
						-22.92	-36.95	-160	0.21
						-22.92	-36.95	-200	[]

A321	A3-20	18	12-Oct-96	286	11:55	-26.60	-39.60	-2	[]
						-26.60	-39.60	-7	0.96
						-26.60	-39.60	-70	0.84
						-26.60	-39.60	-95	0.52
						-26.60	-39.60	-120	0.48
						-26.60	-39.60	-160	0.85
						-26.60	-39.60	-200	[]
A323	A3-21	19	13-Oct-96	287	12:00	-29.85	-42.90	-2	0.40
						-29.85	-42.90	-7	0.33
						-29.85	-42.90	-50	0.48
						-29.85	-42.90	-80	1.17
						-29.85	-42.90	-90	0.51
						-29.85	-42.90	-110	0.84
						-29.85	-42.90	-150	0.36
						-29.85	-42.90	-200	0.49
A324	A3-22	20	14-Oct-96	288	12:00	-32.80	-46.10	-2	[]
						-32.80	-46.10	-7	0.65
						-32.80	-46.10	-20	1.46
						-32.80	-46.10	-50	3.74
						-32.80	-46.10	-60	3.02
						-32.80	-46.10	-100	2.02
						-32.80	-46.10	-200	2.34
Underway	uw10		15-Oct-99	289	8:06	-35.18	-48.76	-7	1.46
A325	A3-23	21	15-Oct-96	289	12:30	-35.70	-49.57	-2	1.14
						-35.70	-49.57	-7	1.68
						-35.70	-49.57	-10	2.12
						-35.70	-49.57	-20	2.68
						-35.70	-49.57	-30	2.33
						-35.70	-49.57	-50	1.64
						-35.70	-49.57	-150	2.03
						-35.70	-49.57	-200	1.84
A327	A3-24	22	16-Oct-96	290	11:50	-37.80	-52.18	-2	[]
						-37.80	-52.18	-7	1.05
						-37.80	-52.18	-20	1.70
						-37.80	-52.18	-40	1.68
						-37.80	-52.18	-60	0.80
						-37.80	-52.18	-100	1.94
						-37.80	-52.18	-150	1.42
						-37.80	-52.18	-200	2.54
A328	A3-25	23	23-Oct-96	297	12:55	-43.57	55.00	-2	1.04
						-43.57	55.00	-7	0.99
						-43.57	55.00	-30	1.60
						-43.57	55.00	-40	0.99
						-43.57	55.00	-100	0.78
						-43.57	55.00	-150	0.92
						-43.57	55.00	-200	0.99
A329	A3-26	24	24-Oct-96	298	12:55	-48.00	-55.87	-2	1.32
						-48.00	-55.87	-7	0.88
						-48.00	-55.87	-20	0.89
						-48.00	-55.87	-60	0.59
						-48.00	-55.87	-80	0.50
						-48.00	-55.87	-100	1.16
						-48.00	-55.87	-150	0.97
						-48.00	-55.87	-200	1.17
A330	A3-27	25	25-Oct-96	299	11:00	-51.90	-57.88	-2	5.92
						-51.90	-57.88	-7	2.71
						-51.90	-57.88	-40	2.89
						-51.90	-57.88	-60	6.07

Notes:

*Total dissolvable (II+III) Fe; includes colloidal and labile particulate fractions

[] Contamination suspected (12 out of 163 samples, ca. 7% of dataset)